UTS UNIVERSITY OF TECHNOLOGY SYDNEY

DEVELPOMENT OF GEL MATERIALS FOR WATER PURIFICATION

by Lilyan Yaaqub Matti Alsaka

Thesis submitted in fulfilment of the requirements for the degree of

Doctor of Philosophy

under the supervision of Dr Ali Altaee and Distinguished Professor T M Indra Mahlia

University of Technology Sydney
Faculty of Engineering and Information Technology

May 2026

CERTIFICATE OF ORIGINAL AUTHORSHIP

I, Lilyan Alsaka, declare that this thesis is submitted in fulfillment of the requirements for the award of Doctor of Philosophy in the School of Civil and Environmental Engineering/ Faculty of Engineering and Information Technology at the University of Technology Sydney.

This thesis is wholly my own work unless otherwise referenced or acknowledged. In addition, I certify that all information sources and literature used are indicated in the thesis.

This document has not been submitted for qualification at any other academic institution.

This research was supported by an Australian Government Research Training Program (RTP) Scholarship doi.org/10.82133/C42F-K220.

Signature: Production Note:
Signature removed prior to publication.

Date: 4th May 2026

ACKNOWLEDGEMENTS

First and foremost, I would like to express my deepest gratitude to God for granting me strength, perseverance, and wisdom throughout my PhD journey. Without His blessings, this achievement would not have been possible.

I want to sincerely thank my principal supervisor, Ali Altaee, for his unwavering support, guidance, and encouragement. His exceptional mentorship has played a pivotal role in shaping me as a scholar and an individual. Ali's faith in my abilities, patience, and insightful advice have been invaluable in helping me flourish academically.

I am also profoundly grateful to my co-supervisor, T M Indra, for his invaluable feedback, direction, and assistance throughout my research. His expertise and constructive guidance have greatly contributed to the success of this work.

A heartfelt thanks to my family my husband Basam, my daughter Lina, and my son Karm for their unconditional love, patience, and unwavering support. Without their constant encouragement and sacrifices, I would not have been able to reach this milestone. Their belief in me has been my greatest motivation.Lastly, I extend my gratitude to the Australian Government for providing the Research Training Program Scholarship (RTPS), which has been instrumental in supporting my research and academic journey.

PUBLICATIONS (ALL INCLUDING CO-AUTHORED)

Alsaka, L., Alsaka, L., Altaee, A., Zaidi, S. J., Zhou, J., & Kazwini, T. (2025). A Review of Hydrogel Application in Wastewater Purification. *Separations*, *12*(2), 51.

Alsaka, L., Altaee, A., Moghaddam, A., Khonakdar, H. A., AL-Ejji, M., Hawari, A. H., Hamdi, F., Aedan, Y., & Al Askar, A. (2025). Fabrication of kappa carrageenan-cellulose nanofiber/graphene oxide composite membrane for water purification. *Journal of Environmental Chemical Engineering*, 120445.

Alsaka, L., Altaee, A., Alsaka, L., Al-Ejji, M., Hawari, A. H., & Zhou, J. (2025). kappa-Carrageenan-based hydrogel for leachate wastewater treatment and resource recovery. *Desalination*, 119208.

Alsaka, L., Ibrar, I., Altaee, A., Zhou, J., Chowdhury, M. H., Maryam, A.-E., & Hawari, A. H. (2024). Performance and analysis of kappa-carrageenan hydrogel for PFOA-contaminated soil remediation wastewater treatment. *Chemosphere*, *365*, 143371.

Ibrar, I[1]., **Alsaka, L[1]**., Yadav, S., Altaee, A., Zhou, J. L., & Shon, H. K. (2023). Kappa carrageenan-vanillin composite hydrogel for landfill leachate wastewater treatment. *Desalination*, *565*, 116826. **1: Equal effort, Lilyan Alsaka with Ibrar Ibrar(Equal effort). The authors would like to acknowledge the research training program scholarship awarded to Lilyan Alsaka by the Government of Australia.**

Altaee, A., Hamdi, F., **Alsaka, L**., Ibrar, I., AL-Ejji, M., Zhou, J., Samal, A., & Hawari, A. (2024). proceedings of the 5th International Conference on Environmental Science and Applications (ICESA 2024). 5th International Conference on Environmental Science and Applications (ICESA 2024),

Ganbat, N., Hamdi, F. M., Ibrar, I., Altaee, A., **Alsaka, L**., Samal, A. K., Zhou, J., & Hawari, A. H. (2023). Iron slag permeable reactive barrier for PFOA removal by the electrokinetic process. *Journal of hazardous materials*, *460*, 132360.

Hamdi, F. M., Altaee, A., Aedan, Y., Zhou, J., Zaidi, S. J., **Alsaka, L**., Almalki, R., Al-Askar, A., & Samal, A. K. (2025). Black tea waste/iron slag reactive filter media-electrokinetic for mixed heavy metals treatment from contaminated site. *Journal of contaminant hydrology*, 104517.

Hamdi, F. M., Altaee, A., **Alsaka, L**., Ibrar, I., Maryam, A.-E., Zhou, J., Samal, A. K., & Hawari, A. H. (2024). Iron slag/activated carbon-electrokinetic system with anolyte recycling for single and mixture heavy metals remediation. *Science of the total environment*, *930*, 172516.

Karbassiyazdi, E., Altaee, A., Ibrar, I., Razmjou, A., **Alsaka, L**., Ganbat, N., Malekizadeh, A., Ghobadi, R., & Khabbaz, H. (2023). Fabrication of carbon-based hydrogel membrane for landfill leachate wastewater treatment. *Desalination*, *564*, 116783.

Kazwini, T., Altaee, A., Ibrar, I., Alkadour, F., Hawari, A. H., Zhou, J., & **Alsaka, L**. (2025). Sodium metasilicate sol-gel draw solution for seawater desalination and supplementing nutrients to soil. *Desalination*, *600*, 118517.

Khanafer, D., Altaee, A., Hawari, A. H., Zhou, J., & **Alsaka, L**. (2024). Innovative stimuli-responsive membrane MSF brine rejection dilution by tertiary treated sewage effluent. *Journal of environmental management*, *365*, 121517.

Kardani, R., Yadav, S., Altaee, A., **Alsaka, L.**, & Zhou, J. (2025). Eco-friendly kappa-carrageenan-nano zerovalent iron hydrogel water and wastewater purification. *Journal of hazardous materials*, 138123.

Aedan, Y., Altaee, A., Mueller, V., Shon, H. K., **Alsaka, L**., & Zaidi, S. J. (2025). PFAS-contaminated groundwater treatment by forward osmosis using pressure-stimuli-responsive nanofiltration membrane: Effects of chain length and operating conditions. *Desalination*, 119425.

Almalki, R., **Alsaka, L**., Hamdi, F., AlAskar, A., Altaee, A., Samal, A., Zhou, J., Mohsen, M., Zaidi, S. J., & Aedan, Y. (2025). Feasibility of combining biological hydrogel reactive filter media with electrokinetic for sustainable site remediation. *Journal of environmental chemical engineering*, 119514.

Kazwini, T., Altaee, A., **Alsaka, L**., Hawari, A., Warmbier, E., Shon, H., Yadav, S., Samal, A. K., Zhou, J., & Aedan, Y. (2025). Fouling mitigation for cellulose triacetate and thin-film composite forward osmosis membranes for seawater desalination by sodium metasilicate sol-gel. *Science of the total environment, 1001*, 180525.

PREFACE

This doctoral thesis is prepared in a "Thesis by compilation" format in accordance with the "Graduate Research Candidature Management, Thesis Preparation and Submission Procedures, 2019" of the University of Technology Sydney. It comprises the published articles.

This thesis contains one published review paper in Chapter 2 and four original research articles in Chapters 3 to 6, which are published. The authorship of these works has been decided after discussing with the supervisory team. Lastly, Chapter 7 includes conclusions and future recommendations.

Chapter 2 comprises the following article:

Alsaka, L., Alsaka, L., Altaee, A., Zaidi, S. J., Zhou, J., & Kazwini, T. (2025). A Review of Hydrogel Application in Wastewater Purification. *Separations*, *12*(2), 51.

Chapter 3 includes the following technical article:

Ibrar, I[1]., **Alsaka, L[1].**, Yadav, S., Altaee, A., Zhou, J. L., & Shon, H. K. (2023). Kappa carrageenan-vanillin composite hydrogel for landfill leachate wastewater treatment. *Desalination*, *565*, 116826. **1: Equal effort, Lilyan Alsaka with Ibrar Ibrar(Equal effort). The authors would like to acknowledge the research training program scholarship awarded to Lilyan Alsaka by the Government of Australia.**

Chapter 4 includes the following technical article:

Alsaka, L., Ibrar, I., Altaee, A., Zhou, J., Chowdhury, M. H., Maryam, A.-E., & Hawari, A. H. (2024). Performance and analysis of kappa-carrageenan hydrogel for PFOA-contaminated soil remediation wastewater treatment. *Chemosphere*, *365*, 143371.

Chapter 5 includes the following technical article:

Alsaka, L., Altaee, A., Alsaka, L., Al-Ejji, M., Hawari, A. H., & Zhou, J. (2025). kappa-Carrageenan-based hydrogel for leachate wastewater treatment and resource recovery. *Desalination*, 119208.

Chapter 6 includes the following technical article:

Alsaka, L., Altaee, A., Moghaddam, A., Khonakdar, H. A., AL-Ejji, M., Hawari, A. H., Hamdi, F., Aedan, Y., & Al Askar, A. (2025). Fabrication of kappa carrageenan-cellulose nanofiber/graphene oxide composite membrane for water purification. *Journal of Environmental Chemical Engineering*, 120445.

Chapter 7 includes the conclusions and future recommendations.

STATEMENT OF CONTRIBUTION OF AUTHORS

The research papers reported on original research I conducted during my Higher Degree by Research candidature are not subject to any obligations or contractual agreements with a third party that would constrain their inclusion in this thesis. I have contributed more than 85% to all the papers reported in this thesis, including conceptualization, methodology, software, validation, formal analysis, investigation, data curation, visualization, writing - original draft, review, and editing. I am the primary author of all the papers reported in this thesis.

Signature: Production Note:
Signature removed prior to publication.

Date: 4th May 2026

TABLE OF CONTENTS

CERTIFICATE OF ORIGINAL AUTHORSHIP i

ACKNOWLEDGEMENTS ii

PUBLICATIONS (ALL INCLUDING CO-AUTHORED) iii

PREFACE vi

STATEMENT OF CONTRIBUTION OF AUTHORS viii

TABLE OF CONTENTS ix

LIST OF FIGURES xvi

LIST OF TABLES xxiii

ABSTRACT xxv

Chapter 1: Introduction 1

1.1 Global water scarcity 1

1.2 Research significance 2

1.3 Research aims and objectives 3

1.4 Research questions 4

1.5 The research hypothesis 5

1.6 Thesis structure 5

Chapter 2: Literature review 7

A Review of Hydrogel Application in Wastewater Purification 7

Abstract 7

2.1 Introduction 8

2.2 Hydrogel classification 11

2.3 Hydrogel separation mechanisms 16

2.3.1. Size exclusion 16

2.3.2. Adsorption....19
2.3.3. Electrostatic interactions....20
2.3.4. Non-sieving process....21
2.4 Functional groups in hydrogels....22
2.5 Hydrogel composites....25
2.6 Hydrogel filtration mechanisms....28
2.7 Hydrogel adsorption effectiveness....30
2.8 Pros and cons of hydrogels and regeneration....31
2.9 Hydration phenomena in hydrogel: mechanisms, measurements....48
2.10 Conclusion....52
Chapter 3: Kappa Carrageenan-Vanillin Composite Hydrogel for Landfill Leachate Wastewater Treatment....54
Abstract....54
3.1 Introduction....55
3.2 Materials and methods....60
3.2.1 Materials....60
3.2.2 Hydrogel Synthesis and Filtration Setup....60
3.2.3 Analytical methods....63
3.2.4 Water contact angle, water uptake, and swelling....65
3.2.5 Wastewater characterization....66
3.2.6 Adsorption capacity....68
3.2.7 Desorption....69
3.2.8 Statistical analysis....70
3.3 Results and discussions....70

3.3.1 Morphological characterization via FE-SEM, FT-IR, and contact angle 70
3.3.2 Water uptake, swelling and pore size analysis 73
3.3.3 Pure water flux 77
3.3.4 Rejection of NaCl and divalent ions 80
3.3.5 Adsorption and desorption 83
3.3.6 Landfill leachate treatment 86
3.3.7 Commercial implications 92
3.4 Conclusion 96
Supplementary information S1 97
Chapter 4: Performance and analysis of kappa-carrageenan hydrogel for PFOA-contaminated soil remediation wastewater treatment 100
Abstract 100
4.1 Introduction 101
4.2 Material and methods 105
4.2.1 Materials 105
4.2.2 Hydrogel fabrication 105
4.2.3 PFOA analysis 107
4.3 Methods of analysis for membrane characterization 108
4.3.1 Membrane morphology 108
4.3.2 Membrane porosity and pore size 109
4.3.3 Water uptake and swelling 110
4.3.4 Membrane performance efficiency 111
4.3.5 PFOA-contaminated water 112
4.4 Statistical assessment 113

4.5 Results and discussion 113
4.5.1 Hydrogel membranes characterization 113
4.5.2 Contact angle and rheology 115
4.5.3 Porosity and pore size 118
4.5.4 Water uptake and swelling degree 120
4.5.5 kC-AC and kC-V performance 123
4.5.5.1 Effect of hydrogel thickness 124
4.5.5.2 Effect of feed pH 126
4.5.5.3 Effect of feed concentration 128
4.5.6 PFOA-contaminated water treatment 131
4.5.7 Reusability of kC-AC and kC-V hydrogel 136
4.5.8 Characterization of kC-AC and kC-V hydrogel after PFOA adsorption 138
4.6 Conclusion 141
Supplementary information S2 142
Performance and analysis of kappa-carrageenan hydrogel for PFOA-contaminated soil remediation wastewater treatment 142
S2.1 The filtration device 142
S2.2 Adsorption-desorption ability/ Adsorption kinetics models 143
S2.3 Adsorption /Desorption of The PFOA solution 144
S2.3.1 Effect AC and Vanillin concentrations 144
S2.3.2 Effect of pH 144
S2.4 Adsorption kinetics 144
Chapter 5: kappa-carrageenan-based hydrogel for leachate wastewater treatment and resource recovery 152

Abstract 152
5.1 Introduction 153
5.2 Materials and methods 157
5.2.1 Materials 157
5.2.2 Synthesis of kC-AC/PEI hydrogel 157
5.3 Hydrogel characterization and analysis 161
5.3.1 Structural features of membranes 161
5.3.2 Swelling, deswelling, and water uptake 161
5.3.3 Hydrogel Filtration Performance 162
5.3.4 Wastewater properties 163
5.3.5 Adsorption-Desorption Mechanism 164
5.3.6 Metal Recovery 165
5. 3.7 Statistical test 165
5.4 Results 166
5.4.1 Morphological characterization of the hydrogel 166
5.4.2 Hydrogel water uptake, swelling, and deswelling 172
5.4.3 Hydrogel Performance Efficiency 175
5.4.4 Impact of temperature and pH on adsorption capacity 179
5.4.5 Leachate wastewater treatment 182
5.4.6 Hydrogel recycling for reuse 187
5.4.7 Metal ions recovery 189
5.5 Conclusion 191
Supplementary information S3 192

kappa-carrageenan-based hydrogel for leachate wastewater treatment and resource recovery 192
Chapter 6: Fabrication of kappa carrageenan-cellulose nanofiber/graphene oxide composite membrane for water purification 195
Abstract 195
6.1 Introduction 196
6.2 Material and methods 199
6.2.1 Materials 199
6.2.2 Synthesis of kC-CNF/GO-GA hydrogel 201
6.3 Hydrogel performance efficiency 204
6.3.1 Flux evaluation and rejection 204
6.3.2 Antifouling Study for Hydrogel 204
6.3.3 Methodology hydrogel properties 205
6.3.4 Adsorption-desorption performance analysis 207
6.4 Results 208
6.4.1 Rheology and Zeta potential of hydrogel composites 208
6.4.2 Porosity and pores size 211
6.4.3 Hydrogel swelling, deswelling, and water uptake 213
6.4.4 Average molecular weight between crosslinks 218
6.4.5 Hydrogel membrane characterization 219
6.4.6 Hydrogel DI water flux and salt rejection 222
6.4.7 Seawater desalination 228
6.4.8 Reusability 234
6.5 Conclusion 236

Supplementary material S4 238
Fabrication of kappa carrageenan-cellulose nanofiber/graphene oxide composite membrane for water purification 238
S4.1 M_c calculations 240
S4.2 Effect of M_c values on properties of hydrogel samples 241
S4.3 Adsorption performance 243
Chapter 7 Conclusions and recommendations for future work 251
References 256

LIST OF FIGURES

Figure1. 1. Factors contributing to water scarcity and various methods to mitigate it. 2

Figure2. 1. (a) Molecular segregation through a semipermeable membrane, (b) schematic representation of the adsorption process, and (c) schematic representation of solute exclusion mechanisms (Roy et al., 2017).....18

Figure2.2.Hydrogel filtration removal mechanisms: (A) size exclusion, (B) hydrophobicity, (C) electrostatic interaction, and (D) adsorption.....22

Figure 2. 3. Mechanisms involved in contaminant removal with hydrogels 29

Figure 2. 4. Illustration depicting the structure of a polymer network. 49

Figure3.1:Hydrogel synthesis and apparatus used a) Hydrogel synthesis and b) a schematic of gravity filtration. 61

Figure3. 2.SEM and FT-IR analysis of the kC-V hydrogel, a) SEM image of the hydrogel at 10 μm at the first focus point, b) SEM images of the hydrogel at 2 μm at the first focus point, c) FT-IR spectra of the kC and kC coated with Vanillin (kC-V). 72

Figure3. 3.a) Water uptake of different concentrations of kC-V hydrogel, b) Swelling degree of various percentages of hydrogel with NaCl concentrations, c) Swelling degree in DI water for different concentrations, d) Swelling degree in NaCl 2g/L solution, e) Contact angle measurements of pure kappa-carrageenan, 1% kappa-carrageenan blended with 1% vanillin, 2% kappa-carrageenan with 1% vanillin and 3% kappa-carrageenan with 1% vanillin. 76

Figure3. 4.a) Hydrogel settlement time, b) Influence of hydrogel thickness on water flux with DI water feed solution, c) influence of hydrogel thickness on rejection, d) Pure water flux with DI water and Pure water permeability for different concentrations of kC-V hydrogel.....80

Figure3. 5.NaCl, MgSO4 and CuSO4 water flux and rejection using 2 g/L feed solution in separate experiments a) water flux, b) $CuSO_4$ solution before on the left, and CuSO4 solution after filtration, on the right, c) hydrogel after $CuSO_4$ filtration, d) gel after $CuSO_4$ filtration, e) SEM of the gel after $CuSO_4$ filtration at 200 µm, f) SEM of the gel after CuSO4 filtration at 100 µm. 83

Figure3.6.Adsorption experiments for $CuSO_4$ solution, a) influence of kC-V concentrations on adsorption of $CuSO_4$, b) adsorption curve for 3kC-V hydrogel for $CuSO_4$, c) adsorption and desorption of $CuSO_4$ in three consecutive cycles. 86

Figure3.7.Particle size distribution of the landfill leachate wastewater conducted through the Malvern Particle Analyser 87

Figure3. 8.a) Water flux (LMH) of the landfill leachate wastewater, b) Colour rejection, c) SEM analysis of fouled hydrogel, d) Rejection of heavy metal ions from the landfill leachate wastewater, e) Grothus mechanism for H^+ and OH^- ion diffusion. 90

Figure3. 9.EDX analysis of hydrogel after filtration with landfill leachate wastewater, a) top surface of the hydrogel, b) inner section of the hydrogel. 91

Figure S1. 1.Hydrogel shrinking. 97

Figure S1. 2.Rejection in multiple cycles 98

Figure S1. 3. Copper sulphate filtration, a) a snapshot of filtration, b) $CuSO_4$ after filtration on the left, $CuSO_4$ before filtration on the right. 98

Figure S1. 4. Comparison of FT-IR spectra of kC-V gel before and after landfill treatment. 99

Figure 4. 1.Hydrogel Fabrication 107

Figure 4. 2.SEM and FT-IR analysis of the hydrogel, a) SEM of the kC-3% V hydrogel before filtration at 20 µm at the first focus point, b) SEM of the kC-3% V hydrogel after

filtration at 20 µm at the first focus point, c) SEM of the 3%kC-0.3%AC hydrogel before filtration at 20 µm at the first focus point, d) SEM of the 3%kC-0.3%AC hydrogel after filtration at 20 µm at the first focus point, e) FT-IR of kC-(1-3)%V before filtration, f) FT-IR of kC-(0.1-0.3)%AC before filtration. 117

Figure 4. 3.a) the contact angle for the 3% kC, 3% kC-AC, b) the contact angle for the 3%kC-V, c,d) viscosity and shear stress of the composite hydrogel, e) the effects of AC content on the porosity and average pore size of kC-AC membranes, f) the effects of vanillin content on the porosity average pore size of kC-V membranes. 119

Figure 4. 4.a) Water uptake of different concentrations of kC-AC hydrogel, b) Water uptake of different concentrations of kC-V hydrogel, c) Swelling degree of kC with various concentrations of AC at different concentrations of PFOA, d) Swelling degree of kC with various concentrations of vanillin at different concentrations of PFOA.The error bar = 1 standard deviation 123

Figure 4. 5.a) The impact of kC-AC hydrogel thickness on water flux with a 1 mg/L PFOA, b) The impact of kC-V hydrogel thickness on water flux with a 1 mg/L PFOA, c) The impact of kC-AC hydrogel thickness on 1 mg/L PFOA rejection, d) The impact of hydrogel thickness (kC-V) on 1 mg/L PFOA rejection, e) The influence pH of a PFOA feed solution on water flux for kC-0.3%AC hydrogel, f) The influence pH of a PFOA feed solution on water flux for kC-3%V hydrogel, g) The influence pH of a PFOA feed solution on rejection for kC-0.3%AC hydrogel, h) The influence pH of a PFOA feed solution on rejection for kC-3%V hydrogel, i) Effect (0.5, 1, 1.5) mg/L PFOA concentration on water flux rate and rejection of 2 cm thick kC-0.3%AC hydrogel, j) Effect (0.5, 1, 1.5) mg/L PFOA concentration on water flux rate and rejection of 2 cm thick kC-3%V hydrogel. 131

Figure 4. 6.a) Water flux rate and rejection of kC-0.3%AC and kC-3%V hydrogel for PFOA wastewater, b) Water flux and rejection in multiple cycles for PFOA feed solution in kC-0.3%AC, c) Rejection of elements and parameters from the PFOA-contaminated water kC-0.3%AC, and d) colour and turbidity rejection. 136

Figure 4. 7.a) adsorption and desorption of 1.5 mg/L PFOA in three consecutive cycles of 3%kC-0.3%AC, b) adsorption and desorption of PFOA in three consecutive cycles of 3%Kc-1%V, c) FT-IR of the different concentration AC (0.1,0.2,0.3)% with 3%kC after filtration, d) FT-IR of the different concentration V (1,2,3)% with 3%kC after filtration, e) SEM of the 3%kC-0.3%AC hydrogel after filtration at 20 µm at the first focus point, f) SEM of the 3%kC-3%V hydrogel after filtration at 20 µm at the first focus point. .. 141

Figure S2. 1.a schematic of gravity filtration. 142

Figure S2. 2.SEM of the 3% kC hydrogel at 100 µm. 143

Figure S2. 3.a and b) influence of kC-0.3%AC and KC-3%V concentrations on adsorption of PFOA, c and d) adsorption curve for kC-0.3%AC and KC-3%V hydrogel for PFOA at different pH with time respectively. PFOA concentration in the feed solution is 1 mg/L. 148

Figure S2. 4.a and b) pseudo-first-order for kC-0.3%AC and KC-3%V hydrogel for PFOA at different pH with time, c and d) pseudo-second-order for kC-0.3%AC and KC-3%V hydrogel for PFOA at different pH with time, e and f) Elovich model for kC-0.3%AC and KC-3%V hydrogel for PFOA at different pH with time, g and h) Intraparticle diffusion model for kC-0.3%AC and KC-3%V hydrogel for PFOA at different pH with time... 150

Figure S2. 5.a and b) EDX of the kC-0.3%AC hydrogel before and after filtration, c and d) EDX of the kC-3%V hydrogel before and after filtration. 151

Figure5.1.Hydrogel preparation a) Hydrogel formation process, b) Synthesis and Structural Composition of PEI-Enhanced kC-AC Hydrogel, and c) Molecular Interactions within PEI-Modified kC-AC Hydrogel Network.....160

Figure5. 2.a & b) SEM of the 3%kC-0.3% AC/2%PEI hydrogel before and after the filtration with NaCl at 20 µm at the first focus point, c & d) SEM of the 3%kC-AC/PEI hydrogel after filtration with $MgSO_4$ and leachate wastewater at 20 µm at the first focus point, e) FT-IR of the 3%kC,0.3%AC,2%PEI and 3%kC-0.3%AC/2%PEI, f) FT-IR of the 3%kC-AC/PEI after filtration with MgSO4, NaCl and leachate wastewater, g) Contact angle measurements of pure kappa-carrageenan and 1-3%kC-AC/PEI, h) viscosity and shear stress of the composite hydrogel membranes.The error bar = 1 standard deviation. 172

Figure5. 3.a) Water uptake of different concentrations of kC hydrogel membranes, b) Swelling degree of hydrogel membranes in DI water at 2 hr and 24 hr, c) Swelling degree hydrogel membranes in 2g/L NaCl and for 2hr, d) Swelling degree of hydrogel membranes in 0.5 to 3 g/L NaCl, e) Deswelling of different hydrogel membranes over time.The error bar = 1 standard deviation. 175

Figure5. 4.a) Hydrogel settlement time, b) Effect of hydrogel thickness on pure water flux, c) Effect of hydrogel thickness on 2 g/L $MgSO_4$ rejection, d) Influence of kC hydrogel membranes $MgSO_4$ and NaCl water flux and rejection, e) Impact of pressure on rejection and water flux in 2 cm thickness hydrogel membranes.The error bar = 1 standard deviation. 178

Figure5. 5.a & b) Influence of temperatures and pH on adsorption of $MgSO_4$ on the 3%kC-0.3%AC/2%PEI membrane, c) Adsorption capacity of the cation metals on the 3%kC-0.3%AC/2%PEI membrane. 181

Figure5. 6.3%kC-0.3%AC/2%PEI membrane performance a) Removal of contaminants from leachate, b) Water flux of the leachate wastewater, c) Rejection of ions in three cycles, and d) Water flux of leachate in three cycles, e) SEM of kC-AC/PEI hydrogel after leachate filtration.The error bar = 1 standard deviation. 186

Figure5. 7.Recovery% of ions from leachate wastewater and concentration of ions in the RO brine.The error bar = 1 standard deviation. 190

Figure S3. 1. an illustrative of gravity-based filtration. 192

Figure S3. 2. The EDS analysis results for the kC AC/PEI hydrogel before and after treatment. 193

Figure S3. 3. Removal of color and reduction of turbidity. 194

Figure S3. 4.SEM of the 3% kC hydrogel at 100 µm 194

Figure 6.1. Hydrogel preparation a) Hydrogel formation process a) Hydrogel formation process, b) Synthesis and structural Composition of kC-CNF/GO-GA (M_1, $M_{1.5}$, M_2, and $M_{2.5}$) hydrogel and molecular interactions within hydrogel Network. 204

Figure 6. 2. a) viscosity and shear stress of kC, CNF, and $M_{2.5}$, b) Zeta potential of kC, CNF, M_1, $M_{1.5}$, M_2, and $M_{2.5}$, c) Contact angle measurements of kC, CNF, M_1, $M_{1.5}$, M_2 and $M_{2.5}$, d) porosity and pore size of the composite hydrogel of M_1, $M_{1.5}$, M_2, and $M_{2.5}$. 213

Figure 6. 3. a) Swelling degree in DI water of M_1, $M_{1.5}$, M_2, and $M_{2.5}$ for 2hr, b) Swelling degree of various hydrogels at various concentrations of NaCl, c) Deswelling of M_1, $M_{1.5}$, M_2, and $M_{2.5}$ hydrogel with time, d)Water uptake ability of M_1, $M_{1.5}$, M_2, and $M_{2.5}$ hydrogel..... 217

Figure 6. 4. a) FT-IR of the M_1, $M_{1.5}$, M_2, and $M_{2.5}$, b) FT-IR of the $M_{2.5}$ after filtration with $MgSO_4$, NaCl, and seawater, c and d) SEM and EDS for the new $M_{2.5}$, e, and f) SEM and EDS for the hydrogel after filtration with seawater. 222

Figure 6.5. a) Influence of hydrogel thickness on pure water flux, b) Influence of hydrogel thickness on 2 g/L NaCl rejection, c) Influence of hydrogel thickness on 2 g/L $MgSO_4$ rejection, d) Influence of hydrogel thickness on 2 g/L NaCl rejection and flux, e) Rejection and flux at 2 cm thickness for M_1, $M_{1.5}$, M_2, and $M_{2.5}$ with NaCl, and $MgSO_4$. 228

Figure 6. 6. a) Ion rejection and TDS reduction performance of $M_{2.5}$ hydrogel by seawater, stage 1, and stage 2, b) Water flux of the seawater with time for stage 1, and 2, c) Particle size distribution of the seawater conducted through the Malvern Particle Analyser, d) Removal of contaminants from seawater using $M_{2.5}$ for stage 1, and 2, e) Fouling (FRR, DR, and IFR) % for $M_{2.5}$ with seawater for three cycles. 234

Figure 6. 7. a) Adsorption/desorption cycles for 2g/L NaCl and $MgSO_4$ on the $M_{2.5}$, b) Rejection of 2g/L NaCl and $MgSO_4$ during three cycles by $M_{2.5}$, and c) Water flux of NaCl 2g/L and $MgSO_4$ 2g/L during c cycles by $M_{2.5}$.....236

Figure S4. 1. An illustration of gravity-based filtration.....238

Figure S4. 2. a) Water flux at 2 cm thickness for M_1, $M_{1.5}$, M_2, $M_{2.5}$, and M_3 with, DI, NaCl, and $MgSO_4$, b) rejection at 2 cm thickness for M_1, $M_{1.5}$, M_2, $M_{2.5}$, and M_3 with, NaCl, and $MgSO_4$. 240

Figure S4. 3. The adsorption capacity of Na^+ and Mg^{2+} on the hydrogel. 244

Figure S4. 4 .Viscosity and shear stress of the composite hydrogel membranes. 244

LIST OF TABLES

Table2. 1: Hydrogel classification. 13

Table2. 2: The functional groups for different hydrogels for contaminant removal from water. 24

Table2. 3:Comparison of various hydrogels for contaminant removal. 36

Table3. 1:Wastewater analysis and composition 67

Table3. 2:Adsorption and Desorption summaries of BET analysis 77

Table3. 3:Comparison of hydrogel filtration driven by gravity vs RO. 95

Table 4. 1.PFOA-contaminated water analysis and composition. 112

Table 4. 2: Adsorption and Desorption summaries of BET analysis. 120

Table 4. 3:Comparative analysis of PFAS removal efficiency by various hydrogel 134

Table S2. 1:Kinetic Equations for different models. 145

Table S2. 2:Kinetic parameters of kC-AC/V hydrogel for different models. 147

Table S2. 3: The EDS analysis results for the kC-AC and kC-V hydrogel. 149

Table5. 1:Hydrogel membrane used for wastewater treatment 160

Table5. 2:Properties of Wastewater 163

Table5. 3: Summaries of BET analysis. 167

Table S3. 1:Comparative of Ionic Radii, Hydration radii, and Electronegativity for Ions. 194

Table 6. 1:Properties of seawater used in the filtration experiments 200

Table 6. 2:Composition of hydrogel membranes used seawater desalination 202

Table S4. 1: Shows Analytic instruments were used to characterize $M_{1,}$ $M_{1.5}$, $M_{2,}$ and $M_{2.5}$ 238

Table S4. 2: Summaries of BET analysis 239

Table S4.3: The EDS analysis results for the $M_{2.5}$ hydrogel. 239

Table S4. 4:Weight content of polymer constituents in hydrogel samples 240

Table S4. 5: Density of polymer constituents in hydrogel samples 241

Table S4. 6: Comparative Summary of CNF, GO, and κc-Based Composite Membranes and Hydrogels for Advanced Water Treatment and Desalination. 245

ABSTRACT

Water purification for human consumption, ecological management, agricultural production, and industrial usage is quickly becoming one of the world's top priorities. The current level of water filtration technology must eventually be improved to provide greater access to clean water in adequate quantities. In recent decades, much research has focused on membrane technology for water filtration; however, more sophisticated membrane technologies are emerging as advances in analytical and manufacturing techniques continue.

Membranes enable water flow while blocking contaminants. Benefits include energy efficiency, customization, and reduced operating requirements compared to other methods, crucial for maintaining water quality and environmental preservation.

Hydrogels are three-dimensional networks of polymers that can absorb large amounts of water. similar in structure to living tissues and have physical and chemical properties that allow them to absorb water. Hydrogels can respond to changes in acidity, temperature, light, electrical current, and salt concentration. The balance between hydrophilic and hydrophobic components influences the swelling behavior of their network structures. Hydrogels can be recycled without losing their adsorption capacity, making them economically and environmentally sustainable. Kappa carrageenan, a linear anionic sulfated polysaccharide derived from seaweeds, has a strong gel-forming capacity and is thermoreversible. The unique physicochemical characteristics make it a viable option for water filtration, and its ability to adsorb various toxins and pollutants provides an alternative to traditional water treatment methods.

Kappa carrageenan is applied as a standalone filtration medium or in combination with other nanomaterials, such as vanillin, activated carbon, and cellulose nanofibers, to

improve its characteristic performance. Vanillin has been studied for its potential use in water purification, particularly as a membrane surface modifier to improve antifouling and filtration properties, and exhibits antibacterial properties, adsorption properties for heavy metals and organic pollutants, and biodegradability. Activated carbon is another adsorbent produced from various organic materials. It can remove organic compounds and other impurities from water due to its large surface area and pore structure. Cellulose nanofibers (CNFs) are nanoparticles derived from biodegradable natural sources and have been used in water filtration due to their unique mechanical strength, large surface area, and flexibility. The hydrophilic character of CNFs allows them to retain water effectively, creating an ideal environment for hydrogel-based systems and environmental applications. The potential of integrating kappa carrageenan hydrogel with vanillin, activated carbon, or cellulose nanofibers to provide exceptional filtration media for water purification, organic and heavy metal removal, and ion recovery from seawater and wastewater solutions has been explored here.

Chapter 1: Introduction

1.1 Global water scarcity

Water is a precious and indispensable natural resource, but unfortunately, there has been rampant overexploitation of surface and groundwater in the past decade, which has led to water scarcity in several regions across the globe. Although water envelops 70% of the earth's surface, a mere 3% is freshwater, and a proportion of this freshwater reservoir is trapped in ice, rendering it inaccessible. In addition to the increased demands on freshwater, misuse of water resources, contamination, industrial growth, and climate change are often blamed for water shortage. There are more than one billion individuals around the world who do not have access to potable water, while 41% of the world population lives in areas suffering from water stress (Service, 2006). As a result, this increase in water demand has created many local and international conflicts for the continuation of survival.

To address the water shortage problem, scientists focused on developing sustainable methods for freshwater supply from unconventional sources, such as seawater and wastewater. Arnal et al. 2010 reported that various technologies were created to provide freshwater, including seawater desalination, wastewater treatment, and water reuse (Arnal et al., 2010). Alternative water reuse methods, such as greywater, New water, and wastewater, have reduced freshwater demand (Hoekstra, 2014). Several solutions for addressing water scarcity include increasing water use efficiency, reducing water pollution, adopting sustainable agricultural practices, promoting rainwater harvesting, investing in water infrastructure, raising public awareness, implementing water pricing policies, and developing new water supply technologies, illustrated in Figure 1.1.

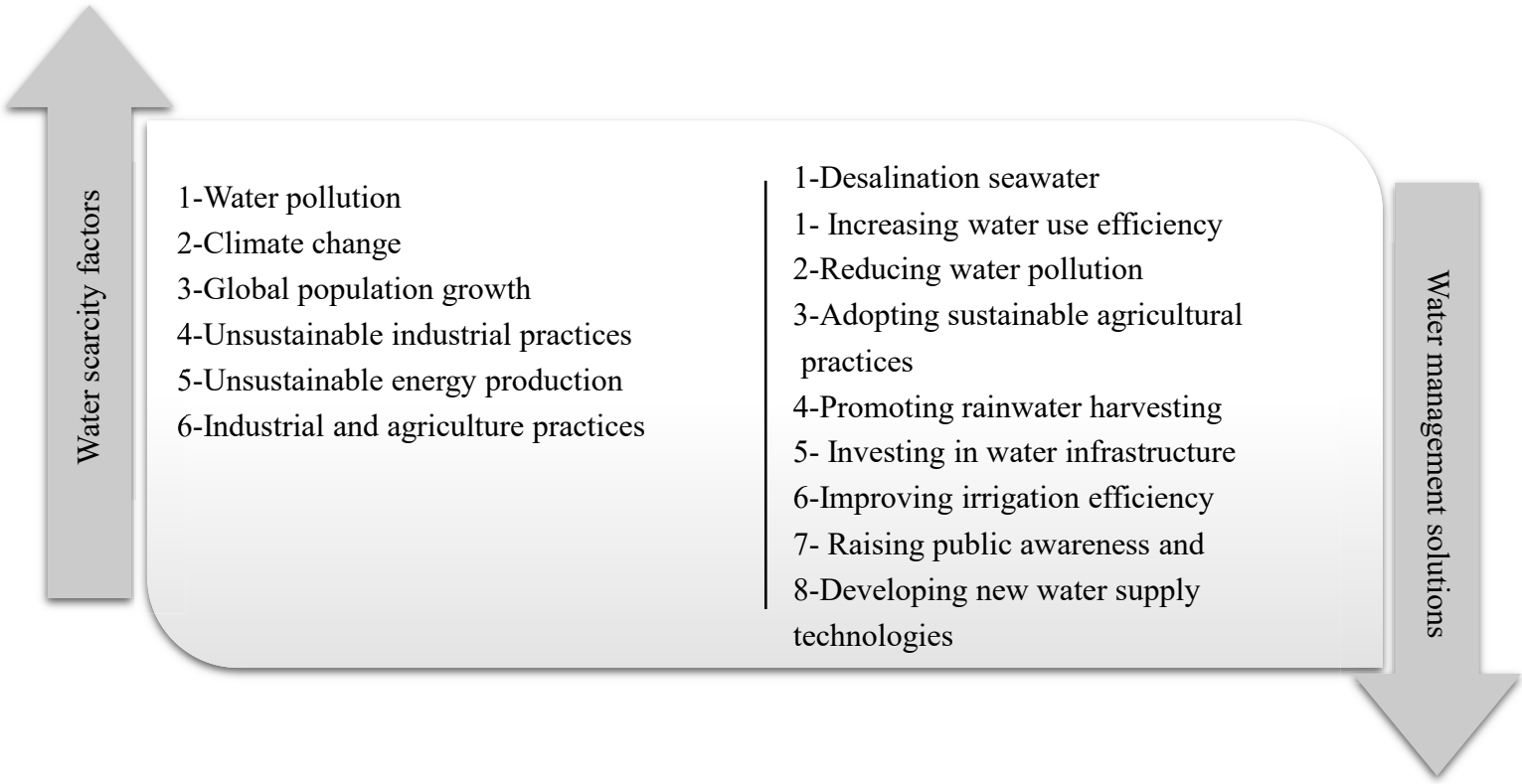


Figure1. 1. Factors contributing to water scarcity and various methods to mitigate it.

1.2 Research significance

Hydrogel membranes and filters were proposed for water purification and wastewater treatment. Most developed and tested HGMs were for oil-water separation to achieve high water flux and selectivity, whilst work on the HGM for desalination/ions separation was scarce. The unique characteristics of good mechanical strength, thermo-reversibility, biodegradability, and excellent adsorption capacity make kappa-Carrageenan (kC) hydrogel novel for water purification and treatment. However, most kC applications in separation technology are a facile method used for dye removal from wastewater by adsorption on kC-based adsorbents. Despite kC being an excellent adsorbent for heavy metals removal from aqueous solution with high performance during wastewater

treatment, adsorption technology experiences shortcomings due to difficulties in separating adsorbates, preparation cost, and requirements for high surface area. Besides, adsorbent technology is a relatively slow treatment process and generates secondary wastewater. This project aims to develop and test super flux kC composite HG filters for purification and wastewater treatment by crosslinking the hydrogel with nanoparticle additives to enhance the water permeability, membrane selectivity, and mechanical strength. The proposed composite hydrogel filter addresses the concerns mentioned above by:

i. Introducing a facile method to prepare a crosslinked kC hydrogel integrated with nanoparticles for improved water flux and pollutant rejection.
ii. Reducing capital and operating costs of water treatment using gravity or low-pressure filtration methods.
iii. Using environmental-friendly materials, biodegradable and recyclable, for sustainable water treatment processes.

1.3 Research aims and objectives

This research aims to develop hydrogel filter media for water and wastewater purification and resource recovery. The developed hydrogel filter is gravity-driven or ultra-low-pressure to reduce operating costs. It will be a cheaper alternative for pressurized membrane technologies, especially when no infrastructures for filtration processes are in place or emergencies. The thesis work objectives are:

1. To investigate the feasibility and performance of kC hydrogel crosslinked with vanillin for water and wastewater treatment. The experimental work will study the impact of feed

pH, concentration, hydrogel thickness, and kC concentration on the performance of the filtration process.

2. To evaluate activated carbon powder and vanillin as a crosslinker with the kC hydrogel for organic-contaminated wastewater treatment. Perfluorooctanoic acid (PFOA)-contaminated wastewater was tested for the hydrogel treatment. The study will also assess the impact of the hydrogel thickness, feed pH, and AC concentration on the water flux and rejection rate.

3. To investigate the feasibility of resource recovery from wastewater by the kC hydrogel. Desorption tests will be conducted for heavy metals recovery from the hydrogel at the end of the filtration process, followed by reverse osmosis treatment of the brine solution for valuable meyal ions recovery. Hydrogel recycling for reuse will also be investigated to reduce the filtration cost.

4. To investigate the feasibility of cellulose nanofibers (CNF) crosslinker to improve the hydrogel membrane's rejection rate and water flux. A parametric study will investigate the impact of CNF concentration, hydrogel thickness, etc., on the water flux and rejection rate for seawater treatment.

1.4 Research questions

1. Will the kC hydrogel be capable of separating a mixture of organic pollutants and dissolved metal ions in an aqueous solution at a high selectivity level?

2. Can a low-pressure kC hydrogel with a high recovery rate be developed to eliminate brine waste production?

3. How readily can sorbed heavy metals be desorbed and recovered?

1.5 The research hypothesis

1. Nanomaterials are crosslinked with kC to control the porosity, functional groups, and hydrophilicity of the composite hydrogel membrane for organic and heavy metals removal from aqueous solution and

2. kC is a thermoreversible hydrogel, i.e. can be melted and hardened by heating and cooling and thermally or chemically treated for metal ions recovery and reused when cooled down.

1.6 Thesis structure

This study focuses on developing and applying novel membrane materials, fabrication techniques to control filtration size, performance testing using analytical tools, and molecular modeling for transport and separation processes. Furthermore, it evaluates the membranes' chemical stability, fouling resistance, and environmental impact. Consequently, the need arose to develop gel-based materials for water filtration, purification, and resource recovery. The dissertation is organized into six chapters.

Chapter 1 highlights the global issue of water scarcity and emphasizes the urgent need for technological advancements in water treatment. It outlines the research hypothesis and significance and defines the study's objectives. Additionally, it provides a comprehensive description of the primary tasks required to fulfill the study's aims and outlines the scope of the research.

Chapter 2 provides a literature review covering recent advancements and fundamental principles of membrane technology.

Chapter 3 explores the utilization of Kappa Carrageenan-Vanillin Composite Hydrogel for landfill leachate wastewater treatment to reduce the treatment cost and brine management problem.

Chapter 4 presents developed an environmentally friendly and cost-effective gravity-driven kappa-carrageenan (kC)-based hydrogel with (Vanillin-activated carbon) for perfluorooctanoic acid (PFOA) removal from synthetic and actual wastewater.

Chapter 5 investigates the effectiveness of a kappa-carrageenan-activated carbon/polyethyleneimine (kC-AC/PEI) hydrogel in removing and recovering metal ions from leachate wastewater.

Chapter 6 investigates the synthesis, optimization, and assessment of kappa-carrageenan-cellulose nanofiber/glutaraldehyde coated with graphene oxide (kC-CNF/GO-GA) hydrogel to improve seawater treatment and divalent and monovalent ions.

Chapter 7 presents the conclusions, recommendations, and future work.

Chapter 2: Literature review

A Review of Hydrogel Application in Wastewater Purification

Alsaka, L., Alsaka, L., Altaee, A., Zaidi, S. J., Zhou, J., & Kazwini, T. (2025). A Review of Hydrogel Application in Wastewater Purification. *Separations*, *12*(2), 51.

Author contributions statement:

Lilyan Alsaka: Conceptualization, methodology, validation, formal analysis, investigation, data curation, original draft preparation, writing review and editing, visualization. Lina Alsaka: Conceptualization, methodology, validation, formal analysis, original draft preparation. Ali Altaee: Conceptualization, validation, investigation, data curation, original draft preparation, writing review and editing, visualization, supervision, project administration, funding acquisition. Syed Javaid Zaidi: methodology, validation, investigation, funding acquisition. John Zhou: investigation, data curation, writing review and editing, supervision. Tayma Kazwini: Conceptualization, methodology, investigation.

Abstract

This chapter provides a literature review that thoroughly examines the use of hydrogels in wastewater treatment. It encompasses their categorization and separation procedures, including size exclusion, adsorption, electrostatic interactions, and non-sieving processes. Furthermore, it examines how functional groups improve the efficiency of pollutant removal. The review examines hydrogel composites and their filtering processes, measuring their adsorption efficacy and evaluating hydrogels' benefits and limits, especially regarding regeneration capabilities. It explores hydration processes in hydrogels, emphasizing the fundamental mechanisms and measuring methods involved.

2.1 Introduction

Two million metric tons of pollutants from sewage, industry, and agriculture are released into the water, threatening public health and resulting in 1.4 million fatalities (Bolisetty et al., 2019). Efficient methodologies are necessary for converting seawater and wastewater into potable water via water purification. The specific procedures used depend on the source of water and its intended application (Ray & Iroegbu, 2021). Many technologies have been used to desalinate seawater and wastewater to provide fresh water. Conventional biological processes are an example of wastewater treatment and reuse in farming activities instead of rivers and groundwaters. Several countries use tertiary treated wastewater for irrigation, compensating for the shortage of freshwater resources. Biological and membrane bioreactors (MBR) technologies for wastewater treatment are widely used for domestic wastewater treatment to supply a source of clean water for irrigation (Acikgoz et al., 2016; Prajapati et al., 2021). Hyperfiltration technology desalinates seawater for various purposes, such as irrigation, industrial use, and drinking water. Membranes with different molecular weight cut-offs are developed for various applications. Nanofiltration (NF) membranes, derived from ultrafiltration (UF), are designed to separate divalent ions and partially remove monovalent ions, showing less than 20% rejection rate for the latter (Mulyanti & Susanto, 2018; Shon et al., 2013). NF membranes are used for water softening, industrial wastewater treatment, and desalinating low-salinity water. Reverse osmosis (RO) membranes can selectively eliminate solutes, making them energy-efficient and adaptable (Anis et al., 2019). Developed in the 1970s, RO membranes for seawater desalination achieved a 99% rejection rate for monovalent ions like NaCl, replacing thermal processes as the dominant technology (Macedonio et al., 2012). Despite their advantages, NF and RO membranes

face challenges such as intensive pretreatment, fouling, and high energy and cost requirements.

Seawater desalination often needs over 60 bars for a TDS above 40 g/L (Jiang et al., 2017; Qasim et al., 2019). Chemical purification techniques are slow and generate large quantities of wastewater, while adsorption methods face challenges in finding ideal adsorbents and high regeneration costs. New, cost-effective water purification methods are needed, especially in emergencies (Mishra et al., 2017; Parsons, 2004). In recent years, the research focus has shifted to designing and developing new polymeric adsorption matrixes that provide economical and efficient treatment technology. In this view, hydrogel materials provide a novel technology that enables cost-effective, reusable, and highly effective methods for purifying and decontaminating water. Hydrogel materials consist of an interconnected three-dimensional polymer network. These materials possess a high surface area, which enables them to adsorb a wide range of pollutants from water, such as heavy metals, organic contaminants, and colors, with significant selectivity. In addition, hydrogel materials have a rapid regenerative capacity, which reduces the amount of waste produced during the purifying process, making them a possible substitute for conventional purification methods and significantly reducing waste production(Lee et al., 2016). Hydrogels have received considerable interest because they can be used in many different sectors, such as water treatment, agriculture, and biomedicine. Chitosan-based hydrogels successfully remove pollutants like heavy metals and organic contaminants from water because they have a high capacity for adsorption (Chelu et al., 2023). In agriculture, hydrogels serve as soil conditioners, augmenting water retention and nutrient accessibility and promoting crop productivity and resilience in dry areas (Patra et al., 2022). In the biomedical domain, hydrogels are

used in drug delivery systems, wound dressings, and tissue engineering owing to their biocompatibility and capacity to replicate natural tissue characteristics (Ho et al., 2022). Hydrogel technology remains challenging to use industrially. Scalability, cost-effectiveness, and environmental impact must be considered. Some hydrogels need sophisticated, non-scalable production techniques (Ansar et al., 2022). Furthermore, a comprehensive assessment of the environmental consequences of hydrogel degrading products is necessary to guarantee sustainability. The limited mechanical strength and possible toxicity of some hydrogel components may also prevent them from being widely used in industry. Despite the improvements in this field, several gaps still exist; firstly, understanding how hydrogel matrices interact with various contaminants is essential for optimizing their design and functionality. Second, although hydrogels have demonstrated potential in laboratory settings, their production and application for large-scale water treatment remain challenging. Key issues that need to be addressed include mechanical stability, regeneration efficiency, and long-term performance for effective practical implementation. Third, it is crucial to thoroughly evaluate the environmental impact of hydrogel synthesis, usage, and disposal to ensure sustainability. Filling these research gaps is vital for advancing hydrogel-based technologies in water purification. This review provides insight into the hydrogel materials used in wastewater treatment, emphasizing the mechanisms involved in removing organic and inorganic pollutants from contaminated solutions and the advantages of hydrogels as an alternative technology for wastewater treatment.

2.2 Hydrogel classification

Hydrogels may be categorized in several different ways depending on the processes used in their production. Homopolymeric hydrogels are characterized by a crosslinked skeletal structure produced from a specific monomer or an essential structural component. Table 1 categorizes hydrogels based on various criteria, including polymer composition, charge, crosslinking method, crystallinity, source, and application, highlighting their diverse structures and functionalities. The polymer and the manner of crosslinking impact this structure. Copolymeric hydrogels are made up of two or more monomer species, with at least one of them being hydrophilic, that are organized in a variety of configurations inside the framework of the hydrogel (Cai et al., 2023). Networks that are formed of two distinct natural or synthetic polymers that have been crosslinked together are known as multipolymeric hydrogels. In addition, hydrogels may be categorized according to their charges (nonionic, ionic, amphoteric electrolyte, and zwitterionic), the procedures used to crosslink them (chemical or physical), and their crystalline state (amorphous, semicrystalline, or crystalline) (Zhao et al., 2023). The polymer scaffold may be made from natural, synthetic, or hybrid hydrogels. Hydrogels are formed using natural biopolymers such as gelatine and collagen and polysaccharides like starch, cellulose, chitosan, etc. The use of pHEMA, polyvinyl alcohol, poly(N-isopropyl acrylamide), polyethylene glycol, and polyacrylamide in the production of synthetic hydrogels results in products that exhibit exceptional water absorption and retention capabilities, as well as extended shelf life and enhanced gel strength. Hydrogels derived from biological sources are more durable, porous, biocompatible, and biodegradable (Kalendova et al., 2021).

Technology advancements in materials science have made it possible to manufacture composite hydrogel materials, creating novel hybrid structures with distinctive physico-

mechanical properties. Physical and chemical methods synthesize and modify these systems, including crosslinking, impregnation, grafting, interpenetration, incorporation, mixing, and imprinting. Depending on their stability, water absorption, and strength, bio-based hydrogels and their modified forms are used in environmental, biomedical, and agricultural applications.

The hydrogel's properties are influenced by the kind of polymer used and the presence of hydrophilic groups (–OH, –COOH, $–CONH_2$, and $-SO_3H$) attached to the polymer chains. The presence of hydrophilic moieties, including alcohol, amides, and carboxylic acids, among other types of molecules, enhances the hydrogel's stiffness and capacity to absorb water (Bashir et al., 2020; Bhat et al., 2025). Furthermore, the presence of functional groups affects the specific crosslinking approach required to create hydrogel from scratch. Hydrogels, which are elastic and soft, have limited applications due to their mechanical weakness. Numerous functional groups and the ease with which they may be crosslinked contribute to the mechanical solid strength of these materials. Hydrogel water absorption depends on polymer and network density. Most polymers absorb more water than their bulk. Hydrogels are available in various sizes and forms, such as slabs, membranes, nanogels, beads, microgels, cryogels, and aerogels (Kuddushi et al., 2019).

Three variables are crucial for successfully manufacturing crosslinked hydrogels: (I) The liquid absorption capacity of the hydrogel network relies on the volume at which the polymer swells. (II) The median molecular weight of the crosslinks determines the crosslinking of the hydrogel. (III) The network mesh's size influences the hydrogel's mechanical strength, degradability, and diffusivity.

Table2. 1: Hydrogel classification.

Classification Criteria	**Types of Hydrogels**	**Description**	**References**
Based on polymer composition	Homopolymeric hydrogels	Crosslinked skeletal networks based on a monomer or key structural component.	(Singhal & Gupta, 2016; Ullah et al., 2015)
	Copolymeric hydrogels	The hydrogel framework consists of many monomer species, at least one of which is hydrophilic and organized in different configurations.	
	Multipolymeric hydrogels	Crosslinked networks consist of two distinct natural or synthetic polymers that are interconnected.	
Based on charge	Nonionic	Hydrogels without any ionic charges.	(Erathodiyil et al., 2020; Mehta et al., 2023; Sargeant et al., 2012)
	Ionic	Hydrogels with ionic charges.	
	Amphoteric electrolyte	Hydrogels contain both positive and negative charges.	

	Zwitterionic	Hydrogels with both positive and negative charges but are neutral overall.	
Based on crosslinking method	Chemically crosslinked hydrogels	Hydrogels are crosslinked using chemical methods.	(Maitra & Shukla, 2014)
	Physically crosslinked hydrogels	Hydrogels crosslinked using physical methods.	
Based on crystallinity	Amorphous hydrogels	Hydrogels without a crystalline structure.	(Bustamante-Torres et al., 2021; Ullah et al., 2015)
	Semicrystalline hydrogels	Hydrogels with partial crystalline structure.	
	Crystalline hydrogels	Hydrogels with a crystalline structure.	
Based on source	Natural hydrogels	Made from natural biopolymers such as proteins (gelatin, collagen) and polysaccharides (starch, cellulose, chitosan).	(Khansari et al., 2017; Ullah et al., 2015)
	Synthetic hydrogels	Made from synthetic polymer compounds such as pHEMA, polyvinyl alcohol, poly(N-isopropyl	

		acrylamide), polyethylene glycol, polyacrylamide, and their derivatives.	
	Hybrid hydrogels	Made from a combination of natural and synthetic polymers.	
Based on application	Environmental hydrogels	Sorbents and flocculants that purify wastewater and sludge.	(Liu et al., 2022; Rabajczyk et al., 2024)
	Biomedical hydrogels	Biomedical applications include medication delivery systems, tissue engineering, and contact lenses.	
	Agricultural hydrogels	Used to release water reservoirs and agrochemicals.	

2.3 Hydrogel separation mechanisms

The main methods of hydrogel separation rely on their distinct three-dimensional, crosslinked structures, which enable selective absorption and filtering. Size exclusion is a fundamental process in which the pore size of a hydrogel controls the molecules that can flow through it, thereby capturing bigger molecules (Ahmed, 2015). Charge interactions are also significant since hydrogels that are ionic or zwitterionic may either attract or repel charged particles, hence increasing separation efficiency (Pooresmaeil & Namazi, 2020). Moreover, due to their hydrophilic properties, the water-absorbing capability of hydrogels facilitates the separation of water from impurities. Hydrogels are essential in water purification and medicine administration (Caló & Khutoryanskiy, 2015).

2.3.1. Size exclusion

Size exclusion is a fundamental separation approach based on the idea that particles cannot flow through holes that are smaller than their diameter (Figure 2.1a). It is rejected when the particles' hydrated ionic diameters exceed the pore size (R. Zhang et al., 2020). Many studies have been performed on the influence of size exclusion on the separation process, particularly emphasizing various molecular features such as size, shape, and molecular weight (MW). Yoon and Lueptow (2005) and Van der Bruggen and Vandecasteele (2002) have confirmed the vital necessity of knowing these molecular features to increase the predictability and effectiveness of size exclusion approaches (Van der Bruggen & Vandecasteele, 2002; Yoon & Lueptow, 2005). MW has been used as an essential parameter for assessing rejection, especially for chemicals that are not charged; nonetheless, its capacity to provide comprehensive insights is restricted. In particular,

molecular weight does not consider molecule shape, significantly affecting how chemicals interact with membrane pores (Chang et al., 2012). Recent research has reached for a more thorough analysis of molecular size features other than MW to satisfy this problem. For example, Miron et al. emphasized the need to precisely describe the size properties of molecules to have a more accurate knowledge of the separation process (Miron et al., 2019). This process enhances the design and use of membrane technologies for targeted solute separation in various industries, from water purification to biochemical processing, and helps explain the dynamics of size exclusion.

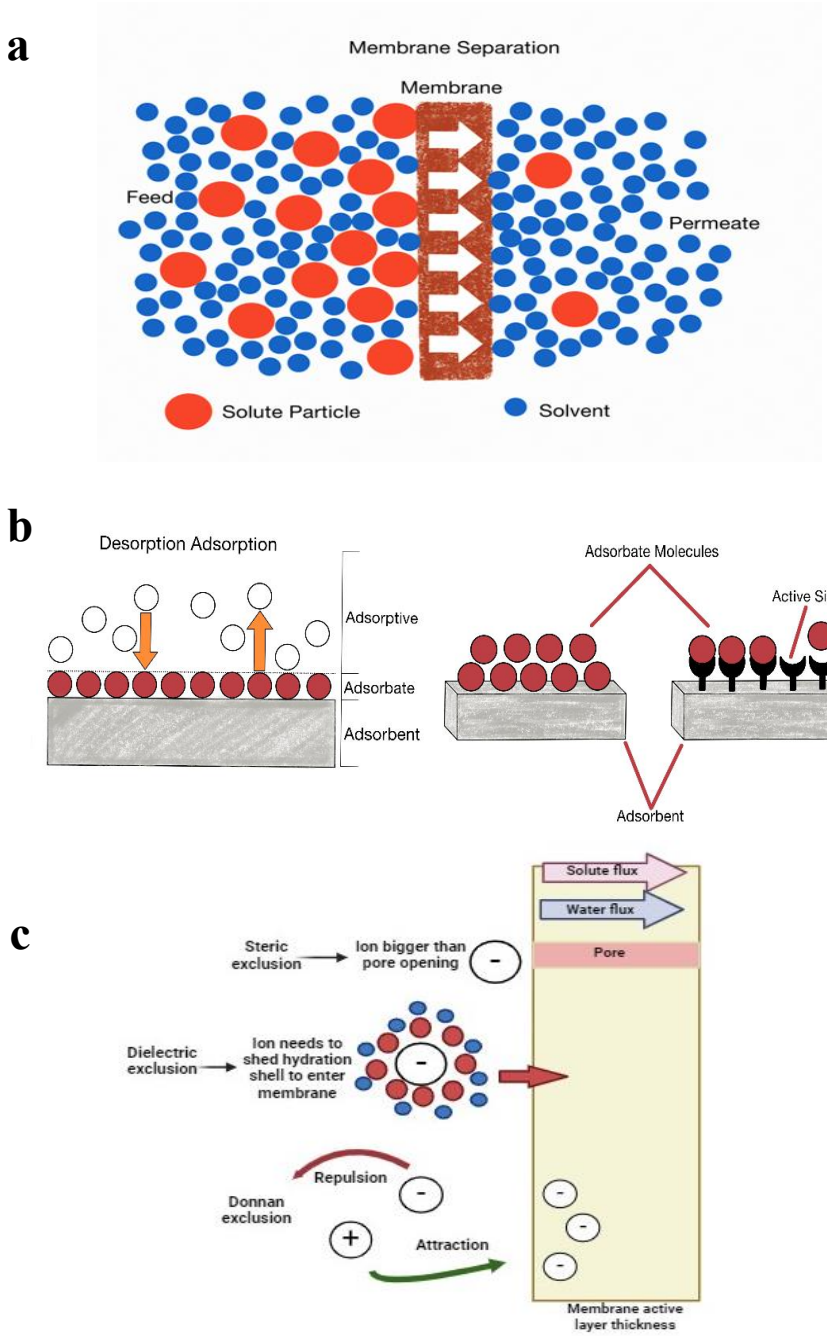


Figure2. 1. (a) Molecular segregation through a semipermeable membrane, (b) schematic representation of the adsorption process, and (c) schematic representation of solute exclusion mechanisms (Roy et al., 2017).

2.3.2. Adsorption

Adsorption is vital in hydrological membrane-based techniques, serving as a critical separation mechanism. Some aspects in the liquid phase, such as organic compounds, heavy metals, or impurities, attach to the membrane's surface through these methods. This method improves filtration and purification efficiency by selectively eliminating undesired substances and enhancing permeate quality (Figure 2.1b). This process is driven by attractive forces between the molecules, including chemical affinity, hydrogen bonding, electrostatic interactions, and Van der Waals forces (Huber et al., 2019). The effectiveness of adsorption is influenced by the characteristics of the adsorbent, such as hydrophobicity, the presence of functional groups, and density, as well as the properties of the adsorbate, including solubility and molecular size. The competitive dynamics between inorganic and organic substances at active adsorptive sites can enhance or hinder adsorption. Environmental conditions like solution pH, temperature, and other factors critically impact adsorption performance, modifying how substances interact with the membrane (de Andrade et al., 2018; Grassi et al., 2012). The performance of adsorbents is also affected by several operational factors, including the initial ion concentration, temperature, pH, adsorbent dosage, contact time, stirring speed, and ionic strength (Ambashta & Sillanpää, 2010). Hydrophobic interactions further influence the adsorption of solute molecules onto membranes, playing a pivotal role in the selective rejection of specific micropollutants. Adsorption offers a highly efficient and cost-effective approach to pollutant removal from wastewater. At the same time, membrane filtration, although more costly and requiring a smaller operational area, is particularly effective in removing heavy metal ions (Ahmed & Ahmaruzzaman, 2016). Materials like activated carbon are favored in adsorption processes for their extensive surface area, effectively eliminating

micropollutants and adsorbing microbes and organic matter from contaminated waters. Similarly, silica gel, with its vast network of voids and a surface area of about 800 m^2/g, shows a remarkable capacity for moisture absorption, especially at 40 °C, underscoring its utility in various adsorptive applications.

2.3.3. Electrostatic interactions

The electrostatic interactions during the use of hydrogel for filtration are crucial and affect the degree to which various materials are separated (Mulder, 2012). A porous hydrogel functions as a physical barrier within a particular filtration system, allowing some molecules or ions to flow through while preventing others from doing so. The charge on the hydrogel's surface and the particles in the feed solution are essential aspects of this process. These charges can either attract or repel particles, substantially impacting the selectivity and efficiency of the separated particles. Electrostatic interactions may be classified as either electrostatic attraction or electrostatic repulsion. When the hydrogel and the particles have the same charge, they repel each other. This repulsion prevents the particles from approaching the hydrogel surface, hindering the particles from getting close to the surface. Alternatively, attraction can facilitate the separation of certain species when the charges are of opposite polarities, promoting adsorption or deposition onto the hydrogel. The efficiency of electrostatic interaction is determined by several factors, including the magnitude and distribution of charges on the hydrogel surface, the charge density of the particles or solutes, the ionic strength of the solution, functional groups in the hydrogel, and pH affecting the hydrogel and contaminants' ionization state (Pendergast & Hoek, 2011). Many theoretical models have been developed to quantify these interactions. Additionally, experimental methods such as zeta potential

measurements have been used to obtain information on the surface charge (Hilal et al., 2004; Verliefde et al., 2007).

2.3.4. Non-sieving process

The diffusion of ions in two solutions separated by a semipermeable barrier is known as Donnan exclusion. The membrane restricts ionic transport selectively. The electrostatic repulsion between ionic compounds and the fixed charges of the membrane matrix causes Donnan exclusion (Yaroshchuk, 1998). Figure 2.1c shows the Donnan exclusion and dielectric exclusion processes. The membranes reject the negative charges while allowing positive charges to pass through them; thus, some of the dissolved substances are transported, and the ions are trapped in the pores of the membranes. Substances are moved by electromigration, diffusion, and convection depending on the membrane potential gradient (Roy et al., 2017). According to Donnan's exclusion principle, ions with significant charges are rejected more than those with lower charges; hence, it is more effective with divalent ions (Y. Liu et al., 2018).

Dielectric exclusion occurs because of ion interactions with bound electric charges at interfaces between dielectrically distinct media, such as a membrane structure and a medium. The well-known forces operating on an electric charge near an infinite planar interface are caused by interactions with polarized interfaces. The reaction with a polarized interface is comparable to an imaginary charge on the opposite side of the interface at the same distance from it as the real charge (Bowen & Welfoot, 2002; Geng et al., 2021; Ritt et al., 2020).

Figure 2.2 shows techniques for removing pollutants from a water system using hydrogel; these techniques enable separation based on various factors such as the size, chemical composition, hydrophilicity, and charge of the contaminants.

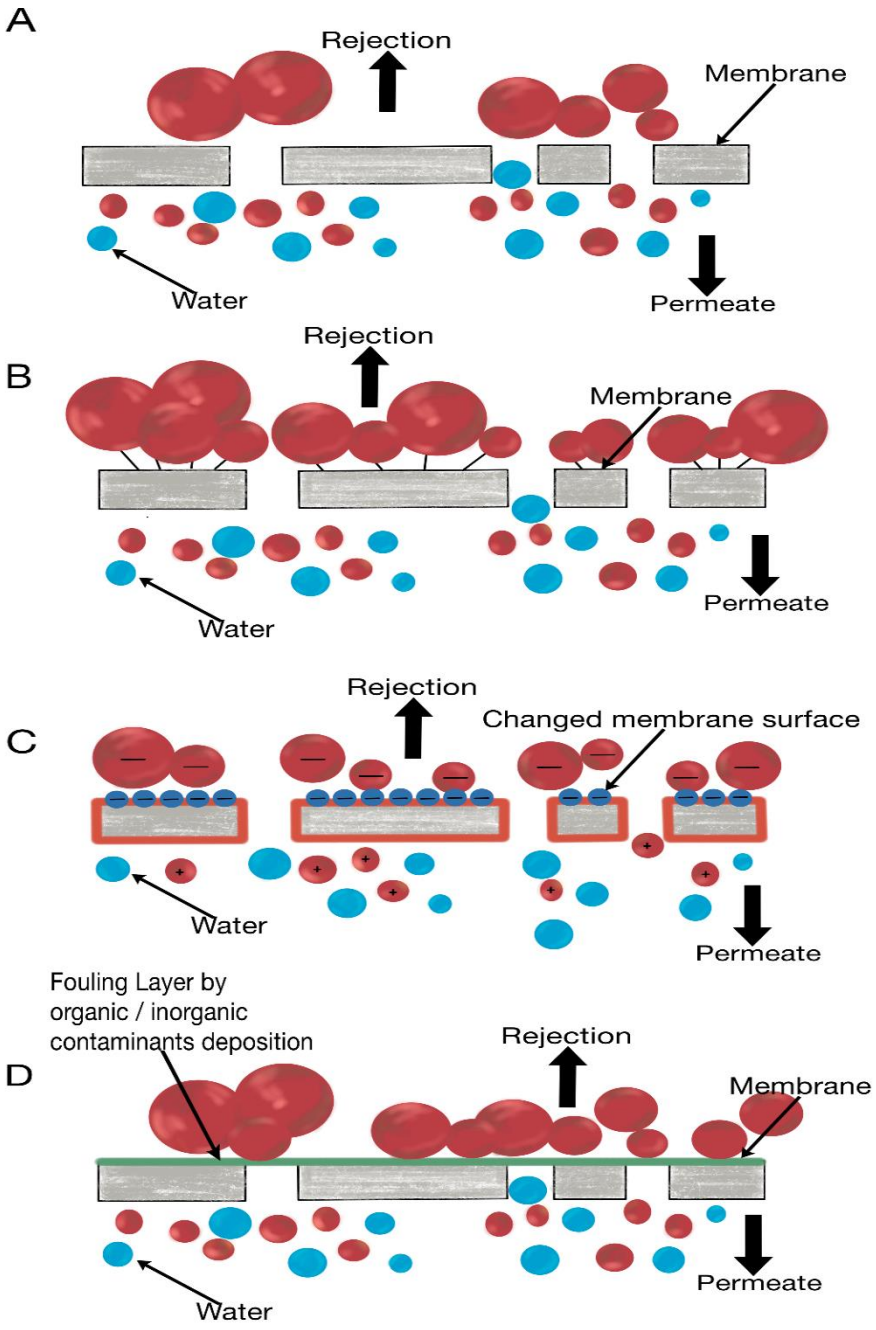


Figure2.2.Hydrogel filtration removal mechanisms: (A) size exclusion, (B) hydrophobicity, (C) electrostatic interaction, and (D) adsorption.

2.4 Functional groups in hydrogels

Based on the crosslinking technique, hydrogen is physically entangled with transitory bonds or chemically linked with excellent stability. Functional groups such as hydroxyl,

carboxyl, and amine provide essential qualities such as hydrophilicity and reactive potential, allowing their use in different fields, including medication delivery and water purification (Caló & Khutoryanskiy, 2015). According to, hydrogels respond to motivating such as via pH and temperature. Therefore, they can be used to develop intelligent materials for sophisticated applications (Hoare & Kohane, 2008). Hydrogels are increasingly used because they selectively remove contaminants via functionalized networks. Preparing hydrogels for this purpose often involves integrating specific functional groups that improve their interaction with pollutants. For instance, hydrogels containing carboxyl groups (–COOH) are effective in binding heavy metal ions such as lead and cadmium, leveraging the ionic interactions between the negative charge of the carboxyl and the positive charge of the metal ions (Perumal et al., 2021). In addition, using amine groups ($–NH_2$) in hydrogels can effectively remove anionic dyes and other negatively charged contaminants from water through electrostatic attraction (Dalalibera et al., 2020; Ferfera-Harrar et al., 2022). It was discovered that composite hydrogels, including natural and synthetic polymers, can improve their structural and functional properties (Table 2.2). For example, a chitosan–polyacrylamide composite hydrogel has shown remarkable effectiveness in removing dyes and heavy metals from aqueous solutions. This hydrogel combines the biocompatibility and cationic character of chitosan with the strength of polyacrylamide (Wang et al., 2020).

Table2. 2: The functional groups for different hydrogels for contaminant removal from water.

Hydrogel Type	**Functional Group(s)**	**Contaminants Removed**	**Example of Application**	**Reference**
Carboxymethyl cellulose hydrogel Polyacrylic acid hydrogel	Carboxyl(-COOH)	Heavy metals (Cd, Pb, Cu, and phosphates)	Removal of heavy metals from wastewater	(Perumal et al., 2021)
Amine-functionalized hydrogel	Amine (-NH_2)	Anionic dyes, heavy metals	Electrostatic removal of negatively charged contaminants	(Dalalibera et al., 2020; Ferfera-Harrar et al., 2022)
Chitosan–polyacrylamide hydrogel	Amine (-NH_2), Amide (-$CONH_2$)	Dyes, heavy metals	Dual functionality for broad-spectrum contaminant removal	(Wang et al., 2020)
Kappa carrageenan hydrogel	Sulfate (-OSO_3)	Heavy metals and organic pollutants	Effective in binding with divalent metal ions	(Kalaiselvi et al., 2023)

			and various organics	
Poly(N-isopropyl acrylamide) hydrogel	Amide (-$CONH_2$)	Temperature-sensitive pollutants	Temperature-responsive contaminant capture	(Saito et al., 2006)
Iron oxide nanocomposite hydrogel	Magnetic groups	Arsenic, chromium	Magnetic separation of heavy metals from drinking water	(Zhang & Li, 2017)
Cyclodextrin hydrogel	Hydroxyl (-OH)	Organic pollutants, pesticides	Encapsulation and removal of organic chemicals	(Cova et al., 2018)

2.5 Hydrogel composites

Polymerization is a simple procedure involving the utilization of monomers and initiators carried out at high temperatures, and it produces very dense hydrogels. Upon contact with water, these hydrogels become more pliable and are stabilized by surfactants. Ionic or neutral monomers are used in solution polymerization, and UV or redox initiators are used to commence the process. Following the polymerization process, the solvents are extracted by immersing the hydrogel in water, which results in phase separation and

purification. Hydrogels are characterized by significant swelling, hydrophilicity, and coordination interactions with heavy metals. FTIR, XPS, SEM, optical microscopy, and compressive strength tests are some methods used for characterization (Chen et al., 2020). Hydrogel composites are becoming more critical in environmental applications and water purification. These composites combine hydrogels with biodegradable, inexpensive materials such as starch, cellulose, lignin, and charcoal, successfully addressing the problems associated with the cost and environmental impact of artificial hydrogels (Sanyang et al., 2016; Sun YaJie et al., 2016). This integration enhances the composite's adsorptive capacity, augments its surface properties, and introduces essential functional groups such as carboxylic, amino, and hydroxyl groups, increasing hydrophilicity and improving pollutant removal efficiency. Integrating biochar with hydrogels, for instance, substantially elevates the composite's swelling capacity and contaminant adsorption effectiveness. Hydrophilic functional groups in the hydrogel–biochar composite allow for more effective capture and removal of waterborne pollutants than either material alone (Karakoyun et al., 2011; Sanyang et al., 2016). Research suggests that these composites may significantly enhance the rate at which pollutants like arsenic are absorbed, showing a higher sorption capacity than more straightforward biochar settings. Moreover, these composites can be tailored according to individual water treatment needs by including different essential ingredients and functional groups. For instance, adding biochar high in silica improves the strength of hydrogel composites and optimizes their ability to adsorb substances due to silica's involvement in the composite synthesis (Sanyang et al., 2016). Researchers have developed a dual-network hydrogel composed of PEDOT:PSS and PAAm, which effectively produces solar steam for desalination and sewage purification. This hydrogel demonstrates a high solar absorption rate of approximately 99.8% and a

steam production rate of 2.15 kg $m^{-2} \cdot h^{-1}$, providing a sustainable solution for water purification (Q. Zhao, Z. Wu, et al., 2022).

Additionally, a Ti_4O_7 membrane, modified with a hydrophobic surface and a thermal insulation layer, attained a high evaporation rate of 7.51 $kg \cdot m^{-2} \cdot h^{-1}$, producing water that met WHO drinkable water requirements (Qiu et al., 2022). A Ti_4O_7-PVA nanocomposite hydrogel has also been designed to generate solar steam efficiently, achieving an evaporation rate of 4.45 $kg \cdot m^{-2} \cdot h^{-1}$ under one-sun irradiation and demonstrating an energy efficiency of 90.69%. This hydrogel effectively desalinated and purified water samples containing high salinity, strong acids or bases, heavy metals, and organic colors (Xu et al., 2024). Moreover, researchers blended and crosslinked PEDOT:PSS nanofibrils with poly(vinyl alcohol), resulting in a mechanically resilient nanocomposite hydrogel. In a 60-day seawater evaporation test, this hydrogel maintained an average energy efficiency of approximately 93.3%. Its scalable manufacturing process enables these solar water evaporators to desalinate saltwater and purify wastewater to meet WHO drinking standards (Q. Zhao, J. Liu, et al., 2022). Researchers are making significant strides in water purification technologies. By incorporating TiO_2 nanoparticles and single-walled carbon nanotubes into a polyacrylamide matrix, they developed a cost-effective hydrogel composite with 88.40% porosity, significantly enhancing photothermal and photocatalytic properties for solar-driven purification (Xu et al., 2025). Kaolin/CNTs/PAM hydrogel (KCAH), a clay-based hydrogel evaporator, exhibits over 99% desalination efficiency and efficient photothermal evaporation, adsorbing heavy metal ions at different salinities (Li et al., 2025). The co-gelation of reduced graphene oxide (rGO), polyvinyl alcohol (PVA), and poly(acrylamide oxime) has produced an integrated solar-driven hydrogel evaporator (GPPH) with 1289 mg/g uranium adsorption

capacity in simulated seawater with 64 ppm uranium (Wang et al., 2025). The development of hydrogel composites represents a notable improvement in water treatment technology, providing an efficient, cost-effective, and environmentally friendly solution to address water contaminants.

2.6 Hydrogel filtration mechanisms

Hydrogels play an essential part in the removal of contaminants via a variety of methods that are controlled by the characteristics of the hydrogel as well as the parameters of the environment, such as the pH and the ionic strength (Benguella & Benaissa, 2002; Zhou et al., 2005), and ion exchange (Figure 2.3). These mechanisms are brought about by functional groups within the hydrogel composition. According to Zhou et al., the adsorption capabilities of hydrogels are mainly influenced by the physical and chemical characteristics of the pollutants as well as the circumstances of the microenvironment that exist in the surrounding area (Zhou et al., 2005). For example, using FTIR analysis, Zhou et al. demonstrated functional groups' role in adsorption. They found that shifts in the bands of the hydroxyl and acetyl groups indicated changes in chemical interactions that occurred after the binding of contaminants. As validated by this research, complexation promoted by electron donation from nitrogen atoms inside the hydrogel structure was shown to be the predominant mechanism for the adsorption of lead ions into the hydrogel structure.

As a consequence, the molecular weight of the hydrogel gradually increased (Zhou et al., 2005). X-ray diffraction (XRD) examination showed changes in the hydrogel's crystalline structure after the contaminants' adsorption, which indicates interactions with contaminants affect the crystalline phases of the hydrogel (Ahmed, 2015). The XRD patterns demonstrated a decrease in crystallinity, which indicates that the amorphous

regions of the hydrogel did play a substantial part in the adsorption process, which was accomplished by the hydrolysis product precipitation and complexation processes. The pH rise detected throughout the adsorption process supported these results, similar to the results on chitin cadmium absorption(Zhou et al., 2005). Moreover, cationic hydrogels have a relatively straightforward mechanism in terms of how they incorporate ionic contaminants into their structure. According to Barakat and Sahiner (Benguella & Benaissa, 2002), these hydrogels can absorb water in aqueous conditions, expanding the network. Because of this, negatively charged metal ions, such as arsenate, can diffuse into the network and participate in electrostatic interactions, making it feasible for other ions to do the same. The pH significantly influences the solution, which in turn has a significant effect on the electrostatic interactions (Barakat & Sahiner, 2008).

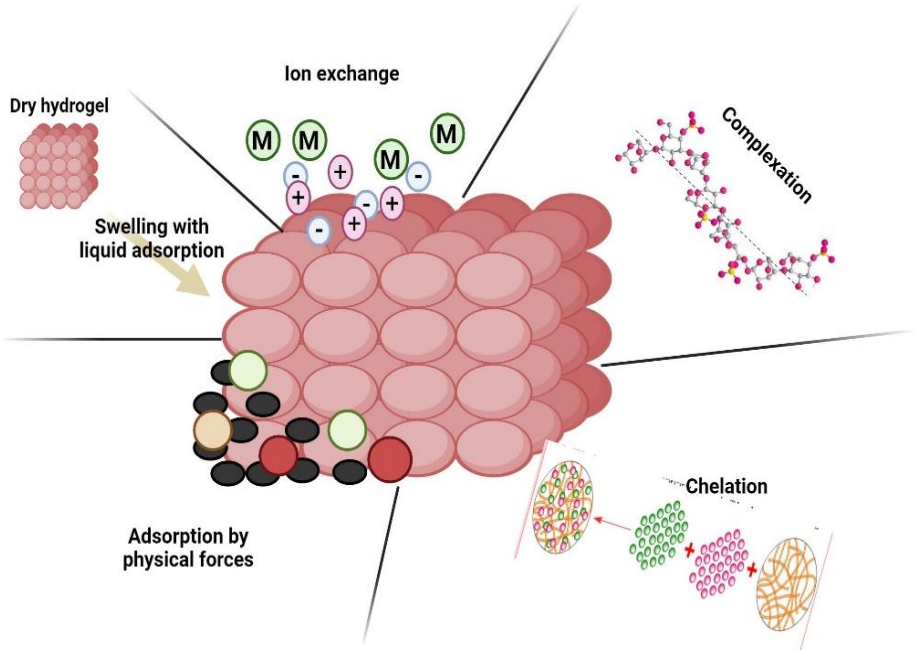


Figure 2. 3. Mechanisms involved in contaminant removal with hydrogels

2.7 Hydrogel adsorption effectiveness

Hydrogels are three-dimensional networks that retain water. Polar or nonpolar monomers make hydrophilic or hydrophobic hydrogels, although application-specific hydrophobic hydrogels are made. Monomers, initiators, and crosslinkers are typical. Polar monomers are polymerized in situ to make hydrophilic hydrogels. Hydrogels are made by bulk, emulsion, and solution polymerization. In removing pollutants from water, the adsorption effectiveness of hydrogels is affected by several parameters, such as the hydrogel's surface morphology, the functional group involved, and ambient circumstances, such as pH and the presence of other ions (Tang et al., 2011). Hydrogels have a network structure, making their surface area much more significant than their monomers or other adsorbents. This characteristic is one of the most critical factors in increasing the adsorption capacity of hydrogels. This surface area may be considerably improved using techniques such as freeze-drying during hydrogel manufacturing. These techniques include creating a highly porous structure with a broad pore size distribution, ultimately improving the hydrogel's total adsorption capacity (Sun et al., 2009). Adsorption efficiency is also significantly impacted by environmental conditions, which play a vital effect. Hydrogels' efficiency in removing contaminants may be diminished by the presence of inorganic ions or natural organic materials that compete with them. Studies conducted by Tang et al. indicated that when the sulfate concentration in groundwater increased, the Cr(VI) adsorption capacity decreased because of the decrease in the number of competitive ion exchange sites. Furthermore, pH variations may substantially impact the performance of hydrogels (Tang et al., 2011). These changes affect the speciation of pollutants such as Cr (VI) and the surface charge of the hydrogel, which in turn modify the properties of adsorption (Barakat & Sahiner, 2008; Gao et al., 2013).

2.8 Pros and cons of hydrogels and regeneration

Modifying hydrogels' physical and chemical properties also increases their adsorption capacities. Ali et al. and Sanyang et al. discovered that adjusting parameters impacted the hydrogel's swelling capacity and mechanical strength. These factors included the monomer content and the crosslinking density. These characteristics are necessary for efficient adsorption and stability during several usage cycles (Ali et al., 2003; Sanyang et al., 2016). Compared to other adsorbents, hydrogels have several significant benefits when removing contaminants. Even though some adsorbents may have more excellent adsorption capabilities, hydrogels are especially advantageous since they are simple to separate from water, which contrasts with other materials, such as activated carbon and biochar, that are difficult to recover after treatment. In addition, hydrogels may be used in a simplified purification method that only requires one step. According to Liang et al., alternative adsorbents, on the other hand, often need intricate pH modifications to function well, which ultimately limits their use in natural water circumstances (Liang et al., 2011). Because of this pH dependence, the application of many adsorbents is restricted. One example is carbon nanofiber membranes, which only work best within particular pH ranges for certain pollutants, such as Cr (VI) and Pb. Hydrogels, however, are effective throughout a more comprehensive pH range, increasing their applicability in various situations. They are economically more viable, especially in low-income regions, due to the lower production costs than those of synthetic adsorbents. Hydrogels can be regenerated and reused multiple times, offering long-term sustainability and cost-effectiveness that is not achievable with most low-cost adsorbents when used independently.

One of the distinguishing characteristics of hydrogels is their capacity to be regenerated and reused, making them an environmentally friendly choice for removing contaminants. Desorbing the adsorbed pollutants is often a part of the regeneration process, which can be accomplished by either pH modifications or magnetic separations (Liu et al., 2012). More specifically, it has been shown that successful desorption may be accomplished using both strong and weak acids, influencing the hydrogel's ability for desorption and its lifetime (Ali et al., 2003; Ozay et al., 2010). HNO_3 and HCl, for example, break down the hydrogel after a few cycles, but H_2SO_4 retains its efficacy even after several cycles (Ozay et al., 2010). Also, magnetic hydrogels have demonstrated various degrees of endurance when subjected to different acids. UV irradiation is another unique method that may be used to regenerate graphene oxide–TiO_2 hydrogels. These hydrogels maintain a high adsorption capacity even after being subjected to several cycles (Zhang et al., 2013). Tang et al. also showed the regeneration and reusability of hydrogels via a column experiment for removing Cr(VI) by a cationic hydrogel (Tang et al., 2011).

Interestingly, after six adsorption and desorption cycles, the adsorption capacity remained unchanged (27 mg/g, 90%), and the desorption efficiency was 93% of the average for each cycle (Tang et al., 2011). During seven adsorption cycles, Liu et al. demonstrated that 95% of copper, iron, and lead could be extracted from an aqueous solution. Furthermore, they revealed that the hydrogel retained its ability to adsorb metals. It has been shown that hydrogels may be reused for an extended period, increasing their efficiency and reducing the amount of money spent on manufacturing the contaminant removal procedures that take place in aqueous medium (Liu et al., 2012). The capacity to reuse hydrogels increases their economic feasibility and demonstrates that they are safe for use in water purification operations from an environmental standpoint. In contrast to

some sorbents, which lose their efficacy over time, hydrogels keep their adsorptive capabilities even after regenerating them. This trait makes hydrogels an excellent option for applications that involve the removal of contaminants over short periods.

Table 2.3 presents a comparison of various hydrogels for contaminant removal. Overall, natural hydrogels, such as lignin, kappa carrageenan, and chitosan, are biodegradable, reusable, and cost-effective media for contaminant removal from aqueous solution. They can be applied as standalone or composite hydrogels for heavy metals and dye treatment. Natural hydrogels' mechanical strength and stability were reported to control their applications in water and wastewater treatment. Combining natural hydrogels with organic and nonorganic nanoparticles was suggested to overcome these problems. Graphene oxide and carbonaceous nanofiber hydrogels were also used for contaminant treatment, although they are more expensive and complicated to fabricate than kappa carrageenan and chitosan ones.

Lignin hydrogels are biodegradable and cost-effective but have limited mechanical strength. They have the ability to remove metals like pb^{2+}, Cr^{3+}, and Cu^{2+} via various interactions, with adsorption capacities of 308, 65.72, and 541 mg/g, respectively (Kwak et al., 2016; Thakur et al., 2017; L. Zhang et al., 2018). The vast surface area of graphene oxide-based hydrogels makes them particularly effective in removing dyes; nevertheless, manufacturing them is expensive and hazardous. Their adsorption capacities for methylene blue are 324 mg/g, whereas their adsorption capacities for rhodamine B are 114.4 mg/g (Guo et al., 2015).

Carbonaceous nanofiber membranes eliminate Pb^{2+}, Cr^{3+}, and methylene blue by electrostatic interactions and complexation, with high adsorption capacity but possible performance reduction over cycles (Liang et al., 2011). Chitosan, maltodextrin, and gum

arabic hydrogels efficiently remove Cd^{2+} while retaining biodegradability but lacking mechanical strength. Chitosan hydrogels are low cost and biodegradable; they have poor mechanical strength (Paulino et al., 2011). Aluminum hydroxide polyhydrate hydrogels reject multiple ions but perform poorly with monovalent ions (Karbassiyazdi et al., 2023a). Kappa carrageenan–vanillin hydrogels are biodegradable and efficient but need optimization owing to the limited mechanical strength to remove metal ions (Ibrar et al., 2023).

The kappa carrageenan–graft–poly(N hydroxyethyl acrylamide)/magnetite nanocomposite hydrogel removes cationic dyes and heavy metals via adsorption and magnetic separation. However, manufacturing is complex, and stability is uncertain (Kulal & Badalamoole, 2020b). Kappa carrageenan/tamarind kernel powder hydrogel absorbs brilliant green and Rose Bengal colors. Biodegradable and cost-effective, it may need regeneration and has water stability difficulties (Vaid & Jindal, 2022). Kappa carrageenan-coated magnetic nanoparticles remove methylene blue swiftly, are eco-friendly, magnetically separate easily, and may be reused four times. While the kappa carrageenan/cellulose hydrogel is cost-effective and eco-friendly, it may lose its adsorption capacity at low pH and in overuse cycles (Salgueiro et al., 2013).

The kappa carrageenan/graphene oxide hydrogel efficiently removes Na^{+} and Mg^{+} ions via electrostatic interactions and increased surface area, resulting in higher capacity and mechanical strength. While graphene oxide has a 95% removal efficiency for $MgSO_4$ and 23% for NaCl, its high cost and production complexity prevent its widespread application (Yadav, Ibrar, Altaee, et al., 2022b). Despite high manufacturing costs and complex synthesis, the titanium dioxide nanoparticle-loaded hydrogel degrades methylene blue via adsorption and photocatalytic degradation under UV light, resulting in excellent

adsorption capacity, mechanical strength, and biocompatibility. Adsorption capabilities range from 349.65 mg/g to 465.12 mg/g, depending on the TiO_2 concentration (Patel et al., 2023).

Chitosan and cellulose composites efficiently remove heavy metals (e.g., Cu, Zn, Cr, Ni, and Pb) by chelation and ion exchange. Biodegradable and eco-friendly, they lack mechanical stability (Sun et al., 2009). The Fe_3O_4–polyvinyl alcohol/chitosan combination adsorbs Cr^{6+} by electrostatic attraction and electron sharing, allowing magnetic separation and recycling, although efficiency drops at neutral pH(Yan et al., 2018). Through multiple interactions, the dual-network chitosan-based hydrogel (CMAPP) eliminates methylene blue (MB) and malachite green (MG) dyes at >2000 mg/g and high recyclability, but not anionic dyes (Miao et al., 2024). Though swelling is minimized, the CMC-g-poly(AM-co-ITA)/clay nanocomposite removes vivid green dye at 1513.55 mg/g (Aljeboree et al., 2024). Finally, the chitosan–ethylene glycol hydrogel (CEGH) eliminates perfluorooctanoic acid (PFOA) via ionic hydrogen bonding at 1275.9 mg/g, but just PFOA (Long et al., 2019).

Table2. 3:Comparison of various hydrogels for contaminant removal.

Hydrogels Type	**Removal Mechanism**	**Metal Ions**	**Advantage**	**Disadvantage**	**Adsorption Capacity (mg/g)**	**References**
Lignin hydrogels (lignosulphonate-based graphene hydrogel Lignin grafted polyacrylic hydrogel Lignocellulose-based composite hydrogel	Hydrogen bonding, electrostatic, and covalent interactions Lignin-grafted polyacrylic hydrogel and lignocellulose-based composite hydrogels remove contaminants through adsorption, ion exchange, complexation,	Pb^{2+} Cr^{3+} Cu^{2+}	The ability to biodegrade, a natural polymer, cost-effective, renewable, and versatile, with hydroxyl, methoxy, carboxyl, phenolic, and ether groups	Lignin hydrogels suffer from limited mechanical strength, poor hydrolysis, and chemical resistance, require pretreatment, and demonstrate potential leaching and lower swelling capacity.	308 65.72 541	(Kwak et al., 2016; Thakur et al., 2017; L. Zhang et al., 2018)

	hydrogen bonding, and electrostatic interactions.		enhancing adsorption			
Graphene oxide-based hydrogels	Graphene oxide-based hydrogels can effectively remove dyes by using π–π interactions, van der Waals forces, hydrogen bonding, electrostatic interactions, and the utilization of their large surface area and porosity.	Food Blue 2 and Food Red 17	Superior adsorption for dyes due to the large surface area and functional groups Easily functionalized to target specific contaminants Robust and durable due to GO	High synthesis and processing costs Possible toxicity if not adequately purified Environmental impact Potential long-term stability issues	For both methylene blue (MB) and rhodamine B (RhB), the absorption capacity was 324 mg/g and 114.4 mg/g.	(Guo et al., 2015)

			Maintains performance under varying temperatures Safe for the environment Efficient dye removal within approximately 4 h Reusable 3–5 times, with some loss of effectiveness			

Carbonaceous nanofiber membranes	Adsorption through electrostatic interactions, hydrogen bonding, and surface complexation	Pb^{2+}, Cr^{3+}, methylene blue	High surface area, fast adsorption rates, high adsorption capacity, regenerable and reusable over multiple cycles, and efficient at high flux	Potential for performance decline over multiple use cycles, complex manufacturing process	Methylene blue: up to 818.6 mg/g Pb(II): up to 423.7 mg/g Cr(VI): up to 221.3 mg/g	(Liang et al., 2011)
Hydrogels based on chitosan, maltodextrin, and gum arabic	Adsorption by physical forces, ion exchange, complexation	Cd^{2+}	Biodegradable, low cost, abundant, high efficiency	Limited mechanical strength, biodegradability	80–150 mg/g	(Paulino et al., 2011)

Polyvinyl alcohol/chitosan	PVA/chitosan hydrogels remove Mn (II) ions from aqueous solutions by physical adsorption, ion exchange, and complexation.	Mn^{2+}	Biodegradable, high adsorption capacity, low cost	Biodegradability, limited mechanical strength	10.5 mg/g	(Abdeen et al., 2015)
Aluminum hydroxide Polyhydrate hydrogel	Adsorption, ion exchange, electrostatic attraction	Pb^{2+}, Cu^{2+}, Mg^{2+}, Ca^{2+}, Ni^{1+}, Zn^{2+}, As^{5+}.	High rejection rates, stable performance, easy to fabricate, reusable 4 times	Limited effectiveness for monovalent ions, the potential for clogging	Removal efficiency for Pb, Cu, and Zn was 99.9%, Ni: 100%, Mg: 85%, Ca: 84%	(Karbassiyazdi et al., 2023a)

Kappa carrageenan–vanillin hydrogel	Adsorption, ion exchange, chelation mechanism	Pb^{2+}, Cu^{2+}, Mg^{2+}, Ca^{2+}, Na^{1+}.	High removal efficiency, low energy consumption, biodegradable	Low mechanical strength requires optimization for stability	Cu: 1.22 mg/g Removal efficiency for Mg: 88%, pb: 79%, Cu: 82%, Ca: 82%, Na: 38%	(Ibrar et al., 2023)
Kappa carrageenan–graft–poly(N hydroxyethyl acrylamide)/magnetite nanocomposite (κ-g-PHEAA/Fe3O4) hydrogel	Adsorption, magnetic separation	Cationic dyes (MB, R6G), heavy metals (Cu^{2+}, Hg^{2+})	High adsorption capacity and reusable, magnetic properties facilitate separation	Complex synthesis, potential stability issues	MB: 196.1, R6G: 307.8, Cu(II): 243.4, Hg(II): 229.9	(Kulal & Badalamoole, 2020b)

Kappa carrageenan/tamarind kernel powder hydrogel	Adsorption	Brilliant green (BG), Rose Bengal (RB)	Biodegradable, cost-effective, high adsorption capacity, pH-responsive	It may require regeneration, stability issues in water	840.33 mg/g (BG), 168.06 mg/g (RB)	(Vaid & Jindal, 2022)
Kappa carrageenan-coated magnetic nanoparticles	Kappa carrageenan sulfonate groups adsorb and electrostatically interact with methylene blue (MB).	Methylene blue (MB)	High adsorption capacity, quick removal (5 min), eco-friendly, facile magnetic separation, and neutral and alkaline chemical stability. Reusable 4 times	This product features rapid removal (5 min) and high adsorption capacity, is eco-friendly, has quick magnetic separation, and shows excellent chemical stability in	185.3 mg/g at pH 9	(Salgueiro et al., 2013)

				neutral and alkaline environments.		
Kappa carrageenan/cellulose hydrogel	Adsorption, electrostatic interactions, and ion exchange between Pb^{2+} ions and functional groups (such as –OH and –COOH)	Pb^{2+} ions	High adsorption capacity, eco-friendly, reusable (with an effectiveness of over 79% after eight cycles), and cost-effective	At low pH, adsorption capability may decrease during reuse cycles.	486 ± 28.5 mg/g	(Kalaiselvi et al., 2023)
Kappa carrageenan/graphene oxide hydrogel	Electrostatic interactions, increased surface area, and hydrophilicity	Na^{1+}, Mg^{2+}	High adsorption capacity, improved mechanical strength, enhanced	Graphene oxide is expensive, and manufacturing complex and performance	Removal efficiency MgSO4: 95%, NaCl: 23%	(Yadav, Ibrar, Altaee, et al., 2022b)

	caused by graphene oxide and kappa carrageenan contribute to adsorption.		selectivity, and antifouling properties	deteriorate over numerous cycles.		
Titanium dioxide nanoparticle-loaded κ-carrageenan hydrogel	Adsorption and photocatalytic degradation TiO2 nanoparticles, when exposed to ultraviolet light, produce reactive oxygen species, which contribute to	Methylene blue	High adsorption capacity, improved mechanical strength, UV-responsive degradation, and biocompatibility	High production costs, complex synthesis process	Methylene blue: 349.65 mg/g to 465.12 mg/g depending on TiO_2 concentration and crosslinking	(Patel et al., 2023)

	the degradation of dyes.					
Chitosan (chitin)/cellulose composite hydrogel	Adsorption via chelation and ion exchange through hydroxyl and amine groups	Cu^{2+}, Zn^{2+}, Cr^{6+}, Ni^{2+}, Pb^{2+}	High adsorption efficiency, eco-friendly, biodegradable, improved stability with freeze-drying	Limited mechanical stability requires regeneration	Cu^{2+} (0.417 mmol/g), Zn^{2+} (0.303 mmol/g), Cr^{6+} (0.251 mmol/g), Ni^{2+} (0.225 mmol/g), Pb^{2+} (0.127 mmol/g)	(Sun et al., 2009)
Fe_3O_4-polyvinyl alcohol/chitosan composite hydrogel	Adsorption via electrostatic attraction and electron-sharing	Cr^{6+}	High adsorption efficiency, magnetic separability, good repeatability	Decreased swelling ratio, limited adsorption under neutral conditions	Cr^{6+} (0.267 g/g)	(Yan et al., 2018)

Dual-network chitosan-based hydrogel (CMAPP)	Adsorption via electrostatic attraction, hydrogen bonding, and n-π interactions	Methylene blue (MB), malachite green (MG), crystalline violet (CV), basic fuchsin (BF)	High adsorption efficiency, strong anti-interference, excellent recyclability	Limited adsorption for anionic dyes	MB: 1800 mg/g, MG: 1797 mg/g, CV: 2495 mg/g, BF: 2938 mg/g	(Miao et al., 2024)
Carboxymethyl cellulose(CMC)-g-poly(AM-co-ITA)/clay	Adsorption via electrostatic interactions and multilayer adsorption	Brilliant green (BG) dye	High adsorption capacity, enhanced stability with clay, easy	Reduced swelling ratio with higher clay content	BG: 1513.55 mg/g	(Aljeboree et al., 2024)

nanocomposite hydrogel			separation, strong reusability.			
Novel chitosan–ethylene glycol hydrogel (CEGH)	Ionic hydrogen bond interaction between carbonyl groups of PFOA and protonated amine groups of CEGH	Perfluorooctanoic acid (PFOA)	High adsorption capacity, simple synthesis via freeze-thawing, eco-friendly	Limited to specific contaminants like PFOA	PFOA: 1275.9 mg/g	(Long et al., 2019)

2.9 Hydration phenomena in hydrogel: mechanisms, measurements

Hydrogel hydration phenomena include water absorption and swelling, which affect their physical and chemical characteristics. Hydrogels made from kappa carrageenan, chitosan, and cellulose absorb water well owing to their hydrophilic and porous properties. When these gels come into contact with water, they undergo swelling driven by osmosis, where water molecules penetrate the gel matrix, causing it to expand. This hydration enhances the gel's mechanical strength and flexibility, making it appropriate for medication administration, wound healing, and environmental cleanup. The gel's crosslinking density affects swelling, water absorption, ionic groups, pH, and temperature. Hydration mechanisms are crucial to the polymer hydrogel sol-gel transition, as responsive hydrogel systems show. A polymer hydrogel's structural makeup is 90% water; hence, understanding hydration processes is vital. Hydrogels may expand their dry weight 1000-fold in water or salt water (Ahmed, 2015), with Gibas and Janik (Gibas & Janik, 2010) expressing sorbed water as equilibrium water content (EWC) in Equation (2.1).

$$EWC\% = \frac{Ww}{Wt} \times 100 \qquad (2.1)$$

Ww is the dry gel weight, and *Wt* is the hydrated gel weight.

Figure 2.4 shows a multi-step technique for hydrating and expanding swellable polymer systems (Gibas & Janik, 2010; Pasqui et al., 2012). Water molecules first hydrate the hydrogel matrix's most polar, hydrophilic active spots to generate primary bound water. This water is essential to the hydrogel structure and cannot be separated. Hydrophobic sites interact with water molecules to create secondary bonded water in the next phase. Total bound water has intermediate qualities from primary and secondary bound fluids

(Pasqui et al., 2012). In the next stage, the covalent or physical crosslinks resist the polymer network's osmotic driving force toward infinite dilution. Thus, they absorb water equal to the polymer's equilibrium swelling capacity. Most free water is between network chains and bigger holes, micropores, or voids (Hoffman, 2012). Due to electrostatic repulsion, polymer chains stretch, generating vacuum regions in the polymer network where much loosely bound water may be absorbed. Thus, the polymer crosslinking strategy during hydrogel fabrication is crucial to network formation. It increases the number of surface-active sites and interstitial domains, makes the copolymer insoluble in water, and increases the polymer network's mechanical strength and swelling.

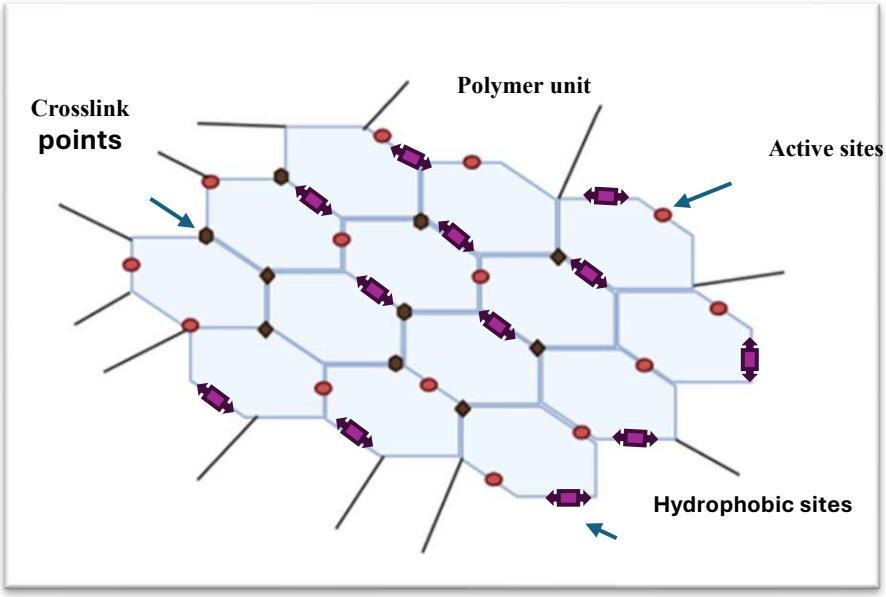


Figure 2. 4. Illustration depicting the structure of a polymer network.

To quantify polymer networks' water absorption (uptake) features, water adsorption/desorption, water retention time (WRt), swelling rates, and repeatability performance were estimated. Equations (2.2) and (2.3) are used to calculate the water adsorption/swelling rate and the reproducibility performance of a hydrogel substance.

WR(t) is defined as the ratio of the weight of the water retained by the hydrogel at a specific time to the weight of the dry hydrogel by Equation (2.4).

$$Swelling\ ratio(SR\%) = \frac{W2-W1}{W2} \times 100 \quad (2.2)$$

$$Water\ uptake(WU\frac{g}{g}) = \frac{W2-W1}{W1} \quad (2.3)$$

$$Water\ retention\ time(WRt\frac{g}{g}) = \frac{(Wt-Wd)}{Wd} \quad (2.4)$$

$$Deswelling(DS\%) = \frac{Ws}{W0} \times 100 \quad (2.5)$$

Equations (2.2) and (2.3) measure the swelling ratio and water uptake. After 24 h of equilibrium swelling, the hydrogel weighs W2 in g, and W1 is the dry material's weight after filtering or oven drying to constant weight. In Equation (2.4), Wt is the weight of the hydrogel at time t after it has absorbed water, and Wd is the hydrogel's initial dry weight. Deswelling refers to the process by which a hydrogel releases absorbed water and contracts, returning closer to its original dry state. This characteristic is essential for applications that require hydrogels to undergo multiple swelling–deswelling cycles while maintaining their structural integrity and functionality. Deswelling (DS) was calculated using Equation (2.5), with Ws representing the weight of the swollen hydrogel and Wo the weight after vacuum drying for 30 min.

The hydrogel's swelling and deswelling phenomenon demonstrates its ability to retain and release water. Equation (2.6) calculates the moisture desorption rate by allowing a sample with a known weight W (g) to absorb and release water at a particular temperature, relative humidity, and time. $W1$ and $W2$ are sample weights after sorption and desorption, while WD is the water desorption rate.

$$Water\ desorption\ (WD\%) = \frac{W1-W2}{W} \times 100\% \quad (2.6)$$

The elastic response of polymer chains and chemical and physical factors affect hydrogel composite water absorption and swelling. Polymer networks swell when water enters the hydrophilic matrix via diffusion and capillary action. The flexibility of crosslink sites allows hydrogel structures to expand and contract in response to physical or chemical stimuli. Hydrogel swelling is affected by crosslinking density, particular surface area, hydrophile–lipophile character, and medium ionic strength.

The salt sensitivity factor Equation (2.7), calculated from equilibrium swelling in saline solution to deionized water, assesses how ionic strength affects polymer swelling. Smaller f-values suggest a lesser electrolyte swelling reaction. Higher cation charges promote crosslinking, diminishing swelling dynamics. Zhang and Francisco et al. examined the effects of monovalent (K^+, Na^+, NH_4^+), divalent (Ca^{2+}), and trivalent (Al^{3+}) ions on chitosan- and starch-based hydrogel swelling. Monovalent, divalent, and trivalent cations limit water absorption. Cationic charge enhances crosslinking density, minimizing swelling (Rodrigues et al., 2012; Q. Zhang et al., 2020). The salt sensitivity factor (f) shows this link, with higher f-values affecting swelling more. The swelling capacity (g/g) of chitosan-based polymers declines with larger f-values: NH_4^+ (0.69; 43.3 g/g) < Na^+ (0.76; 33.6 g/g) < Ca^{2+} (0.93; 10.2 g/g) < Al^{3+} (0.97; 4.7g/g). Chemical complexation and electrostatic interaction with polymer matrix let multivalent cations produce more crosslinks (Alam & Christopher, 2018). Higher crosslink density reduces swelling by limiting access to interstitial polymer domains. Increased ionic strength also lowers osmotic swelling pressure, causing the gel to contract. Alam et al. found that cellulose-based hydrogels' swelling and WR significantly decreased from 725 g/g in deionized

water to 118 g/g in saline water due to the charge screening effect (M. N. Alam et al., 2019).

$$Salt\ sensitivity\ factor = 1 - \frac{Wsaline}{Wwater} \quad (2.7)$$

Water absorption and swelling are stronger in hydrogels of hydrophilic polymers like hydroxyl or carboxyl groups. Due to charge screening, cellulose-based hydrogels expand greatly in deionized water but less in saline (M. N. Alam et al., 2019). Higher environmental ionic strength minimizes the osmotic pressure differential, contracting the hydrogel. The polymer's molecular weight and chemical structure impact the hydrogel's environmental response. Due to differences in polymeric chains and functional groups, chitosan-based hydrogels swell differently than cellulose-based ones (Q. Zhang et al., 2020). Higher-molecular-weight polymers make stronger, more durable hydrogels but may expand less.

2.10 Conclusion

Water purification methods have undergone tremendous development to meet the rising concerns over water pollution produced by contaminants from industrial, agricultural, and sewage sources. The efficiency of membrane technologies such as microfiltration (MF), ultrafiltration (UF), nanofiltration (NF), and reverse osmosis (RO) in removing a wide variety of pollutants depends on size exclusion, adsorption, and electrostatic interactions. These technologies have become a vital part of the different approaches. Fouling, high energy consumption, and high operating expenses are obstacles these technologies confront, even though they have beneficial applications. In light of this, novel materials such as hydrogels provide potentially promising alternatives. Because of their one-of-a-kind three-dimensional polymer networks, large surface area, and quick regeneration

capabilities, hydrogels provide a solution for water purification that is both cost-effective and efficient. They can absorb various pollutants, including organic toxins and heavy metals, making them appropriate for emergencies and environmentally responsible water treatment procedures. Hydrogel composites have been developed to further improve their functioning by merging the characteristics of natural and synthetic materials, increasing these composites' adsorptive capacity and compatibility with the environment. The adsorption processes of hydrogels, which functional groups and ambient circumstances regulate, make it possible for hydrogels to effectively remove pollutants via complexation, ion exchange, and physical adsorption. Hydrogels are a better option than traditional adsorbents because they can undergo regeneration via various mechanisms. This guarantee of long-term sustainability and cost-effectiveness positions hydrogels as a superior choice. Despite these advantages, several challenges remain that require further investigation. These include improving the structural integrity of hydrogels to withstand prolonged operational use, tailoring hydrogel compositions to maximize adsorption capacity for specific pollutants and developing cost-effective synthesis methods for large-scale production and real-world implementation. Additionally, there is a need to explore the long-term environmental impact and degradation mechanisms of hydrogel-based materials and investigate multifunctional hydrogels that incorporate nanomaterials for selective adsorption and self-regeneration properties. Addressing these research gaps will pave the way for more effective, sustainable, and commercially viable hydrogel-based water purification technologies.

Chapter 3: Kappa Carrageenan-Vanillin Composite Hydrogel for Landfill Leachate Wastewater Treatment

Ibrar, I[$]., **Alsaka, L**[$]., Yadav, S., Altaee, A., Zhou, J. L., & Shon, H. K. (2023). Kappa carrageenan-vanillin composite hydrogel for landfill leachate wastewater treatment. *Desalination*, *565*, 116826.

$: Equal effort

Author contributions statement:

Lilyan Alsaka: Conceptualization, Methodology, Writing - original draft, and Data curation. Ibrar Ibrar: Methodology, Writing - original draft, Data curation. Ali Altaee: Supervision, Writing - review & editing. Sudesh Yadav: Visualization, Investigation, reviewing. John L. Zhou: Supervision, Writing -review & editing. Ho Kyong Shon: Visualization, Investigation.

Acknowledgment

The authors would like to acknowledge the research training program scholarship awarded to **Lilyan** Alsaka by the Government of Australia.

Abstract

Removing heavy metals from landfill leachate wastewater treatment is an environmental challenge because of its complicated characteristics and composition. Although several chemical and physical processes were developed for landfill wastewater treatment, membrane technologies are still common. Nevertheless, membrane fouling, energy requirements and brine management are drawbacks of membrane technologies. This study proposed a biodegradable, gravity-driven kappa-Carrageenan-vanillin hydrogel for biologically treated leachate wastewater treatment to reduce the treatment cost and brine

management problem. The composite hydrogel was synthesized using a facile method, with an average pore size of 2.58±0.5 nm and acts as a water filter with super high flux and excellent rejection for heavy metal ions, divalent ions and other contaminants in the landfill leachate wastewater. The hydrogel filter achieved high rejection for divalent ions from salt feed solutions such as sodium chloride, magnesium sulphate, and copper sulphate. An average rejection of 42 ±5% was achieved for sodium chloride, 78%±5% for copper, 72%±5% for divalent magnesium ion, and 17%±5% for sulphate rejection. The hydrogel filter achieved a flux of 27 ±5 LMH for landfill leachate wastewater with high rejection efficiency for total organic carbon, turbidity, and heavy metal separation. The filtration of the landfill leachate with the hydrogel resulted in a high rejection of total organic carbon (77±3 %), 95±3 % turbidity removal, 73 ±5 % TDS removal, and 95-97% colour removal. Heavy metal ions were rejected in the following order: Al (80±3%)> Ba (88 ±2%) > Pb (79 ±3%) > Cd (72±3%). The composite hydrogel filter is inexpensive, reliable, and highly efficient in removing contaminants under gravity filtration, requiring no external energy or high hydraulic pressures and ease of scalability for commercial applications.

3.1 Introduction

Rapid urbanization and industrialization have led to increased heavy metal pollution, which is detrimental to our environment, food chain, water bodies, and agriculture (Oves et al., 2012). Every year, millions of industries worldwide discharge waste laden with heavy metals into soil, water and the environment (Umoren & Eduok, 2016; Zhou et al., 2023). Heavy metals generally refer to metals having densities greater than 5 g/cm^{3,} such as Copper (Cu), lead (Pb), zinc (Zn), barium (Ba), cadmium (Cd), mercury (Hg), and chromium (Cr) are the most well-known in literature on heavy metals (Fang et al., 2018;

Li et al., 2014; Oves et al., 2012). At least 20 metals are classified as toxic and pose a significant risk if discharged into the environment in high concentrations (Akpor & Muchie, 2010). These metals have hazardous effects on living beings and the environment. For instance, lead can disrupt our food chain, decrease plant growth, and cause human cancer (Ahmed et al., 2022). Cadmium toxicity can also promote soil pollution, inhibit plant growth, and can cause damage to human kidneys, renal tubular impairment, and other pulmonary diseases (Mahajan & Kaushal, 2018). Chromium in water above regulatory levels has been linked to human cancer and kidney and liver damage (Pradhan et al., 2017). Barium is harmful to aquatic organisms, and due to its high solubility in water, it can travel easily in the aquatic environment, such as lakes, oceans, etc., covering longer distances (Ghaemi et al., 2011). Hence, there is a dire need for robust wastewater treatment technologies to remove heavy metal ions efficiently, besides the stricter regulations for environmental protection. At the same time, new cost and energy-efficient technologies should be developed for water purification and wastewater treatment where alternative technologies remain questionable.

Over the past few decades, several technologies have been adapted for removing heavy metals from wastewater, such as membrane technologies, adsorption, and several others, such as coagulation/flocculation and precipitation (N. Abdullah et al., 2019). Membrane processes such as reverse osmosis, ultrafiltration, and nanofiltration are more effective for removing heavy metal ions from wastewater effluent. However, these technologies are not cost-effective, require hands-on experience, and require expensive capital investment. Additionally, these technologies are prone to fouling and high energy consumption (X. Zhang et al., 2018). Adsorption remains the most cost-effective option for contaminants such as heavy metal adsorption (Sun et al., 2019), especially

advancements in graphene-related composites (Qin et al., 2014; Reshmy et al., 2022). The most common adsorbent commonly used is activated carbon; however, regeneration is a drawback and cost (Nesic et al., 2012). Several researchers have also reported that activated carbon is inefficient for heavy metal removal (Barakat, 2011). These technologies also leave behind toxic by-products, an environmental issue that needs serious attention.

In addition to heavy metals, organic matter and microorganisms remain significant challenges for the membranes technology of wastewater treatment (K. Zhao et al., 2022). Researchers used nanoparticles to improve membrane properties and resistance to fouling (Yadav, Ibrar, Samal, et al., 2022b). Graphene oxide (GO) membranes were developed for desalination and water purification due to their excellent water permeability and fouling resistance of the GO material (Ashfaq et al., 2020). GO-modified polyamide reverse osmosis membrane exhibited improved antiscaling characteristics to conventional RO membrane treating $CaSO_4$ feed solution. The antifouling properties of the polysulfone-GO membrane used to filtrate 200 mg/L bovine serum albumin feed solution exhibited a 99% rejection rate and 88.55% water flux recovery. Despite the advantages of GO material, it is still considered expensive to use in membrane applications for water purification. Vanillin was reported to improve the membrane biofouling properties for wastewater treatment due to its biocidal properties (Yadav, Ibrar, Samal, et al., 2022b). Esmaeili et al. (2020) applied vanillin to enhance the hydrophilicity and antifouling properties of the polyethersulfone (PES) membrane. The PES membrane with 6 wt% of vanillin showed 40% higher water flux than the PES membrane. The study concluded that vanillin antifouling and hydrophilic properties would significantly improve the membrane performance.

Recently, several researchers have investigated novel hydrogels with chemical crosslinking, which are recyclable and biodegradable for heavy metal removal from wastewater (Zeng et al., 2020). These hydrogels, however, are limited to laboratory scale, as they have complex synthesis and involve rather expensive chemicals coupled with intricate synthesis. Kappa-Carrageenan (kC) was proposed to remove organic matter and heavy metals from an aqueous solution (Kulal & Badalamoole, 2020b; Pacheco et al., 2021; Wang et al., 2017). Researchers applied a hybrid nanocomposite kC-magnetite adsorbent to remove methylene blue (MB), Hg^{2+} and Cu^{2+} from the solution (Kulal & Badalamoole, 2020b; Tranquilan-Aranilla et al., 2012). The study found that kC-magnetite adsorption increased with the adsorbate concentration and reached equilibrium at 800 mg/L for MB and Hg^{2+} and 600 mg/L for Cu^{2+}. In another study, kC-GO hydrogel for methylene blue adsorption revealed a remarkable adsorption capacity of 658.4 mg/g at 25 °C (Wang et al., 2017). The adsorption capacity of the kC-GO hydrogel was almost constant after five cycles. Cañizares et al. (1994) used kG hydrogel for Spirulina maxima immobilization in a repeated cycle for 7 to 10 days, depending on the feed concentration. The removal of total phosphorus and ammonium nitrogen was >90% at 25% wastewater dilution, but it decreased to >80% for ammonium nitrogen and 90% for total phosphorus at 50% wastewater dilution. Despite the advantages of adsorption purification technology, it suffers drawbacks, including low surface area, difficulty separating adsorbent from adsorbate, and slow operation since it is a time-dependent process. Unlike membrane technologies, adsorption technology is time-dependent; hence, treatment takes a long time. In a recent study, Sudesh and coworkers(Yadav, Ibrar, Altaee, et al., 2022a) used a kC-GO solution for commercial nanofiltration (NF) membrane coating in leachate wastewater treatment. The modified membrane exhibited 95.73% water flux recovery and

low fouling percentage compared to the NF without kC-GO coating. As a pressure-driven membrane technology, kC-GO-coated NF membrane is a relatively energy-intensive process and generates a brine solution.

There is a need for a cost-effective separation and purification technology with low environmental impact. In this research, we designed and tested a hydrogel filter media for the first time, combining the advantages of thin membrane permeability and the adsorption properties of polymers for heavy metals treatment using landfill leachate wastewater as a feed solution. The gravity-driven kappa-carrageenan-vanillin (kC-V) composite hydrogel operates in dead-end mode to address some of the shortcomings of commercially available filtration systems, such as brine wastewater management, requirements for expensive infrastructure, and energy consumption. Vanillin was used to improve the hydrophilicity of kC hydrogel and impart a biocidal effect required for wastewater treatment (Yadav, Ibrar, Samal, et al., 2022b). The kC hydrogel mixed with vanillin exhibited increased hydrophilicity and biocidal characteristics for treating wastewater. The research questions are i) how does kappa-carrageenan concentration impact the hydrogel water flux and ions rejection? ii) what is the composite kC-V hydrogel rejection of divalent and monovalent ions? and iii) what is the kC-V performance when treating real landfill leachate wastewater? Different kC-V hydrogel concentrations were investigated and optimized for ions and heavy metal separation from biologically treated landfill leachate wastewater under gravity-assisted filtration. The experimental work investigated the impact of operating parameters on ions separation, water flux, and rejection rate for different hydrogel filters. Furthermore, the rejection rate of the kC-V hydrogel to divalent and monovalent ions in the solution was assessed using different solutions such as sodium chloride, magnesium sulphate, and copper sulphate,

and the feasibility of the hydrogel for the separation of heavy metal ions was assessed using real landfill leachate wastewater.

3.2 Materials and methods

3.2.1 Materials

Analytical grades, kC (sulphated plant polysaccharide), and vanillin were procured from Sigma-Aldrich (Australia) and used in all experiments. The wastewater sample was landfill leachate wastewater obtained from the Hurstville Golf Centre, and the wastewater was collected after biological treatment. Analytical grade sodium chloride (NaCl), magnesium sulphate ($MgSO_4$), and copper sulphate ($CuSO_4$) were also procured from Sigma-Aldrich and used in some experiments for rejection studies. A fabric material of 30 μm pore size was used as a support layer for the kC-V hydrogel filter. The hydrogel was set on the fabric layer in a filtration column for water treatment.

3.2.2 Hydrogel Synthesis and Filtration Setup

The kC hydrogel was made by dissolving different concentrations (1- 3% wt/v) of kappa-carrageenan powder in DI water at 60 ^oC and left on a magnetic stirrer for 3 hours to make a homogenous gelatinous solution (Figure 3.1a).

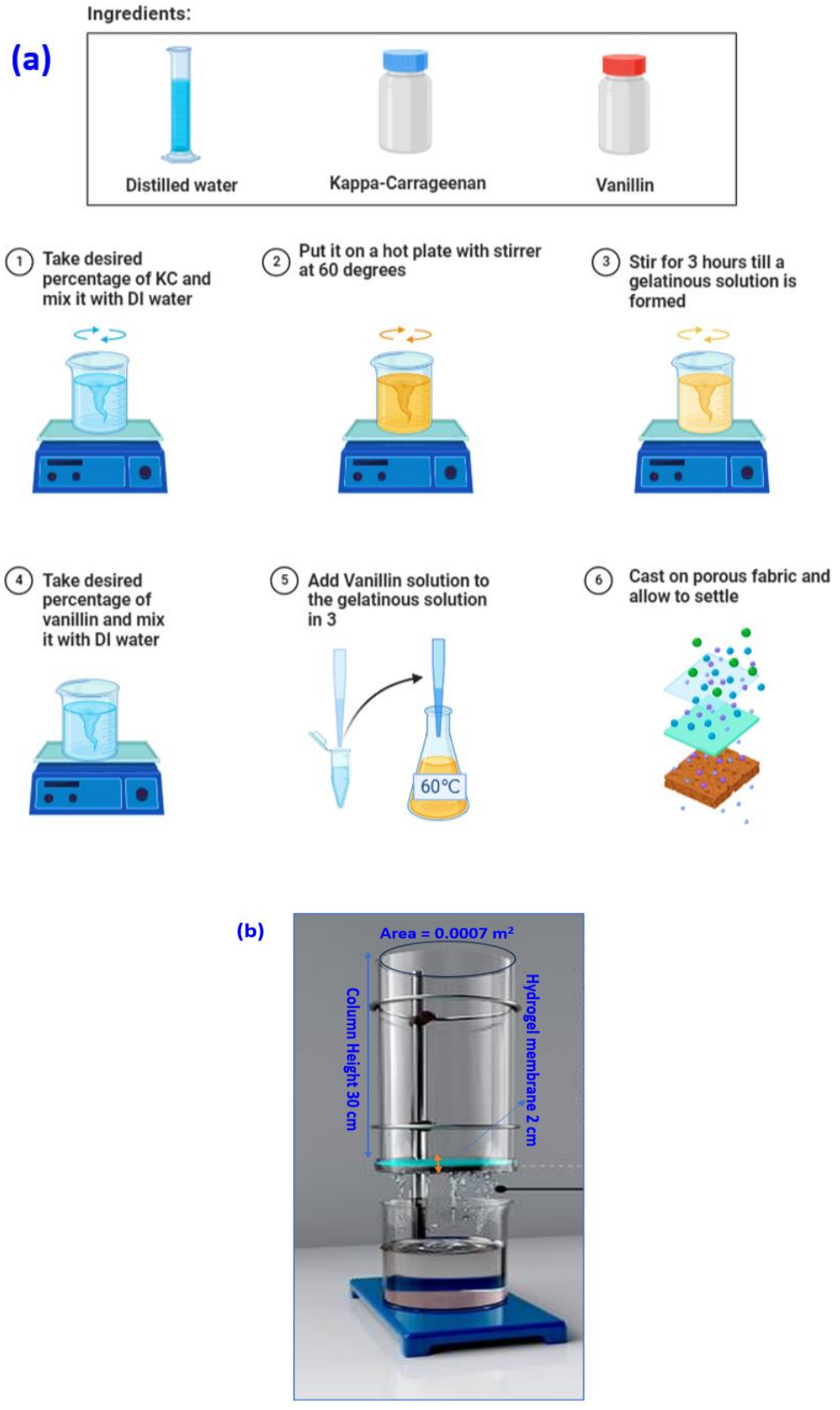


Figure3.1:Hydrogel synthesis and apparatus used a) Hydrogel synthesis and b) a schematic of gravity filtration.

Kappa-carrageenan gelling temperature usually ranges from 60 - 80 ºC. It was noticed that a higher temperature of 80 ºC affects the separation performance of the hydrogel as usually a firm hydrogel is formed, and it gets blocked quickly, compared with hydrogel synthesized at 60 ºC. In a separate beaker, 1% wt/v of vanillin powder was dissolved in DI water and stirred on a magnetic stirrer for homogenization simultaneously. Then, the vanillin solution was mixed with the hydrogel and vigorously shaken with a shaker (ThermoScientific, Australia). When kappa-carrageenan and vanillin are mixed, the vanillin molecules become trapped within the three-dimensional structure of the kappa-carrageenan molecule, forming a complex. This complexation can result in changes in the physical properties of the kappa-carrageenan, such as its viscosity and hydrogel strength. In general, the vanillin molecules can interact with the carrageenan chains through a combination of hydrogen bonding, electrostatic interactions, and hydrophobic interactions. The interaction between kappa-carrageenan and vanillin is believed to be due to the formation of hydrogen bonds between the sulphate groups of kappa-carrageenan and the hydroxyl groups of vanillin.

The kC-V hydrogel was cast on a fabric material (pore size about 30 μm) to provide a support layer for the hydrogel. The experimental work was performed using a homemade column filtration of 30 cm height made of plexiglass material (Figure 3.1b) to facilitate visual observation with a 0.0007 m^2 filtration area. In all the experiments, the head was kept constant at 30 cm. In the filtration setup, the fabric support layer was tightly placed at the bottom of the filtration column, and the kC-V hydrogel was poured slowly on top of the substrate using a syringe and allowed 10-15 minutes to settle down. The hydrogel was allowed to settle and set for 10-15 minutes at least whilst hydrated. The pure water was then poured slowly on column filtration. Care was taken during the filtration process

as the sudden falling of the water onto the hydrogel would deform it, compromising its performance. The feed solution's water flux and rejection rate of contaminants were measured using analytical equipment. All experiments were repeated at least three times to confirm the results. The water flux was measured using the following Equation.

$$Jw = \frac{W}{1000*A*t} \quad (3.1)$$

The rejection of pollutants was measured using Equation (3.2)

$$R = (1 - \frac{Cp}{Cf}) * 100 \quad (3.2)$$

In Equation (2), C_p represents the concentration of the pollutants in the permeate solution, whereas C_f is the initial concentration of the same contaminants in the feed solution. All experiments for water flux rejection studies were repeated at least three times.

3.2.3 Analytical methods

Fourier Transform infrared spectroscopy (FT-IR) was conducted for functional group analysis of the kC hydrogel and the kC-V using a Thermo Scientific Nicolet spectrometer (0.9 cm^{-1} optical resolution) connected to an IR- microscope (Thermofisher, Sydney, Australia). All samples were dried in an oven at 105 ºC for 24 hours. The FT-IR analysis was performed for the wavenumber ranging from 4000 to 1000 cm^{-1}. Each scan was conducted three times, and the average of the three scans was reported for the final spectra. Field-emission scanning electron microscopy (FE-SEM) for the hydrogel samples was conducted using a Zeiss EVO LS15 SEM (Zeiss, Sydney, Australia). Before the SEM analysis, all samples were coated with a 6nmlayer of Gold using a sputtering machine. The EDX (Energy dispersive X-ray) was conducted with a Bruker SDD XFlash 5030 detector (Zeiss, Australia). The same samples were subjected to SEM and EDX analysis. Pore size analysis was conducted through a porometer (TECHPoro Capillary

flow Porometer) using the Barret-Joyner-Hallena (BJH) model for adsorption and desorption. The kC-V hydrogel underwent a standardized procedure for analysis. Initially, all samples were precisely cut into a 4 cm^2 area. Subsequently, they were immersed in a wetting liquid known as Techporo fill liquid for 24 hours before analysis to ensure that the wetting liquid thoroughly permeated the pores within the samples. Besides, the hydrogel samples were carefully positioned within the module. A range of nitrogen gas pressures was applied across the active layer to investigate the characteristics of the hydrogel. The gas pressure was incrementally increased from 10 Psi (0.68 bar) to 120 Psi (8.27 bar). This pressure gradient facilitated the displacement of the fluid trapped within the pore possessing the largest pore throat. It is worth noting that the applied pressure had to surpass the capillary pressure of the liquid in the largest pore throat, a determination made through the bubble point method. This process aimed to expel any trapped fluid by employing a gas pressure that exceeded the capillary pressure. Once the gas was passed through the membranes under fully saturated conditions, the same pressure range was applied while the hydrogel samples were dry. Collecting data from both wet and dry states made it possible to calculate the maximum, mean, and minimum pore sizes exhibited by the membranes. The Laplace equation was utilized to measure the pore radius. This Equation considers the change in pore size as the pressure increases.

Consequently, the size of displaced pores decreased progressively from larger to smaller as the pressure was incrementally raised. The through-pore distribution was determined by measuring the pressure and flow rate of the gas passing through the membranes. Finally, the Washburn equation was employed to calculate the pore size, which provides a method of estimating pore characteristics based on the measured pressure and flow rate.

The dried hydrogel's pore size diameter (D) was estimated using Equation (3.3), also called the Washburn equation.

$$D = 4\gamma \cos\theta \Delta P \quad (3.3)$$

In Equation (3 γ represents the surface tension of the liquid, θ is the contact angle of the liquid, and P is the differential gas pressure. Nitrogen gas (N2) was used as adsorbate for BET analysis. One gram of dried hydrogel was placed in a glass column of BET and left for degas for 5 to 6 hours. The samples were then analyzed for 10 hours for pore size analysis.

3.2.4 Water contact angle, water uptake, and swelling

The contact angle of the pure kappa carrageenan and different percentages of kappa carrageenan (1% to 3%) were measured to get an insight into the surface wettability and the hydrophilicity of the different hydrogel surfaces. The water contact angle was measured by a sessile-drop method using the DM 211 Contact angle measurement system (Kyowa Interface Science, Chennai, India). For each sample, at least three different locations were selected for measurement, and the average water contact angle was reported as the final result with an error value. Further hydrogel analysis was conducted for water content analysis and assessment of swelling behaviour. Hydrogel with 2 cm thickness was subjected to water content and swelling tests. All the tests were conducted at a neutral pH value. The following Equation measured the water uptake (WU) of the hydrogel.

$$WU = \frac{(Wmoistgel - Wdriedgel)}{Wdriedgel} * 100 \quad (3.4)$$

water uptake (WU) was determined using a previously dried membrane by cutting the membrane into dimensional pieces of (3×3×1) cm. The hydrogel pieces were dried in an oven at 105 °C for 6 hours. Dry weight was recorded ($W_{driedhydrogel}$). After drying, the pieces were immersed in distilled water for 24 hours at room temperature and weighed after removing all excess m on a surface using blotting paper $W_{moisthydrogel}$ finally, water uptake was determined by Equation (4). A total of 5 samples were tested, and the average results were reported. Additionally, the swelling degree of the hydrogel was determined to measure the anti-swelling properties of the hydrogel. The hydrogel's initial weight was recorded ($W_{initial}$) and placed in DI water for 2 hours or NaCl solution of different concentrations. The final weight was re-recorded (W_{final}), and the swelling degree (SD) was estimated using Equation (3.5).

$$SD = \frac{(Wfinal - Winitial)}{Winitial} * 100 \quad (3.5)$$

3.2.5 Wastewater characterization

The wastewater was obtained from a former landfill site in Sydney, New South Wales. The landfill site generates mature leachate wastewater, which is hard to treat with biological treatment processes. The landfill leachate was collected after biological treatment at the landfill site with a membrane bioreactor (MBR). Despite being biologically treated, the leachate wastewater still shows high total dissolved solids (TDS), total organic carbon (TOC) and turbidity, which requires further treatment to meet environmental discharge guidelines. In the case of the landfill generated from this landfill site (methane formation and matured leachate), biological treatment is ineffective in treating the toxic pollutants (Andreja Žgajnar & Aleksander, 2015). The wastewater was

analyzed by Inductively coupled mass spectroscopy (ICP-MS) for the heavy metals concentrations, and the results are presented in Table (3.1).

Table3. 1:Wastewater analysis and composition

Parameter	Measurement tool	Value
pH	LAQUA-pH meter (Horriba, Japan)	7.9
Conductivity	LAQUA meter (Horriba,Japan)	14.53 ±2 ms/cm
Total dissolved Solids	LAQUA meter (Horriba,Japan)	2600± 100 mg/L
Salinity	LAQUA meter (Horriba,Japan)	
Turbidity	Turbidity meter (Horriba, Japan)	36 ±2 NTU
Total organic Carbon	TOC Analyser (Shimatzu, Japan)	155.2 mg/L
Mg	ICP-MS (Agilent, United States)	89.3 ±3 mg/L
Ca	ICP-MS (Agilent, United States)	71 ±2 mg/L
Cd	ICP-MS (Agilent, United States)	0.008 0.002 mg/L
Pb	ICP-MS (Agilent, United States)	0.007 ±0.002 mg/L
Al	ICP-MS (Agilent, United States)	0.06 ± 0.01 mg/L
Cr	ICP-MS (Agilent, United States)	0.09 ± 0.01 mg/L
Mn	ICP-MS (Agilent, United States)	0.07 ±0.01 mg/L
Ba	ICP-MS (Agilent, United States)	0.42 ± 0.1 mg/L
Na	ICP-MS (Agilent, United States)	132 ±5 mg/L
K	ICP-MS (Agilent, United States)	39± 5 mg/L

3.2.6 Adsorption capacity

The adsorption capacity experiment for Cu^{2+} ions was conducted using a thermostatic shaker under pH 6, 25°C, and 150 rpm for 24 hours. A solid-to-liquid ratio of 2 g/L of $CuSO_4$ was utilized. The investigation encompassed three concentrations (1%, 2%, and 3%) of kappa-carrageenan gel combined with 1% Vanillin. Following the adsorption process, separation performance of the kappa-carrageenan gel with Vanillin (kC-V) was accomplished through centrifugation at 5000 rpm for 8 minutes. Copper concentration in the samples was determined via ICP analysis, and the adsorption capacity ($mg.g^{-1}$) was calculated utilizing Equation (3.6).

$$Adsorption\ capacity\ \left(\frac{mg}{g}\right) = (Ci - Cf) \times \frac{V}{W} \qquad (3.6)$$

Equation (3.6) incorporates Ci (initial concentration of copper sulphate in mg/L), Cf (residual concentration of copper sulphate at equilibrium in mg/L), V (volume of the solution in L), and W represents the weight of the hydrogel samples in grammes.

The assessment of pollutants adsorption on the kC-V hydrogel layer involved conducting experiments to construct breakthrough curves of Cf/Ci. Equation (3.6) was used, with Ci representing the initial concentration of $CuSO_4$ and Cf indicating the concentration after passing through the fixed bed at a specific time (t). The breakthrough curve experiments aimed to determine the breakthrough point, which indicates the moment when the concentration of pollutants in the effluent reaches a predetermined percentage of the concentration in the influent. This point serves as a crucial indicator of the adsorption capacity and efficiency of the hydrogel layer in removing pollutants from the water or gas stream. By analyzing and interpreting the breakthrough curves, crucial insights can be

gained into the kinetics and performance of the kC-V hydrogel, allowing for optimization and further improvement of the adsorption process (N Abdullah et al., 2019). The quantity ($mg \cdot g^{-1}$) can be calculated using Equation (3.7) to ascertain the maximum adsorption capacity(Godiya et al., 2019).

$$\text{Maximum capacity adsorption (mg/g)} = \frac{Q.Ci}{m} \int_{t=0}^{t=total} \left(1 - \frac{Cf}{Ci}\right) \quad (3.7)$$

The maximum adsorption capacity in Equation (3.7) takes into account the flow rate (Q in Liter/minute), the adsorbent mass (g), and Ci (initial concentration of copper sulphate in mg/L) and Cf (residual concentration of copper sulphate at equilibrium in mg/L). The integral represents the cumulative adsorption over the specified time.

3.2.7 Desorption

In the desorption test, 50 mL of 0.1 M hydrochloric acid (HCl) was added to the kC-V hydrogel vial. The desorption process was done using a thermostatic shaker operating at 25°C and a stirring speed of 150 rpm for 2.5 hours. Then, the kC-V hydrogel was centrifuged at 5000 rpm for 8 minutes to separate from the solution, and copper concentration was measured using inductively coupled plasma (ICP). Equation (3.8) determines the desorption capacity (expressed as mg. g^{-1}).

$$Desorption \left(\frac{mg}{g}\right) = \frac{C_e * V}{W} \quad (3.8)$$

Where Ce represents the residual concentration of copper sulphate at equilibrium in mg/L, V is the volume of the solution in Litres, and W is the weight of the kC-V hydrogel. Consequently, adsorption-desorption experiments were conducted in three cycles to evaluate the adsorbents' reusability. The desorption studies were performed in acidic conditions around pH 1.2. The percentage of desorption (D) was determined using Equation 13.

$$Desorption\ (\%) = \frac{C_d}{C_a} \qquad (3.9)$$

In Equation (3.9), C_d represents the desorbed ions measured via ICP-MS analysis, and C_a represents the adsorbed ions.

3.2.8 Statistical analysis

Each experiment was conducted at least three times, and the average result ± standard deviation is reported there. The Analysis of Variance (ANOVA) was used to test the difference between multiple experimental data.

3.3 Results and discussions

3.3.1 Morphological characterization via FE-SEM, FT-IR, and contact angle

The surface morphology of the kC-V hydrogel was conducted via FE-SEM analysis. It should be noted that the hydrogel analysis was not conducted in its native state (not feasible with SEM). The hydrogel was dried for 24 hours and thus shrank before doing the SEM analysis. All the SEM pictures show no cracks at even smaller resolutions (2

and 10µm), as evident from Figures 3.2a and 3.2b, which show the integrity of the kC-V hydrogel, even after drying at high temperatures (105 ºC). All SEM images reveal tiny nanostructures of vanillin on the top of the hydrogel surface and ridges and valley-like structures for contaminants entrapment (Figure 3.2b). The structure resembles a thin-film composite membrane with a ridge and valley-like structure (Hamid, Abdullah, Yusof, Lau, Ismail, Wan Salleh, et al., 2021). The kC and vanillin interaction can be visualized with FT-IR analysis of the kC and the kC hydrogel mixed with vanillin (kC-V). Dry kC and kC-V hydrogel samples were subjected to FT-IR analysis (n=3). The FT-IR spectra of the kC and kC with different concentrations (1 to 3%) with 1% vanillin are presented in Figure 2c for wavenumber 4000 to 1000 cm^{-1}. The O-H stretch, C-H stretch, and possible triple bond formation of C and N are also highlighted in Figure 3.2c.

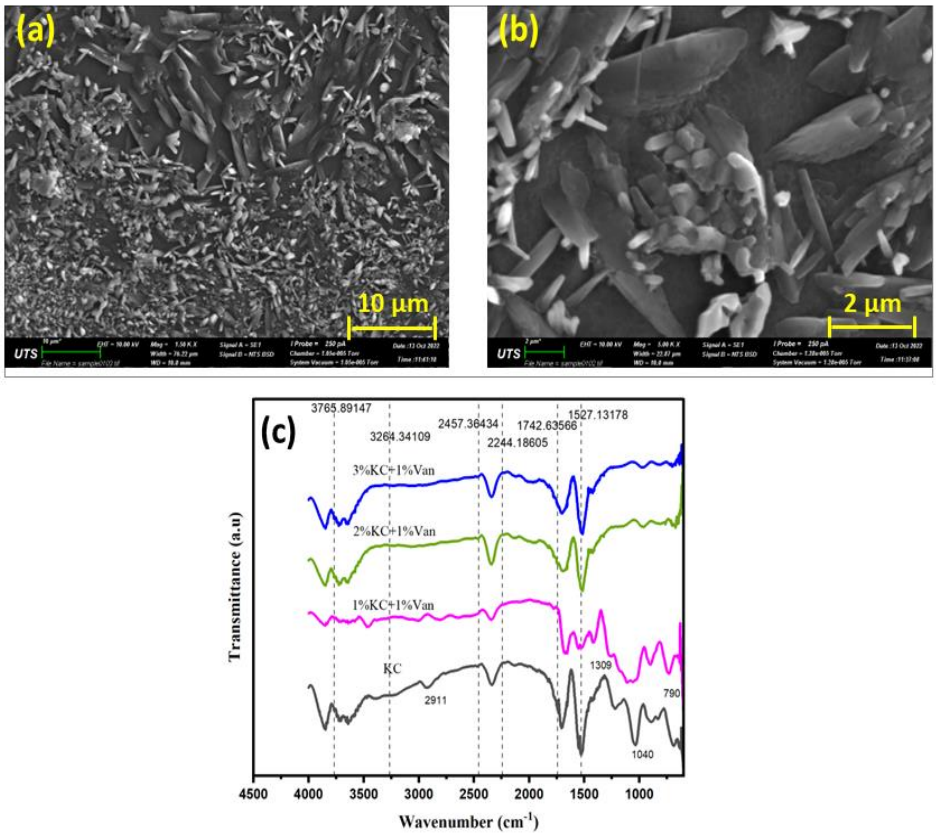


Figure3. 2.SEM and FT-IR analysis of the kC-V hydrogel, a) SEM image of the hydrogel at 10 µm at the first focus point, b) SEM images of the hydrogel at 2 µm at the first focus point, c) FT-IR spectra of the kC and kC coated with Vanillin (kC-V).

The spectrum of the pure kC shows several characterization bands. These peaks correspond to wavenumber 3765, 2457, 2244, 1742, and 1527 cm^{-1}. The bands at 1155, 923, and 844 cm^{-1} in the kC spectrum indicate polysaccharide units, 3,6-anhydride-galactose and d-galactose-4-sulfate, and are in agreement with the previous literature on FT-IR analysis of the kC hydrogel (Wang et al., 2017; Pacheco et al., 2021). These peaks wavenumber 923,1155,1527 cm^{-1}, assigned to stretching bands C-O, O=S=O, C-H, and O-H groups and the FT-IR spectrum confirmed the existence of carboxyl (-COOH), hydroxyl (-OH), and additional polar functional groups. All membranes demonstrated broadband performance between 2457 and 3765 cm^{-1}. The FT-IR of the kC-V hydrogel is also presented, and these bands are also present in the kC-V spectra with a slight stretching of some bands. The presence of new heights confirms the interaction of vanillin with the kC hydrogel, this confirms that the addition of vanillin to the kappa carrageenan contributes to increasing the presence of the hydroxyl group, which leads to an increase in the intensity of the hydroxyl expansion at 3200-3600cm^{-1}, and this is consistent with the theory that helps to bond with H (Yadav, Ibrar, Altaee, et al., 2022a). Vanillin is a pore-forming agent to improve the hydrogel's hydrophilicity and biocidal properties. Research suggests that the membrane porosity increases with increasing concentration of vanillin, and vanillin functions as a porogen by introducing polar functional groups, such as alcohol and aldehyde, which result in a negative surface charge on the membrane (X. Zhang et al., 2022a). The FT-IR of the kC-V also shows the formation of new peaks compared to the kC spectra in the 1kC-V (1% kC+1%Van). The FT-IR of 2kC-V and

3kC-V are almost identical. The broad rounded peak at 3765 cm^{-1} is slightly suppressed by adding vanillin, and this peak is a characteristic peak of hydroxyl (OH) groups. The dense peaks from 1500 to 1000 cm^{-1} can be attributed to the presence of sulphate groups in the kC and are also visible in the kC-V spectra. These peaks appear very dense, possibly due to small moisture in the hydrogel after drying. The presence of small moisture usually introduces an interference in the resulting absorption spectrum (X. Zhang et al., 2022a).

3.3.2 Water uptake, swelling and pore size analysis

The WU was measured by comparing fresh and dried hydrogel samples. The fresh hydrogel was placed in an oven at 105 ^{0}C for 6 hours. The kappa-carrageenan-vanillin (kC-V) composite hydrogels of similar thickness (2 cm) were tested for the WU. Upon losing water, the hydrogel shrinks, folds at the sides, and turns into a tiny plastic-like structure upon heating (Figure S1.1 Supplementary information S1). The WU for the 1% kC-V hydrogel was the highest, followed by the 2% and 3% hydrogels as presented in Figure 3.3a. The WU of the hydrogel with 1%kC-V indicates that 1g can take up to 1100g of water, significantly higher than most hydrogels reported in the literature. The increase in the water uptake of the hydrogel indicates an increase in the diffusion rate of protons. The protons are transferred by hydrogen bonding from the water molecule, and the same happens to the hydroxyl ions, thus increasing the flux (Yadav, Ibrar, Samal, et al., 2022b). Additional tests were conducted for the swelling behaviour of the different kC-V hydrogel concentrations in NaCl solution of different concentrations and DI water (Figures 3.3b, 3.3c and 3.3d). The swelling behaviour of different percentages of kC-V hydrogels was studied by immersing the hydrogel in different concentrations of NaCl (Figure 3.2b and 3.2d) and DI water (Figure 3.3c). Swelling tests were performed for 2 hours for all the solutions and hydrogel concentrations. Swelling behaviour in the presence of salt is a vital

metric for practical applications, such as water release systems in agriculture (Hamid, Abdullah, Yusof, Lau, Ismail, Salleh, et al., 2021). The impact of different concentrations on swelling is reported here in Figure 3b, and the other results are presented in Figures 3.3c and 3.3d for DI water and 2g/L NaCl. The swelling degree increases with the increasing salt concentrations for 1% kC-V hydrogel, compared to the other two hydrogels following an erratic path. The increase in salt concentrations after 2g leads to a decline in the swelling degree. It also agrees with the literature, where an increase in salt concentrations reaches a saturation point and the swelling degree of kappa-carrageenan declines after this point (Distantina et al., 2016). The sorption ability behaviour depended on the crosslinker of the hydrogel structure. An increase in the swelling agent leads to an increase in the hydrogel's hydrophilicity ability to absorb water, and the ions present in water affect the ability of the hydrogel to absorb water. For DI water swelling tests (Figure 3.3c), the 3% kC-V hydrogel exhibited good anti-swelling behaviour compared to the 2% and the 1% hydrogel.

The water contact angles were measured for pure kC and kC-V hydrogels to determine the hydrogel's surface hydrophilicity and wetting ability. Surface wettability refers to how liquids spread or stick to the hydrogel surface, while hydrophilicity specifically relates to water's interaction with the hydrogel. Surface wettability determines how well a liquid spreads or sticks to the hydrogel, while hydrophilicity focuses on water's affinity for the hydrogel surface. A smaller contact angle indicates high surface wettability and hydrophilicity (Andreja Žgajnar & Aleksander, 2015). The water contact angle of the pure kappa carrageenan was reduced substantially by adding 1% vanillin to the 1%, 2% and 3% kC hydrogels, as presented in Figure 3.3e. The decrease in hydrophobic properties of the pure kappa-carrageenan can be attributed to the addition of highly hydrophilic

vanillin. The result agrees with previous studies, where incorporating vanillin into PSf (Polysulfone) membranes decreased the contact angle substantially (Yadav, Ibrar, Samal, et al., 2022b). The highest decline in the hydrophobicity was in the 1% kC-V hydrogel, where the water contact angle was dropped to 58 ±1°. Increasing the concentrations of the kappa-carrageenan hydrogel led to a slight increase in the contact angle of the 2% kC-V and 3% kC-V hydrogels, 61 ±1° and 63 ±1°, which can be attributed to the increase in surface tension or high viscosity imparted by the increase in the concentration of the kappa-carrageenan. Increasing surface tension generally increases the contact angle by making the liquid more compact (Yadav & Chiu, 2019) (liquid tends to form a sphere). In contrast, an increase in viscosity may hinder the spreading of the liquid and lead to a larger contact angle (Keller et al., 2007). Similar results were also reported for the lower contact angle of sodium alginate hydrogel, where increasing concentration led to an increase in contact angle (Jin et al., 2022).

BET results for sorption data indicated that the average pore diameter of the 3kC-V hydrogel is 2.58 ±2 nm for a sample weight of 0.0318g. Furthermore, the BJH (Barrett-Joyner-Halenda) adsorption summary provides information about a material's micropores and mesopores based on the gas adsorption data analysis. The BJH (Barrett-Joyner-Halenda) adsorption and desorption summaries were imported from the BET analysis and are presented in Table3.2. The pore volume of the 3kC-V hydrogel is 0.047cc/g with a pore diameter of 3.228 nm for adsorption and 0.036 cc/g with a pore diameter of 3.31 nm for desorption.

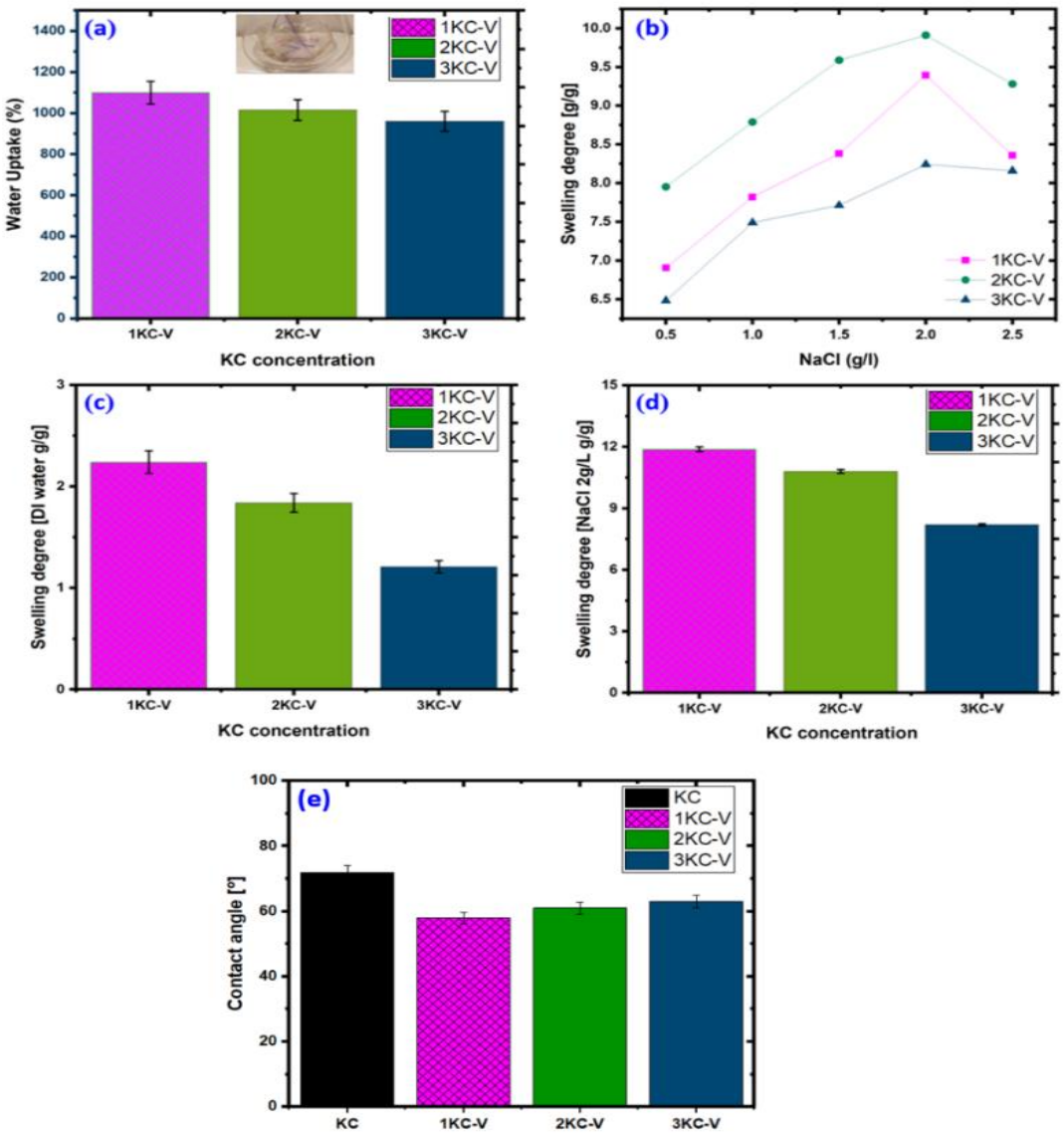


Figure3. 3.a) Water uptake of different concentrations of kC-V hydrogel, b) Swelling degree of various percentages of hydrogel with NaCl concentrations, c) Swelling degree in DI water for different concentrations, d) Swelling degree in NaCl 2g/L solution, e) Contact angle measurements of pure kappa-carrageenan, 1% kappa-carrageenan blended with 1% vanillin, 2% kappa-carrageenan with 1% vanillin and 3% kappa-carrageenan with 1% vanillin.

Table3. 2:Adsorption and Desorption summaries of BET analysis

BJH Adsorption summary		BJH desorption summary	
Surface area	33.15 m^2/g	Surface area	23.7 m^2/g
Pore Volume	0.047 cc/g	Pore Volume	0.036 cc/g
Pore Diameter	3.228 nm	Pore Diameter	3.318 nm

3.3.3 Pure water flux

A DI water feed solution was used to estimate the pure water flux of 1% to 3% kappa-carrageenan hydrogel mixed with 1% vanillin. Different hydrogel thicknesses were tested for optimal water flux and rejection. The best performance for 2 cm hydrogel regarding water flux and rejection was obtained. After 15 to 20 minutes of settling time, the permeate flux initiates as the water penetrates the kC-V hydrogel (Figure 3.4a), making channels through the gelatinous layer. The column height was fixed at 30 cm (0.29 bar), and the percentage of vanillin was kept at 1%. An increase in the concentration of vanillin from 2% to 3 % reduced the water flux due to the increased hydrogel's hydrophilicity enhanced by the vanillin, making the water difficult to permeate through or leave the matrix. Higher hydrophilic hydrogels will bind the water molecules inside the hydrogel, making it harder for the water to leave the porous hydrogel matrix (Sun et al., 2019). Initial tests were done for different hydrogel concentrations with different thicknesses, and water flux with DI water feed solution was evaluated, as presented in Figure 3.4b. The rejection tests with magnesium sulphate solutions were conducted for different hydrogel concentrations and thicknesses for process optimization, as presented in Figure 3.4c.

Hydrogels with 2 cm thickness exhibited better performance than smaller thicknesses; therefore, 2 cm thickness is the optimal hydrogel width for good water flux and rejection. Figure 3.4c presents the rejection of different hydrogel concentrations (1 to 3%) with

varying thicknesses. The best rejection was observed at 2 cm thickness for all the hydrogels. The rejection of 1% hydrogel was 36 ±2 %, followed by 48 ±2% for 2% hydrogel, and the highest rejection of 72 ±2% was observed for 3%. The rejection and water flux of the kC-V hydrogel can be tuned by changing the hydrogel thickness and or the kappa carrageenan concentration to achieve the desired water flux and concentration. In contrast, 1% and 2% hydrogels exhibited high water flux compared to the 3% hydrogel. The comparison of various hydrogel concentrations for 2 cm thickness is presented in Figure 3.4d. The highest water flux was obtained for 1% hydrogel (118 LMH), followed by 2% (104 LMH), and the lowest water flux was obtained for 3% kC hydrogel (85 LMH) (Figure 3.4d). Subsequently, higher concentrations of 4% of kC were also tested for water flux; however, the greater percentage of the kC hydrogel had insignificant water permeation even after one hour of the experiment and therefore was not further investigated.

The water permeation through the kC-V hydrogel can be attributed to the molecular structure of the kC-V hydrogel and the improved kC hydrogel hydrophilicity by vanillin. The pure kappa-carrageenan chemical consists of anionic sulphate ions. Due to electrostatic repulsions between these ions, the space between the polymer chain increases, leading to the penetration of water molecules through the hydrogel structure. Also, the mechanism of water permeation can be explained via the swelling process of the kC-V hydrogel. During the swelling process, the water penetrates the kC-V hydrogel's structure and is opposed by the elastic properties of the hydrogel, which tries to maintain the structure intact. The gravity filtration setup exerts additional pressure from the top, leading to a drag of the water across the hydrogel channels and hence the water flux across. Adding vanillin to the pure kappa-carrageenan improved the hydrogel's porosity,

as vanillin is a pore-forming agent. Furthermore, using vanillin can significantly influence the formation of pores and increase the permeation rate in filtration applications (R et al., 2017). The addition of vanillin also imparts a negative charge on the hydrogel surface and decreases the contact angle measurement (Yadav, Ibrar, Samal, et al., 2022b). The kC and vanillin have been successfully used in several membrane fabrication studies to improve membrane porosity and increase membrane hydrophilicity. Adding the kC and vanillin also led to enhanced membrane permeability and better antifouling properties (Alam et al., 2017; Yadav, Ibrar, Altaee, et al., 2022a). The main advantage of using the composite kC-V hydrogel in filtration processes is reducing desalination's energy requirements since the hydrogel operates under gravity. The only energy consumed in the process is during the synthesis of the kC-V hydrogel. The kC-V hydrogel operates in a dead-end mode; hence, no brine solution would be generated from filtration.

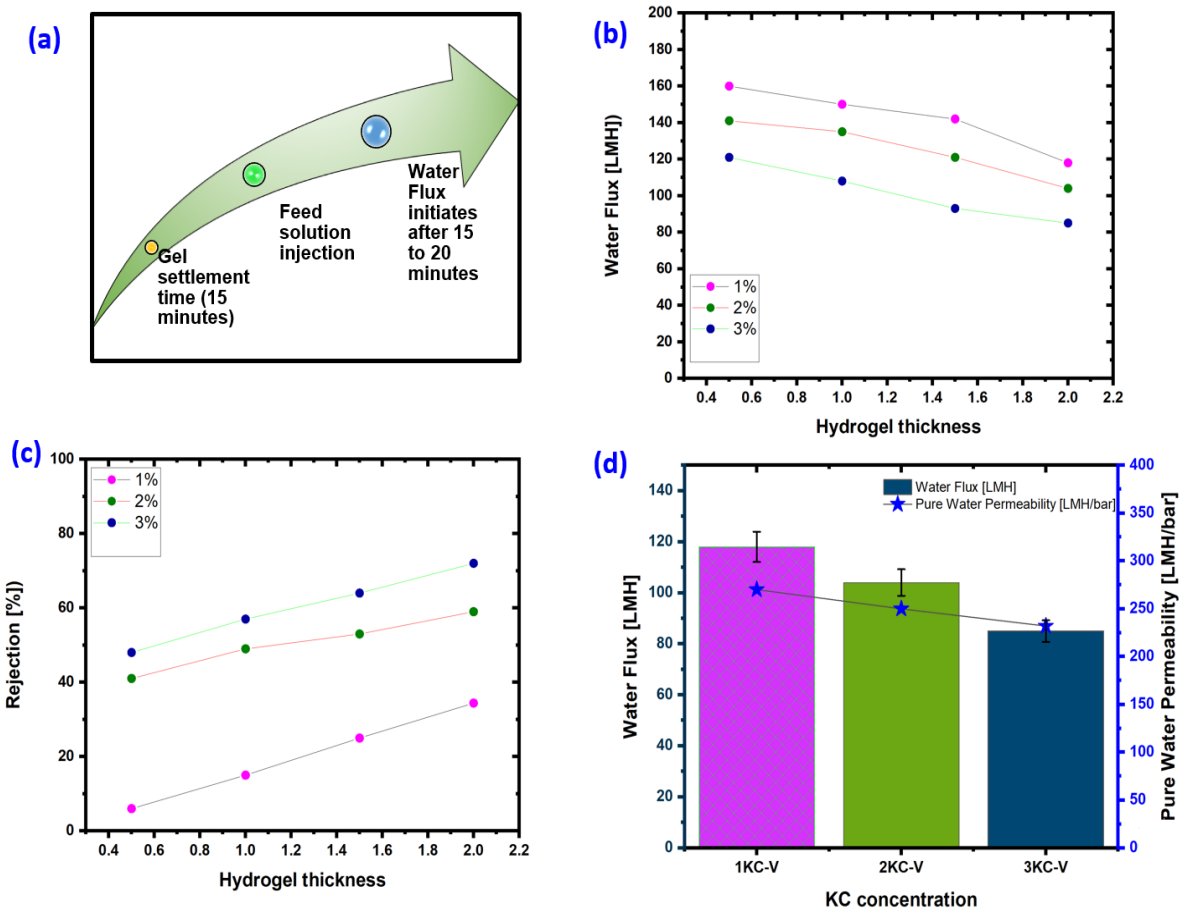


Figure3. 4.a) Hydrogel settlement time, b) Influence of hydrogel thickness on water flux with DI water feed solution, c) influence of hydrogel thickness on rejection, d) Pure water flux with DI water and Pure water permeability for different concentrations of kC-V hydrogel.

3.3.4 Rejection of NaCl and divalent ions

The NaCl water flux and rejection measurements were conducted using a 2 g/L NaCl feed solution. The highest rejection was obtained for the 3% kC-V hydrogel (42 ±5 %), followed by the 2% kC-V (13 ± 5%), and 1% kC-V hydrogel had the lowest NaCl rejection (5 ±2 %). The average water flux and the rejection of the 3% kC-V hydrogel are

presented in Figure 3.5. The 3% kC-V hydrogel has the best performance in terms of NaCl rejection, with an average water flux of 30.8 LMH under a 30 cm gravity head. This rejection is substantially higher than most of the hydrogels reported in the literature for NaCl rejection (K. Zhao et al., 2022).

Figure 3.5a also presents the water flux curves for 3% kC-V hydrogel for two representative divalent feed solutions, $CuSO_4$ and $MgSO_4$, both in a concentration of 2 g/L. The best performance for divalent ion rejection was obtained for 3% kC-V hydrogel. Lower percentages of 1% and 2% kappa-carrageenan had a very low rejection for divalent ions, around 29% for 2% hydrogel and 15% for 1% hydrogel, respectively, for the $MgSO_4$. The best performance was obtained for 3% kC-V hydrogel for $MgSO_4$ feed solution with an average water flux of 44 ± 3 LMH and rejection rate of 72 ± 2% (ICP-MS for Mg). An average water flux of 36 ±2 LMH was obtained for the $CuSO_4$ feed solution with a rejection rate of 76 ±2% (ICP-MS for Cu). Lower rejection of Mg^{2+} ions compared to the Cu^{2+} ions can be attributed to the smaller ionic radius of the Mg^{2+} ion (0.65 A) compared to 0.73A for the Cu^{2+} ion. High copper rejection is one of the main advantages of this filter media since most of the wastewater from different industries contains copper (Dil et al., 2017).

The rejection of the 3% hydrogel with 2 cm thickness was also investigated in three consecutive cycles, as presented in Figure S1.2 (Figure S1.2, Supplementary information, S1). Each cycle lasted one hour. At the end of each cycle, the DI water solution was filtered through the hydrogel for at least 15 minutes. A fresh solution was poured onto the hydrogel, and water flux and rejection were recorded again. The hydrogel maintained a water flux of 45 ±5 LMH and 74% ±4 rejection for three consecutive filtration cycles.

The mechanisms of pollutant rejection by the kC-V hydrogel include steric hindrance when particles are rejected because of their size, adsorption onto the hydrogel surface due to charge differences such as heavy metals, or Donnan exclusion. The latter mechanism applies to ionic species, for example, metal salts such as copper sulfate solution. The kC hydrogel contains immobile, negatively charged $–OH^-$ (hydroxyl) groups. On the hydrogel-copper sulfate solution interface, some SO_4^{2-} ions from the feed solution pass to the product water, while Cu^{2+} ions are rejected due to Donnan's potential. As such, the gel side of the interface will be negatively charged, and the solution side will be positively charged. Figure 3.5b shows the colour of the copper sulphate before filtration (B) and after filtration (A). The permeate water appears slightly yellowish, possibly due to the reaction of vanillin with the copper sulphate. However, it can be seen that the permeate seems quite transparent, indicating a high rejection of copper. Additional images of the permeate before and after filtration are presented in the supplementary information (Figure S1.2, Supplementary information S1). Figure 3.5c shows the kC-V hydrogel after filtration of $CuSO_4$. The 2 cm hydrogel thickness was cut into two parts, as shown in Figure 3.5d. Evidently, the Cu^{2+} ions were not rejected on the hydrogel surface since both parts of the hydrogel were stained in blue due to Cu^{2+} contamination. The results confirm that Cu^{2+} rejection was achieved by adsorption onto the kC-V hydrogel, as evident from the light blue colour of the hydrogel. Most copper treatment methods are expensive or require toxic solutions or solvents. The kC-V hydrogel can also recover copper ions from wastewater for reuse since contaminants will be trapped on the hydrogel materials in the dead-end filtration mode. Future studies could investigate the recovery of copper from wastewater, such as electroplating wastewater (Zhang et al., 2014), which contains high copper content.

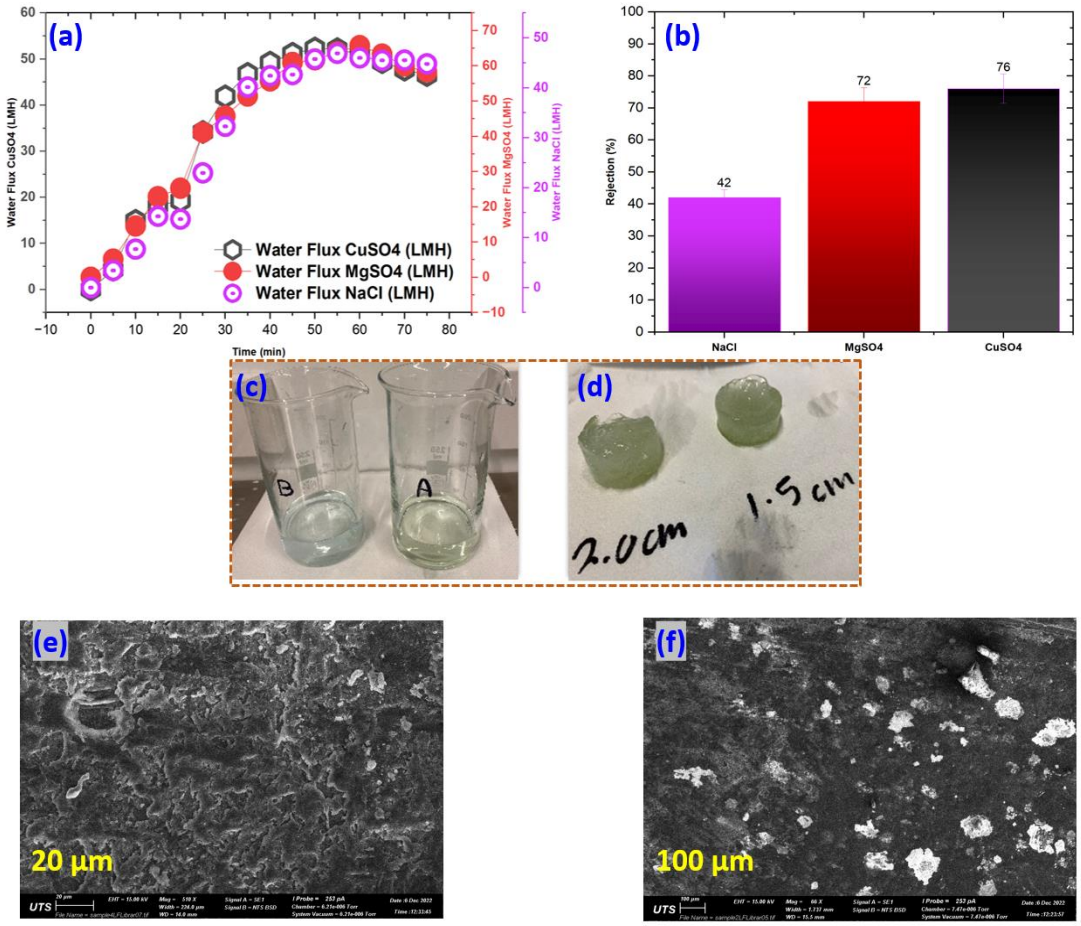


Figure3. 5.NaCl, MgSO4 and CuSO4 water flux and rejection using 2 g/L feed solution in separate experiments a) water flux, b) $CuSO_4$ solution before on the left, and CuSO4 solution after filtration, on the right, c) hydrogel after $CuSO_4$ filtration, d) gel after $CuSO_4$ filtration, e) SEM of the gel after $CuSO_4$ filtration at 200 µm, f) SEM of the gel after CuSO4 filtration at 100 µm.

3.3.5 Adsorption and desorption

The initial concentration of the adsorbate material influences the adsorption capacity. Figure 3.6 illustrates the influence of the initial adsorbate concentration of $CuSO_4$ on the adsorption of kC-V, demonstrating a direct correlation between the concentration of the

adsorbate and the extent of adsorption. The adsorption enhancement attributable to higher adsorbate concentrations can be ascribed to the increased availability of adsorption sites on the adsorbents and the heightened driving force from the amplified solute concentration. This intensified driving force facilitates the surmounting of mass transfer resistance between the solid and liquid phases (Mohammadzadeh Pakdel & Peighambardoust, 2018).

The experimental findings derived from dynamic adsorption experiments conducted with 3% kC-V are presented in Figure 3.6b. The maximum adsorption capacity was systematically investigated for Cu, and it was found that the gel has the maximum adsorption capacity of 1.22 mg/g for Cu. Initially, metal ions are rapidly extracted, signifying a high adsorption rate. However, as the system approaches equilibrium, the extraction rate gradually declines. This phenomenon can be explained by the proliferation of unoccupied sites accessible for adsorption during the early stages of the process. As the adsorbate molecules occupy these vacant sites, a repulsive force emerges between the adsorbate at the adsorbent site and those in the bulk phase, decelerating the adsorption process. Moreover, the rate at which adsorbate molecules are eliminated from the solution is governed by their transfer from surface sites to the interior regions of the adsorbent material (Zhang et al., 2014). Equilibrium is attained within 60 minutes for the examined metal ions, where adsorption and desorption rates reach a state of equilibrium.

The potential for reusing adsorbents in multiple cycles provides economic benefits by reducing the cost associated with the adsorption process. This reusability feature is particularly advantageous for large-scale industrial applications. Three adsorption-desorption cycles were conducted using 2000 mg/L $CuSO_4$ feed concentration to investigate the adsorption/desorption performance of the hydrogel for Cu^{2+} ions. The

percentage of copper removal during the three cycles was 81.9 ± 2 %, 80.03 ±2 %, and 75.43 ±2 %. Furthermore, the desorption concentration for the three cycles was 80.68 ± 1.5 %, 78.85 ±2 %, and 73.09 ±1%, respectively, as shown in Figure **3.6c**. The results show that the hydrogel adsorption performance can be recovered significantly in multiple filtration cycles. The hydrogel's desorption mechanism involves releasing previously adsorbed or absorbed Cu^{2+} ions. This can be achieved through various mechanisms, including diffusion, exchange reactions, solvent effects, or external stimuli. Diffusion relies on concentration gradients, where the adsorbed Cu^{2+} ions move from high-concentration areas to lower-concentration regions. Exchange reactions occur when species with higher affinity displace the previously adsorbed ones. Solvents can influence desorption by affecting the interactions between hydrogels and adsorbed species.

Additionally, external stimuli such as changes in temperature or pH can induce structural modifications in the hydrogel, leading to the release of the adsorbed species. In the case of an acidic solution, the presence of protons competes with the binding sites of the adsorbents, weakening the interaction between the adsorbents and the targeted Cu^{2+} ions. Therefore, the adsorbed Cu^{2+} ions are effectively released, highlighting the impact of solution conditions on the desorption process. Overall, the 3kC-V hydrogel membrane exhibits promising performance in terms of its ability to be repeatedly used for filtration, as demonstrated by its good desorption efficiency during consecutive cycles.

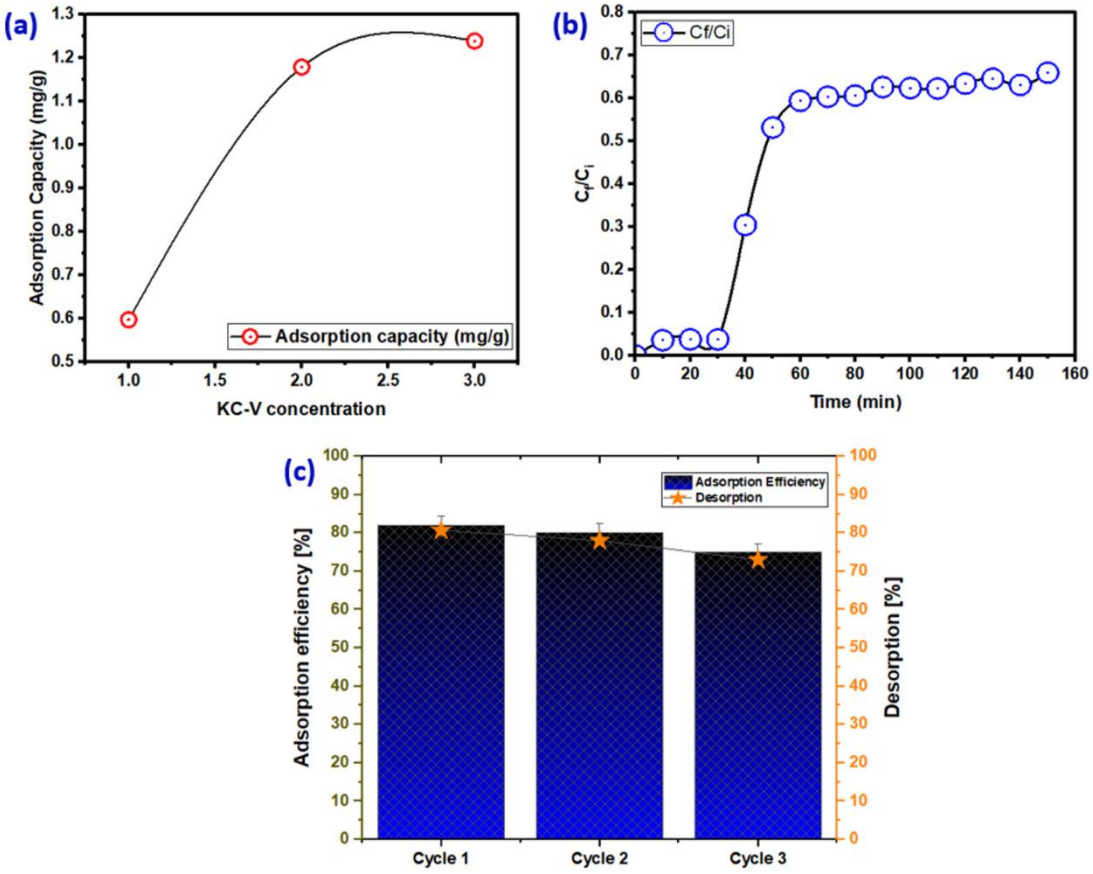


Figure3.6.Adsorption experiments for $CuSO_4$ solution, a) influence of kC-V concentrations on adsorption of $CuSO_4$, b) adsorption curve for 3kC-V hydrogel for $CuSO_4$, c) adsorption and desorption of $CuSO_4$ in three consecutive cycles.

3.3.6 Landfill leachate treatment

Due to its strong metal binding capacity, kappa-carrageenan has been used to create drugs to remove heavy metal ions from the human body (Khotimchenko et al., 2010). The feasibility of the kC-V hydrogel filtration for heavy metal separation was evaluated using real landfill leachate wastewater. The landfill leachate wastewater was analyzed through a Malvern Particle analyzer for size distribution, as shown in Figure 3.7. The particle size of the landfill leachate wastewater falls in the two ranges from 0 to 20 nm and 40 to 100 nm.

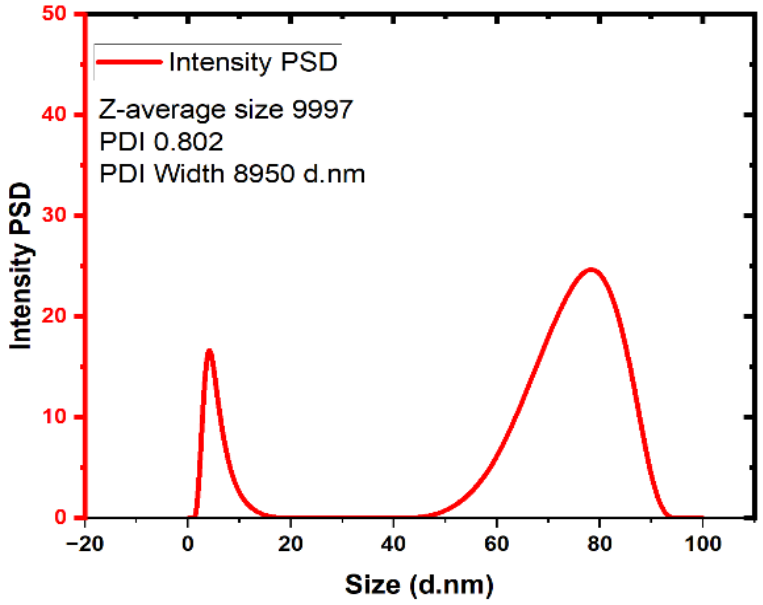


Figure3.7.Particle size distribution of the landfill leachate wastewater conducted through the Malvern Particle Analyser

The filtration of the landfill leachate wastewater with the hydrogel resulted in a high water flux (Figure 3.8a), colour removal (Figure 3.8b) and a high rejection of total organic carbon (77±3 %), 92% turbidity removal, 60-73% TDS removal and 95-99% (Figure 3.8d). The turbidity removal mechanism involves the steric hindrance mechanism when particles are rejected because they are larger than the hydrogel pore size (circa 2.5 nm). The filtration of feed solution with the kappa-carrageenan-vanillin composite filter left no landfill leachate wastewater/or brine solution behind. The hydrogel achieved high water flux, excellent turbidity, and an organic matter rejection rate. These features are particularly important for treating wastewater, where the waste contains potentially toxic materials, and their management is highly regulated, critical, and costly. Figure 3.8c reveals the SEM micrographs of the hydrogel after the landfill leachate treatment. The white crystalline structures can be attributed to the fouling due to inorganic contaminants

in the landfill leachate wastewater. Figure 3.8b shows the water flux and the landfill leachate colour before (B) and after treatment (A). The landfill leachate is more transparent than the yellowish appearance before. An average flux of 26 ±3 LMH was obtained for the landfill leachate wastewater (Figure 3.8a). During the 80 minutes operation for landfill leachate wastewater, 24.5 mL was recovered from 100 mL in 80 minutes, and a 100% recovery rate was achieved at the end of the filtration process. Water flux in the kC-V hydrogel is governed by the Grouthuss mechanism, where proton (H+) and hydroxyl ions (OH-) (Figure 3.8e) diffuse through the hydrogen-bonded network of kappa-carrageenan and vanillin hydrogel via the formation and simultaneous cleavage of covalent bonds between neighbouring molecules. Further, the transport mechanism is believed to include Eigen to Zundel to Eigen (E–Z–E) and Zundel to Zundel (Z–Z) mechanisms.

Heavy metal ions were rejected in the following order: Pb>Ba>Al>Cr>Cd (Figure 3.8d). The lowest rejection amongst all the heavy metals was for the Cd^{2+} ion, attributed to the competitive adsorption of different heavy metals and their affinity to the hydrogel molecules. The rejection efficiency ranges from 65-75% for heavy metal removal. Amongst all the heavy metals, the highest rejection was for the Pb^{2+} ion, probably due to the larger ionic radius of the Pb^{2+} ion compared to the other ions. For divalent ions in the landfill feed solution, the rejection of Mg^{2+} was slightly higher than that of Ca^{2+} ions. The interplay of different ions simultaneously in the landfill leachate wastewater can also affect the rejection efficiency of each ion. The rejection for Mg^{2+} ions in the landfill leachate wastewater was 88 ±5 % higher than when the synthetic $MgSO_4$ feed solution (section 3.5) and can be attributed to the bridging of Mg^{2+} ion to the high organic content (TOC of the landfill in Table 1) in the landfill leachate wastewater, leading to the higher

rejection. Energy dispersive X-ray (EDX) analysis was conducted for the hydrogel's top surface and middle part to get insights into the rejection.

All the experiments were conducted at neutral pH (7-8) since the kC-V hydrogel is more stable at this pH range and has a high affinity towards heavy metal ions. In effect, several synergistic mechanisms, such as adsorption, ion exchange and chelation, can govern the hydrogel rejection of metal ions. As an ionic carrageenan polysaccharide, kappa-carrageenan is significantly affected by other charged species in solution that can reorient the conformation from ordered to disordered. By forming bridges with the cation at its d-galactose sulphate group and interacting electrostatically with an anhydrous-O-3,6 ring of another d-galactose ring, it demonstrates high sensitivity to several metal ions. Kappa-carrageenan has been shown to have a high affinity for binding to heavy metals such as cadmium, lead, and mercury. This property is due to sulphate groups in the kappa-carrageenan molecule, which can form coordinated covalent bonds with heavy metal ions (Alam et al., 2017). The binding of kappa-carrageenan with heavy metal ions can also be attributed to chelation. The chelation process involves the formation of coordination bonds between the sulphate groups on kappa-carrageenan and the heavy metal ions. These bonds can be quite strong and help remove heavy metals from the solution by forming insoluble complexes easily removed through filtration or sedimentation. In addition to its chelation properties, kappa-carrageenan also can sequester heavy metals by adsorption. This process involves the physical binding of heavy metal ions to the surface of kappa-carrageenan without forming coordination bonds.

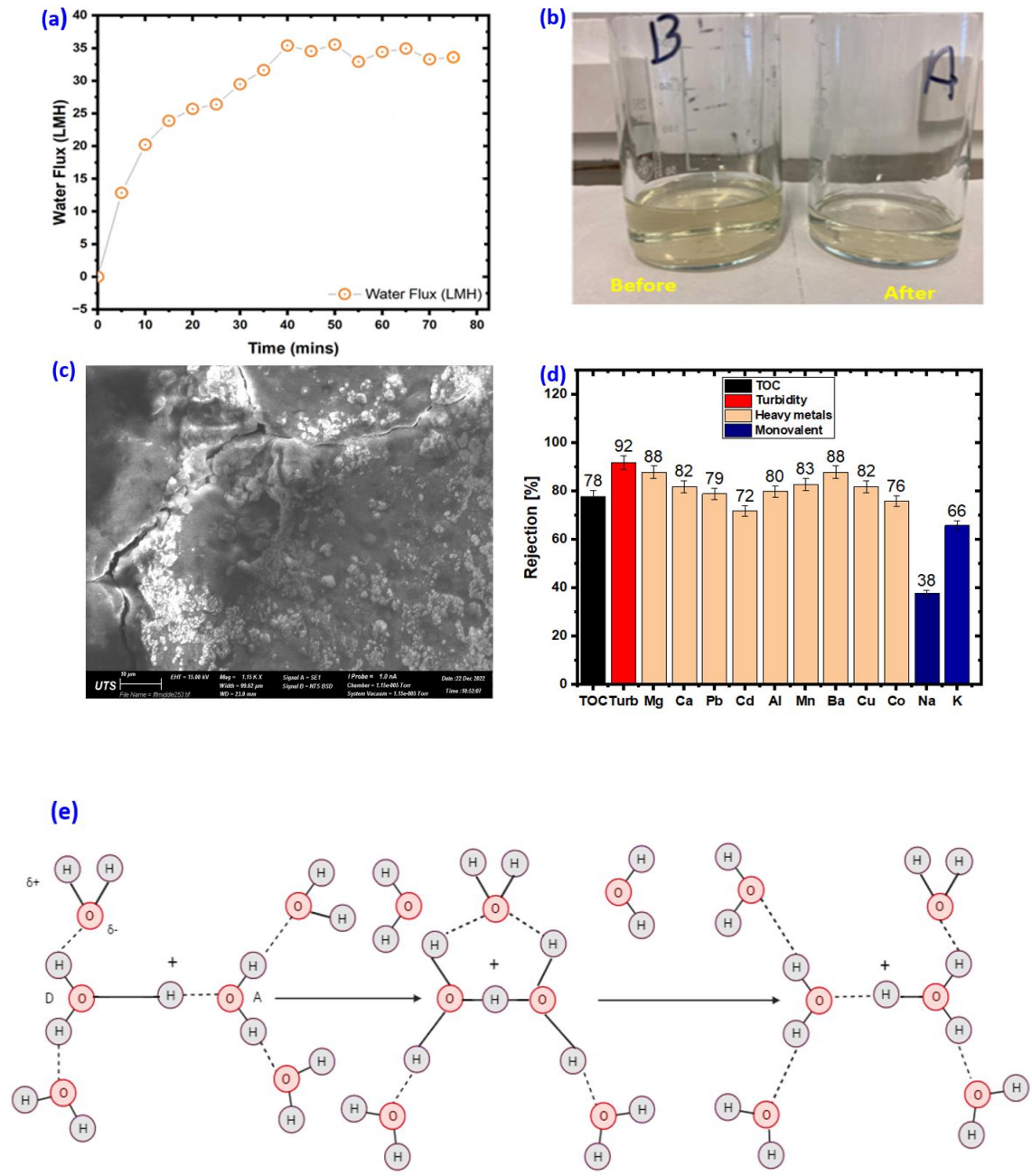


Figure3. 8.a) Water flux (LMH) of the landfill leachate wastewater, b) Colour rejection, c) SEM analysis of fouled hydrogel, d) Rejection of heavy metal ions from the landfill leachate wastewater, e) Grothus mechanism for H^+ and OH^- ion diffusion.

In addition to heavy metals binding to sulphate ions, the kC-V rejection mechanism also includes the Donnan exclusion theory mentioned in section 3.5. The binding of heavy metals to kappa-carrageenan can have several beneficial applications. For example, it can be used as a means of removing heavy metals from contaminated water sources or as a way of reducing the levels of heavy metals in food products. Based on these properties, the kC-V hydrogel can be a viable option for wastewater with heavy metals, such as landfill leachate wastewater. Figures 3.9a and 3.9b present the EDS analysis of the top surface and middle section of the kC-V hydrogel after the landfill treatment. The highest intensities in the EDS spectrum are obtained for Cr, Mn and Fe ions. Besides these elements, Al, Cu, Ca, and Si were the main occupants of the hydrogel after filtration. The SEM and EDS of the middle part of the hydrogel after landfill leachate filtration show much sharper peaks and intensities compared to the top surface (Figure 3.9b).

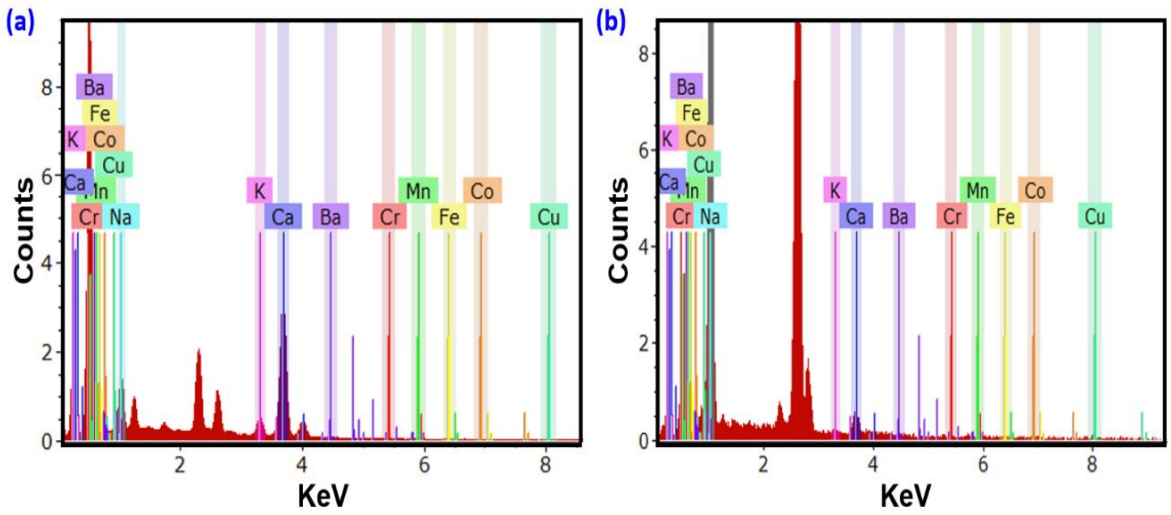


Figure3. 9.EDX analysis of hydrogel after filtration with landfill leachate wastewater, a) top surface of the hydrogel, b) inner section of the hydrogel.

Further analysis was conducted through FT-IR spectroscopy. The FT-IR spectra (Figure S1.4, Supplementary Information, S1) show several peaks diminished in the landfill leachate wastewater fouled hydrogel spectrum compared to the kC-V spectrum. A slight stretching is observed in the peak at the wavenumber 3765 cm^{-1} (O-H stretching, alcohol) and 3155 cm^{-1} for the kC-V hydrogel after the landfill leachate wastewater treatment, which is attributed to several polysaccharides in the landfill, leachate wastewater or protein fouling. The peaks at 3271 cm^{-1}, 2900 cm^{-1} and 2260 cm^{-1} are completely diminished. The diminished peak at 2900 cm^{-1} reveals the presence of humic acid fouling from the landfill leachate wastewater.

3.3.7 Commercial implications

The kC-V hydrogel technology is an inexpensive and simple method for wastewater treatment that operates in dead-end filtration to minimize brine waste generation. Unlike pressure-driven membranes such as reverse osmosis, kC-V does not require expensive infrastructure and is easy to use. It is a suitable method for wastewater treatment and freshwater supply for remote areas or when infrastructures are unavailable. Compared to existing treatment technologies such as reverse osmosis, composite hydrogel filter technology is cost-effective, made of biodegradable materials and requires low energy. The specific power consumption (Es) is a function of feed pressure (P), pump efficiency (η), feed flow rate (Q_f) and the permeate flow rate (Q_p) as the following:

$$E_s = \frac{Q_f * P}{n * Q_p} \tag{3.14}$$

The kC-V hydrogel has high water flux, excellent turbidity, and organic matter removal. These features are particularly important for treating wastewater, where the waste contains potentially toxic materials, and their management is highly regulated and costly. The gravity-driven kC-V hydrogel requires less than 1 bar compared to 10 to 30 bar for RO membranes (Zhou et al., 2012).Table 6compares the current hydrogel filtration technology with the RO. The specific energy required for wastewater treatment by advanced RO technology is between 0.8 kWh/m^3 and 1.6 kWh/m^3 (Wakeel et al., 2016). RO recovery rate in the wastewater treatment plant could reach 85%, depending on the feed characteristics. For example, for an RO system processing wastewaters of variable feed concentrations at 30 bar, recovery rates between 75% to 85%, and pump efficiency of 0.8%, the expected specific power consumption will range from 1.39 kWh/m^3 to 1.23 kWh/m^3, which is in the range reported in the literature. In contrast, the specific power consumption of the kC-V for leachate wastewater treatment at 1 bar was about 0.034 kWh/m^3, significantly reducing power consumption and greenhouse emissions. With a dead-end filtration process, the recovery rate is almost 100%, eliminating brine waste generation.

Another main issue in pressure-driven membrane processes such as reverse osmosis is the fouling and scaling of membranes, and eventually, reverse osmosis membranes require replacement. The cost of the kC-V hydrogel is very cheap (1$ per m^2) and, therefore, would be very economical for commercial applications. Moreover, the kC-V hydrogel can recover valuable resources in future applications, such as lithium-ion from brine and precious metal from industrial wastewater. Industrial wastewaters, contaminated groundwaters, hospital wastewater, food processing wastewater, and pharmaceutical wastewater are among the wastewater types suitable for the kC-V

hydrogel filter treatment. Many businesses could benefit from this new technology for wastewater treatment to reduce the treatment cost while meeting the environmental guidelines of wastewater disposal. The hydrogel filter's technology lends itself to treating wastewater containing heavy metal ions and organic matter, as the hydrogel and vanillin materials have an affinity to heavy metals and organic matter.

Table3. 3:Comparison of hydrogel filtration driven by gravity vs RO.

Technology	**Membrane fabrication**	**Membrane mechanical strength**	**Lifetime**	**Emissions**	**Equipment**	**Energy consumption kWh/m^3**	**Pressure Required**	**Membrane cost per 1m^2**
Reverse osmosis	Complicated and requires expensive infrastructure	High	6 months	High	Expensive infrastructure	0.8 to 1.6	1 to 30 bars	102-238$ (Sterlitech Corporation, WA, USA, 2023)
kC-V Hydrogel	Easy	Low	Low lifetime	Low emissions	Cheap and easy to operate	0.034	0.1 to 1 bar	1$

3.4 Conclusion

Kappa-carrageenan-vanillin composite hydrogel filter was investigated for the treatment of ions and wastewater. The composite filter shows great potential in contaminants removal from synthetic and natural landfill leachate feed solutions. Furthermore, the gravity filtration in a dead-end mode of feed solution with the kappa-carrageenan-vanillin composite filter leaves no wastewater stream that often occurs in conventional membrane filtration processes. This advantage is an important feature in the developed composite hydrogel filter to reduce or eliminate the environmental impact of the treatment method. Compared to existing treatment technologies, composite hydrogel filter technology is cost-effective, easy to use, environmentally friendly, and low-energy process for wastewater treatment. The hydrogel's water flux decreased with increasing its concentration from 1 to 3%, whilst its rejection increased. Amongst all the hydrogels, the 3% kC-V hydrogel achieved a rejection of 80% ±5 for divalent ions and 42%±5 for monovalent ions. Moreover, the hydrogel exhibited a high-water flux, between 30.8 L/m^2h and 44 L/m^2h for synthetic feed solutions and 26 L/m^2h for leachate wastewater, and an excellent rejection rate to turbidity, organic matter, and metal ions. These features are particularly important for treating biomedical, and hospital wastewater, where the waste contains potentially infectious materials and their management is highly regulated, critical, and costly. The hydrogel filter media can be retrofitted in existing wastewater treatment as a polishing stage to remove recalcitrant pollutants. The hydrogel has weak mechanical strength, and long-term stability should be explored in future studies. The mechanical strength can be improved by adding different additives to the kappa-carrageenan in the fabrication process. Future research will also focus on tuning the hydrogel for different types of wastewater treatment and optimizing operational

parameters. Furthermore, it is important to study fouling mitigation and investigate the hydrogel for valuable resource recovery from different types of waste streams.

Supplementary information S1

Kappa Carrageenan-Vanillin Composite Hydrogel for Landfill Leachate Wastewater Treatment

Ibrar Ibrar[1$], Lilyan Alsaka[1$], Sudesh Yadav[1], Ali Altaee[1*], John L Zhou[1], Ho Kyong Shon[1]

$: Equal effort



Figure S1. 1.Hydrogel shrinking.

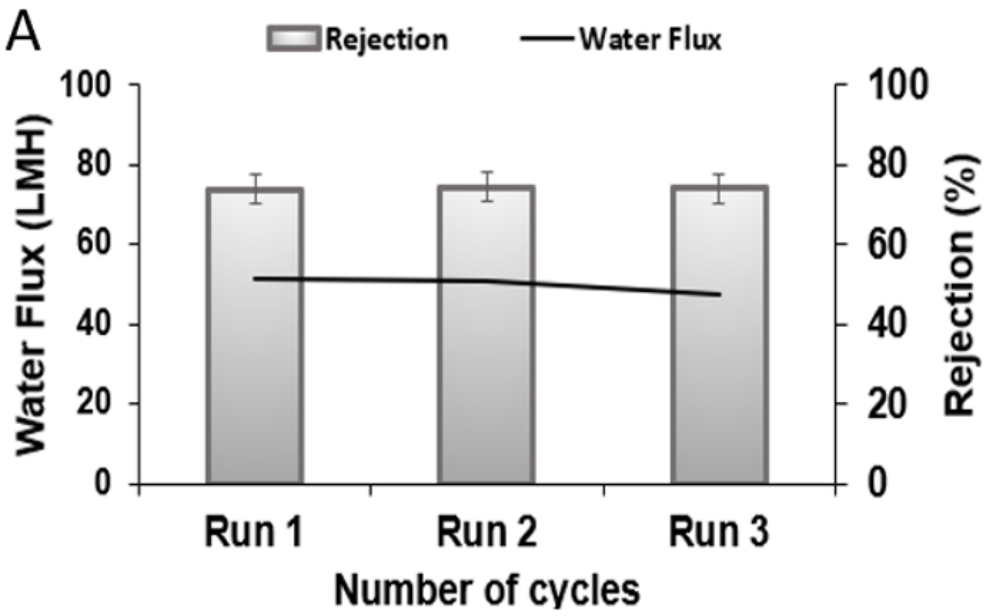


Figure S1. 2.Rejection in multiple cycles

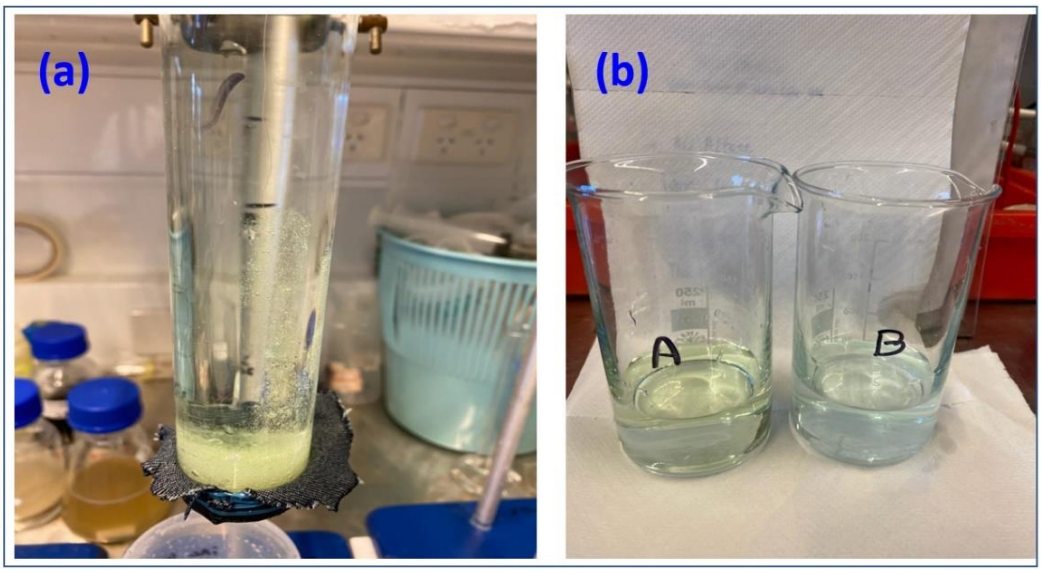


Figure S1. 3. Copper sulphate filtration, a) a snapshot of filtration, b) $CuSO_4$ after filtration on the left, $CuSO_4$ before filtration on the right.

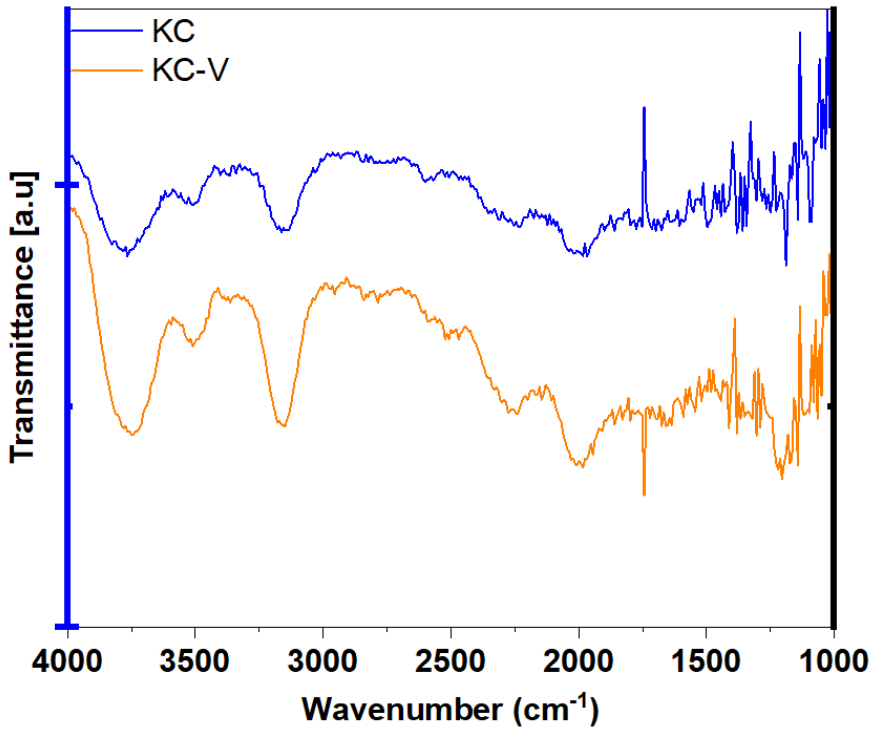


Figure S1. 4. Comparison of FT-IR spectra of kC-V gel before and after landfill treatment.

Chapter 4: Performance and analysis of kappa-carrageenan hydrogel for PFOA-contaminated soil remediation wastewater treatment

Alsaka, L., Ibrar, I., Altaee, A., Zhou, J., Chowdhury, M. H., Maryam, A.-E., & Hawari, A. H. (2024). Performance and analysis of kappa-carrageenan hydrogel for PFOA-contaminated soil remediation wastewater treatment. *Chemosphere*, *365*, 143371.

Author contributions statement:

Lilyan Alsaka: Investigation, conceptualization, Data Analysis and curation, Validation, Writing –original draft, Writing – review and editing. Ibrar Ibrar: Investigation, Data Analysis and curation, writing. Ali Altaee: Supervision, Methodology, Conceptualization, Funding, Investigation, data analysis and curation, Writing – review, and editing. John Zhou: Supervision, Data curation, Writing– review and editing. Mahedy Hasan Chowdhury: Data analysis, Data Curation. Maryam AL-Ejji: Investigation, Data analysis, Funding. Alaa H. Hawari: Data analysis, Funding, Writing – review and editing.

Abstract

Perfluorooctanoic acid is an emerging pollutant with exceptional resistance to degradation and detrimental environmental and health impacts. Conventional physical and chemical processes for Perfluorooctanoic acid are either expensive or inefficient. This study developed an environmentally sustainable and cost-effective gravity-driven kappa-carrageenan (kC)-based hydrogel for perfluorooctanoic acid (PFOA) removal from

synthetic and actual wastewater. Two kC filters were prepared by mixing activated carbon (AC) or vanillin (V) with the kC hydrogel to optimize the hydrogel selectivity and water permeability. Experimental work revealed that the PFOA rejection and water permeability increased with the AC and V concentrations in the kC hydrogel. Experiments also evaluated the impact of feed pH, PFOA concentration, hydrogel composition, and hydrogel thickness on its performance. Due to pore size shrinkage, the AC-kC and V-kC hydrogels achieved the highest PFOA rejection at pH 4, whereas the water flux decreased. Increasing the PFOA concentration reduced water flux and increased PFOA rejection. For 2 cm hydrogel thickness, the water flux of 3%kC-0.3%AC and 3%kC-3%V hydrogels was 25.6 LMH and 21.5 LMH, and the corresponding PFOA rejection was 86.9% for 3%kC-0.3%AC and 85.7% for 3%kC-3%V. Finally, the kC-0.3%AC hydrogel removed 81.1% of PFOA from wastewater of 179 mg/L initial concentration compared to 79.3% for the kC-3%V hydrogel. After three filtration cycles, the water flux decline of 3%kC-0.3%AC was less than 10%. The gravity dead-end kC hydrogel provides sustainable PFOA wastewater treatment with biodegradable and natural materials.

4.1 Introduction

Polyfluoroalkyl substances (PFAS) are synthetic compounds widely utilized for their water and grease resistance and thermal stability in diverse industrial and consumer applications. Characterized by robust fluorine-carbon bonds, PFAS exhibit exceptional chemical stability, contributing to their persistence in the environment. PFAS are categorized into perfluoroalkyl sulfonates (PFAS) and perfluoroalkyl carboxylates (PFCA). Despite their versatility, PFAS have raised environmental concerns due to their pervasive presence and potential adverse effects on human health and ecosystems globally. Consequently, developing effective PFOA removal strategies has become an

area of intense research and innovation (Buck et al., 2011; Milley et al., 2018; Zheng et al., 2017). PFOA, typically found at low concentrations, is treated by one of these methods: adsorption, ion exchange, or membrane filtration (Appleman et al., 2014). Adsorbents used for PFAS treatment include activated carbon (AC), silica, zeolites, aminated rice husk, g-C_3N_4, MOFs, COFs, and modified chitosan(Lei, 2023). PFAS adsorption relies on electrostatic and hydrophobic forces influenced by molecular structure and physicochemical properties. Solution pH, regeneration costs, and ionic strength affect the adsorption broad application for PFAS treatment. Also, short-chain PFAS (<C6) presents difficulties for conventional adsorbers like AC (Das & Ronen, 2022).

Several studies recommended nanofiltration (NF) and reverse osmosis (RO) for PFAS treatment, knowing that RO outperforms NF membranes for PFAS rejection. RO membranes consistently exhibit rejection rates of over 99% for multiple PFAS species, including PFOS, PFHxA, PFOA, and PFDA (Tang et al., 2006; Zeng, Tanaka, Suzuki, Yukioka, et al., 2017), in contrast to approximately 95% rejection observed with NF membranes (Franke et al., 2019; Tang et al., 2006). In a study by (Flores et al., 2013), RO effectively removed over 99% of fluorinated compounds (PFOA and PFOS) from wastewater, resulting in trace concentrations (PFOA <4.2–5.5 ng/L, PFOS 3–21 ng/L) below the US-recommended limit for drinking water (70 ng/L). However, it is crucial to note that while membrane technologies, particularly RO, are highly effective, they pose economic challenges, and handling residual PFAS concentrate remains problematic.

Recent focus has been on innovative hydrogel substances derived from natural and synthetic polymer sorbents for addressing PFAS contamination in aqueous environments. The adsorption of PFOA to chitosan and ethylene glycol exhibits a maximum capacity

adsorption of 1275.9 mg/g, rendering them attractive adsorbents for PFOA removal from wastewater (Long et al., 2019). For example, hydrogel based on poly(acrylamide) with incorporated powdered AC demonstrated removal efficiencies of up to 98% for perfluorooctanoic sulfonic acid (PFOS) and 96% for perfluorooctanoic acid (PFOA) (Klaus et al., 2023). Ateia et al. reported the functionalized cellulose achieved a rapid 70–80% removal of PFOA and PFOS within the first 100 seconds (Ateia et al., 2019). Researchers enhanced PFAS affinity by incorporating ionic fluorogels through thermally initiated radical copolymerization of perfluoropolyethers PFPE with methacrylate chain-end functionality (Fluorolink MD 700) and an amine-containing monomer (2-dimethylaminoethyl methacrylate, DMAEMA). This approach achieved >95% removal of diverse PFAS, including PFOA and PFOS, from wastewater treatment plant samples (Kumarasamy et al., 2020). Chitosan, a polysaccharide containing amine groups, manifests adsorptive properties concerning PFAS through ionic interactions involving the carboxylic/sulfonic groups of PFAS and the cationic groups inherent in the polymer (Zhang et al., 2011). Crosslinking with epoxy epichlorohydrin (ECH) enhances affinity, forming a molecularly imprinted hydrogel that adsorbs over 50% of PFAS, even in competing pollutants (Yu et al., 2008).

Kappa-carrageenan (kC) is another polysaccharide widely used in adsorption and membrane filtration. It has a robust gel-forming capacity due to its helicoidal shape, which plays a crucial role in gelation (Liu & Li, 2016). Ibrar and co-workers developed a kC-vanillin hydrogel filter for landfill leachate wastewater treatment, which achieved a 27 LMH water flux, 77% rejection of organic carbon (TOC), and 95% for color removal (Ibrar et al., 2023). Esmaeili et al. (2020) enhanced polyethersulfone (PES) membrane hydrophilicity and antifouling properties by incorporating 6 wt% vanillin, resulting in a

40% increase in water flux compared to the control (Esmaeili et al., 2020). The study examined the influence of kC content in PVDF/kC composite membranes and found that 1.0 wt% of kCg significantly improved membrane properties, enhancing characteristics and increasing dye rejection and water permeance (J. Alam et al., 2019). Yadav et al. (2022) enhanced a nanofiltration (NF) membrane with a kC-GO solution for leachate wastewater treatment, achieving a 95.73% water flux recovery and reduced fouling compared to the uncoated NF membrane.

Although kC was investigated for wastewater treatment, studies on kC applications for PFAS removal from wastewater are scarce. kC, with excellent characteristics, such as plenty of functional groups, high adsorption capacity, biodegradable, thermal stability, outstanding mechanical strength, and exceptional gelling mechanisms, would be suitable for treatment from organic and inorganic pollutants (Ibrar et al., 2023). This study has developed novel gravity-driven kC-based hydrogel filters that operate in dead-end mode for PFOA removal from aqueous solutions. The dead-end filtration mode will facilitate hydrogel recovery at the end of the filtration process. The kC hydrogels were mixed with AC and vanillin (V) nanoparticles to improve their adsorption capacity. Two hydrogel filters, kC-vanillin (kC-V) and kC-AC, were investigated for PFOA treatment. kC-V, already used for ions removal from leachate wastewater, will be tested for PFOA removal. Vanillin was used as a crosslinker and pore-forming agent to enhance the hydrophilicity and water permeability of the hydrogel. Besides, the kC-AC hydrogel filter was investigated for the first time for PFOA treatment. Adding AC to hydrogel improved the hydrogel water permeability and adsorption capacity. A parametric study evaluated the impact of feed concentration, hydrogel thickness, and feed pH on PFOA removal. The research questions for this study are: i) What is the efficacy of kC-V and kC-AC hydrogels

as filters for PFOA removal from aqueous solutions? ii) What is the influence of vanillin and AC concentration on kC hydrogel performance, and iii) What is the capability of kC hydrogels to treat PFOA-contaminated wastewater from soil remediation? The outcomes of this study will provide data about the feasibility of applying a kC-based gravity hydrogel filter as a potential technology for PFOA treatment. Furthermore, kC is environmentally friendly, cost-effective, and biodegradable, making it a sustainable water purifying option.

4.2 Material and methods

4.2.1 Materials

All materials in this research were procured from Sigma Aldrich Australia. The sulphated plant polysaccharide (kC), vanillin, and AC were acquired from the Australian branch of Sigma-Aldrich and utilized in all experimental methods. The perfluorooctanoic solution (POFA) was prepared with different concentrations of 0.5, 1, and 1.5 mg/L to test it with the novel membrane filter to find the efficiency of rejection and flux. Polyvinyl alcohol solution (PVA) was obtained from Sigma Aldrich, Australia.

4.2.2 Hydrogel fabrication

The kC hydrogel was prepared by dissolving 3 g in 100 mL (3% wt/v) of kC powder in deionized (DI) water. The dissolution process took place at temperatures between 60-80 °C. The mixture was then continuously stirred on a magnetic stirrer for 3 hours at 800 rpm, forming a homogeneous hydrogelatinous solution (Figure 4.1). It is worth noting that the hydrogelling temperature for kC typically falls within the range of 60-80 °C. Observations revealed that utilizing a higher temperature of 80 °C significantly impacted

the separation performance of the hydrogel, which led to the formation of a more rigid hydrogel structure, the result of quick blockage of the filtration system.

In contrast, hydrogels synthesized at a lower temperature of 60 °C exhibited improved separation performance due to their comparatively softer and more flexible nature. The hydrogel was then subjected to purification steps, such as washing with DI water, to remove residual impurities. Finally, the hydrogel was characterized using various techniques, such as rheological analysis, microscopy, and spectroscopy, to evaluate it.

In a controlled experiment, 1%, 2%, and 3% vanillin and 0.1%, 0.2%, and 0.3% AC powder (weight/volume) were individually dissolved in deionized water (Figure4.1). The solutions were then incorporated into separate hydrogel matrices through vigorous mixing using a shaker apparatus. When kC was combined with either vanillin or AC, the respective molecules became entrapped within the three-dimensional structure of kC, forming distinct complexes. This complexation process led to notable alterations in the physical properties of kC, encompassing changes in viscosity and mechanical strength. Moreover, vanillin and AC exhibited specific interactions with kC chains, including hydrogen bonding, electrostatic attractions, and hydrophobic interactions. In the case of vanillin, hydrogen bonds formed between the sulphate groups of kC and the hydroxyl groups of vanillin, while AC showed adsorption onto the surface of kC. These interactions played pivotal roles in influencing the overall structure and properties of the respective composite materials. The kC-V and kC-AC hydrogel were carefully layered onto fabric support within a plexiglass column filtration setup 30cm in height. With a filtration area of 0.0007 m^2, the hydrogel was given 10–15 minutes to settle and hydrate. Observational data revealed that water seepage through the column walls was occurring, potentially diminishing the efficacy of the filtration process. To address this issue, a PVA solution

was applied to the outer edges of the hydrogel. Subsequently, pure water was introduced slowly to prevent any disruption to the hydrogel structure, ensuring optimal performance Figure S2.1.

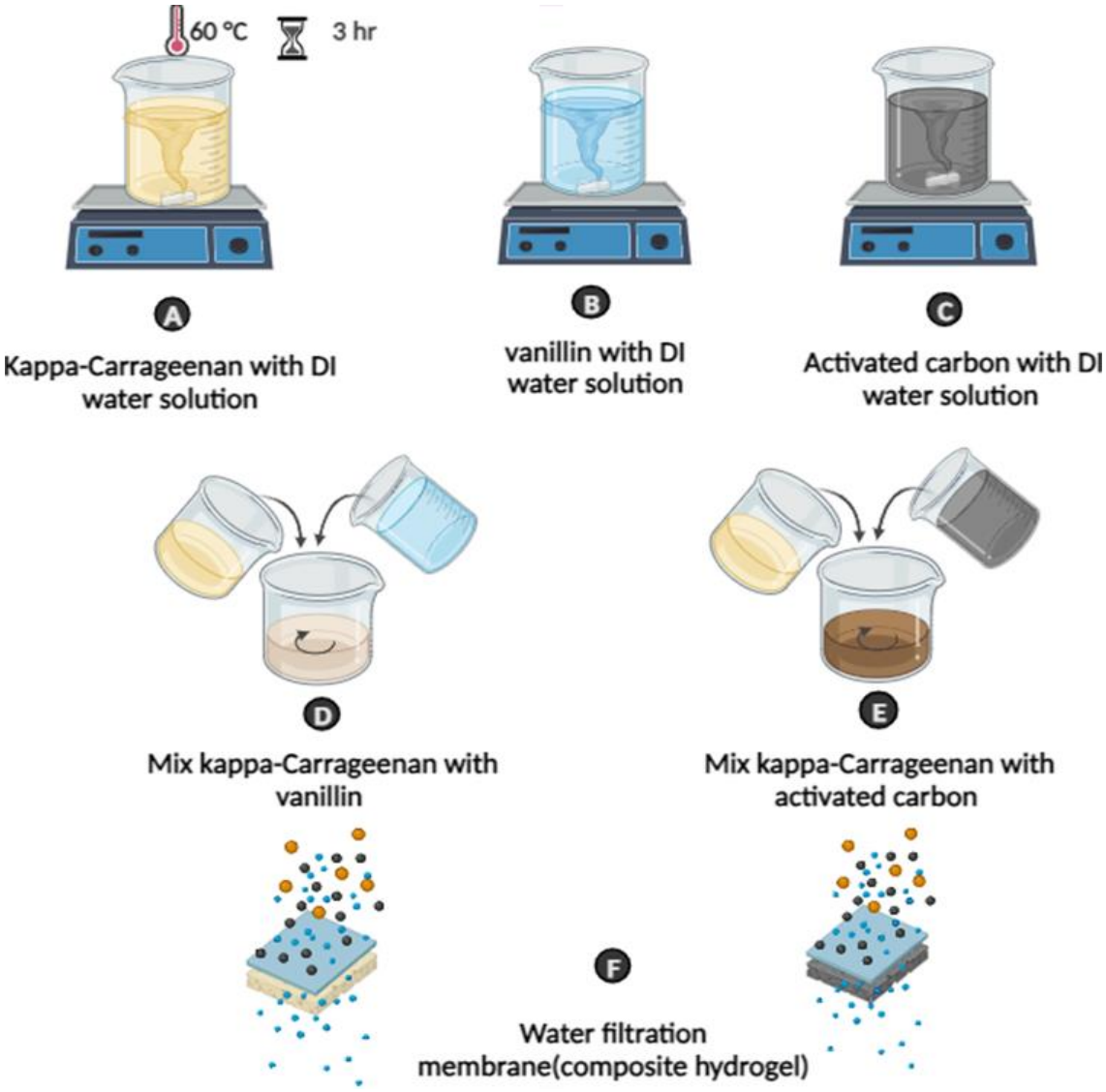


Figure 4. 1.Hydrogel Fabrication

4.2.3 PFOA analysis

PFOA in water samples was analyzed by a triple quadrupole ultra-high-performance liquid chromatograph-tandem mass spectrometer (UHPLC-MS/MS) from Shimadzu

(model 8060), following a method by Xu et al. (2020)(Xu et al., 2020). Compound separation was through a Shim-pack column (1.6 μm, 2.0 mm × 50 mm), using mobile phase A (Milli-Q water) and mobile phase B (methanol). Under a flow rate of 0.4 mL min^{-1}, samples of 1 μL were injected. The elution of PFOA from samples began with 50% B for 2.5 min, then 100% B for the next 1 min, followed by 50% B for another 1.5 min, with a total run time of 5 min. The mass spectrometer was operated in multiple reaction monitoring mode, using ions (*m/z* 169.1, *m/z* 219.0) as the qualitative ions and ion (*m/z* 369.0) as the quantitation ion. Quality assistance procedures included the regular checks of blanks, regular calibration by PFOA standards, and derivation of the limit of detection.

4.3 Methods of analysis for membrane characterization

4.3.1 Membrane morphology

The functional groups in kC gel, kC-V, and kC-AC were analyzed using FT-IR (Fourier Transform Infrared) with a Thermo Scientific Nicolet spectrometer. The spectrometer was equipped with an IR microscope with an optical resolution of 0.9 cm^{-1}. Before analysis, the samples were dried at 105 °C for 24 hours. The study encompassed the wavenumber range of 4000-500 cm^{-1}. The gel samples were subjected to field-emission scanning electron microscopy (FE-SEM) using a Zeiss EVO LS15 SEM. Before imaging, a thin coating of gold with a thickness of 6nm was applied to the samples using a sputtering machine. Three SEM tests were performed and averaged to generate the final spectra for precise outcomes. In addition, energy-dispersive X-ray spectroscopy (EDX) was performed on the same SEM samples using a Bruker SDD X flash 5030 detector. The TECHPoro Capillary Flow Porometer was utilized for pore size analysis, employing the BJH model for both the adsorption and desorption processes. The contact angles of 3%kC

and kC with 1% to 3% concentrations of vanillin and 0.1% to 0.3% AC were measured to assess hydrogel surface wettability and hydrophilicity. The DM 211 contact angle measurement system (Kyowa Interface Science, Chennai, India) was used to measure water contact angles using the sessile-drop method. For each sample, a minimum of three locations were chosen to obtain contact angle measurements. The result was the average water contact angle with an error value.

4.3.2 Membrane porosity and pore size

The porosity of the hydrogel membrane was calculated by cutting the membrane into dimensional pieces of (3×3×1) cm and immersing it in distilled water for 15 hours, then weighing it after removing all excess water on a surface using blotting paper (*weight1*). After that, it was dried in an oven at 60 °C for 6 hours and weighed (*weight2*). The porosity was calculated by Equation (4.1).

$$P\% = \left(\frac{weight1 - weight2}{A * l * \rho}\right) \quad (4.1)$$

weight1 and *weight2* are the gel membrane's wet and dry weight values, respectively. *A* is the gel membrane sample area cm^2. *l* is the membrane thickness cm, and ρ is the water density ($1 g/cm^3$).

The gel membrane's average pore radius size rm was calculated using the membrane porosity and pure water flux through the membrane by Equation (4.2).

$$rm = \sqrt{\frac{(2.9 - 1.75p) \times (8 \times lQ\eta)}{(p \times A \times \Delta P)}} \quad (4.2)$$

ΔP is the operation pressure, p is the membrane porosity, and l and A are the membrane thickness and effective membrane area. Q is the volume of pure water flux per time (m^3/s)(Alsalhy et al., 2013).

4.3.3 Water uptake and swelling

Water uptake (WU) was determined using a previously dried membrane by cutting the membrane into dimensional pieces of (3×3×1) cm. The hydrogel pieces were dried in an oven at 105 °C for 6 hours. Dry weight was recorded (*Wdry*). After drying, the pieces were immersed in distilled water for 24 hours at room temperature and weighed after removing all excess water on a surface using blotting paper (*Wwet*). Finally, water uptake was determined using Equation (4.3). Three samples underwent testing, and the average outcomes were subsequently reported.

$$Wu = \left(\frac{Wwet - Wdry}{Wdry}\right) x100 \quad (4.3)$$

The hydrogel's swelling degree was also determined to assess its anti-swelling properties. The initial weight of the hydrogel (Winitial) was recorded, then placed in DI water and PFOA solution at 0.5, 1, and 1.5 mg/L concentrations for 2-24 hours. The final weight (*Wfinal*) was re-recorded, and the swelling degree (*SD*) was estimated using Equation (4.4).

$$SD = \frac{(Wfinal - Winitial)}{Winitial} * 100 \quad (4.4)$$

4.3.4 Membrane performance efficiency

The kC-AC and kC-V hydrogel were cast on a fabric material with a pore size of about 30 μm, providing a support layer. Experimental work was conducted using a 30 cm tall homemade plexiglass column Figure.S1 with a filtration area of 0.0007 m^2 and a constant head of 30 cm, facilitating visual observation. The fabric support layer was tightly placed at the bottom of the column, and the kC-AC and kC-V hydrogel were poured slowly on top of the substrate. It was allowed to settle for 10-15 minutes while remaining hydrated. Care was taken to avoid sudden impacts that could deform the hydrogel and compromise its performance. Then, 1 mg/L PFOA solution was gradually poured onto the column for filtration. Analytical equipment measured the contaminants' water flux and rejection rate. All experiments were repeated at least three times to ensure reliability. The water flux was determined using the provided Equation (4.5).

$$J = \frac{V}{A*t} \tag{4.5}$$

V represents the accumulated permeate volume (m^3) over time (t), and A denotes the efficient membrane area (m^2) utilized in the filtration process. The rejection of pollutants was measured using Equation (4.6).

$$R\% = (1 - \frac{Cp}{Cf}) * 100 \tag{4.6}$$

In Equation 6, Cp refers to the pollutant concentration in the permeate solution, and Cf is the initial concentration of the same contaminants in the feed solution. Experiments were repeated at least three times for water flux rejection studies.

4.3.5 PFOA-contaminated water

The perfluorooctanoic acid (PFOA) solution was prepared at concentrations of 0.5, 1, and 1.5 mg/L to evaluate the novel membrane filter's efficiency in terms of rejection and flux. PFOA quantification was performed using liquid chromatography-mass spectrometry (LC-MS). Calibration curves for PFOA quantification were established using a six-point calibration range from 5 µg/L to 50 µg/L. The data were fitted to a quadratic, weighted regression equation. The calibration curve's coefficient of determination (R^2) exceeded 0.99 in all analyses. The accuracy for PFOA analysis across all quality control (QC) concentration levels was within ±5%.

The hydrogel membrane was tested with PFOA-contaminated wastewater from electrokinetic soil remediation in Sydney, Australia. Liquid chromatography-mass spectrometry (LC-MS) and inductively coupled mass spectroscopy (ICP-MS) were used to measure the PFOA and metal concentrations, respectively (Table 4.1).

Table 4. 1.PFOA-contaminated water analysis and composition.

Parameter	Measurement tool	Value
pH	LAQUA-pH meter (Horriba, Japan)	9.53
Conductivity	LAQUA meter (Horriba,Japan)	1.871 ±2 ms/cm
Total dissolved Solids	LAQUA meter (Horriba,Japan)	1774± 5 mg/L
Turbidity	Turbidity meter (Horriba, Japan)	>100 ±2 NTU
PFOA	LC-MS	179.2±3 mg/L
Na	ICP-MS (Agilent, United States)	25 ±5 mg/L
K	ICP-MS (Agilent, United States)	18 ± 5 mg/L

Si	ICP-MS (Agilent, United States)	10 ± 5 mg/L
Cl	ICP-MS (Agilent, United States)	33 ± 5 mg/L
Al	ICP-MS (Agilent, United States)	104 ± 5 mg/L

4.4 Statistical assessment

Every experiment was replicated at least three times, and the outcomes are presented as the mean values. The Analysis of Variance (ANOVA) was employed to assess variations among multiple experimental data sets. Single-factor ANOVA analysis for experimental data showed a *P-value* less than 0.05, indicating statistically significant differences between treatment groups.

4.5 Results and discussion

4.5.1 Hydrogel membranes characterization

FE-SEM analysis examined the surface morphology of the kC-AC and kC-V hydrogels after drying for 24 hours at 60 °C, during which it experienced shrinkage. Figure S2 (Supplementary Materials) shows the surface of the pure kC hydrogel, which exhibits a relatively smooth texture with irregular folds and indications of brittle fractures. The SEM image in Figure 4.2a illustrates the presence of diminutive nanostructures composed of vanillin in the uppermost layer of the hydrogel surface and configurations like canals and valleys to facilitate the entrapment of contaminants. This structural arrangement resembles a thin-film composite membrane characterized by ridge and valley-like topography (Hamid, Abdullah, Yusof, Lau, Ismail, Wan Salleh, et al., 2021). Figure 4.2c describes the surface of kC-0.3%AC hydrogel, which has diverse properties, including roughness and porosity. AC becomes an integral part of the kC matrix, featuring

irregularly shaped particles with porous structures, while kC particles exhibit organized, helical structures. Notably, SEM images unveil the existence of pores or voids within the composite, impacting its adsorption capacity, particularly when AC assumes the role of the adsorbent. Figures 4.2b and 4.2d show the alteration of kC-AC and kC-V hydrogel surface morphology after PFOA filtration, including swelling, pore size, and surface roughness. It provides evidence of PFOA adsorption on the hydrogel's surface, manifested by potential pore blockage.

The Fourier-transform infrared spectroscopy (FT-IR) analysis of the kC-(1-3)%V hydrogel confirmed the presence of discernable peaks (Figure 4.2e). The heightened peaks indicated the interaction between vanillin and kC, particularly increased hydroxyl groups' intensity at 3200-3600 cm^{-1}. This analysis aligns with the theory of hydrogen bonding, suggesting that vanillin contributes to the hydroxyl groups. Furthermore, vanillin acted as a pore-forming agent, enhancing hydrogel hydrophilicity and biocidal properties. Studies showed increased membrane porosity due to vanillin concentration, attributed to the polar functional groups like alcohols and aldehydes, resulting in a negatively charged membrane surface (X. Zhang et al., 2022b). Compared to kC spectra, new peaks were observed in kC-1%V, while kC-2%V and kC-3%V exhibited similar profiles. A broad peak at 3765 cm^{-1}, representing hydroxyl (OH) groups, was slightly increased in the presence of vanillin.

FT-IR analysis of the kC-(0.1-0.3)%AC hydrogel offers valuable molecular insights. The kC exhibits - OH groups as a broad absorption band 3000-3500 cm^{-1} signifying O-H stretching vibrations. The spectrum reveals strong absorption of 1240-1260 cm^{-1} corresponding to sulfate ester bonds (O=S=O) in kC, referring to potential interactions with AC. In the 1600-1800 cm^{-1} range, absorption bands arise from carbonyl (C=O)

stretching vibrations originating from various kC and AC surface functional groups (e.g., COOH, OH, C=O). AC introduces distinctive peaks, representing its surface functional groups, notably COOH, OH, and C=O (Figure 4.2f). Tracking any shifts or changes in absorption bands during FT-IR analysis can reveal chemical interactions between kC and AC, including hydrogen bonding or chemical adsorption. Zhou's study highlighted the complexity of AC adsorption, driven by diverse forces. The AC surface primarily features oxygen-containing functional groups such as carbonyl, carboxyl, lactone, and phenolic hydroxyl, influencing its adsorption capabilities (Zhou et al., 2021).

4.5.2 Contact angle and rheology

The hydrogel's surface hydrophobicity was determined by measuring the water contact angle (Figures 4.3a and 4.3b). According to Bhushan et al. (2011), a contact angle between 0° and 90° indicates a hydrophilic surface, while angles exceeding 90° indicate hydrophobicity. Surface wettability is influenced by chemical composition and morphology, with roughness affecting contact angles through models like the Wenzel or Cassie–Baxter models (Bhushan & Yong Chae, 2011). kC's chemical structure imparts hygroscopic properties, making hydrogel surfaces wets hydrophilic with a measured contact angle of 72°. AC has both hydrophobic and hydrophilic sites on its surface. While it naturally leans towards hydrophobicity, filtration processes demand hydrophilic characteristics for enhanced performance, achievable through various treatments (Kostov et al., 2014). Incorporating 0.1 to 0.3% of AC into a kC solution decreased the contact angle to 53.8° ± 3 for 0.1%AC, followed by a slight increase to 55.5° ± 3 for 0.2%AC and 57.4° ± 3 for 0.3%AC. Adding 1% to 3% vanillin to kC hydrogels substantially reduced the water contact angle (Figure 4.3a, and 4.3b), mainly due to vanillin's high hydrophilicity. The results align with previous studies that showed reduced contact angles

when vanillin was added to Polysulfone (PSf) membranes (Yadav, Ibrar, Samal, et al., 2022a). The most significant decrease in hydrophobicity was observed in the kC-1%V hydrogel, resulting in a water contact angle of 58° ± 3. Increasing vanillin concentrations in the hydrogel led to a slight decrease in contact angles for the kC-2%V and kC-3%V hydrogels, reaching 55° ± 3 and 53° ± 3, respectively. During phase inversion, vanillin's hydrophilic nature migrated to the surface, enhancing membrane hydrophilicity (Arthanareeswaran et al., 2009).

Essential to understanding the rheological properties of the kC response to shear forces and deformation when combined with vanillin or AC, examining changes in its viscosity that measures resistance to flow and shear stress that characterizes the internal stress when subjected to mechanical forces. Adding vanillin to the kC hydrogel increased viscosity and was further amplified upon adding AC (Figures 4.3c and 4.3d). The viscosity for all hydrogel decreased with increased shear stress; for the middle point in the graph, the viscosity values of kC, kC-3%V, and kC-0.3%AC were 61116 mPa.s, 187430 mPa.s, and 420610 mPa.s, respectively. The corresponding shear stress for the 3%kC, kC-3%V, and kC-0.3%AC hydrogels was 136.4 Pa, 419.63 Pa, and 941.46 Pa, respectively, closely related to water contact angle changes. Notably, the viscosity properties exhibited marked distinctions compared to the hydrogel without vanillin or AC serving as controls.

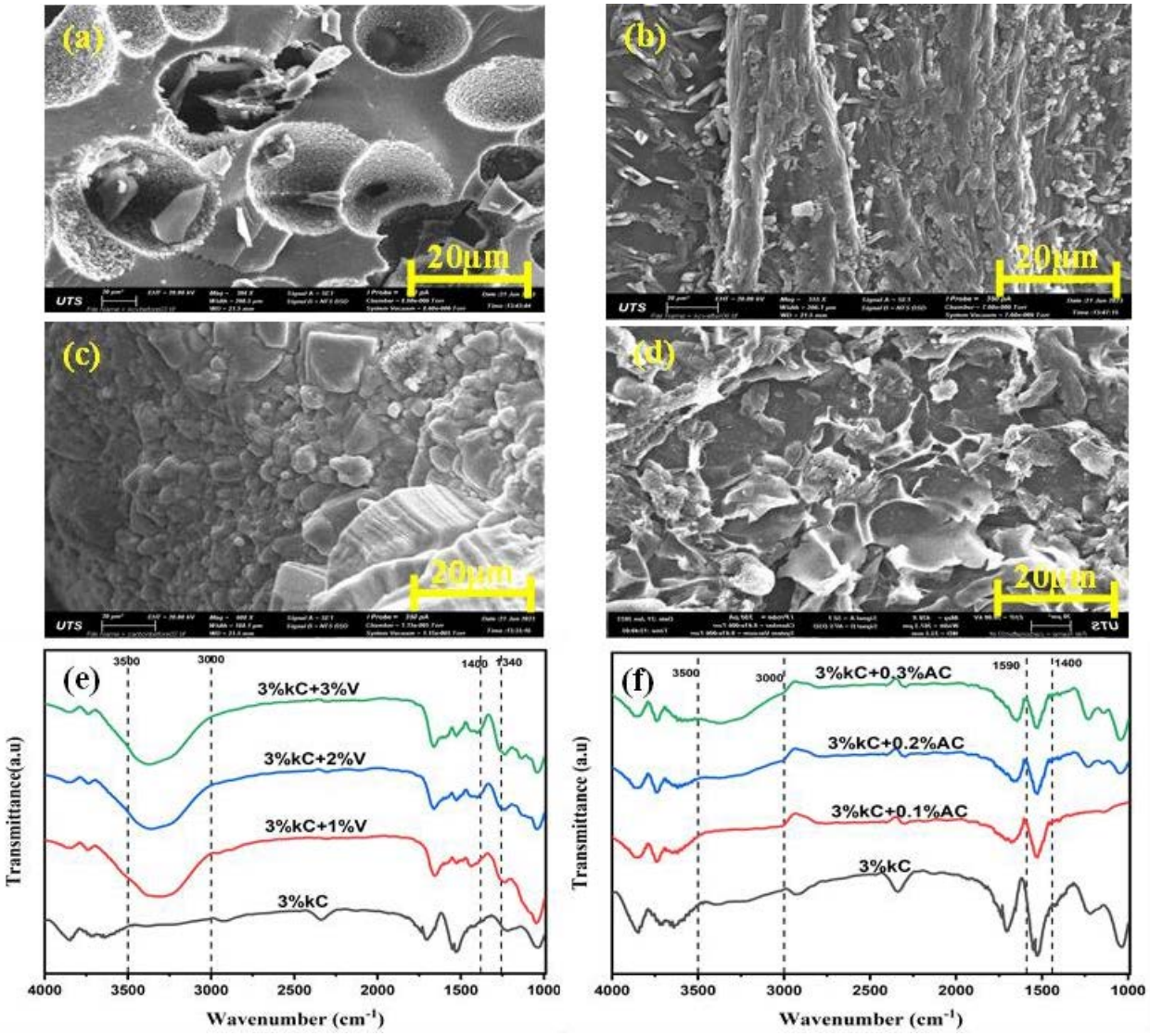


Figure 4. 2.SEM and FT-IR analysis of the hydrogel, a) SEM of the kC-3% V hydrogel before filtration at 20 µm at the first focus point, b) SEM of the kC-3% V hydrogel after filtration at 20 µm at the first focus point, c) SEM of the 3%kC-0.3%AC hydrogel before filtration at 20 µm at the first focus point, d) SEM of the 3%kC-0.3%AC hydrogel after filtration at 20 µm at the first focus point, e) FT-IR of kC-(1-3)%V before filtration, f) FT-IR of kC-(0.1-0.3)%AC before filtration.

4.5.3 Porosity and pore size

Figures 4.3e and 4.3f depict vanillin and AC influence on the porosity of kC membranes. The introduction of 1% to 3% vanillin into the kC hydrogel enhanced the membrane porosity from 62.8% ± 5 to 75.8% ± 5, 77.5% ± 5, and 79.1% ± 5. Similarly, the incorporation of 0.1% to 0.3% AC into the kC hydrogel increased the porosity from 62.8% ± 5 to 85.4% ± 5, 87.6% ± 5, and 89.7% ± 5, respectively. Hydrophilic additives help expedite solvent-nonsolvent exchange in hydrogels and facilitate the formation of highly porous membrane structures.

Furthermore, the increase in porosity is accompanied by a gradual transition in void morphology within the membranes, shifting from microcavities to valley-like voids characterized by a more constrained size distribution. According to Equation (4.2) and Figures 4.3e and 4.3f, the pore radius for kC was 3.2nm ± 1, kC-(1-3)%V was 2.63 nm ± 1, 2.59 nm ± 1, 2.57 nm ± 1, and kC-(0.1-0.3)%AC was 1.95 nm ± 1, 1.86 nm ± 1, 1.68 nm ± 1, respectively. Membranes featuring a confluence of smaller, uniformly dispersed pores tend to exhibit elevated porosity due to the abundance of void space within the matrix. Conversely, membranes characterized by larger or irregularly distributed pores often yield lower porosity. This matches the results obtained for both hydrogels composite. Surface area is a crucial parameter that characterizes the surface properties of an adsorbent. The Brunauer-Emmett-Teller (BET) method is widely employed for quantifying the surface area of an adsorbent, utilizing nitrogen gas as an adsorbate interacting with the material's surface. The specific surface area of kC is 10.872 m^2/g, 33.15 m^2/g for kC-3%V, and 95.61 m^2/g for kC-0.3%AC (Table 2). In addition, the total pore volume of the kC hydrogel is 0.015 cc/g compared to 0.047 cc/g and 0.099 cc/g for the kC-3%V and kC-0.3%AC.

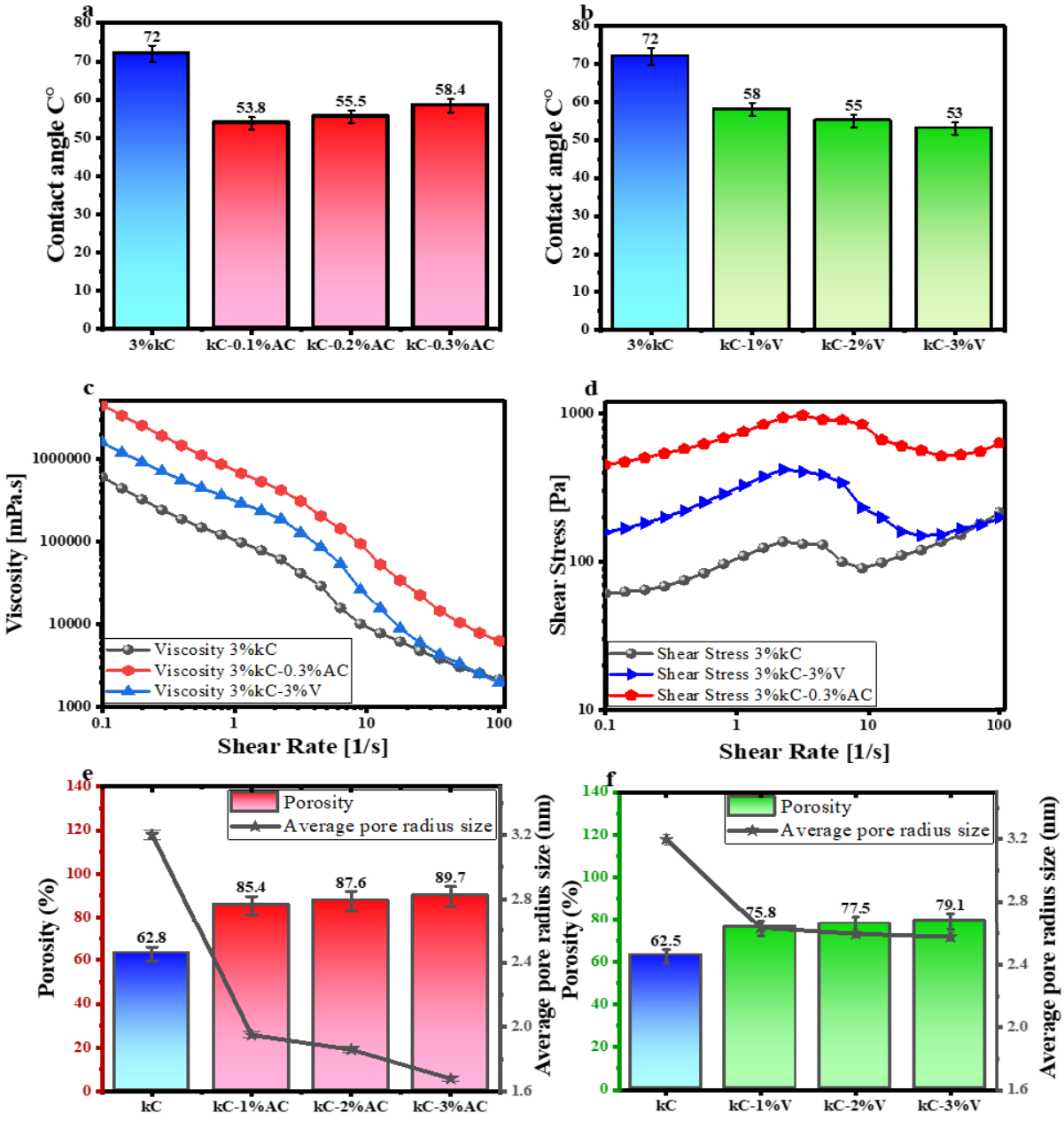


Figure 4. 3.a) the contact angle for the 3% kC, 3% kC-AC, b) the contact angle for the 3%kC-V, c,d) viscosity and shear stress of the composite hydrogel, e) the effects of AC content on the porosity and average pore size of kC-AC membranes, f) the effects of vanillin content on the porosity average pore size of kC-V membranes.

Table 4. 2: Adsorption and Desorption summaries of BET analysis.

BET analysis		**3%kC**	**3%kC-3%V**	**3%kC-0.3%AC**
Adsorption summary BJH	Surface area	10.872 m^2/g	33.15 m^2/g	95.61m^2/g
	Pore Volume	0.015 cc/g	0.047 cc/g	0.099 cc/g
	Pore Diameter	3.231 nm	3.228 nm	5.83 nm
Desorption summary BJH	Surface area	5.776 m^2/g	23.7 m^2/g	60.80 m^2/g
	Pore Volume	0.009 cc/g	0.036 cc/g	0.0504 cc/g
	Pore Diameter	3.309 nm	3.318 nm	3.492 nm

4.5.4 Water uptake and swelling degree

Water uptake for the kC hydrogel composite represents its ability to absorb and retain water, a critical attribute determined by factors such as hydrogel concentration, formulation, and environmental conditions. The kC-AC and kC-V composite hydrogels of equal thickness of 2 cm were tested for the water uptake capacity. The hydrogel contracted during drying, folding at the edges and transforming into a compact, plastic-like structure (Figures 4.4a and 4.4b). The impact of different concentrations on swelling degree is reported in Figures 4.4c and 4.4d; water uptake increases with the increasing vanillin and AC concentrations. The kC-(1-3)%V hydrogel exhibited 966.22% ± 2, 1038.8% ± 2, and 1045.5% ± 2, water uptake, respectively. The corresponding kC-(0.1-0.3)%AC results were 892.31% ± 2, 902.2% ± 2, and 918.4% ± 2, respectively. The kC-3%V and kC-0.3%AC displayed an exceptional water uptake capacity, absorbing 1045.5% ± 2 and 918.4% ± 2 of water, significantly outperforming most hydrogels. This

increase in water uptake implies an enhanced proton diffusion rate facilitated by hydrogen bonding with water molecules and increased hydroxyl ion flux, causing distinct water-absorbing capabilities for different formulations of the kC hydrogel. Hydroxyl groups in the hydrogel enhance its hydrophilicity, increasing water uptake as the nanoparticle percentage rises. Vanillin and AC, forming hydrogen bonds with kC, boost water uptake in the composite hydrogel. Higher vanillin and AC concentrations significantly amplify water uptake. The relationship between water uptake and sulphate group content varies, as sulphate content affects moisture absorption differently. The sulphate content, molecular weight, crosslinking percentage, and microstructure void volume influence moisture content in polysaccharide hydrogels. The hydrogel's structure and chemical composition are vital in water uptake properties (Balasubramanian et al., 2018).

The swelling degree measures how much a hydrogel expands when exposed to a solvent, typically expressed as the ratio of the swollen volume to its initial dry volume. Factors like polymer network structure, ionic groups, and solubility influence this degree. In loosely crosslinked domains, polymer chains deform more upon swelling than densely crosslinked domains. The kC-based hydrogels consist of polymer chains with charged sulphate groups that repel each other due to their negative charge. The electrostatic repulsion increases the distance between chains, making the network more permeable to large molecules and allowing more water to enter, resulting in a higher swelling degree. The maximum swelling degree was observed to rise with longer sub-chain lengths, representing the length of chains between crosslinks. The introduction of PFOA into a hydrogel may also impact its swelling degree. PFOA's hydrophobic properties can diminish the hydrogel's attraction to water, potentially reducing swelling. However, it's essential to consider that the concentration of PFOA and the specific polymer chemistry

of the hydrogel will determine the extent of this effect. Swelling studies have shown that hydrogel composites achieve equilibrium swelling after being immersed overnight in different PFOA concentrations (0.5, 1, 1.5) mg/L. Figures 4.4c and 4.4d illustrate the extent of swelling in kC-AC and kC-V hydrogel composites. Among the kC-AC formulations, the kC-0.3% AC hydrogel demonstrated the highest swelling degree of 11.8 ± 1 g/g when exposed to 1 mg/L of PFOA. This result was statistically significant when compared to other kC-AC formulations.

Additionally, hydrogels exposed to PFOA concentrations of 0.5 and 1.5 mg/L exhibited 11.1 ± 1 g/g and 11.8 ± 1 g/g swelling, respectively, with minimal variations in sol fraction over time. The swelling of the kC-V hydrogels was assessed by immersing them in a PFOA solution for 24 hours (Figure 4.4d). The kC-3%V hydrogel displayed favourable swelling behaviour of 11.5 ± 1 g/g, outperforming the kC-2%V and the swelling of the kC-1%V hydrogel of 11.2 ± 1 g/g and 10.7 ± 1 g/g, respectively. This behavior is attributed to hydrophilic functional groups, including -OH, $-CONH_2$, $-CONH^-$, and $-SO^3$ (Hamidi et al., 2008).

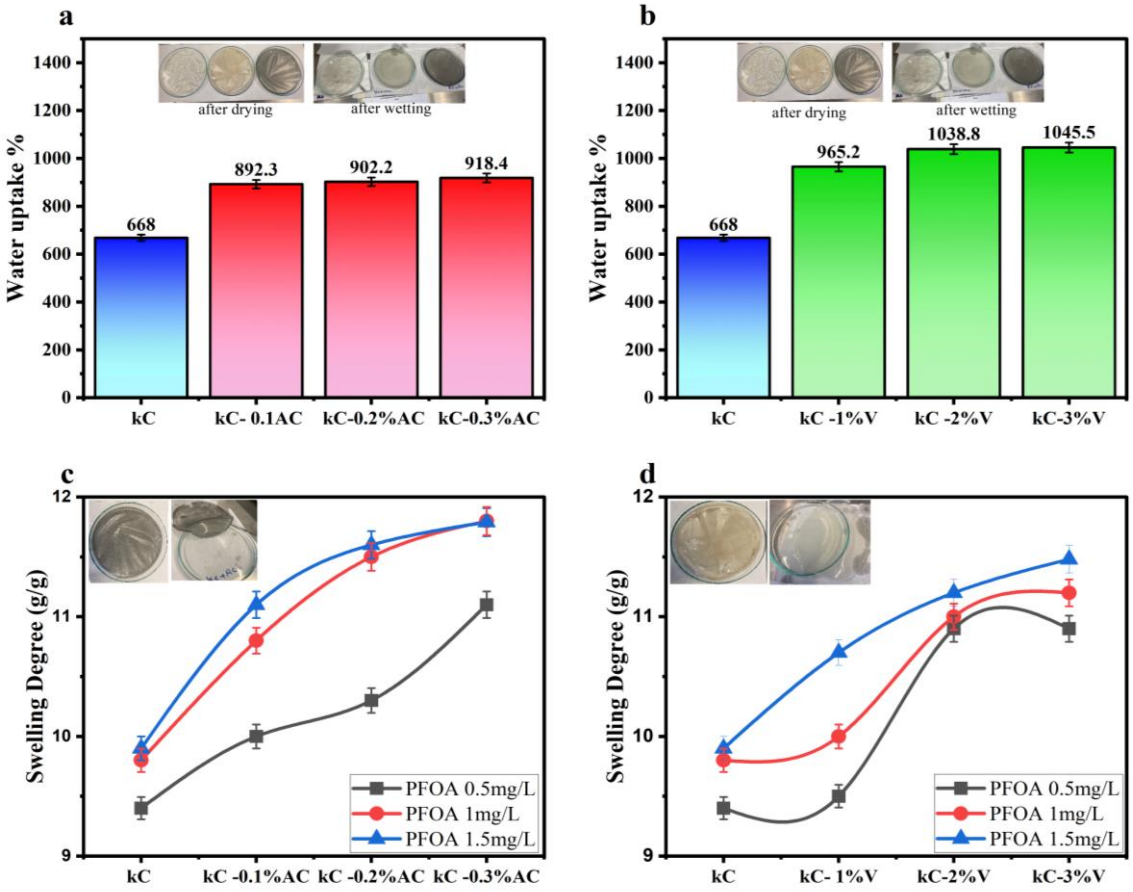


Figure 4. 4.a) Water uptake of different concentrations of kC-AC hydrogel, b) Water uptake of different concentrations of kC-V hydrogel, c) Swelling degree of kC with various concentrations of AC at different concentrations of PFOA, d) Swelling degree of kC with various concentrations of vanillin at different concentrations of PFOA.The error bar = 1 standard deviation

4.5.5 kC-AC and kC-V performance

Several factors, including hydrogel thickness, feed concentration, pH of the feed solution, solute volume, viscosity, and ionic interactions, influence the water flux of the hydrogel. In the filtration experiments, the hydrogel membrane was tested with PFOA-contaminated wastewater from soil remediation. A support layer made of fabric material

with a pore size of 30 μm was selected for the kC-V and kC-AC hydrogel membrane filter. The hydrogel was manually applied to the fabric layer within a specialized filtration column designed for water treatment. This support layer serves as a structural foundation for the hydrogel during filtration.

4.5.5.1 Effect of hydrogel thickness

A feed solution containing 1 mg/L of PFOA was employed to evaluate water flux at 0.5 cm, 1 cm, 1.5 cm, and 2 cm hydrogel thicknesses. The height of the filtration column was 30 cm (0.029 bar. The hydrogel comprises a 3% kC, blended with 1% to 3 % vanillin or 0.1% to 0.3% AC. Hydrogel thicknesses were examined to determine the optimal water flux and rejection performance. There is a trade-off between the hydrogel water flux and rejection as the membrane thickness increases from 0.5 cm to 2 cm (Figures 4.5a and 4.5b). In general, the results demonstrate that a substantial enhancement in the water flux can be achieved by increasing the vanillin and AC content within the kC hydrogel. For example, the water flux in the kC-0.3%AC decreased from 32.4 LMH in 0.5 cm hydrogel thickness to 25.6 LMH in 2 cm kC-0.3%AC thickness (Figure 4.5a). On the contrary, water flux increased with increased AC and vanillin concentration in the kC hydrogel. The water flux was 23.4 LMH in the kC-0.1%AC, 24.1 LMH in the 0.2%AC, and 25.6 LMH in the kC-0.3%AC (Figure 4.5a). The corresponding water flux for kC-V hydrogel was 20.9 LMH for kC-1%V, 21 LMH for kC-2%V, and 21.5 LMH for kC-3%V.

Increasing the water flux with the AC and vanillin concentration in the hydrogel is attributed to increased surface hydrophilicity, pore density, porosity, and macro voids, alongside the formation of vertically interconnected finger-like pores (Zhu et al., 2021). Due to enhanced membrane hydrophilicity, the water flux in the kC-3%V and kC-0.3%AC membranes achieved 25.6 LMH ± 2 and 21.5 LMH ± 2, respectively. These

outcomes align with the increase in porosity and pore size radius for hydrogels composite, which were 89.7% and 1.68 nm in kC-0.3%AC, 79.1% and 2.57 nm in kC-3%V, 1.68 nm. The water flux enhancement is facilitated by vanillin and AC additives that accelerate solvent exchange during membrane preparation, increasing porosity and larger cavities. Also, the structural changes in the membrane's cross-morphology, from delicate finger-shaped pores in the kC membrane to broader valley-shaped pores with macro voids in kC-AC and kC-V membranes, facilitate smoother water molecule passage, further increasing water flux, and Figures 2a and 2c confirm that. Although water flux increased the AC and vanillin concentration in the hydrogel, PFOA adsorption reduced water flux due to pore narrowing, exacerbated by higher AC or vanillin particle concentrations, resulting in a rougher membrane texture. Besides, adding vanillin plays a pivotal role in the generation of pores and the augmentation of permeation rate (R et al., 2017). Adding vanillin imparts a negative charge to the hydrogel surface, increasing the hydrophilicity of hydrogel (Yadav, Ibrar, Samal, et al., 2022a). The interaction between kC and vanillin further enhances membrane permeability and fortifies its resistance to fouling (Alam et al., 2017; Yadav, Ibrar, Samal, et al., 2022a). When combined with kC, AC provides a robust framework for the entrapment of impurities due to its vast surface area and high porosity. The porous architecture of kC and AC improves the hydrogel's permeability, allowing water to pass while retaining contaminants (Mahdavinia et al., 2015).

The results demonstrate that a substantial enhancement in rejection was achieved by increasing the hydrogel thickness or the concentration of AC and vanillin due to the increased hydrogel adsorption capacity (Supplementary Materials S2.3.1). For example, the rejection in the kC-0.3%AC increased from 70% in 0.5 cm hydrogel thickness to 82% in 2 cm kC-0.3%AC thickness (Figure 4.5c). On the contrary, rejection increased with

increased AC and vanillin concentration in the kC hydrogel. The rejection was 78% in the kC-0.1%AC, 81% in the 0.2%AC, and 82% in the kC-0.3%AC (Figure 4.5c). The corresponding rejection for kC-V hydrogel was 72% for kC-1%V, 75% for kC-2%V, and 80% for kC-3%V (Figure 4.5d). The results showed that 2 cm hydrogels demonstrated superior PFOA rejection compared to thinner hydrogels, i.e., 0.5 cm, 1 cm, and 1.5 cm. A 2 cm thickness is optimal for achieving high water flux and rejection, as Figures 4.5a,4.5b,4.5c, and 4.5d illustrate. Although the contact angles of kC-AC and kC-V hydrogels were very close (Figures 3a and 3b), the kC-AC exhibited greater water flux than kC-V due to the higher porosity (Figures 4.3e and 4.3f). Also, kC-AC hydrogels exhibited more PFOA rejection than kC-V hydrogels because of i) the smaller average pore size of kC-AC hydrogels (Figures 4.3e and 4.3f) and ii) the higher adsorption capacity of kC-AC hydrogel compared to kC-V (Figure 4.6a,4.6b). Therefore, kC-AC hydrogel exhibited better water flux and rejection rates than kC-V.

4.5.5.2 Effect of feed pH

A feed solution containing 0.5 mg/L, 1 mg/L, and 1.5 mg/L of PFOA was used in the 3%kC-0.3%AC and 3%kC-3 %V hydrogels to evaluate water flux and PFOA rejection at different feed pHs. Changing the feed pH can affect the electrostatic interactions between the membrane and PFOA compounds (Ouyang et al., 2019; Zhao et al., 2011). The pH was adjusted to pH 4, 7, and 10 to assess the hydrogel's performance using 0.1M NaOH and 0.1M HCl. The alkalinity of the feed solution can significantly impact the performance of the filtration process due to the change in surface charge, pore size, water flux, and rejection rates. For 2 cm hydrogel thickness, results show an increase in water flux with a pH increase and an increase in rejection with a pH decrease. The 2 cm hydrogel

thickness results show increased water flux at alkaline pH and PFOA rejection at acidic pH (Figures 4.5e, 4.5f, 4.5g, and 4.5h).

In general, the results demonstrate that a substantial enhancement in the water flux can be achieved at feed pH 10 and PFOA concentration 0.5 mg/L. For example, the water flux in the kC-0.3%AC increased from 27.8 LMH at feed pH 4 to 30.4 LMH at feed pH 10 (Figure 4.5e). On the contrary, water flux decreased with increased PFOA concentration in the feed solution. The water flux at feed pH 10 was 30.4 LMH at 0.5 mg/L, 29.9 LMH at 1 mg/L, and 30.1 LMH at 1.5 mg/L PFOA (Figure 4.5e). The corresponding water flux for kC-3%V hydrogel was 29.5 LMH at 0.5mg/L, 28.7 LMH at 1mg/L, and 27.4 LMH at 1.5mg/L PFOA (Figure 4.5f).

For kC-0.3%AC and kC-3%V hydrogels, results show PFOA rejection increased at pH 4 and decreased at pH 10 (Supplementary Materials S2.3.2). For example, the rejection in kC-0.3%AC at pH 4 was 86.9%, while it decreased to 78.3% at pH 10 for 1.5 mg/L PFOA concentration. In contrast, the rejection in kC-3%V hydrogel was 85.7% at pH 4 and decreased to 79.5% at pH 10. The results also exhibit a substantial rejection enhancement was achievable at increased PFOA concentration. For example, the kC-0.3%AC rejection of PFOA increased from 81% at 0.5 mg/L feed solution to 86.9% at 1.5 mg/L. Similarly, in the kC-3%V hydrogel, the rejection increased with increasing PFOA concentration. For example, the PFOA rejection was 78.4%, 86.5%, and 85.7% in 0.5 mg/L, 1 mg/L, and 1.5 mg/L, respectively (Figure 4.5g and 4.5h).

The surface charge of a membrane, determined by functional groups and pKa, significantly influences PFOA separation efficiency based on the feed pH. Moreover, pH alterations impact membrane pore size, affecting PFOA removal. A positively charged surface enhances rejection through electrostatic attraction. Acidic feed pH also reduces

the repulsion forces, causing pore shrinkage and improved rejection, while higher pH increases hydrogel porosity, resulting in a lower PFOA rejection. The pH-dependent behaviour of hydrogel ionizable groups influences the solvent flow and PFOA interactions, leading to varying rejection rates. Thus, pH is a crucial parameter in membrane and hydrogel filtration for effective PFAS removal (Jin et al., 2021; Pensini et al., 2019; Yang et al., 2017; Zeng, Tanaka, et al., 2017a, 2017b).

4.5.5.3 Effect of feed concentration

To investigate the effects of the PFOA feed concentration on the water flux and rejection by KC-0.3%AC and kC-3%V hydrogels, 0.5, 1, and 1.5 mg/L PFOA concentrations were tested (Figures 4.5i and 4.5j). For the kC-0.3%AC at 2 cm thickness and pH 7, The water flux slightly decreased with increasing the PFOA concentration, and it was 29.5 LMH ± 0.5 at 0.5 mg/L, 28.4 LMH ± 0.5 at 1 mg/L, and 28.4 LMH ± 0.5 at 1.5 mg/L. On the contrary, PFOA rejection increased with an increase in the PFOA concentration, and it was 60.4 % ± 1 at 0.5 mg/L, 65.7 % ± 1 at 1 mg/L, and 67.3 % ± 1 at 1.5 mg/L. For KC-3%V at 2 cm and pH 7, the water was 27.8 LMH ± 0.25 at 0.5 mg/L, 26.7 LMH ± 0.25 at 1 mg/L, and 26.5 LMH ± 0.25 at 1.5 mg/L. The corresponding PFOA rejection was 67.6% ± 0.25 at 0.5 mg/L, 69.4 % ± 0.25 at 1 mg/L, and 71.4 % ± 0.25 at 1.5 mg/L. Also, higher PFOA feed concentration decreases water flux since it occupies available pore spaces, restricting the passage of water. Increased solute concentration reduces the effective hydrogel porosity. However, the reduction in porosity reduces permeability, i.e., water flows more slowly through the hydrogel, increasing the likelihood of interactions between the solutes and the hydrogel. These interactions can result in more significant adsorption or trapping of solutes within the hydrogel structure, leading to better removal efficiency. Therefore, the hydrogel's rejection capability increases with increasing the

PFOA concentration. The results also agree with the literature (AlSawaftah et al., 2021; Eke et al., 2020) that delved into the PFAS removal efficiency in scenarios involving elevated 100 mg/L PFOA concentration. The potential for micelle formation arises at such PFOA concentrations, particularly as the concentration surpasses the critical micelle concentration threshold.

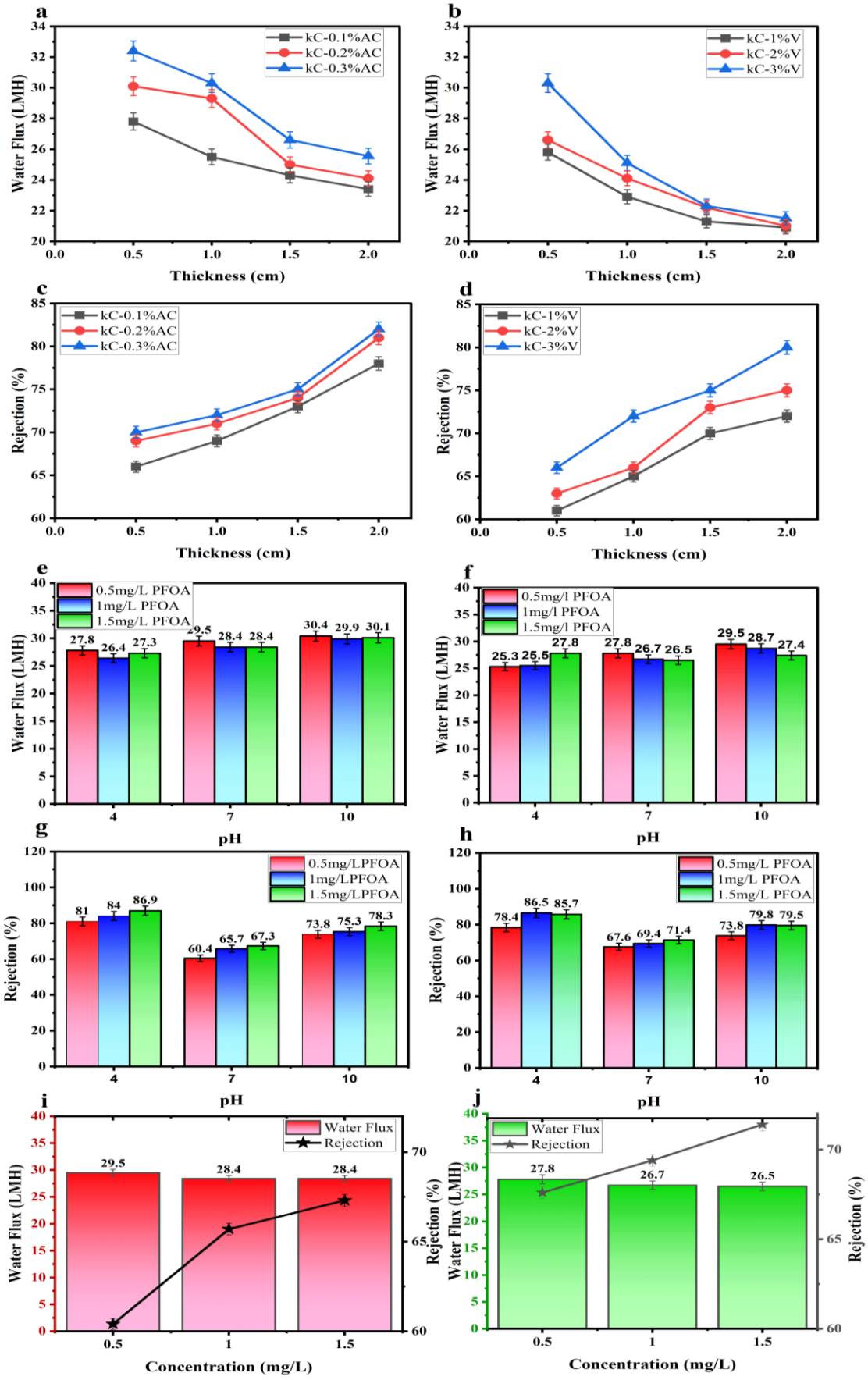

a
Water Flux (LMH)
Thickness (cm)
kC-0.1%AC
kC-0.2%AC
kC-0.3%AC
b
Water Flux (LMH)
Thickness (cm)
kC-1%V
kC-2%V
kC-3%V
c
Rejection (%)
Thickness (cm)
kC-0.1%AC
kC-0.2%AC
kC-0.3%AC
d
Rejection (%)
Thickness (cm)
kC-1%V
kC-2%V
kC-3%V
e
Water Flux (LMH)
pH
0.5mg/L PFOA
1mg/L PFOA
1.5mg/L PFOA
27.8 26.4 27.3
29.5 28.4 28.4
30.4 29.9 30.1
f
Water Flux (LMH)
pH
0.5mg/l PFOA
1mg/l PFOA
1.5mg/l PFOA
25.3 25.5 27.8
27.8 26.7 26.5
29.5 28.7 27.4
g
Rejection (%)
pH
0.5mg/LPFOA
1mg/LPFOA
1.5mg/LPFOA
81 84 86.9
60.4 65.7 67.3
73.8 75.3 78.3
h
Rejection (%)
pH
0.5mg/L PFOA
1mg/L PFOA
1.5mg/L PFOA
78.4 86.5 85.7
67.6 69.4 71.4
73.8 79.8 79.5
i
Water Flux (LMH)
Rejection (%)
Concentration (mg/L)
Water Flux
Rejection
29.5 28.4 28.4
j
Water Flux (LMH)
Rejection (%)
Concentration (mg/L)
Water Flux
Rejection
27.8 26.7 26.5

Figure 4. 5.a) The impact of kC-AC hydrogel thickness on water flux with a 1 mg/L PFOA, b) The impact of kC-V hydrogel thickness on water flux with a 1 mg/L PFOA, c) The impact of kC-AC hydrogel thickness on 1 mg/L PFOA rejection, d) The impact of hydrogel thickness (kC-V) on 1 mg/L PFOA rejection, e) The influence pH of a PFOA feed solution on water flux for kC-0.3%AC hydrogel, f) The influence pH of a PFOA feed solution on water flux for kC-3%V hydrogel, g) The influence pH of a PFOA feed solution on rejection for kC-0.3%AC hydrogel, h) The influence pH of a PFOA feed solution on rejection for kC-3%V hydrogel, i) Effect (0.5, 1, 1.5) mg/L PFOA concentration on water flux rate and rejection of 2 cm thick kC-0.3%AC hydrogel, j) Effect (0.5, 1, 1.5) mg/L PFOA concentration on water flux rate and rejection of 2 cm thick kC-3%V hydrogel.

4.5.6 PFOA-contaminated water treatment

A 2 cm hydrogel gravity filter of 30 cm height was employed to remove 179.2 mg/L PFOA from electrokinetic soil-remediation wastewater. The kC-0.3%AC hydrogel exhibited excellent performance with 25.6 LMH ±1 water flux and 81.1% PFOA rejection (Figure 4.6a). The corresponding water flux and rejection for kC-3%V hydrogel were 21.5 LMH±1 and 79.3%, respectively. The water flux enhancement in the kC-0.3%AC hydrogel is facilitated by AC, which accelerates solvent exchange during membrane preparation, increasing porosity and creating larger cavities (Table 4.2). Also, the structural changes in the membrane's cross-morphology, from delicate finger-shaped pores in the kC membrane to broader valley-shaped pores with macro voids in the kC-0.3%AC filter, facilitate smoother water molecule passage. Compared to kC-3%V hydrogel, kC-0.3%AC hydrogel showed better PFOA rejection due to its higher surface area (Table 4.2) and adsorption capacity (Supplementary Materials S2.2 and S2.3).

The long-term performance, i.e., rejection and water flux, of the kC-0.3%AC hydrogel was also investigated in three consecutive filtration cycles. Each filtration cycle lasted one hour. The hydrogel was cleaned with DI water for 30 minutes at the end of each cycle before conducting the following filtration cycle with fresh wastewater. The results show decreased water flux and rejection of the kC-0.3%AC hydrogel in the consecutive filtration cycles. For example, the water flux in the kC-0.3%AC decreased slightly from 26.4 LMH in run 1 to 24.1 LMH in run 2 and 23 LMH in run 3. Besides, PFOA rejection decreased from 81.1% in run 1 to 75.1 in run 2 and 70.5% in run 3 (Figure 4.6b). Understanding the equilibrium dynamics is crucial for optimizing PFOA removal at varying concentrations. Particle size or morphology changes can affect the hydrogel's ability to capture and retain contaminants, influencing its performance in consecutive filtration cycles. The PFOA-loaded kC-AC hydrogel consistently maintained its capacity for PFOA removal over three complete cycles. However, the decline in PFOA removal was noticeable in the second and third cycles. Adsorption tests confirm a decrease in the hydrogel's PFOA adsorption capacity in multiple filtration cycles. The decreased PFOA rejection may be attributed to the progressively diminished binding strength between PFOA and the hydrogel in the consecutive filtration cycles. The reduction in rejection efficiency likely arises from the saturation of adsorbent sites with adsorbate molecules after each cycle, resulting in fewer available sites for the adsorbate over time and consequently influencing the PFOA removal efficiency. The competition between PFOA and metal ions on the adsorption sites is another reason for the reduced hydrogel rejection of PFOA in cycles 2 and 3 (Figure 4.6b).

Furthermore, Figures 4.6c and 4.6d show that the kC-0.3%AC hydrogel removed the colour, 92% turbidity, 59% TDS, and 58% EC. Eliminating turbidity operates through the

steric hindrance mechanism, wherein particles are excluded due to their size exceeding the hydrogel pore size, approximately 3.49 nm, as indicated in Table 4.2. In addition, the hydrogel has removed metal ions, for example, 76% Na, 90% K, 75% Si, 83% Cl, and 99% Al. AC's extensive surface area and porous structure facilitate efficient organic and inorganic adsorption. The kC-0.3%AC, incorporating ionizable groups from kC, selectively exchanges ions in applications like removing elements. The kC's diverse functional groups, including hydroxyl and sulfate, enhance element removal through electrostatic or chemical interactions. Concurrently, complexation contributes to the holistic capture and removal of specific elements from the solution, outlining the nuanced mechanisms underlying kC-AC hydrogel's targeted element removal.

Previous studies on the applicability of various hydrogels for PFAS wastewater treatment are listed in Table 4.3. V/AC-kC hydrogels have competitive performance with other hydrogels, with 79% to 81% removal of PFOA from contaminated wastewater, knowing that the concentration of PFOA in this study was at least 1.8 times greater than those in Table 4.3. Also, this study used mixed wastewater from soil remediation containing metal ions such as silica, aluminium, and potassium in moderate concentrations. Also, V/AC-kC hydrogels are easy to fabricate at an affordable cost, about $ 1.5 per kilogram.

The kC-V and kC-AC hydrogels offer sustainable and environmentally friendly water and wastewater treatment methods. The hydrogel is made of natural and decomposable materials and does not require high energy for operation. Besides being gravity-driven, the kC-0.3%AC and kC-3%V hydrogel operate in a dead-end mode, leaving no wastewater/or brine solution behind, which is a problem in reverse osmosis and nanofiltration processes. Also, kC-0.3%AC performed better than kC-3%V hydrogel for PFOA removal from synthetic and actual wastewater.

Table 4. 3:Comparative analysis of PFAS removal efficiency by various hydrogel

Type of Hydrogel	**PFAS Type and Concentration**	**Type of Wastewater**	**Removal (%)**	**Reference**
CTAB-functionalized alginate hydrogel	PFOA/50 mg/L	River water matrix	94.8 ± 2.1%	(Naim Shaikh & Nawaz, 2024)
Quaternized nanocellulose (QNC)	PFBA, PFBS, PFOA, & PFOS (N/A)	Contaminated groundwater	>95% for C7-C9 PFAS, 0% for PFBA, 10% for PFPeA	(Li et al., 2023)
PEI-modified bio-adsorbents (PEI-BA, PEI-LF, PEI-PP)	PFOA/-	Synthetic water matrix	Up to 279.3 mg/g adsorption capacity	(Qin et al., 2023)
Chitosan/F-COF	PFOS & PFOA/-	Lake water, sewage	Over 88.4% for three PFASs, maximum adsorption capacities: PFOS (8307.1 mg/g), PFOA (6177.1 mg/g), GenX (4603.3 mg/g)	(He et al., 2022)

Chitosan-based hydrogel (CEGH)	PFOA/-	Synthetic water matrix	Maximum adsorption capacity: 1275.9 mg/g	(Long et al., 2019)
CNC/PTMAEMA nanocomposite film	PFOA/(1, 10, and 100 mg/L)	Synthetic water matrix	61 %, 67 %, and 76 % respectively.	(Gomri et al., 2023)
COF@CS composite gel	PFOA/-	Synthetic water matrix	Maximum adsorption capacity: 2.8 mmol/g	(Zhang et al., 2024)
Acrylamide-based hydrogel composites with PAC	PFOS & PFOA (N/A)	Synthetic water matrix	98% for PFOS, 96% for PFOA	(Klaus et al., 2023)
kappa carrageenan - Activated carbon	PFOA/(179.2 mg/L)	Soil-remediation wastewater	81.1%	This study
kappa carrageenan - vanillin	PFOA/(179.2 mg/L)	Soil-remediation wastewater	79.3%	This study

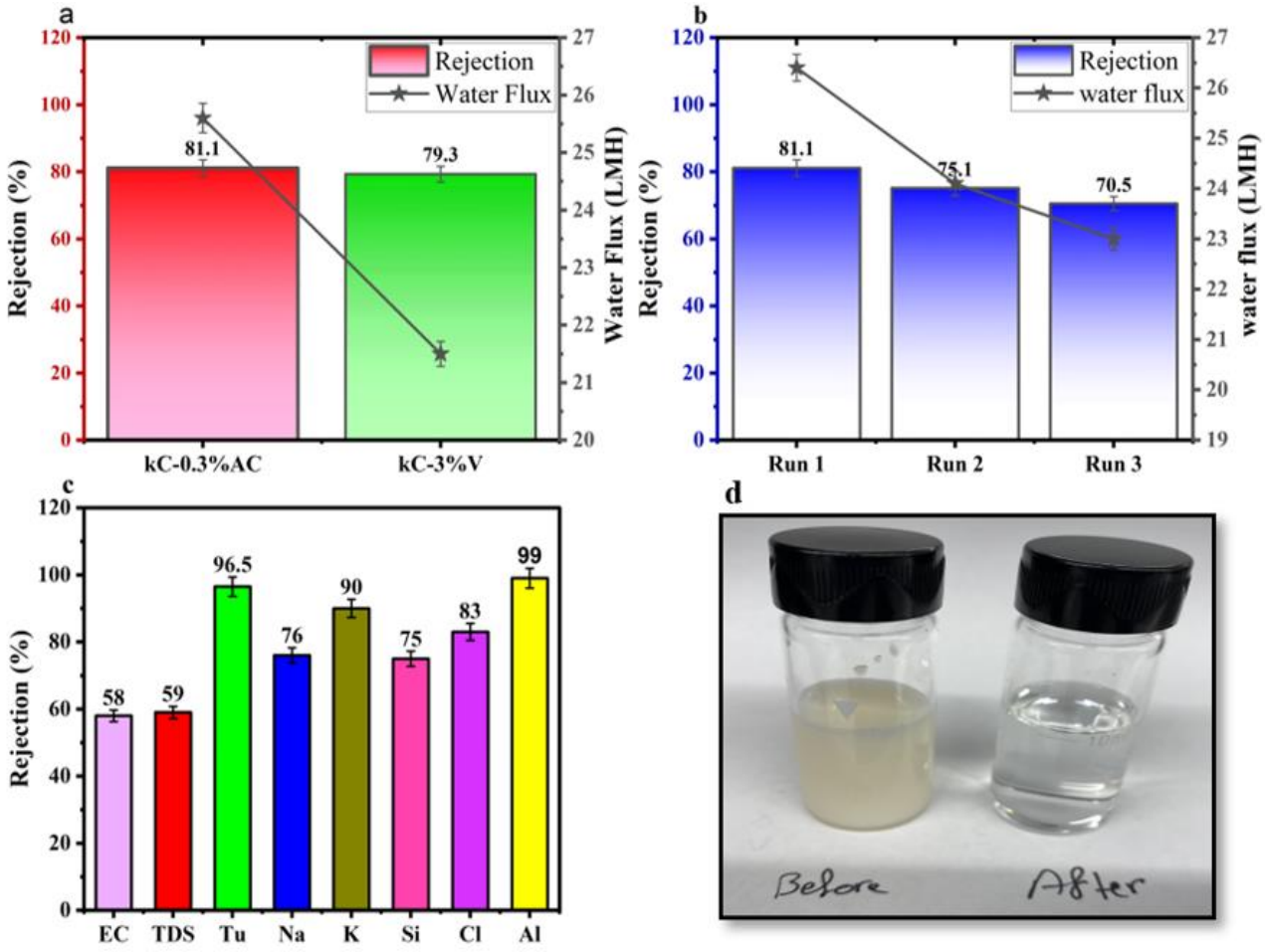


Figure 4. 6.a) Water flux rate and rejection of kC-0.3%AC and kC-3%V hydrogel for PFOA wastewater, b) Water flux and rejection in multiple cycles for PFOA feed solution in kC-0.3%AC, c) Rejection of elements and parameters from the PFOA-contaminated water kC-0.3%AC, and d) colour and turbidity rejection.

4.5.7 Reusability of kC-AC and kC-V hydrogel

The reusability of adsorbents is crucial for mitigating waste production and reducing treatment costs. This study investigated the reusability of the kC-0.3%AC and kC-3%V hydrogels regarding % PFOA removal by repeating adsorption tests. Then, desorption experiments were carried out to assess the reversibility of the process and quantify the quantity of adsorbed PFOA in consecutive cycles. In the desorption procedure, methanol

was introduced into vials containing 20 g of kC-0.3%AC-kC-3%V under monitor conditions. Subsequently, these isolated hydrogel specimens were suspended in methanol (MeOH), which can desorb PFOA from the hydrogel matrix. This method can be employed during regeneration processes, enabling the hydrogel's reutilization in successive cycles of PFOA adsorption.

In Figures 4.7a and 4.7b, the percentage of PFOA removal in three cycles with kC-0.3%AC hydrogel was 82.8 ± 2 %,79.6 ± 2 %, and 77.9 ± 2 %, while in the kC-3%V was 81.5 % ± 2, 77.7% ± 2, and 74.8 % ± 2. The desorption concentration for the three cycles with kC-0.3%AC hydrogel was 77.8 ± 1 %, 70.9 ± 1%, and 67.7 ± 1 %. The corresponding PFOA desorption values for kC-3%V were 77.2 % ± 4,67.1 % ± 4, and 60.5 % ± 4.

Throughout the experimental procedure, it became evident that the PFOA-loaded kC-0.3%AC and kC-3%V hydrogels relatively maintained their capacity for PFOA removal over three complete adsorption-desorption cycles. A noticeable decline in removal efficiency was observed beyond the third cycle, attributed to the progressively diminished binding strength between PFOA and the hydrogel with each successive cycle. The reduction in adsorption efficiency likely arises from the saturation of adsorbent sites with adsorbate molecules after each cycle, resulting in fewer available sites for the adsorbate in subsequent cycles and, consequently, influencing the overall efficiency of the removal process. The capacity for successive adsorption-desorption cycles using the same adsorbent quantity, coupled with its effectiveness in removing PFOA from water, underscores the exceptional efficiency of the kC-AC- kC-V hydrogel as an adsorbent, suggesting a promising and potentially innovative and cost-effective approach for wastewater treatment.

4.5.8 Characterization of kC-AC and kC-V hydrogel after PFOA adsorption

SEM imaging enables a detailed assessment of kC-AC and kC-V hydrogel surface morphology after PFOA adsorption Figures 4.7e and 4.7f. It has been observed that upon exposure to PFOA, the hydrogel's surface undergoes discernible changes manifested by surface roughening, formation of irregularities, or variations in surface topography. The nature and extent of these changes depend on factors such as PFOA concentration, exposure time, and the specific characteristics of the hydrogel material. Investigations indicated that PFOA can exhibit different distribution patterns, ranging from uniform coverage to localized clustering. The hydrogel's affinity for PFOA and the prevailing solution conditions may also influence the nature of the distribution. PFOA may preferentially adsorb in specific regions, forming aggregates or islands. These clusters' degree of aggregation and size can offer insights into the adsorption mechanism.

FTIR is a powerful tool for studying hydrogel and PFOA interactions. It detects shifts in absorption bands and signaling interactions between functional groups in the hydrogel and PFOA. New bands indicate the formation of chemical bonds. FTIR also confirms PFOA adsorption and offers insights into the adsorption mechanism, distinguishing between physical and chemical interactions. The FTIR spectra in Figures 4.7c and 4.7d reveal discernible bands associated with different concentrations of PFOA (0.5, 1, and 1.5) mg/L, indicating its adsorption by the kC-0.3%AC and kC-3%V hydrogel. Notably, a peak at 1,640 cm^{-1} in all kC-0.3%AC and kC-3%V hydrogel spectra post-adsorption indicates the deprotonated carboxylate group (COO^-) (Chen et al., 2017). Importantly, there is an escalation in the intensity of the 1640 cm^{-1} peak, mirroring the increase in the COO- concentration in the solution. This relationship underscores the role of attractions

between the PFOA anion and the positively charged conjugate acid active sites on the kC-0.3%AC and kC-3%V surface as the principal driving force behind adsorption.

Additionally, the FTIR spectra in the 1000–1250 cm^{-1} capture the typical C-F bonds associated with PFOA. Various peaks at specific wavenumbers represent distinct features of the PFOA molecule, including the C-C bond at 1032 cm^{-1}, symmetric CF_2 stretches at 1227 cm^{-1}, asymmetric stretching of CF_2 and CF_3 at 1200-1240 cm-1, and another asymmetric CF_2 stretch (Gao & Chorover, 2012). As the pH during adsorption increases, a noticeable reduction in the intensity of the C-F peaks on kC-0.3%AC and kC-3%V is observed. This effect can be attributed to decreased positively charged conjugate acid active sites on the kC-0.3%AC and kC-3%V surfaces, increasing repulsion between the negatively charged conjugate base active sites on kC-0.3%AC and kC-3%V and the PFOA anion.

EDS and EDX mapping analyses were conducted to characterize the nanoparticles and understand their distribution within the hydrogel cross-section. Figures S2.5a, S2.5b, S2.5c, S2.5d, and Table S3 illustrate the EDS analysis of the section of the kC-0.3%AC and kC-3%V hydrogel after PFOA filtration. The results revealed the presence of carbon and oxygen in all membrane structures, indicating the composition of kC with either AC or vanillin (Figures S2.5a, S2.5b, S2.5c, and S2.5d). Additionally, the detection of gold elements can be attributed to the surface deposition of gold during SEM imaging. Carbon, oxygen, sulfate, and a small amount of fluorine (0.03 wt.%) were identified in the kC-0.3%AC and kC-3%V membrane structures. The EDS spectrum exhibited the highest intensities for fluorine and chloride ions, along with the presence of sodium, calcium, and sulfur as the primary constituents of the hydrogel after filtration. This finding suggests a relatively uniform distribution of elements within the membrane structure. After

filtration, increased fluorine was observed in the hydrogel, 5.12 wt% and 4.04 wt% in the kC-0.3%AC and kC-3%V, respectively. Moreover, chloride was observed in the hydrogel, with concentrations of 2.24 wt% in kC-0.3%AC and 1.73 wt% in kC-3%V.

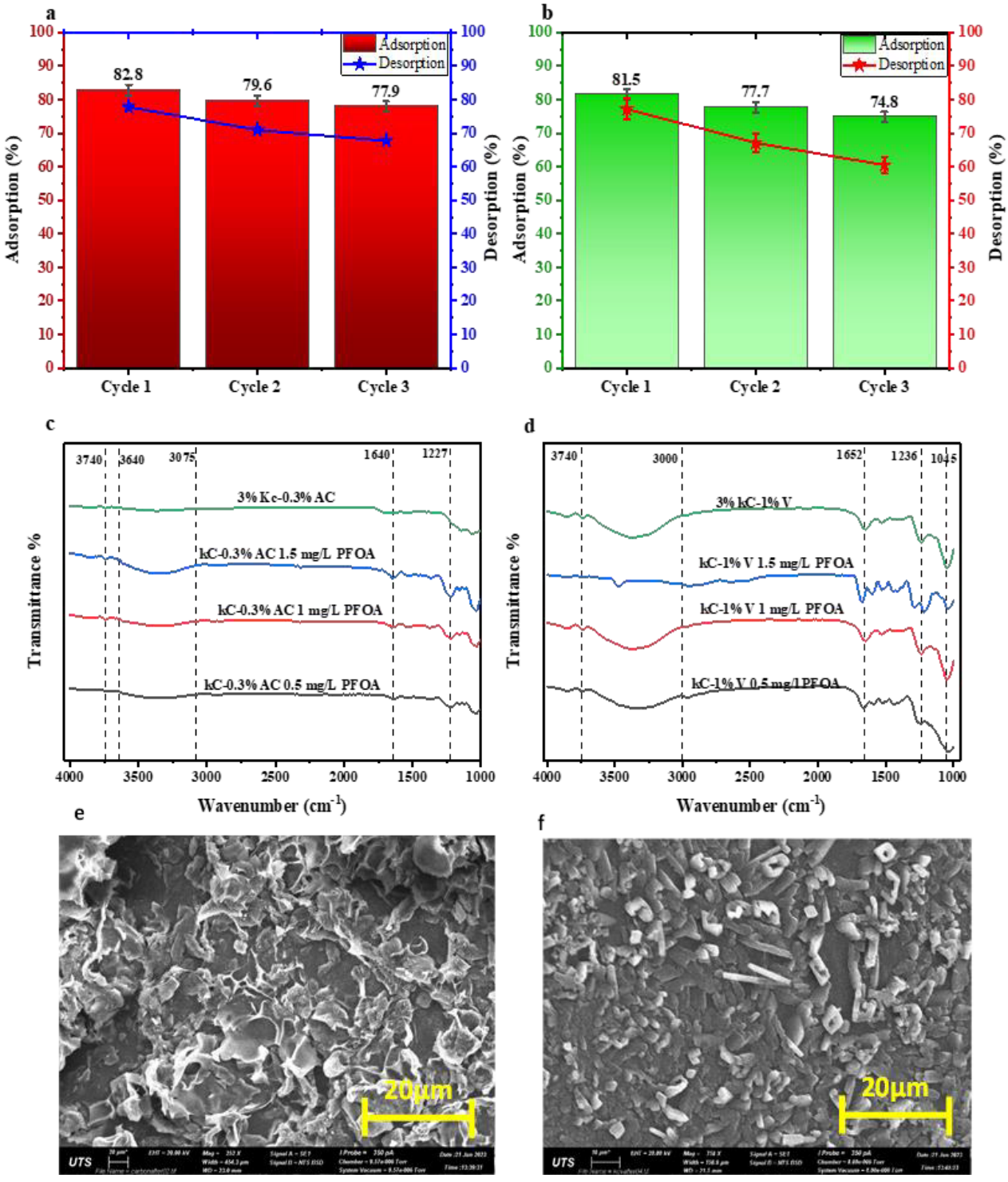


Figure 4. 7.a) adsorption and desorption of 1.5 mg/L PFOA in three consecutive cycles of 3%kC-0.3%AC, b) adsorption and desorption of PFOA in three consecutive cycles of 3%Kc-1%V, c) FT-IR of the different concentration AC (0.1,0.2,0.3)% with 3%kC after filtration, d) FT-IR of the different concentration V (1,2,3)% with 3%kC after filtration, e) SEM of the 3%kC-0.3%AC hydrogel after filtration at 20 μm at the first focus point, f) SEM of the 3%kC-3%V hydrogel after filtration at 20 μm at the first focus point.

4.6 Conclusion

The study revealed kC-based hydrogel's exceptional efficiency in adsorbing various PFOA and pollutants, making it a compelling alternative for water purification. Incorporating vanillin and AC into the kC hydrogel significantly enhanced the kC-3%V membrane porosity, from 62.8% ± 5 to 79.1% ± 5 and up to 89.7% in the kC-0.3%AC. When evaluating the hydrogel's performance against PFOA, notable pH-dependent variations in rejection were observed. The hydrogel rejection of PFOA is pH-dependent, with the kC-0.3%AC hydrogel achieving an 86.9% rejection at pH 4, while the kC-3%V showed 85.7% rejection. Experiments also exhibited a decline in the water flux at higher PFOA concentrations and pH levels for both kC-0.3%AC and kC-3%V hydrogels. The study revealed that PFOA rejection increased with concentration, indicating that elevated PFOA levels restrict water passage by occupying pore spaces. When it was tested for soil remediation wastewater treatment, the kC-0.3%AC hydrogel removed 81.1% PFOA at 25.6 LMH water flux, while the kC-3%V hydrogel removed 79.3% PFOA at a water flux of 21.5 LMH. However, due to pore blocking, consecutive filtration cycles revealed a slight decline in the hydrogel's performance. More characterization results, such as pH at zero-point charge (pHpzc), X-ray diffraction (XRD), and X-ray photoelectron

spectroscopy (XPS), should preferably be included in future work to understand the mechanisms of PFOA removal better.

Supplementary information S2

Performance and analysis of kappa-carrageenan hydrogel for PFOA-contaminated soil remediation wastewater treatment

Alsaka, L., Ibrar, I., Altaee, A., Zhou, J., Chowdhury, M. H., Maryam, A.-E., & Hawari, A. H. (2024). Performance and analysis of kappa-carrageenan hydrogel for PFOA-contaminated soil remediation wastewater treatment. *Chemosphere*, *365*, 143371.

S2.1 The filtration device

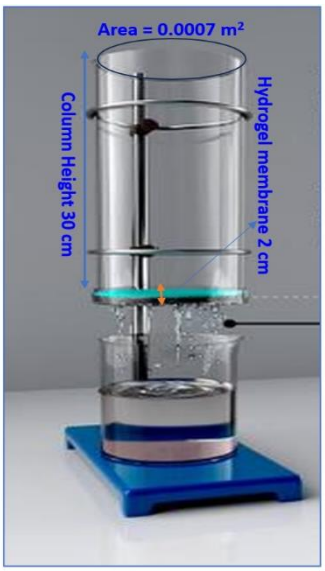


Figure S2. 1.a schematic of gravity filtration.

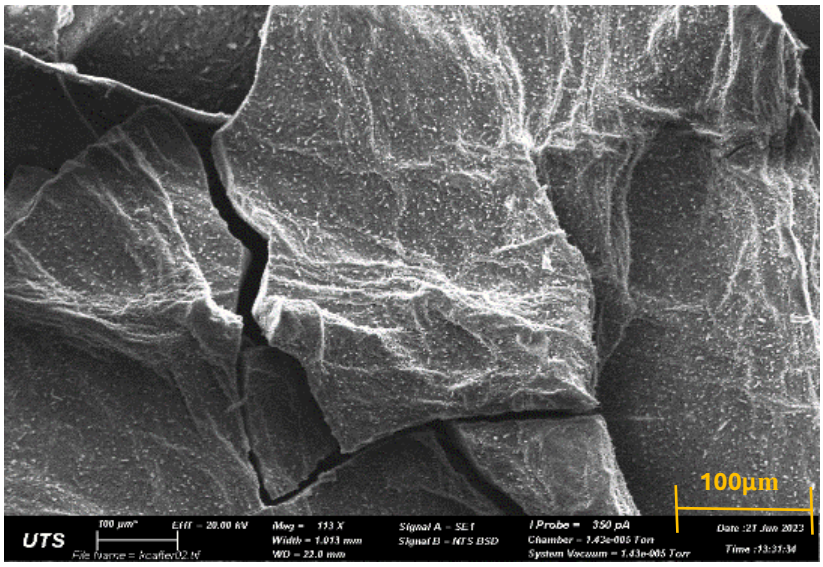


Figure S2. 2.SEM of the 3% kC hydrogel at 100 µm.

S2.2 Adsorption-desorption ability/ Adsorption kinetics models

In a controlled batch study, adsorption capacity was assessed using a thermostatic shaker at varying pH levels (2.8, 4.2, 7, 9.2) with PFOA solutions. Experiments utilized two hydrogels: 3%kC mixed with 1-3%vanillin (V) and 3%kC mixed with 0.1-0.3%AC. LC-MS analysis determined PFOA concentration and adsorption capacity (mg/g), calculated using Equation S1 in Table S1. Desorption experiments assessed reversibility by employing a thermostatic shaker with 30 mL methanol. The 3%kC-3%V and 3%kC-0.3%AC materials were separated via centrifugation, and desorption capacity (mg. g^{-1}) was computed using Equation S2.3 in Table S1. Established mathematical models, including the pseudo-first-order, pseudo-second-order, intraparticle diffusion, and Elovich models, were employed to unravel the intricacies of adsorption kinetics PFOA using kC-AC/V hydrogel in Table S2.1.

S2.3 Adsorption /Desorption of The PFOA solution

S2.3.1 Effect AC and Vanillin concentrations

Increasing adsorbent amount (Figures S2.3a and S2.3b) correlates with higher PFOA adsorption capacity, indicating the pivotal role of hydrogel concentration. Higher concentrations offer more active sites, enhancing mass transfer.

S2.3.2 Effect of pH

Testing PFOA adsorption on kC-0.3%AC and kC-3%V at pH levels 2.8, 4.2, 7, and 9.2 revealed rapid surface adsorption in the initial five hours, followed by slower mesopore diffusion. Optimal adsorption occurred at pH 4.2, with lower capacities at 2.8, 7, and 9.2 due to protonation and charge variations (Figures S2.3c and S2.3d).

S2.4 Adsorption kinetics

Figures S2.4a to S2.4h illustrate PFOA (1 mg/L) adsorption kinetics in kC-0.3%AC and kC-3%V hydrogels at pH levels 2.8, 4.2, 7, and 9.2. Table S2.2 details parameters for diverse adsorption models, with the pseudo-second-order (PSO) model exhibiting a strong correlation (R^2 = 0.992 to 0.998). The pseudo-first-order (PFO) model also demonstrates a good correlation (R^2 = 0.995 to 0.999). The PSO model effectively captures chemisorption-dominated PFOA adsorption across pH ranges, depicting rapid initial adsorption followed by slower diffusion into hydrogel mesopores. The Elovich equations align closely with experimental results at pH 4.2, indicating prolonged adsorption. Intra-particle diffusion analysis reveals multi-phased dynamics, emphasizing process complexity. The relatively lower R^2 value for intra-particle diffusion suggests potential for better-fitting kinetic models, as indicated in Table S2.2.

Table S2. 1:Kinetic Equations for different models.

Eq No.	Equations	Definition of parameters
S2.1	$Adsorption\ capacity\left(\frac{mg}{g}\right) = \frac{(CiPFOA - CfPFOA) * VPFOA}{Wgel}$	*CiPFOA* (initial PFOA concentration in mg/L) *CfPFOA*(equilibrium residual PFOA concentration in mg/L) *VPFOA* (solution volume in L) *Wgel* (weight of kC-AC and kC-V in g).
S2.2	$\text{Maximum capacity adsorption (mg/g)} = \frac{Q.Ci}{m}\int_{t=0}^{t=total}(1-\frac{Cf}{Ci})$	*Q* the flow rate (L/min) *m* is the quantity of adsorbent (hydrogel) in g. *Ci* is the initial concentration of the PFOA solution (mg/L). *Cf* is the redidual concentration of the PFOA solution at equilibrium (mg/L).
S2.3	$Desorption\left(\frac{mg}{g}\right) = \frac{(CrPFOA * VPFOA)}{Wgel}$	*CrPFOA* represents the residual concentration of PFOA (mg/L) *VPFOA* is the volume solution of methanol in Liters (L), *Wgel* is the weight of gel in grams (g).
S2.4	$D\% = \left(\frac{CPFOA\ desorbed}{CPFOA\ adsorbed}\right)X100$	*D%* (degree of desorbed). *CPFOA desorbed* (concentration of PFOA mg/g). *CPFOA adsorbed* (concentration of PFOA mg/g).
S2.5	$qt = qe(1 - e^{k1t})$	*qt*(mg/g) amount adsorbed at time t. *qe* (mg/g) amount remaining after of adsorption reaction. *K1* Pseudo first rate constant (mg/(g*min)).

S2.6	$$qt = \frac{qe^2 k2t}{1 + qtk2t}$$	*qt*(mg/g) amount adsorbed at time t. *qe* (mg/g) amount remaining after of adsorption reaction. *K2* Pseudo second rate constant (mg/(g*min)).
S2.7	$$qt = kdifft^{1/2} + c$$	*Kdiff* denotes the intraparticle diffusion rate constant(mg/(g*min)). *c* signifies the boundary layer thickness.
S2.8	$$qt = \frac{1}{\beta} ln(\alpha\beta) + \frac{1}{\alpha\beta} lnt$$	α the initial adsorption rate (mg/(g*min)). β desorption constant (mg/(g*min)).

Table S2. 2:Kinetic parameters of kC-AC/V hydrogel for different models.

Kinetic adsorption for 3%kC-3%V					
Kinetic model	**Parameters**	**pH 2.8**	**pH 4.2**	**pH 7**	**pH 9.2**
Pseudo first order	K1(1/min)	3.06±0.33	2.84±0.11	3.08±0.25	2.33±0.24
	qe cal (mg/g)	0.00174±9.2E-6	0.0018±3.9E-6	0.0016±6.2E-6	0.00169±1.4E-5
	qe exp(mg/g)	0.001742	0.001799	0.00161	0.001605
	R^2	0.998	0.999	0.998	0.995
Pesudo second order	K2 mg/(g min)	11425.94±4839.95	9116.12±2270.2	10615.99±215.9	4393.75±746.7
	qe cal (mg/g)	0.00176±1.4E-5	0.00182±1.02E-5	0.00162±7.2E-5	0.00174±1.3E-5
	qe exp(mg/g)	0.001748	0.001805	0.001605	0.00175
	R^2	0.997	0.998	0.992	0.998
Elovich model	qe(mg/g)	0.00175	0.0018	0.00161	0.00171
	α mg/ (g min)	4.41E37±3.29E39	2.53E30±1.13E39	9.02E26±2.7E26	2.37E8±2.0E9
	β mg/ (g min)	57211.52±43775.87	46050.37±25531.47	46711.77±19127.94	18323.99±5247.36
	R^2	0.996	0.997	0.998	0.995
Intraparticle diffusion model	qe(mg/g)	0.00176	0.00182	0.00162	0.00172
	Ki mg/ (g min)	2.49E-4±1.22E-1	2.59E-4±1.25E-1	2.32E-4±1.11E-1	2.58E-4±2.77E-1
	C mg/g	0.00103±2.98E-4	0.00106±3.06E-4	9.4E-4±2.7E-4	9.57E-4±2.77E-4
	R^2	0.343	0.350	0.354	0.393
Kinetic adsorption for 3%Kc-0.3%AC					
Kinetic model	**Parameters**	**pH 2.8**	**pH 4.2**	**pH 7**	**pH 9.2**
Pseudo first order	K1(1/min)	1.63±0.19	1.57±0.22	1.51±0.162	2.75±0.29
	qe cal (mg/g)	0.0021±2.87E-5	0.00221±3.73E-5	0.00197±2.66E-5	0.00193±1.22
	qe exp(mg/g)	0.00205	0.00212	0.00196	0.00194
	R^2	0.987	0.982	0.989	0.997
Pseudo second order	K2 mg/(g min)	1597.51±200.13	1394.57±219.07	1541.41±175.40	5552.61±865.73
	qe cal (mg/g)	0.00222±2.25E-5	0.00233±3.142E-5	0.00208±2.05E-5	0.00197±1.0E-5
	qe exp(mg/g)	0.00214	0.002246	0.0019965	0.001992
	R^2	0.997	0.995	0.997	0.999
Elovich model	qe (mg/g)	0.00215	0.00226	0.0020	0.00195
	α mg/ (g min)	66.28±176.14	21.43±49.6	24.09±61.05	2.51E12±2.26E13
	β mg/ (g min)	7119.97±1392.17	6220.19±1167.14	7131.56±1435.95	20922.02±2844.49
	R^2	0.990	0.989	0.988	0.998

Intraparticle diffusion model	qe(mg/g)	0.00215	0.00224	0.00202	0.0021
	Ki mg/ (g min)	3.51E-4±1.32E-1	3.75E-4±1.36E-	3.29E-4±1.22E-1	2.91E-4±1.30E-1
	C mg/g	0.0011±3.23E-4	0.00113±3.34E-4	0.00101±2.99E-4	0.00111±3.19E-4
	R^2	0.469	0.485	0.476	0.383

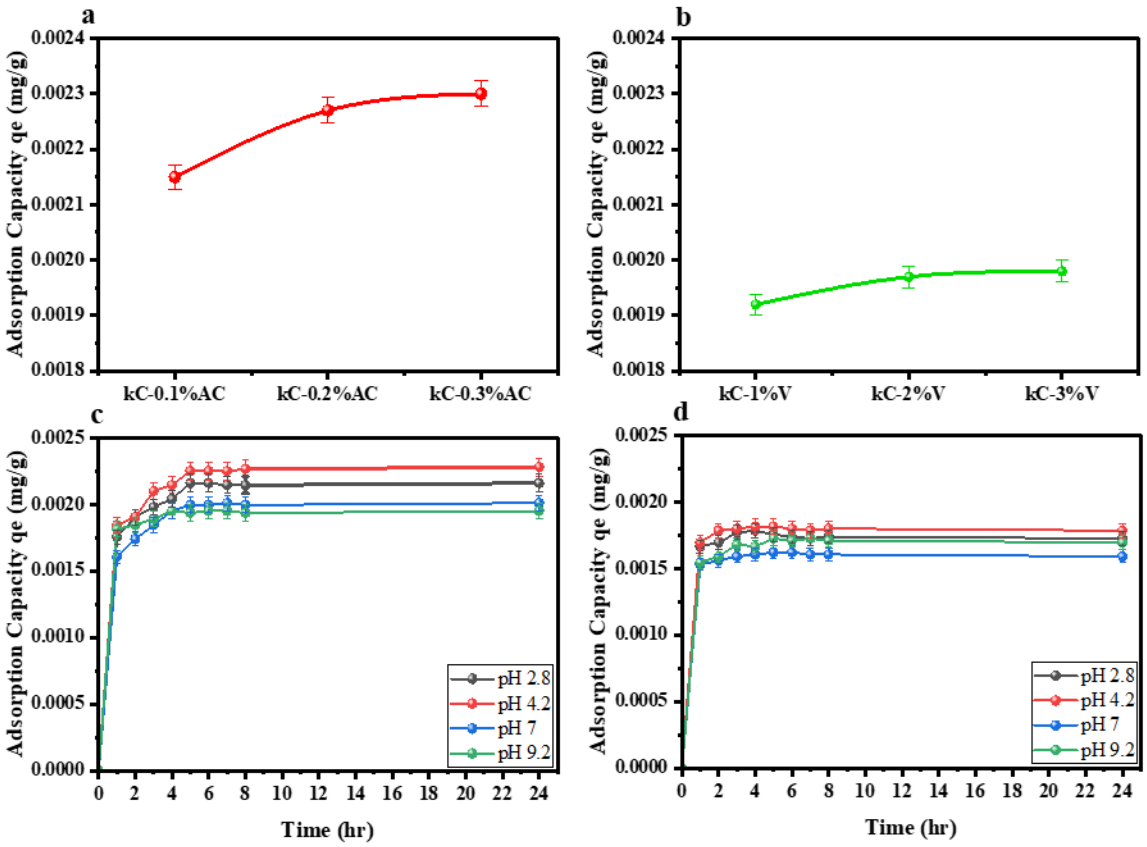


Figure S2. 3.a and b) influence of kC-0.3%AC and KC-3%V concentrations on adsorption of PFOA, c and d) adsorption curve for kC-0.3%AC and KC-3%V hydrogel for PFOA at different pH with time respectively. PFOA concentration in the feed solution is 1 mg/L.

Table S2. 3: The EDS analysis results for the kC-AC and kC-V hydrogel.

Element	**Quantitative Results (wt.%)**			
	kC-AC	kC-AC	kC-V	kC-V
	Before	After	Before	After
C	83.60	55.05	85.15	41.79
O	13.64	35.08	12.64	47.79
S	----	3.02	0.03	4.14
F	2.76	5.12	2.18	4.04
Cl	----	1.73	----	2.24
Total	100	100	100	100

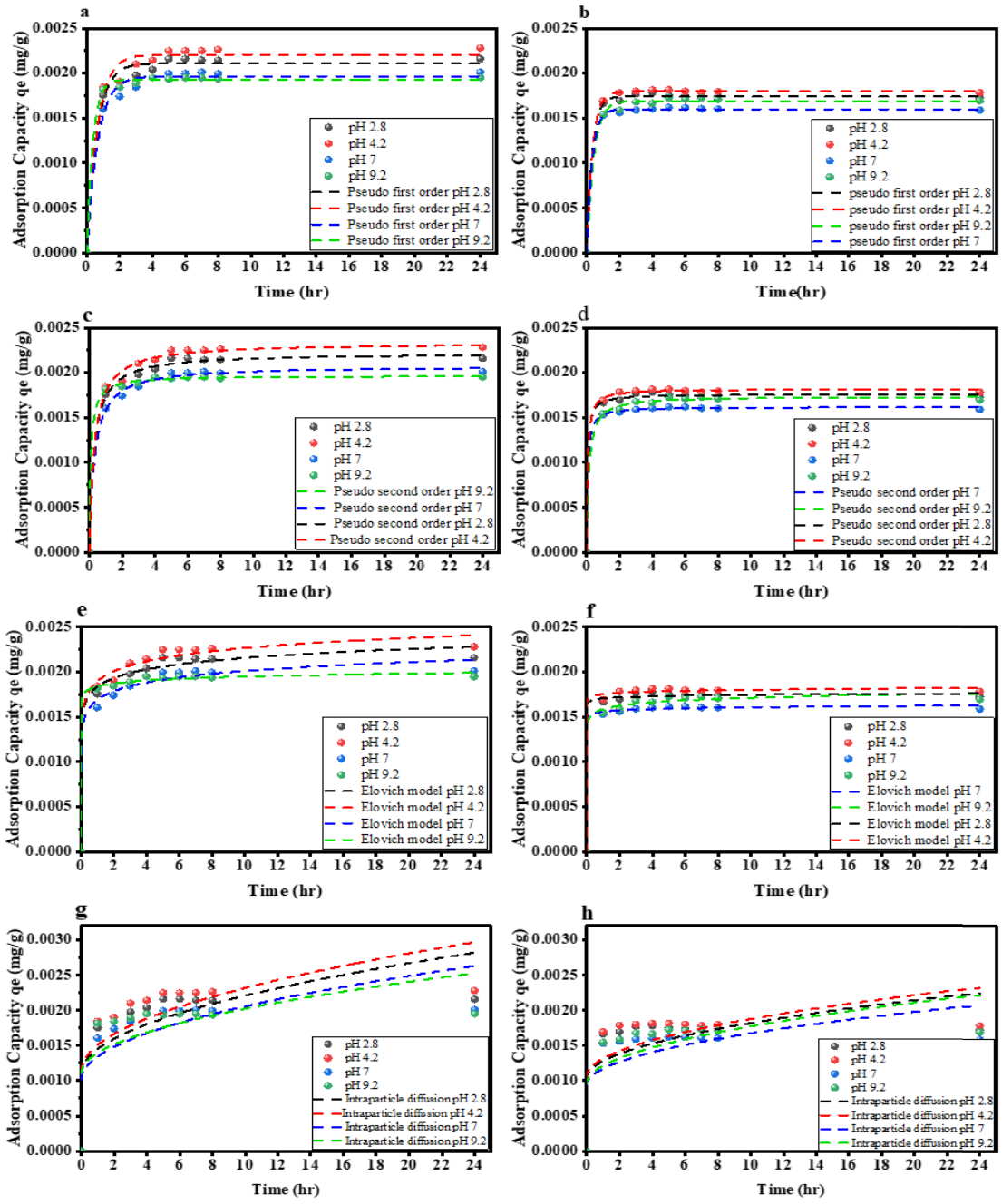


Figure S2. 4.a and b) pseudo-first-order for kC-0.3%AC and KC-3%V hydrogel for PFOA at different pH with time, c and d) pseudo-second-order for kC-0.3%AC and KC-3%V hydrogel for PFOA at different pH with time, e and f) Elovich model for kC-0.3%AC and KC-3%V hydrogel for PFOA at different pH with time, g and h) Intraparticle diffusion model for kC-0.3%AC and KC-3%V hydrogel for PFOA at different pH with time.

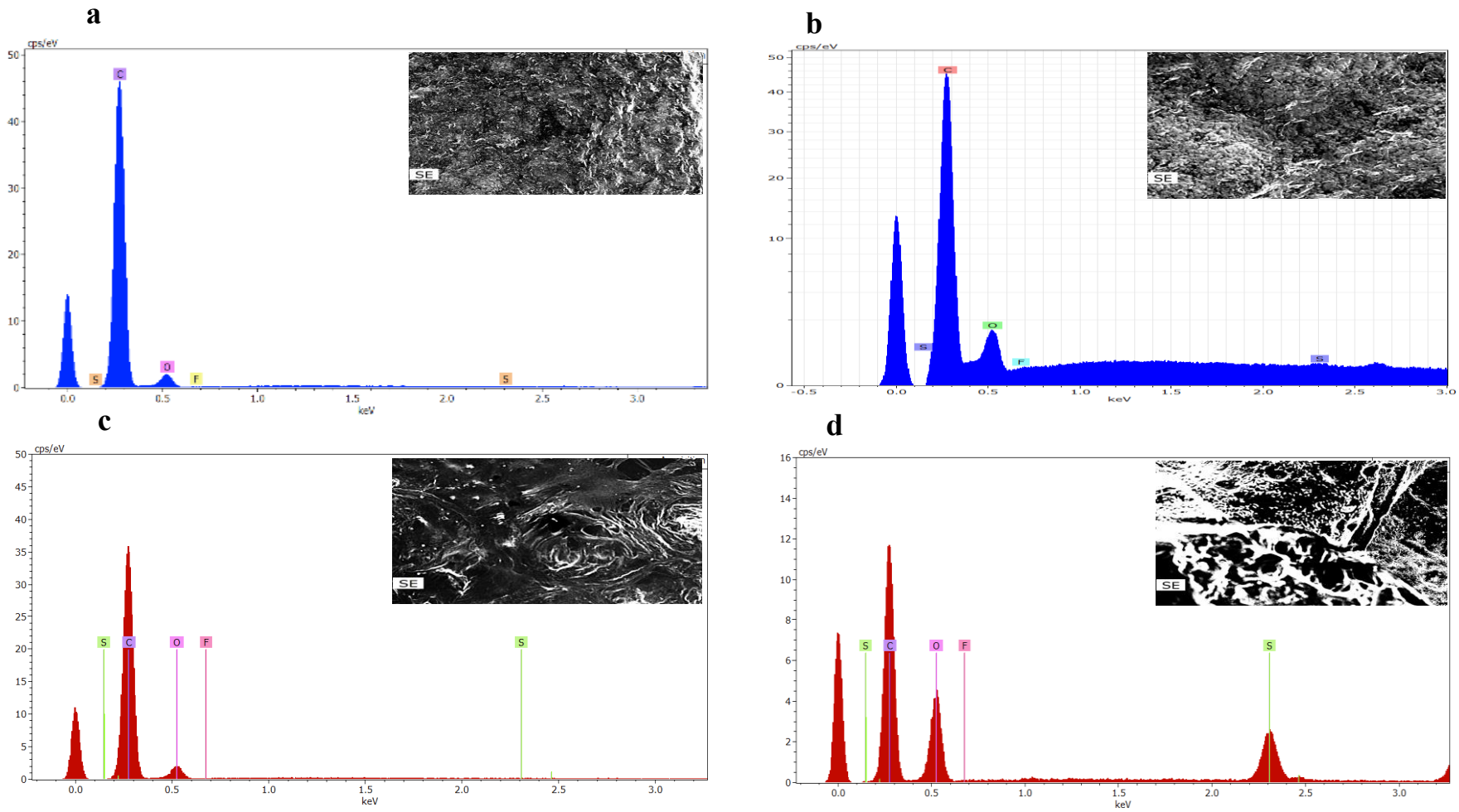


Figure S2. 5.a and b) EDX of the kC-0.3%AC hydrogel before and after filtration, c and d) EDX of the kC-3%V hydrogel before and after filtration.

Chapter 5: kappa-carrageenan-based hydrogel for leachate wastewater treatment and resource recovery

Alsaka, L., Altaee, A., Alsaka, L., Al-Ejji, M., Hawari, A. H., & Zhou, J. (2025). kappa-Carrageenan-based hydrogel for leachate wastewater treatment and resource recovery. *Desalination*, 119208.

Author contributions statement:

Lilyan Alsaka: Investigation, methodology, conceptualization, data Analysis, Writing and editing. Ali Altaee: Supervision, Conceptualization, Curation, investigation, data analysis, writing and editing. Lina Alsaka: Investigation, data analysis, writing. Maryam AL-Ejji: Data analysis and writing. Alaa H. Hawari: Data analysis, Curation, investigation. John L. Zhou: Supervision, writing and editing.

Abstract

The current investigation examined the effectiveness of a kappa-carrageenan-activated carbon/polyethylenimine (kC-AC/PEI) hydrogel, with a surface area of 95.61 m^2/g, in the removal and recovery of metal ions from leachate wastewater. Variations in kC concentrations are analyzed for their influence on the hydrogel's structural characteristics, adsorptive performance, water absorption capacity, and swelling behaviour. Additionally, optimization of operational parameters, including temperature and pH, is explored to achieve maximum adsorption efficiency. The hydrogel demonstrated exceptional efficiency in treating leachate, with rejection rates of 97.8% for total organic carbon (TOC) and 94.4% for turbidity. The kC-AC/PEI hydrogel exhibited 82.9% to 87.1% rejection for divalent ions and 46.9% to 74.4% for monovalent ions. In addition, permeation flow declined 12% over three cycles, starting at 32.3 LMH and decreasing to

28.2 LMH in the third cycle. The kC-AC/PEI hydrogel exhibited excellent reusability after recycling, achieving 80.6% rejection of Mg^{2+} and 40.3% for Na^{+} ions. Other metal ions exhibited slight declines in rejection rates, demonstrating the hydrogel's enduring efficiency in removing ions even after recycling. At the end of the hydrogel tests, reverse osmosis effectively recovered approximately 70% of metal ions from the hydrogel, making the hydrogel-RO system a sustainable and affordable approach for metal recovery from wastewater in small-scale treatment plants.

5.1 Introduction

Annually, industries release into the environment heavy metal-containing waste solutions laden with copper, lead, zinc, cadmium, mercury, and chromium. These toxic metals will impact the food chain and aquatic life, causing significant health problems, including kidney damage and cancer. Extensive pollution stresses the pressing need for innovative wastewater treatment methods that should be effective and affordable to protect the environment and public health (Zhou et al., 2023). Membrane processes, such as reverse osmosis (RO) and nanofiltration (NF), efficiently separate heavy metals from solutions, but they suffer significant disadvantages, including the need for extensive pretreatment, high energy consumption, and membrane fouling. In contrast, adsorption-based techniques, particularly those using activated carbon (AC), zeolites, clay minerals, and hydrogels, provide a comparatively economical strategy but with restricted efficacy and varying effectiveness in eliminating various pollutants (N Abdullah et al., 2019).

Hydrogels are adept at absorbing organic and inorganic pollutants(Kwon et al., 2025). Remarkably, kappa-carrageenan (kC) hydrogel, comprising crosslinked polymers with anionic sulphate groups ($–OSO^{3-}$), exhibited potential for heavy metal treatment (Aguilan et al., 2003). In addition, it possesses numerous hydroxyl and carboxyl groups along its

polysaccharide backbone, presenting potential reaction and coordination sites for the adsorption of diverse pollutants (Kulal & Badalamoole, 2020b). These attributes render carrageenan an outstanding biopolymer for crafting adsorbent and filtration materials. The kC's anionic nature enables the formation of a robust hydrogel, particularly effective in adsorbing positively charged pollutants from wastewater and water softening (Rocha et al., 2021). The advancement of adsorption technologies is contingent upon the development of efficacious adsorbents. Although powdered materials, such as AC, possess notable adsorptive properties, they are impeded by agglomeration issues and subsequent separation complexities (Singh et al., 2018). Hydrogel, characterized by a three-dimensional polymer network saturated with water, gained attention for wastewater treatment due to its cost-effectiveness, recyclability, and ease of fabrication (Weerasundara et al., 2021). However, many reported hydrogels experience poor mechanical performance, low adsorption capacity, or slow diffusion kinetics (Kalcioglu et al., 2012; Yang et al., 2013). Incorporating adsorptive nanoparticles into a hydrogel matrix effectively enhances its mechanical properties and adsorption capacity (Makhado et al., 2020). Graphene oxide (GO) (Hou et al., 2012), titanium dioxide, metal or metal oxide, and biochar (Weerasundara et al., 2021) were integrated with hydrogels to address physicochemical challenges.

AC was widely used in water purification for its considerable adsorption ability, large surface area, pore structure, chemical stability, low toxicity, and renewability. It is a robust adsorbent in wastewater treatment (Cheng et al., 2016; Liu et al., 2014). Graphene-based hydrogels also showed advanced adsorption capacities toward heavy metals and metalloids (Chen et al., 2013). An adsorption capacity of 52.63 mg/g was observed at an optimal pH of 6 by chitosan with an AC layer, achieving completed cadmium ions

removal (Hydari et al., 2012). Polyethyleneimine (PEI), a hydrophilic branched polymer rich in amine (-NH_2) functionalities, is known for its strong attraction to metal ions. The abundant -NH_2 groups on PEI can be effectively crosslinked with epoxy or aldehyde groups to form functional materials of various forms, such as hydrogels, membranes, and fibers (Jin et al., 2017). Yang et al. developed a PEI-modified chitosan electrospun membrane for removing metal ions from water, which showed enhanced adsorption capabilities post-PEI modification (Yang et al., 2019). Similarly, Arshad et al. produced GO-infused alginate-PEI beads specifically for capturing heavy metals, exhibiting 602, 374, and 181 mg/g adsorption for Pb^{2+}, Hg^{2+}, and Cd^{2+} ions following PEI integration (Arshad et al., 2019). Keränen et al. reported the removal of Ni^{2+} and vanadium from natural industrial wastewater, noting that AC had an adsorption efficiency of 4.36 mg/g at pH 5.5 and 5.0 g/L feed concentration (Keränen et al., 2015). Another investigation revealed the adsorption capacity of Ciprofloxacin (CIP) by kC/SA composite double-network hydrogels at a remarkable rate of 229 mg/g, with optimal performance at pH 4 and an increasing trend with ion concentration (Yu et al., 2019). The kC hydrogel was also reported for organic matter and dye removal from wastewater. Liu et al. reported that the demonstrated efficacy of methylene blue (MB) removal surpassed 92% after 120 minutes of employing carboxymethyl cellulose (CMC)/ kC/activated montmorillonite (C. Liu et al., 2018). Furthermore, the CS/kC hydrogel demonstrated exceptional phenol adsorption capabilities, achieving an uptake of 80% (Hamid et al., 2023). Soares et al. used kC-coated magnetic iron oxide nanoparticles for efficient methylene blue removal (530 mg/g), achieving >97% removal in six consecutive experiments (Soares et al., 2017). Duman et al. engineered magnetic OMWCNT-kC-Fe_3O_4 nanocomposites for effective methylene blue removal (Duman et al., 2019). Yang et al. developed eco-friendly κ-

carrageenan and graphene oxide gel beads (κ-Car/GO-GBs) for methylene blue adsorption, demonstrating stable, high adsorption capacity of 658.4 mg/g after five cycles (Yang et al., 2017). Despite the wealth of literature on hydrogel treatment of wastewater, there are scarce studies on the kC-based membrane long-term performance and reusability after metal ions recovery by desorption.

Most literature used hydrogel in adsorbent beads for metals removal from wastewater, with limited removal percentage and generating large brine volumes. In this study, a hydrogel membrane was fabricated and tested in a dead-end filtration cell for metal recovery and reuse from leachate wastewater. The advantage of kC is a thermoreversible hydrogel, i.e., it can be melted and hardened by heating and cooling, and hence it can be thermally or chemically treated for metal ions recovery and recycled for reuse. The hydrogel adsorption capacity, hydrophilicity, and mechanical strength were improved by blending with AC and crosslinking with PEI. The AC provides additional sites for the adsorption of metal ions, while amine groups in the PEI will chelate heavy metal ions (Lu et al., 2020). The hydrogel was cast as a thin composite membrane for metal ions recovery from wastewater in a dead-end filtration cell to reduce the generation of brine and facilitate the ions recovery using a hydrogel-reverse osmosis (RO) system. The leachate wastewater treatment was conducted using a dead-end gravity filtration column, followed by metal ions desorption from the hydrogel and heavy metals recovery by an RO system. The research questions are: i) what is the impact of AC and PEI on the kC hydrogel swelling and permselectivity? ii) what is the impact of the operating conditions, such as feed temperature and pH, on the hydrogel performance and ion removal? And iii) is the cross-linked hydrogel reusable after metal ions recovery? Metal ions were desorbed from the hydrogel filter at the end of the experiments and recovered by an RO system using a

brackish water RO membrane. The kC features an environmentally friendly, cost-effective, and biodegradable filter, making it a sustainable wastewater purifying option.

5.2 Materials and methods

5.2.1 Materials

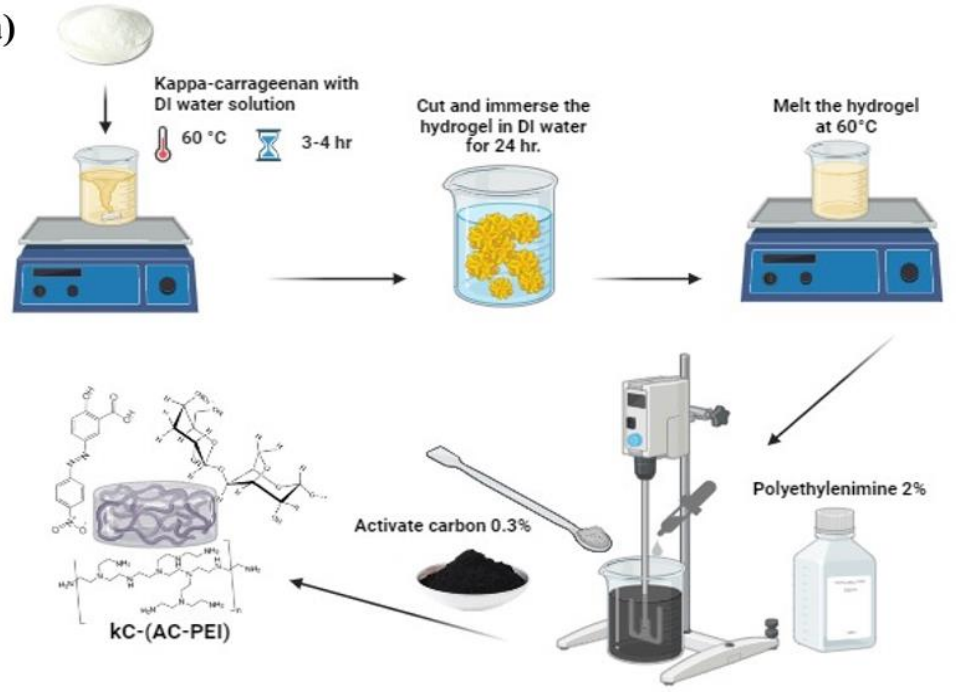
All substances were sourced from Sigma Aldrich in Australia, including the kappa-Carrageenan (kC,1->4-3,6-anhydro-alpha-d-galactopyranosyl-1->3-4-o-sulfonato-beta-d-galactopyranan, CAS number 11114–20-8, molecular weight 788.647 g/mol, purity 99 %, Molecular Formula C24H36O25S2-2), activated carbon (AC, MW 12.01 g/mol, CAS number 7440-44-0), Polyethyleneimine (PEI, MW ~ 2000 by LS,50 wt% in H_2O, CAS number 9002-98-6), and Polyvinyl alcohol (PVA, MW 89000~ 98000, 99% hydrolysed, CAS number 9002-89-5), all of which were utilized in the hydrogel synthesis. For the rejection studies, analytical grade chemicals such as magnesium sulphate ($MgSO_4$) (MW 120.37 g/mol, CAS number 7487-88-9, purity ≥ 99.99 %), copper sulphate ($CuSO_4$) (MW 159.61 g/mol, CAS number 7758-98-7, purity ≥ 99 %), and sodium chloride (NaCl) (MW 58.44 g/mol, CAS number 7647-14-5, purity ≥ 99 %) were procured from Sigma-Aldrich. The landfill leachate wastewater, post-biological treatment, was obtained from Hurstville Golf Centre. A layer of cotton was used as a support layer for the KC-AC/PEI hydrogel filter, which was incorporated into a filtration column designed for water treatment. The hydrogel was manually applied to the cotton layer within a specialized filtration column for water treatment.

5.2.2 Synthesis of kC-AC/PEI hydrogel

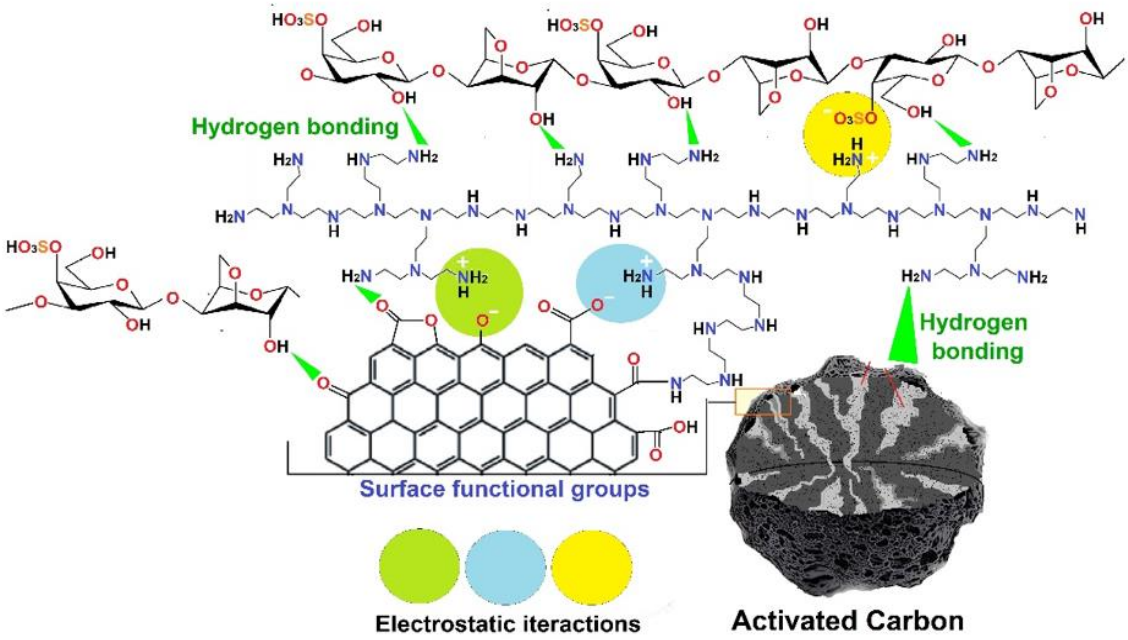
To prepare the kC hydrogel, different concentrations of kC powder (1% to 3%) wt/v were dissolved in deionized (DI) water. Then, the mixture was heated to 60 °C and left on a

magnetic stirrer for 3-4 hr to ensure a homogenous gelatinous solution. The hydrogel was washed with DI water to remove residual impurities. Then, the hydrogel was placed on the magnetic stirrer at 60 °C, and the solubilized hydrogel was mixed at 800 rpm using an electric mixer with (0.3% wt/v) AC and (2% wt/v) PEI. The mixing process continues for four hr until the consistency of a soft, easy-to-pour hydrogel is formed. The hydrogel was cast into a filtration column and left to settle for 10 to 15 minutes before the test. After casting in the filtration column, the hydrogel filter top was sealed with a 10% PVA to prevent water leakage (Figure 5.1a). The acrylic filtration column made from polycarbonate (PC) material in a 13 cm^2 active area (Figure S3.1) was used for wastewater treatment. During all experiments, the feed solution level in the column was maintained at 22 cm height. The composite Figure 5.1b represents integrating PEI into the aqueous solution comprising kappa carrageenan and activated carbon to synthesize a hydrogel. Introducing PEI enhanced the hydrogel's stability and augmented its mechanical robustness during the membrane filtration procedure. Figure 5.1c shows the amine functionalities in PEI form hydrogen bonds with the hydroxyl groups in kappa-carrageenan while concurrently engaging in electrostatic interactions with the sulfate groups of kappa-carrageenan. Additionally, activated carbon participates in hydrogen bonding and electrostatic interactions with PEI. While AC offers a large surface area, enhancing the hydrogel's capacity to remove pollutants, PEI contributes numerous amine groups, enhancing kC-AC hydrogel crosslinking, strengthening its structure, and improving reusability. Owing to its chemical nature, meticulous regulation of crosslinking density and prudent disposal methods are needed to mitigate environmental effects and guarantee sustainability. Table 5.1 shows the kC-AC/PEI hydrogel membranes investigated in this study.

(a)


Kappa-carrageenan with DI water solution
60 °C
3-4 hr
Cut and immerse the hydrogel in DI water for 24 hr.
Melt the hydrogel at 60°C
Polyethylenimine 2%
Activate carbon 0.3%
kC-(AC-PEI)

(b)


Hydrogen bonding
Hydrogen bonding
Surface functional groups
Electrostatic iteractions
Activated Carbon

(c)

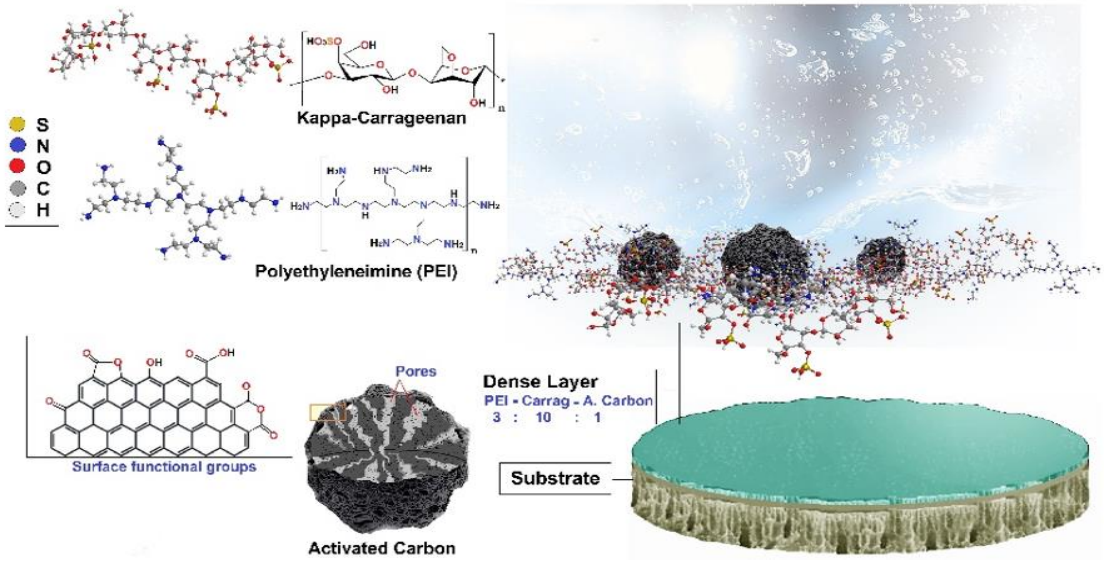


Figure5.1.Hydrogel preparation a) Hydrogel formation process, b) Synthesis and Structural Composition of PEI-Enhanced kC-AC Hydrogel, and c) Molecular Interactions within PEI-Modified kC-AC Hydrogel Network.

Table5. 1:Hydrogel membrane used for wastewater treatment

Membrane	**kC (%)**	**PEI (%wt/v)**	**AC (%wt/v)**
3%kC	3.0	-	-
1%kC + 2%PEI + 0.3% AC	1.0	2.0	0.3
2%kC + 2%PEI + 0.3% AC	2.0	2.0	0.3
3%kC + 2%PEI + 0.3% AC	3.0	2.0	0.3

5.3 Hydrogel characterization and analysis

5.3.1 Structural features of membranes

The FT-IR analysis of kC and 1-3%kC-AC/PEI functional groups was conducted using a Thermo Scientific Nicolet spectrometer with an IR microscope featuring an optical resolution of 0.9 cm^{-1}. Before analysis, hydrogel samples underwent a 24-hour drying at 105 °C. The wavenumber range studied was 4000-400 cm^{-1}. Field-emission scanning electron microscopy (FE-SEM) employing a Zeiss EVO LS15 SEM was used to characterize hydrogel microstructures. A 6 nm-thick gold coating was applied before imaging using a sputtering machine. Three SEM tests were conducted and averaged for precision, followed by Energy-dispersive X-ray spectroscopy (EDX) was performed utilizing a Bruker SDD X flash 5030 detector. Pore size analysis was carried out with the TECHPoro Capillary Flow Porometer, applying the Barett-Joyner-Halenda (BJH) model for adsorption and desorption. Hydrogel surface wettability and hydrophilicity were assessed by measuring the contact angles of kC and composite 1-3%kC with (0.3% AC/2%PEI). The DM 211 contact angle measurement system from Kyowa Interface Science in Chennai, India, was used for water contact angle measurements, with a minimum of three locations chosen for each sample to obtain average contact angles and error values. It is noteworthy that the hydrogel tests were conducted at room temperature, ~22 ºC, at which the kC hydrogel remains thermally stable.

5.3.2 Swelling, deswelling, and water uptake

Water uptake (W_u) was evaluated using pre-dried hydrogel segments (2×2×2 cm). After oven-drying at 105 °C for 6 hr, dry weight (W_d) was recorded. Subsequently, the segments were immersed in distilled water for 24 hr at room temperature, and the post-soaking

weight was recorded after removing excess water (W_w). The water uptake was then calculated using Equation 5.1.

$$Wu = \left(\frac{Ww - Wd}{Wd}\right) \times 100 \quad (5.1)$$

Additionally, the swelling degree, indicative of anti-swelling properties, was determined by recording the initial weight (W_i) and measuring the final weight (W_f) after immersion in DI water and NaCl solutions at varying concentrations for 2-24 hr. The swelling degree (SD) was calculated using the relevant Equation 5.2. Three samples underwent testing, and the averaged results were reported.

$$SD = \frac{(Wf - Wi)}{Wi} \times 100 \quad (5.2)$$

The deswelling characteristics of kC-(AC-PEI) hydrogels with varying kC concentrations were evaluated in a 60 °C oven. Freeze-dried gel samples achieved swelling equilibrium in ultrapure water for 24 hr before being placed in the oven. Weights were recorded at 30-minute intervals, and deswelling (DS) was calculated using Equation 5.3, with W_s representing the weight of the swollen hydrogel and W_o the weight after vacuum drying for 30 minutes.

$$DS = \left(\frac{Wo}{Ws}\right) \times 100 \quad (5.3)$$

5.3.3 Hydrogel Filtration Performance

The kC-AC/PEI hydrogel was poured over a cotton base within a transparent acrylic filtration column, enabling visual observation. The hydrogel was carefully cast into the filtration column and allowed to settle for 10-15 minutes, and a 1 ml layer of PVA was used to seal the hydrogel top. All experiments were conducted three times to ensure reliability. Water flux was determined using Equation 5.4, while pollutant rejection was calculated using Equation 5.5.

$$J = \frac{V}{A \times t} \quad (5.4)$$

$$R\% = (1 - \frac{Cp}{Cf}) \times 100 \quad (5.5)$$

In the filtration process, V denotes the accumulated permeate volume (m^3) over time (t), and A represents the effective membrane area (m^2) used. C_p refers to pollutant concentration in the permeate, while C_f is the initial concentration of contaminants in the feed solution.

5.3.4 Wastewater properties

This investigation employed wastewater from a landfill site in Sydney (Australia) as the feed solution. This landfill site produced mature leachate wastewater with inherent resistance to conventional biological treatment processes. The leachate sample was acquired after biological treatment at the landfill site. A thorough assessment of the heavy metal concentrations in this wastewater was conducted using Inductively Coupled Mass Spectroscopy (ICP-MS), as delineated in Table 5.2.

Table5. 2:Properties of Wastewater

Parameter	leachate wastewater
pH	7.9
Conductivity	14.53 ± 2 ms/cm
Total dissolved Solids	2600 ± 100 mg/L
Turbidity	36 ± 2NTU
Total organic carbon TOC	1870 ± 100 mg/L
Na	132 ± 5 mg/L
K	22.9 ± 2 mg/L
Al	0.02 ± 0.01 mg/L
Mg	89.3 ± 5 mg/L
Ca	71.0 ± 2 mg/L
Cr	0. 23 ± 0.01 mg/L
Mn	1.3 ± 0.01 mg/L
Co	0. 25 ± 0.01 mg/L
Ni	0.17 ± 0.01 mg/L
Cu	0. 19 ± 0.01 mg/L
Zn	0. 13 ± 0.01 mg/L
Cd	0. 15 ± 0.01 mg/L

Pb	0. 14 ± 0.01 mg/L
Ba	0.24 ± 0.01 mg/L

5.3.5 Adsorption-Desorption Mechanism

A single cycle of adsorption-desorption experiments was carried out to evaluate the reusability of the hydrogel. The experimental work tested the effect of temperature (15, 25, 35, 45, and 60 °C) on the adsorption capacity of hydrogel for 2 g/L $MgSO_4$. The best adsorption temperature was used to evaluate the impact of pH 4, 7, and 10 on the adsorption for 2 g/L $MgSO_4$. Adsorption tests for Cu^{2+}, Mg^{2+}, and Na^{+} ions were assessed in a controlled environment using a thermostatic shaker at 35°C, pH 4, and 150 rpm for 3 hr, followed by 10 minutes of centrifugation at 10,000 rpm for hydrogel-solvent separation. Inductively Coupled Plasma Mass Spectrometry (ICP-MS), Agilent Technologies model was used to evaluate each ion's concentration in the samples, and Equation 5.6 calculates the adsorption capacity (mg/g), where C_i represents the initial concentration in mg/L, C_f represents the residual ion concentration at equilibrium in mg/L, V is solution volume in L, and W is hydrogel sample weight in grams.

Desorption experiments were performed by adding 30 mL of 0.1M HCl to vials with 20 g of kC-AC/PEI hydrogel after the adsorption test. For 3 hr, a thermostatic shaker at 35 °C stirred at 150 rpm to desorb. The kC-AC/PEI materials were centrifuged at 10,000 rpm for 10 minutes. Desorption capacity ($mg \cdot g^{-1}$) was estimated using Equation 5.7.

$$Adsorption\ capacity\ \left(\frac{mg}{g}\right) = (Ci - Cf) \times \frac{V}{W} \quad (5.6)$$

$$Desorption\left(\frac{mg}{g}\right) = \frac{(CR \times V)}{Wgel} \quad (5.7)$$

CR represents the residual concentration of ions (mg/L), *V* is the volume of the HCl solution in Liters (L), C_i is the initial concentration (mg/L), and W_{gel} is the weight of the hydrogel in g. The desorption (*D%*) was determined by applying Equation 5.8.

$$D\% = \left(\frac{Cdesorbed}{Cadsorbed}\right) \times 100 \quad (5.8)$$

5.3.6 Metal Recovery

After metal desorption, metal ions from wastewater were extracted using a kC-AC/PEI hydrogel. The desorption involved treating the metal-saturated kC-AC/PEI hydrogel with 0.1M HCl. In a thermostatic shaker at 35°C, 150 rpm agitation was used for three hr. The hydrogel was separated by centrifuging at 10,000 rpm for 10 minutes from the metal-rich solution. The solution underwent RO processing using a BW30LE membrane at 20 bar pressure, 22 ± 2 °C, 0.00146 m² membrane area, and 0.7 L/min flow rate. The recovery percentage (*Re%*) of the metals was calculated by the RO system using Equation 5.9.

$$Re = C_{RO}/C_{fi} \times 100 \quad (5.9)$$

C_{RO} is the concentration of RO concentrate (mg/L), and C_{fi} is the initial concentration of wastewater (mg/L).

5. 3.7 Statistical test

Each experiment was repeated three times, and the results are shown as mean values. Variations across many experimental data sets were evaluated using the analysis of variance (ANOVA). Treatment groups' statistically significant variations were indicated by a P-value less than 0.05 in single-factor ANOVA analysis for experimental data.

5.4 Results

5.4.1 Morphological characterization of the hydrogel

The physical and chemical properties of the kC-AC/PEI hydrogel were studied to understand metal ion rejection processes. The BET analysis in Table 5.3 shows that the hydrogel's surface area, pore volume, and pore diameter significantly increased. For example, the surface area rose from 10.87 m^2/g for 3% kC to 95.61 m^2/g for 3% kC-AC/PEI. Similarly, the pore diameter expanded from 3.31 nm to 4.6 nm, while the pore volume increased from 0.015 cc/g to 0.099 cc/g. These changes suggest that the hydrogel provides more adsorption sites and can accommodate larger molecules with increased kC concentration mixed with AC-PEI. Desorption Analysis mirrors these trends but at reduced magnitudes, a result of adsorption-desorption hysteresis. This hysteresis is caused by the discrepancy between pore filling and emptying mechanism since pore filling in adsorption occurs via capillary condensation while evaporation of the condensed gas lags in the desorption test due to the presence of narrow pore necks, postponing the adsorbed gas release. Also, due to capillary condensation, the adsorption test overestimates the pore size and volume because gas condenses faster into pores than it evaporates out in the desorption test. The 2% kC-AC/PEI pore diameters revealed a contraction during desorption, indicating potential pore restructuring post-substance release.

Table5. 3: Summaries of BET analysis.

BET analysis		3%kC	1%kC-AC/PEI	2%kC-AC/PEI	3%kC-AC/PEI
Adsorption BJH	Surface area m^2/g	10.87	30.410	82.310	95.61
	Pore Volume cc/g	0.015	0.055	0.081	0.099
	Pore Diameter nm	3.309	4.00	4.20	4.60
Desorption BJH	Surface area m^2/g	5.776	29.694	60.80	82.769
	Pore Volume cc/g	0.009	0.055	0.0504	0.111
	Pore Diameter nm	3.309	4.00	3.70	4.00

After 24 hr of drying at 60 °C, the FE-SEM analysis of the kC-AC/PEI hydrogel revealed a rough, porous structure with irregularly shaped granules or clusters, indicating a non-homogeneous surface. The visible micro-porous architecture supports a potentially high surface area (Figure 5.2a). The AC and PEI crosslinking in the kC matrix introduced porous, irregularly shaped, and organized helical kC structures, improving the hydrogel's adsorption capabilities compared to the 3% kC (Figure S4 supplementary material). According to Figure 5.2b, the hydrogel displayed a denser surface after being filtered with NaCl at 2 g/L due to the deposition of salt crystals, indicating the presence of electrostatic interactions. The filtration with $MgSO_4$ at 2 g/L resulted in intricate pore structures and morphological alterations ascribed to the interactions between magnesium and sulfate with the surface (Figure 5.2c). In addition, the leachate wastewater altered the hydrogel's texture, which affected the pore size and surface topology due to the deposition of pollutants (Figure 5.2d).

Figure 5.2e shows how to form a composite hydrogel 3%kC-0.3%AC with 2%PEI based on the FT-IR analysis during preparation. kC, which is a sulfated polysaccharide, exhibits

peaks such as the stretching of O-H at 3400 cm^{-1}, the stretching of C-O-C at about 1250 cm^{-1}, a sulfate ester band at 1150 cm^{-1}, and glycosidic linkages in the region of 950-900 cm^{-1} (Fan et al., 2013). O-H stretching occurs at around 3400 cm^{-1}, C=O stretching occurs for carbonyls between 1700-1650 cm^{-1}, and further C-O vibrations occur close to 1250 cm^{-1}, referring to AC properties(Chen & Wu, 2004). At the same time as PEI displays aliphatic C–H stretching from 810 to 2930 cm^{-1}, it also displays N–H stretching between 3300 and 3450 cm^{-1} (Pattarith et al., 2023). Two critical bands correspond to N–H vibrations of amino groups essential for crosslinking with kC and AC. These bands are located at 1595 cm^{-1} and 1456 cm^{-1}. Peaks at 1306 cm^{-1} and 1040–1120 cm^{-1} correlate with C–N stretching vibrations, enhancing the overall stability of the hydrogel structure(Wang & Li, 2015) (Figure 5.2e). During the process of amalgamation, these components, kC, AC, and PEI, engage in interactions that have the potential to cause shifts or alterations in the FT-IR peaks that are already present, eventually leading to the formation of new spectral characteristics. Following filtering using 2 g/L of $MgSO_4$ and 2 g/L of NaCl, Figure 5.2f displays the FT-IR spectrum of the 3%kC-AC/PEI hydrogel composite. Within the 500–1500 cm^{-1} range, particularly about the sulphate and carbonate functional groups, there was a change in peak shape. Significant spectral shifts and intensity changes in key regions confirm the involvement of specific functional groups in ion binding. Especially the wide O–H and N–H stretching area 3200–3400 cm^{-1} displays intensity variations after ion exposure, suggesting hydrogen bonding and electrostatic interactions with cations. Furthermore, the sulfate group (S=O), which is changed by interaction with $MgSO_4$, spans approximately 1220–1260 cm^{1}, indicating the active engagement of sulfate groups from kappa-carrageenan in ion complexation. Further supporting structural rearrangement and binding activity between the hydrogel matrix and

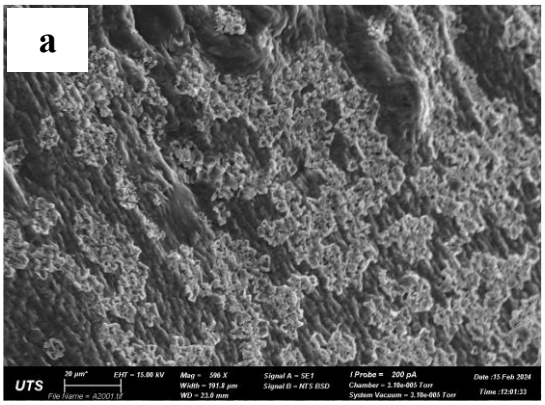
ions are the peak alterations in the C–O–C stretching area (~1040–1150 cm^{-1}) and variations in the fingerprint region 600–900 cm^{-1}.

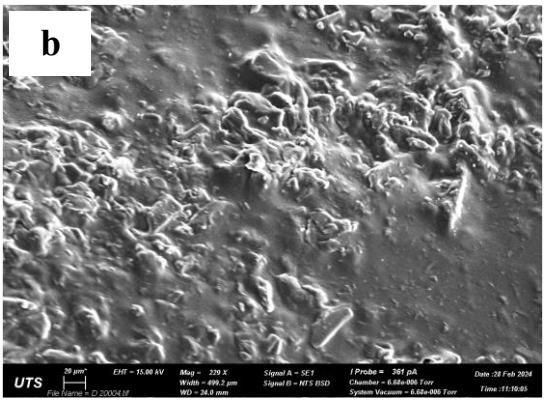
EDX spectroscopic examination showed a significant elemental composition change in the kC-AC/PEI hydrogel at the end of the filtration, stemming from pollutant adsorption from leachate solution. For example, diminished carbon, oxygen, and sulphate content is an indicator of the adsorption process, while K^+ and Na+ increase from 6.23% to 16.73% and 0.63% to 2.2%, respectively, indicating selective ion exchange. The following elements appeared post-filtration: Fe^{2+}, Mg^{2+}, Mn^{2+}, and Al^{3+} were (1, 1.45, 1.04, and 0.42) wt%, respectively, which explains the ability of the hydrogel to sequester inorganic ions and heavy metals from the leachate wastewater. This elemental absorption matches the hydrogel matrix's composite structure's physicochemical interactions to target pollutants (Figure S3.2).

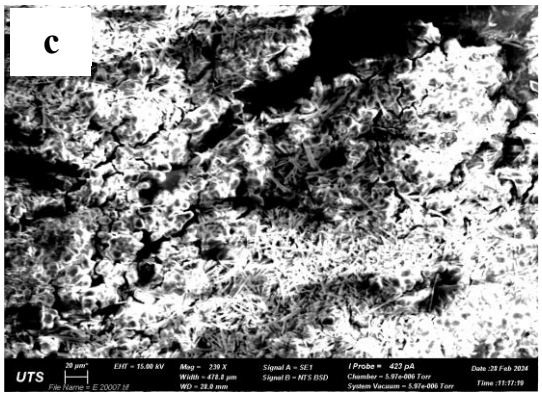
The contact angle measurements provide crucial knowledge of hydrogels' wettability and surface features. Pure kC and kC-AC/PEI hydrogels' water contact angles were tested to evaluate surface hydrophilicity and wetting capabilities. The molecular structure of kC attracts moisture, creating a hydrophilic hydrogel surface with a 72° contact angle. AC exhibits water-attracting and water-repelling regions on its molecular surface, predominantly displaying hydrophobic behaviour. However, a shift towards hydrophilicity is essential for optimal functionality for filtration applications. The measured contact angle was 46.9° ± 1.9 at 1% kC, increased to 51.2° ± 2.05 at 2% kC, and reached 56.8° ± 2.7 at 3% kC, indicating that the hydrogel hydrophilicity decreased with increasing its concentration (Figure 5.2g).

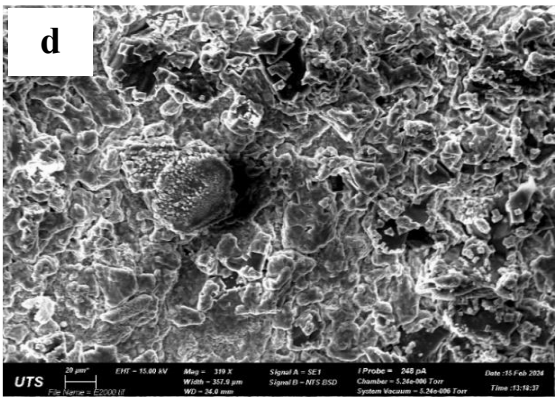
Figure 5.2h illustrates the rheological properties of kC hydrogels that have been changed with AC and PEI. These features give very important insights into the viscoelastic

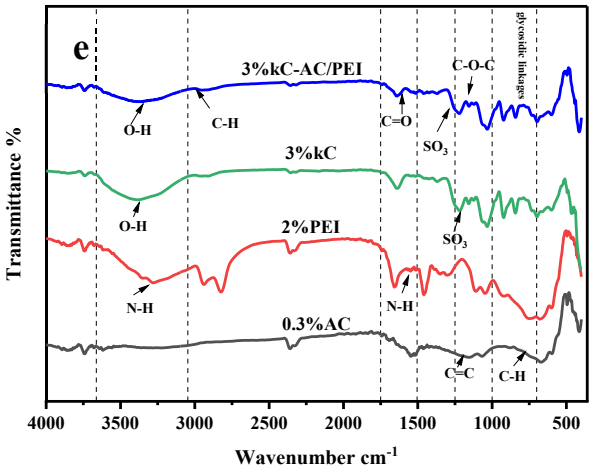
characteristics of the hydrogels at various concentrations. It is clear from the shear stress and viscosity responses at increased shear rates that these gels display shear-thinning behaviour, which reduces flow resistance when shear is applied. The viscosity behaviour intensifies with higher concentration; the 3% kC-AC/PEI hydrogel has the greatest viscosity and shear stress, indicating a more robust gel network than the 1% and 2% formulations. The almost linear connection between shear stress and shear rate on a logarithmic scale throughout concentrations indicates a power-law relationship, typical of materials exhibiting yield stress behaviour and time-independent viscosity at low shear rates. The notable disparity in the slopes of the viscosity curves indicates the degree of shear-thinning, which is particularly evident at higher concentrations (Mokhtari et al., 2019).

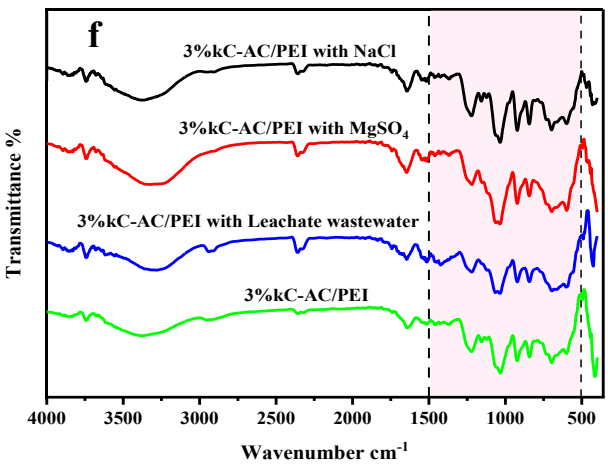

a

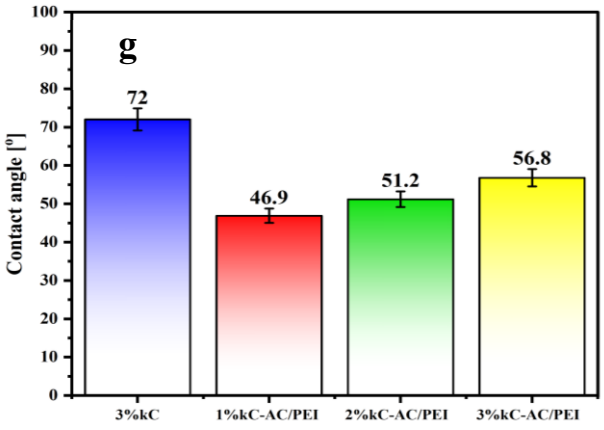

b


c


d


e
3%kC-AC/PEI
3%kC
2%PEI
0.3%AC
O-H
C-H
C=O
C-O-C
SO3
glycosidic linkages
N-H
C=C
Transmittance %
Wavenumber cm-1


f
3%kC-AC/PEI with NaCl
3%kC-AC/PEI with MgSO4
3%kC-AC/PEI with Leachate wastewater
3%kC-AC/PEI
Transmittance %
Wavenumber cm-1


g
Contact angle [°]
72
46.9
51.2
56.8
3%kC
1%kC-AC/PEI
2%kC-AC/PEI
3%kC-AC/PEI

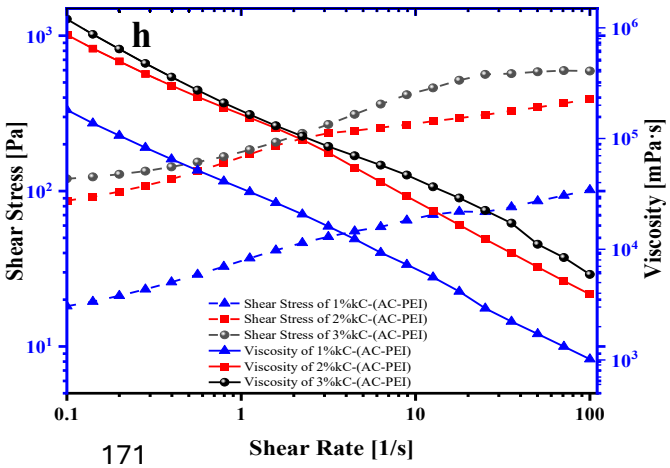

h
Shear Stress [Pa]
Viscosity [mPa·s]
Shear Rate [1/s]
Shear Stress of 1%kC-(AC-PEI)
Shear Stress of 2%kC-(AC-PEI)
Shear Stress of 3%kC-(AC-PEI)
Viscosity of 1%kC-(AC-PEI)
Viscosity of 2%kC-(AC-PEI)
Viscosity of 3%kC-(AC-PEI)

Figure5. 2.a & b) SEM of the 3%kC-0.3% AC/2%PEI hydrogel before and after the filtration with NaCl at 20 µm at the first focus point, c & d) SEM of the 3%kC-AC/PEI hydrogel after filtration with $MgSO_4$ and leachate wastewater at 20 µm at the first focus point, e) FT-IR of the 3%kC,0.3%AC,2%PEI and 3%kC-0.3%AC/2%PEI, f) FT-IR of the 3%kC-AC/PEI after filtration with MgSO4, NaCl and leachate wastewater, g) Contact angle measurements of pure kappa-carrageenan and 1-3%kC-AC/PEI, h) viscosity and shear stress of the composite hydrogel membranes.The error bar = 1 standard deviation.

5.4.2 Hydrogel water uptake, swelling, and deswelling

Increasing the kC concentration in the hydrogel changes its structure and water absorption, with higher kC concentration enhancing the hydrogel crosslinking density and restricting molecular mobility. Therefore, a stiffer and stronger hydrogel is produced by improving chain homogeneity and alignment while reducing water absorption. Water adsorption was greatest at 1% hydrogel, 1777.4% ± 53, reduced to 1664.2% ± 50 at 2%, and 1433% ± 43 at 3% kC concentration. Figure 5.3a indicates an inverse relationship between kC concentration and water uptake, suggesting that when kC concentrations are higher, network structures become denser, making it harder for water to enter. This response that changes based on concentration shows the trade-off between improving the structure by making it stiffer and more crystallized and limiting the hydrogel's ability to absorb and hold water (Hezaveh & Muhamad, 2013).

Figure 5.3b shows swelling degrees of kC-AC/PEI hydrogels with DI water at 2hr and 24 hr for 1%, 2%, and 3% kC. At 2 hr, the hydrogel swelling was 5.2 g/g ± 0.3 for 1%kC, 3.3 g/g ± 0.2 for 2%kC, and 1.9 g/g ± 0.1 for 3%kC. Due to the increased water retention, the swelling of 1%kC reached 9.3 g/g ± 0.4, 7.8 g/g ± 0.3 for 2%kC, and 4.3 g/g ± 0.2 for 3%kC after 24 hr. The swelling degree decreased as the KC concentration increased due

to higher crosslinking density and rigidity, which reduced water absorption in the hydrogel matrix. Figure 5.3c shows the swelling capacity of kC-AC/PEI hydrogels in 2 g/L NaCl solution at 2 hr. The 1% hydrogel swelled the most at 9.7 g/g, indicating better saline solution absorption per unit mass. As kC concentration rose to 2% and 3%, swelling capacity reduced to 8.4 and 7.8 g/g, suggesting reduced saline absorption. Figure 3d shows kC-AC/PEI hydrogel swelling at 0.5 to 3 g/L NaCl. At 2 g/L NaCl, 1% kC swelled to 10 g/g ± 0.2, demonstrating an optimum osmotic equilibrium for water absorption. Greater KC concentrations lowered the hydrogel's swelling; the 2% kC at 9.6 g/g ± 0.19, and the 3% kC at 9 ± 0.18 g/g at the same concentration of NaCl (2 g/L). The salting-out effect, where high ionic strength in the surrounding solution collapses the hydrogel network, may explain the decline in swelling degree above 2 g/L NaCl concentrations across all hydrogel concentrations. The swelling degree dropped to 7.3 g/g ± 0.15, 6.9 g/g ± 0.14, and 6.2 g/g ± 0.13 for the 1%, 2%, and 3% kC at 3 g/L NaCl.The results show that low kC concentration in the hydrogel matrix enabled water to enter more easily due to a less dense polymeric network, whereas high kC concentrations cause a denser matrix that swells less in saltwater.

Figure 5.3e depicts the deswelling behaviour of kC-AC/PEI hydrogels over 330 minutes, demonstrating a rapid water release within the first 90 minutes across all kC concentrations. The greater deswelling of 1%kC than the 2% and 3% concentrations is indicative of a less densely packed polymer network and, thus, a higher water release rate. The hydrogels' water release rate slows with time, indicating a shift to a more controlled release phase. Despite the initial rapid loss, the hydrogels do not fully deswell by the end of the observation period, with the 1%kC hydrogel showing the least water retention, suggesting concentration-dependent differences in the structural integrity and mechanical

strength that influence water retention. Higher concentrations of kC lead to an increased crosslinking density in the hydrogel, creating a tighter polymer network(Nam et al., 2004). This denser structure limits the movement of water, making it harder for water to escape. Consequently, the hydrogel retains water for a longer period, swells more slowly, and experiences a slower deswelling rate as the kC concentration increases.

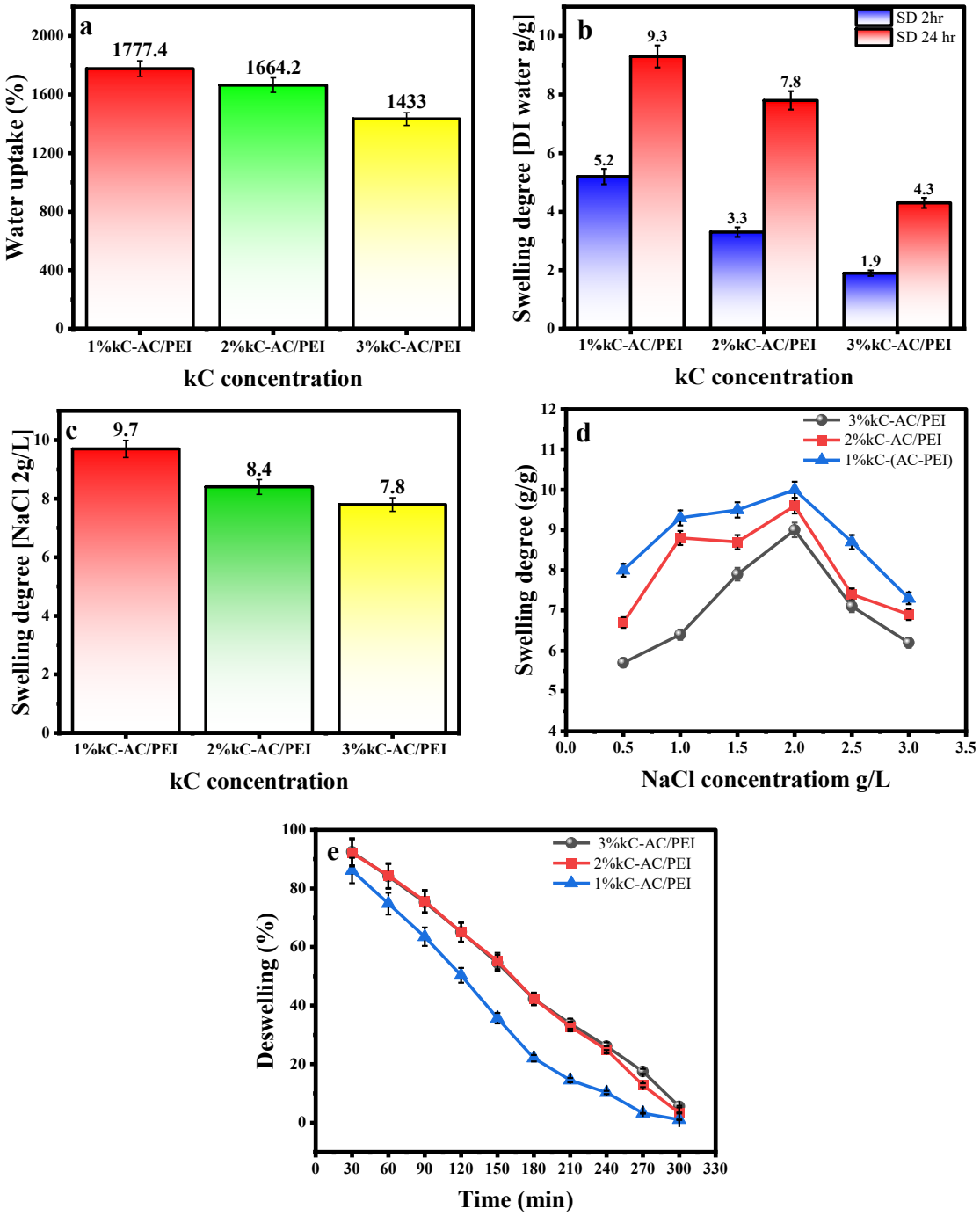


Figure5. 3.a) Water uptake of different concentrations of kC hydrogel membranes, b) Swelling degree of hydrogel membranes in DI water at 2 hr and 24 hr, c) Swelling degree hydrogel membranes in 2g/L NaCl and for 2hr, d) Swelling degree of hydrogel membranes in 0.5 to 3 g/L NaCl, e) Deswelling of different hydrogel membranes over time.The error bar = 1 standard deviation.

5.4.3 Hydrogel Performance Efficiency

Filtration experiments evaluated the performance of 1% to 3%kC hydrogel combined with 0.3%AC and 2%PEI. The feed solution was DI water with 2 g/L $MgSO_4$ or NaCl to measure the water flux and rejection rates of monovalent and divalent ions across hydrogel thicknesses from 0.5 to 2.5 cm under constant hydrostatic pressure of 22 cm, 0.022 bar (Figure 5.4a).

Figure 5.4b shows the inverse correlation between kC thickness and pure water flux, with the 1% kC hydrogel exhibiting a significant decline in water flux from 128.8 ± 3.9 LMH at 0.5 cm to 88.9 ± 2.7 LMH at 2.5 cm. The 2% and 3%kC hydrogels followed a similar pattern, recording respective decreases from 114.3 ± 3.4 LMH to 78 ± 2.3 LMH and 110.7 ± 3.3 LMH to 70.8 ± 2.1 LMH as hydrogel thickness increased from 0.5 to 2.5 cm. A notable water flux reduction of approximately 10 to 15% was observed when the hydrogel thickness was augmented from 0.5 cm to 1 cm, underscoring the impact of structural dimensions on the filtration process. The investigation revealed distinct pure water flux rates by comparing different hydrogel concentrations at a thickness of 2 cm. The highest water flux, 101.6 ± 3 LMH, was observed for the 1% hydrogel, followed by 87.1 ± 2.6 LMH for the 2% hydrogel, and the lowest recorded pure water flux was 78 ± 2.1 LMH for the 3%kC (Figure 5.4b). The water flux decreased in the presence of 2 g/L NaCl and $MgSO_4$ solutions. For 2 g/L $MgSO_4$, the water flux was 47.9 LMH for the 1%kC, 46.4

LMH for the 2%kC, and 45.5 LMH for the 3%kC. Similarly, for the 2 g/L NaCl, the water flux was 36.1 LMH for 1%kC, 30 LMH for 2%kC, and 27.6 LMH for 3%kC at a 2 cm thickness hydrogel (Figure 5.4d).

The hydrogel rejection of 2 g/L $MgSO_4$ solution varies with the kC concentration and thickness. At 0.5 cm, the 1%kC hydrogel exhibited a 40.8% rejection rate, increased to 51.4% for 2%kC, and reached 57.6% for 3%kC (Figure 5.4c). $MgSO_4$ rejection at 2 cm hydrogel thickness was the best, achieving 70 ± 2.1%, 77.5 ± 2.3%, and 80.2 ± 2.4% for 1%, 2%, and 3%kC concentrations, respectively. A parallel trend was observed for 2 g/L NaCl, with a rejection of 37.2 ± 1.1% for 1%kC, 38.2 ± 1.2% for 2%kC, and 41.2 ± 1.2% for 3%kC hydrogels (Figures 5.4c and 5.4d). This pattern suggests that thicker and more concentrated hydrogels are more effective at rejecting solutes due to a denser network that restricts solute passage, but that would be at the expense of water flux. These observations affirm that the hydrogel's water flux and solute rejection parameters are tunable by adjusting the hydrogel thickness and kC concentration, allowing for the calibration of these materials to meet specific performance criteria in filtration and separation processes.

kC hydrogel crosslinked with AC and PEI offers a robust framework for impurity entrapment owing to its extensive surface area, and the high porosity of AC and PEI allows good permeation flow due to its hydrophilic nature and efficiently binds pollutants through its abundant amine groups. The porous architecture from the kC crosslinked with AC/PEI significantly enhances the hydrogel's permeability, allowing water to permeate while effectively retaining contaminants (Mahdavinia et al., 2015). The intrinsic anionic sulphate ions in pure kC lead to electrostatic repulsions, increasing the space between polymer chains and enabling water penetration. The swelling process in the kC-AC/PEI

hydrogel further aids water penetration, with the gravity filtration setup applying additional top pressure for increased water flux. Both kC and AC have proven successful in membrane fabrication studies, improving the hydrogel's porosity, hydrophilicity, permeability, and antifouling properties (Ibrar et al., 2023). The results indicate the hydrogels' structural and functional tunability, which is crucial for optimizing water treatment processes by manipulating the kC content and hydrogel thickness. A desirable balance between water flux and solute rejection is achievable by tailoring the hydrogel properties to the stringent requirements of filtration and separation technologies.

Figure 5.4e explains the interdependence between hydrostatic pressure and Mg^{2+} ions rejection efficacy in a kC-AC/PEI hydrogel filtration system. With an incremental rise in pressure from 0.07 to 0.48 bar, a corresponding reduction in Mg^{2+} rejection from 77% ± 2.3 to 71.4% ± 2.1 is observed, alongside an enhancement in water flux from 45.0 ± 0.9 LMH to 68.2 ± 1.4 LMH. These findings were compared to the gravity-driven experiments of 2 cm hydrogel (Figure 5.4d), representing an elevated Mg^{2+} rejection rate of 80.2% and a diminished flux of 45.5 LMH. The data suggest that increasing pressure adversely affects the selective binding of Mg ions within the hydrogel matrix due to alterations in the hydrogel structure or amplified Mg^{2+} ion kinetics under pressure. Such results highlight the imperative of meticulously modulating pressure in kC-AC/PEI hydrogel systems to achieve an optimal balance between high permeate throughput and selective ion rejection.

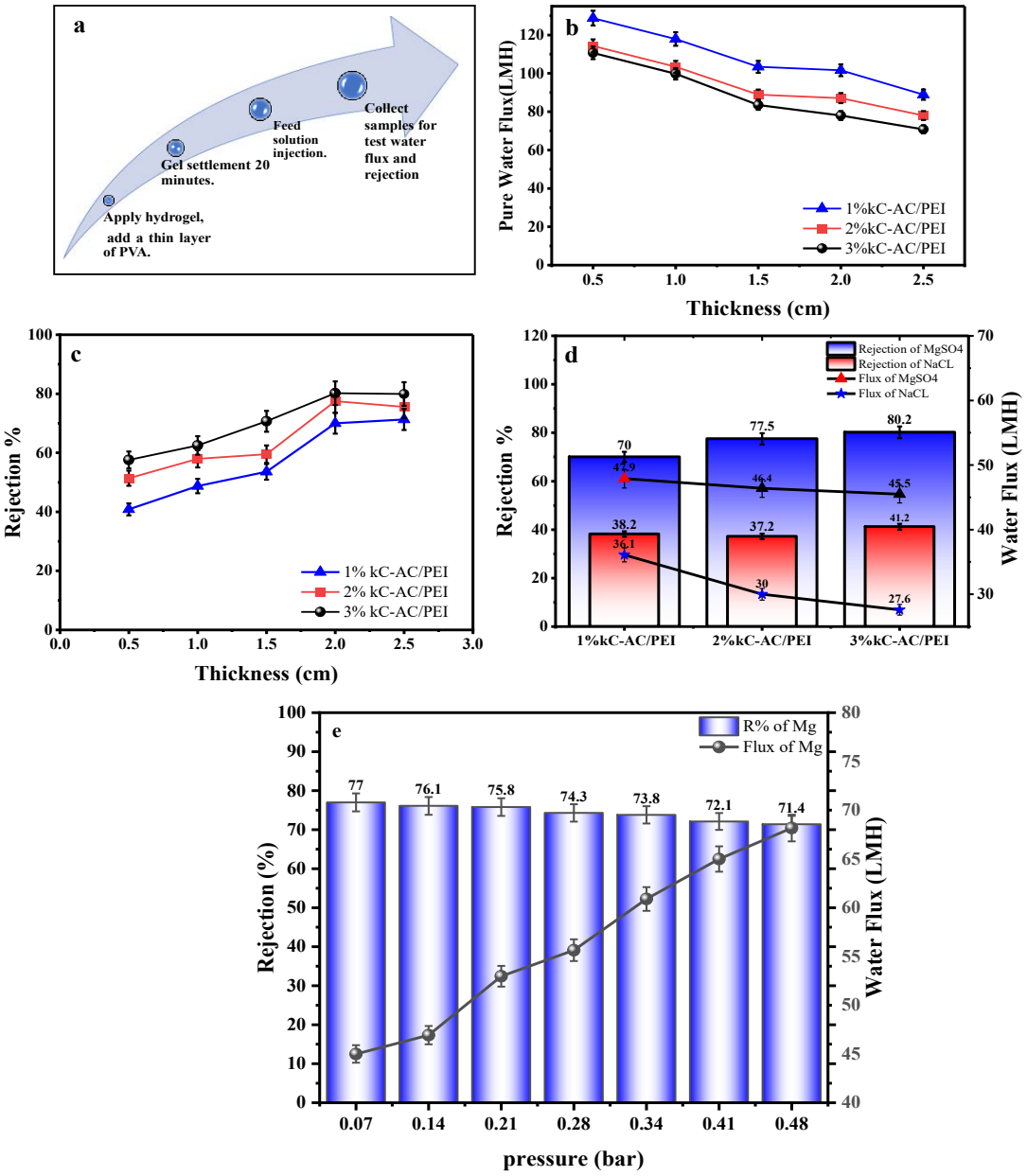


Figure5. 4.a) Hydrogel settlement time, b) Effect of hydrogel thickness on pure water flux, c) Effect of hydrogel thickness on 2 g/L $MgSO_4$ rejection, d) Influence of kC hydrogel membranes $MgSO_4$ and NaCl water flux and rejection, e) Impact of pressure on rejection and water flux in 2 cm thickness hydrogel membranes.The error bar = 1 standard deviation.

5.4.4 Impact of temperature and pH on adsorption capacity

Temperature variations affect ion adsorption, the hydrogel structure, and pore accessibility, with greater mobility and adsorption of ions at elevated temperatures (Karbassiyazdi et al., 2023b). At 35 ºC, the ideal adsorption capacity of magnesium ions was 1.01 mg/g after 90 minutes, but it dropped to 0.83 mg/g at 60 ºC (Figure 5.5a). From 15°C to 35°C, the adsorption process of $MgSO_4$ by the hydrogel was endothermic, manifested by increased adsorption with temperature due to improved ions mobility and diffusion, improving interaction with active sites. As the temperature increases to 45°C and 60°C, adsorption decreases, probably due to the weakening of physical adsorption, desorption becoming more favourable, and potential structural changes or swelling in the hydrogel matrix that compromises the availability of active sites. Also, excessive thermal agitation could disrupt the hydrogel network or adsorbate-adsorbent interaction.

The kC-AC/PEI hydrogel's surface charge changes with pH because functional groups' ionization states change on the hydrogel surface. Electrostatic interactions for ion adsorption depend on surface charge. Figure 5.5b shows fast surface adsorption followed by slow diffusion within the hydrogel's mesopores. The hydrogel adsorption capacity was 1.9 mg/g at pH 4, 1.6 at pH 7, and 1.8 at pH 10. Mg^{2+} removal rates peak at lower pH due to solution protonation, which positively charges the hydrogel surface and repels Mg^{2+} ions. Deprotonation gives hydrogel surfaces a negative charge at alkaline pH, boosting ion adsorption. The pH solution was controlled to optimize kC-AC/PEI hydrogel ion adsorption to promote electrostatic interactions.

Based on previous experiments on pH and temperature with Mg^{2+}, 35 ºC and pH 4 were adopted to calculate the adsorption capacity for Mg^{2+}, Cu^{2+}, and Na^{+}. Figure 5.5c illustrates the adsorption capacity of Mg^{2+}, Cu^{2+}, and Na^{+} on the kC-AC/PEI over time.

At 45 min, Mg^{2+} showed the highest adsorption capacity, 1.31 mg/g, compared to Cu^{2+}, 1.25mg/g. The best adsorption capacity of Na^{+} observed at 75 min was 0.95 mg/g. The adsorptive behaviour of kC-AC/PEI hydrogel towards Mg^{2+}, Cu^{2+}, and Na^{+} ions is significantly influenced by the relationship between the hydrogel's functional groups and the ionic characteristics of the metals. Mg^{2+} ions, divalent cations with a small radius (0.072 nm), adsorb well on the hydrogel via electrostatic interactions with negatively charged functional groups ($-OSO_3$) (Şengil & Özacar, 2009). The small size of Mg^{2+} ions allows them to coordinate with oxygen-containing functional groups in activated carbon, such as carbonyl groups and kappa carrageenan. Cu^{2+} ion, with a greater radius (0.077 nm) than Mg^{2+}, exhibits complexation and coordination interactions during adsorption. The aromatic structure of AC promotes π-electron interactions, whereas oxygen-containing functional groups like carboxyl and hydroxyl aid in Cu^{2+} ion complexation (Rahmani et al., 2022). Electrostatic and physical adsorption are the main methods for adsorption of monovalent Na^{+} ions (0.102 nm). Electrostatic forces and van der Waals interactions allow Na^{+} to adsorb on kC's carboxyl and hydroxyl groups and AC's porous structure. Na^{+} ions' greater ionic radius results in weaker interactions than divalent metal ions. Na^{+} cations neutralize or screen anionic sulfate ($-OSO_3$) groups on kC, reducing electrostatic interactions between cationic and anionic groups on the adsorbent and decreasing composite hydrogel adsorption capacity (Mahdavinia et al., 2014).

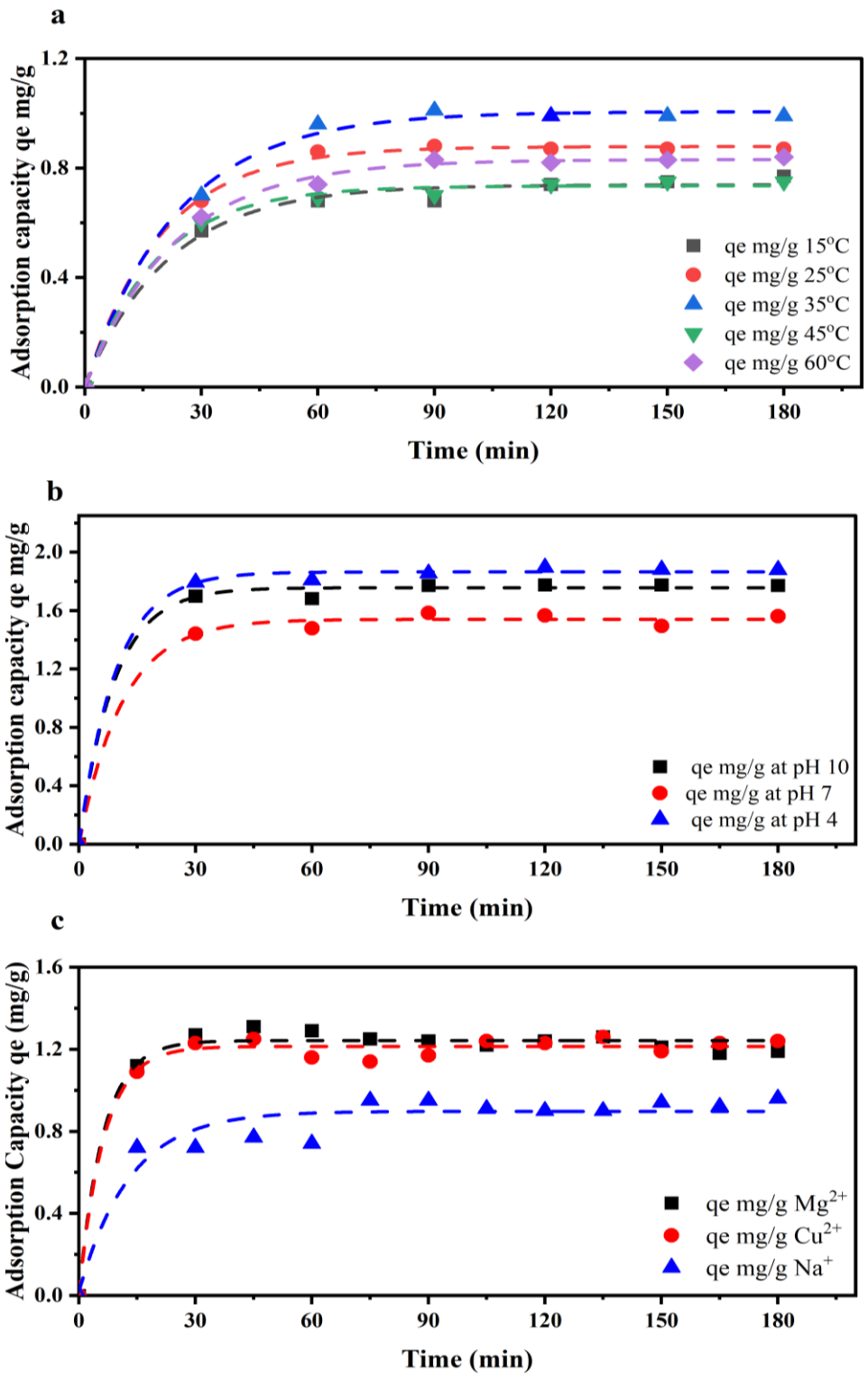


Figure5. 5.a & b) Influence of temperatures and pH on adsorption of $MgSO_4$ on the 3%kC-0.3%AC/2%PEI membrane, c) Adsorption capacity of the cation metals on the 3%kC-0.3%AC/2%PEI membrane.

5.4.5 Leachate wastewater treatment

Landfill Leachate wastewater typically comprises a mixture of organic and inorganic contaminants, including heavy metals, organic compounds, ammonia, and various pollutants. kC-AC/PEI hydrogel filtration ability was tested for pollutant removal at ambient temperature and gravity pressure (30 cm water column). The kC-AC/PEI hydrogel was highly effective for total organic carbon (TOC) and turbidity (Tu) removal, showing rejection rates of 97.8% ± 2.9, 97.5% ± 2.9, and 94.4% ± 2.8 of TOC, TC, and Tu, respectively, indicating excellent contaminants treatment (Figure 5.6a). The hydrogel demonstrated a good colour rejection, comparable to its efficacy in reducing TOC and turbidity (Figure S3.2).

The experimental results (Figure 5.6a) revealed a lower rejection of Na^+ than K^+. In effect, Na^+ has a smaller ionic radius of 0.102 nm but a larger hydrated radius (0.358 nm) than K^+, which has a 0.138 nm ionic radius and a 0.331 nm hydrated radius. Although Na+ has a bigger hydration shell, its rejection rate is lower at 46.9% ± 1.4 than K^+'s 74.4% ± 2.2 because it loses its hydration shell faster and passes through the membrane (Figure 5.6a and Table S3.1). In contrast, K^+'s larger ionic size and smaller hydrated radius correlate with its higher rejection rate, as it maintains its hydration shell during membrane passage (Tansel et al., 2006). For divalent ions, due to their high charge densities, Mg^{2+} and Ca^{2+} exhibited strong electrostatic interactions with the hydrogel surface. The rejection of divalent ions and heavy metals is greater than Na^+ and K^+ due to the stronger electrostatic interaction with the negatively charged hydrogel surface. Mg^{2+}, with a significant rejection rate of 82.9% ± 2.5, demonstrates a robust affinity for its hydration shell, impeding its approach to the hydrogel. However, Ca^{2+}, with a slightly larger ionic radius of 0.099 nm and a higher rejection rate of 87.1% ± 2.6, is theoretically predicted to shed

its hydration shell more readily than Mg^{2+}. The results showed a stronger hydrogel interaction with Ca^{2+} since it loses its hydration shell more quickly when it approaches the membrane surface and establishes a stronger bond with the membrane than Mg^{2+}. The variations in hydrated ion size determine which ions can pass through the hydrogel pores, with ions of the smallest ionic radii, i.e., Ca^{2+} and Mg^{2+}, having the highest hydration numbers compared to those with larger ionic radii, i.e., K^{+} and Na^{+}.

The results conclude that the smaller Mg^{2+} and Ca^{2+} ions hold the water molecules in their hydration shells more strongly, and they cannot detach from them easily, enhancing their rejection by the hydrogel. However, ions with larger ionic radii, like K^{+} and Na^{+}, can leave their hydration shells and pass through the hydrogel (Tansel et al., 2006). Cr^{3+}, with an ionic radius of 0.073 nm, hydrated radii of 0.4 nm, and an electronegativity of 1.66, exhibited an 84.3% ± 2.5 rejection rate for heavy metals. In contrast, Mn^{2+} shows a marginally higher rejection rate of 85.1% with a hydrated radius of 0.438 but a lower electronegativity of 1.55. Ions such as Co^{2+} and Ni^{2+} with analogous ionic and hydrated radii have comparable rejection rates of 82.5% ± 2.5 and 83.9% ± 2.5, respectively. Conversely, Cu^{2+} and Zn^{2+} have larger ionic radii but similar hydrated radii and lower rejection rates. Pb^{2+} stands out with a high rejection rate of 85.8% ± 2.6, attributed to its high electronegativity of 2.33 despite a large ionic radius and a smaller hydrated radius. Ba^{2+} exhibited the lowest rejection rate at 81.5% ± 2.4 due to its lowest electronegativity (0.89) (Figure 5.6a and Table S3.1). The order of metal ions rejection by the kC-AC/PEI hydrogel was as follows: Ca > Pb > Mn > Cr > Ni > Cd=Mg > Co > Zn > Ba > Cu > K > Na.

Furthermore, results suggest that ion rejection is not solely dictated by ionic and hydration size but rather affected by several chemical characteristics. An ion's electron affinity

increases with electronegativity, promoting water molecule binding to its hydration shell and increasing the ion's hydrogel interaction and rejection rates. Pb^{2+}, with 2.33 electronegativity, demonstrated high adhesion affinity to the hydrogel, recording an 85.8% ± 2.6 rejection rate. However, these parameters do not function autonomously; ion-specific chemistry, hydrogel characteristics, and experimental conditions critically modulate ions' rejection. Complex formation and chemical affinity between ions and hydrogel can override the anticipated size-based exclusion, indicating a multifaceted filtration dynamic governed by physical and chemical factors (pH, temperature, ionic strength, etc.). AC acts mainly through adsorption, capturing metal ions within its extensive porous surface.

The rejection rate of Mg^{2+} ions in landfill leachate wastewater was 82.9 ± 2.4%, surpassing the rejection (80.2%) observed with synthetic $MgSO_4$ **(**Figure 5.4d), probably due to the interaction between Mg^{2+} ions and the organic matter in the solution. The EDS results (Figure S3.2) confirm the appearance of these elements by selective ion exchange and change peak morphology in FT-IR (Figure 5.2f). Also, higher ionic strength decreases ion adsorption on adsorbents due to greater competition for surface sites. As ionic strength rises, the concentration of ions in the solution increases, enhancing electrostatic interactions with the adsorbent's surface(Gu et al., 2020). Figure 5.6b illustrates a rise in water flux by the kC-AC/PEI hydrogel, with a water flux reaching 32.2 ± 3 LMH at 80 minutes and an average water flux of 22 ± 3 LMH throughout the treatment of landfill leachate wastewater.

The efficiency of the kC-AC/PEI hydrogel was also evaluated in multiple cycles to investigate its rejection and water flux. In three filtration cycles, a slight reduction was noted in the rejection of metal ions of 6.3% for Cr^{2+}, 5.3% for Co^{2+}, 6.3% for Ni^{2+}, 4.9%

for Cu^{2+}, 4% for Zn^{2+}, 4.3% for Cd^{2+}, 4.2% for Ba^{2+}, 3.7% for Pb^{2+}, 6.2% for Mg^{2+}, and 12.2% for Na^{+}. The reduction in ion rejection arises from the progressive accumulation of these ions within the hydrogel's structure. This accumulation persists even through hydrogel washing with deionized water between treatment cycles, depleting the hydrogel filtration efficiency Figure 5.6c. Furthermore, water flux decreased from 32.3 LMH ± 0.97 to 28.2 LMH ± 0.85 after three filtration cycles, a consequence of trapped particles or ions' incremental blockage of the hydrogel's porous network. The rinse by deionized water dislodges only the easily accessible contaminants, whereas those more deeply embedded will impact the water flux (Figure 5.6d). The SEM image showcases a porous hydrogel surface with a distinctly rough texture, indicating its filtration capabilities (Figure 5.6e). Amidst the maze of interconnected pores, a conspicuous agglomerate comprises contaminants from the leachate wastewater, evidencing the material's effectiveness in capturing and retaining particulate matter. The variation in pore size and the preservation of the hydrogel's structural integrity post-filtration suggest its potential for repeated use in wastewater treatment applications.

Previous studies have examined the suitability of different kC-based hydrogels for purifying wastewater (Table S3.2). Additives like polyethyleneimine, chitosan, graphene oxide, and magnetic nanoparticles made the hydrogel better at absorbing substances and being used multiple times. kC-AC/PEI hydrogel has competitive performance with other hydrogels, 82.9% to 87.1% rejection for divalent ions and 74.4% for monovalent ions. Another KC-V gravity-driven hydrogel study showed removal efficiencies of Na^{+} 42%, Cu^{2+} 76%, and Mg^{2+} of 72%. kC/graphene oxide demonstrated the removal efficiency of Mg^{2+} at 95% and Na^{+} at 23%, while PEI/κC hydrogel composites remove over 98% of Cu^{2+} (Table S5.2).

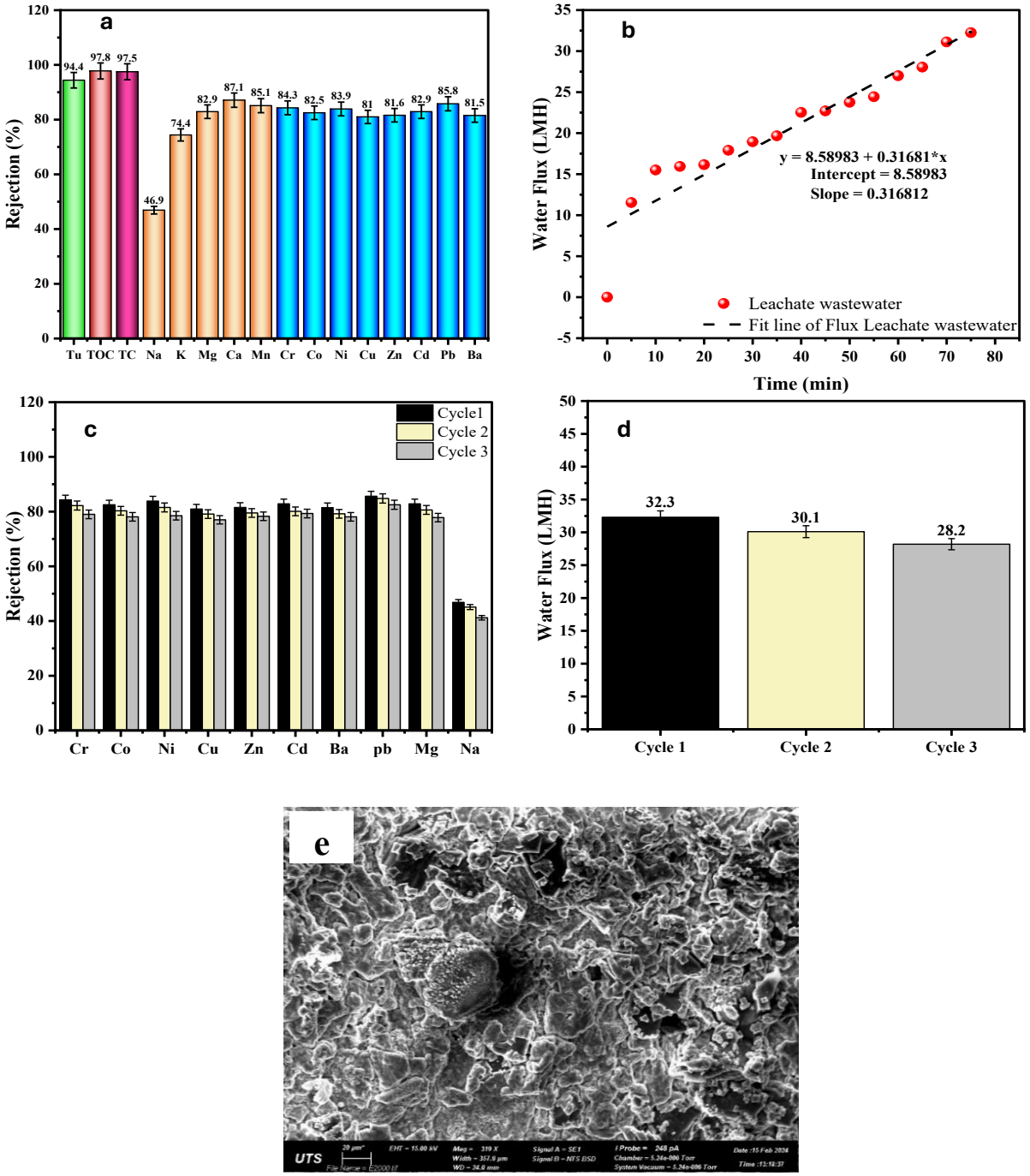


Figure5. 6.3%kC-0.3%AC/2%PEI membrane performance a) Removal of contaminants from leachate, b) Water flux of the leachate wastewater, c) Rejection of ions in three cycles, and d) Water flux of leachate in three cycles, e) SEM of kC-AC/PEI hydrogel after leachate filtration.The error bar = 1 standard deviation.

5.4.6 Hydrogel recycling for reuse

The long-term performance, i.e., rejection of the kC-AC/PEI hydrogel, was also investigated in three consecutive filtration cycles. Each filtration cycle lasted one hour. At the end of each cycle, the hydrogel was cleaned with DI water for 30 minutes before conducting the following filtration cycle with fresh wastewater. The recycled hydrogel demonstrated exceptional Mg^{2+} removal in three consecutive filtration cycles, with a rejection rate of 82.9% ± 1.7 in the first cycle and a decrease to 77.8% ± 1.6 in the third cycle. Conversely, the rejection of Na^{+} decreased by 12.2 % throughout three cycles, from 46.9% ± 1.0 in the initial cycle to 41.2% ± 1.0 in the final cycle. The disparity in rejection behaviour for Mg^{2+} and Na^{+} may be attributed to their unique ionic properties, which affect their affinity for the hydrogel and the potential for reusability in water purification processes (Figure 5.6c). The ion removal efficacy of the kC-AC/PEI hydrogel is contingent upon pH-dependent functionalities, such as hydroxyl and sulphate groups that function as proton donors or acceptors. These functionalities are significantly influenced by the hydrogel's ionization levels and surface charge. Reusability tests were performed for various ions, spanning three filtration cycles.

The maximum reduction of heavy metals rejection was 3.9% and 6.3% for Cr^{2+} in filtration cycles 2 and 3, while it was 8.6% and 12.2% for Na^{+} in filtration cycles 2 and 3 (Figure 5.6c, Table S3.3). The kC hydrogel sulphate groups form covalent and coordination bonds that bind heavy metals, thus facilitating their removal (Rahmani et al., 2022). Compared to the new hydrogel (Figure 5.6a), the kC-AC/PEI hydrogel rejection did not decline after recycling, demonstrating it maintains its property to a large extent after reuse. FT-IR spectrum (Figure 5.2f) shows 3%kC-AC/PEI hydrogel sulphate, carbonate, and hydroxyl peaks changing, demonstrating wastewater adsorption.

Experimental results showed the recyclability and reusability of kC-AC/PEI hydrogel with a reasonable reduction in water flux and metal ions rejection due to several factors. Firstly, partial blockage or saturation of active sites, particularly the amine groups in PEI and the porous surface of activated carbon, limits further adsorption without complete regeneration. Secondly, structural degradation or weakening of the hydrogel matrix after repeated swelling and desorption processes can reduce mechanical integrity, leading to loss of material or reduced interaction with target contaminants. Additionally, strong binding of metal ions to PEI's chelating sites may hinder complete desorption during regeneration, reducing available sites in subsequent cycles. There was also a 6.8% and 6.2% reduction in water flux in cycles two and three after regeneration due to pore clogging, hydrogel structural compaction, and partial loss of functional groups caused by the alteration of surface chemistry. Experimental results showed the recyclability and reusability of kC-AC/PEI hydrogel with a reasonable reduction in water flux and metal ions rejection due to several factors. Firstly, partial blockage or saturation of active sites, particularly the amine groups in PEI and the porous surface of activated carbon, limits further adsorption without complete regeneration. Secondly, structural degradation or weakening of the hydrogel matrix after repeated swelling and desorption processes can reduce mechanical integrity, leading to loss of material or reduced interaction with target contaminants. Additionally, strong binding of metal ions to PEI's chelating sites may hinder complete desorption during regeneration, reducing available sites in subsequent cycles(Alsaka, Ibrar, Altaee, Zhou, Chowdhury, Al-Ejji, et al., 2024). There was also a 6.8% and 6.2% reduction in water flux in cycles two and three after regeneration due to pore clogging, hydrogel structural compaction, and partial loss of functional groups caused by the alteration of surface chemistry.

5.4.7 Metal ions recovery

A hybrid kC-AC/PEI hydrogel-RO system was evaluated to recover metal ions from wastewater after the desorption test with 0.1M HCl solution. The desorption process was done using a thermostatic shaker operating at 35 ºC and 150 rpm stirring for 3 hr. Then, the kC-V hydrogel was centrifuged at 10000 rpm for 10 min to separate from the metal-enriched solution. Then, the solution undergoes filtration with a low-pressure brackish water (LPBW) BW30LE membrane (Filmtec, USA). The membrane area is 0.00146 $m^{2,}$ and the feed flow rate is 0.7 L/min. The LPBW was carried out at 20 bar feed pressure and 22 ± 2 °C feed temperature.

The LPBW membrane recovery rate (%Rr) was 70% at 6 hr, as the ratio of permeate flow to the feed flow rate. The TDS for the feed solution was 1185 mg/L before filtration and increased to 2497 mg/L after filtration, whereas the permeate TDS was 52 mg/L. Figure 5.7 presents the recovery percentages of various elements from leachate wastewater at the end of the RO test (Equation 5.9). The recovery rates reflect the hydrogel's specificity and affinity for different ions due to ion size, charge, functional groups in the hydrogel that can bind these ions, and the conditions of the wastewater treatment process. A high recovery rate suggests that the hydrogel effectively removes these elements from the wastewater, likely through mechanisms such as adsorption, ion exchange, and chelation. Na^{+} shows the recovery rate at 43.9 % ± 2.2, followed closely by Mg^{2+} at 69.9% ± 2.1. The recovery rates for Al^{3+} and Ca^{2+} were relatively lower, at 55.9% ± 1.7 and 66.3% ± 2, respectively. Cr^{2+} and Ni^{2+} were 63.3 ± 1.9 % and 52.5% ± 1.6. Cu^{2+} exhibits a recovery rate of 53.3% ± 1.6 , while Zn^{2+} recovery was 68.1% ± 2, among the higher recovery rates. Cd^{2+} and Ba^{2+} have recovery rates of around 58.6% ± 1.8 and 63.6% ± 1.9. Pb^{2+} and Co^{2+} recovery rates were 62.9% ± 1.9 and 64.9% ± 1.9, which were also

comparatively high. The recovery percentages of metal ions by the RO system vary based on different factors, including the membrane selectivity for various ions, the concentration of ions in the solution, and the efficiency of the desorption process for the extraction of ions from the hydrogel. For example, Na^+ is weakly adsorbed on the hydrogel and hence was easily desorbed by the acid reaction. The results indicate the feasibility of the kC-AC/PEI hydrogel-RO system for ion removal and recovery from leachate wastewater.

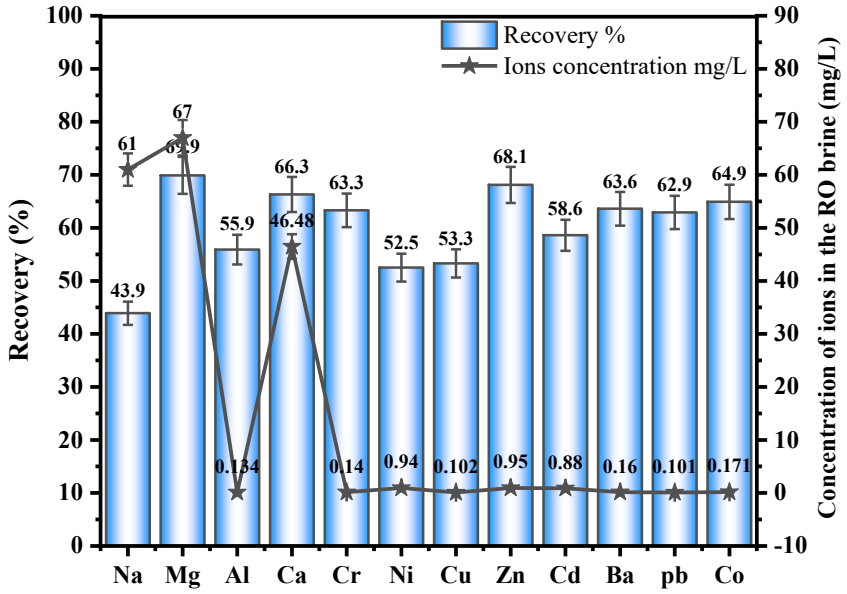


Figure5. 7.Recovery% of ions from leachate wastewater and concentration of ions in the RO brine.The error bar = 1 standard deviation.

5.5 Conclusion

The study proved the efficiency of the kC-AC/PEI hydrogel's wastewater treatment potential. Experimental results showed that 3% kC and 2 cm were the best concentration and thickness of the kC-AC/PEI composite. This composite material rejected divalent ions in wastewater with 87.1% Ca^{2+} and 82.9% Mg^{2+} selectivity. Monovalent ions like Na^{+} and K^{+} were rejected at 46.9% and 74.4%, respectively. The best rejection for divalent ions was at pH 4 and 35 ^{o}C. As for feed pressure, the water flux increased with the feed pressure, while the rejection rate decreased slightly with the feed pressure. The hydrogel removed 94%–97% of turbidity and TOC, 47% of sodium ions, and 81%–87% of divalent ions from leachate wastewater. Its structural integrity and performance remained stable over multiple cycles, showing only slight reductions in heavy metal rejection and water flux, from 32.3 LMH to 28.2 LMH.

Furthermore, the study demonstrated the feasibility of hydrogel reuse after metal desorption without significantly reducing its rejection rate of divalent ions, which was less than 5%. About 70% of heavy metals were reclaimed through an RO system. Future work should include investigating alternative, eco-friendly crosslinkers to improve long-term hydrogel durability and develop innovative regeneration techniques to minimise the loss of hydrogel over multiple cycles. Also, field tests are recommended to assess hydrogel performance and reusability for wastewater treatment. Adsorption isotherm tests are recommended in future studies to provide more data about hydrogel behaviour. Hybrid hydrogel membrane systems should also be investigated to improve their performance.

Supplementary information S3

kappa-carrageenan-based hydrogel for leachate wastewater treatment and resource recovery

Lilyan Alsaka[1], Ali Altaee[1]*, Lina Alsaka[1], Maryam Al-Ejji[2], Alaa H. Hawari[3], John Zhou[1]



Figure S3. 1. an illustrative of gravity-based filtration.

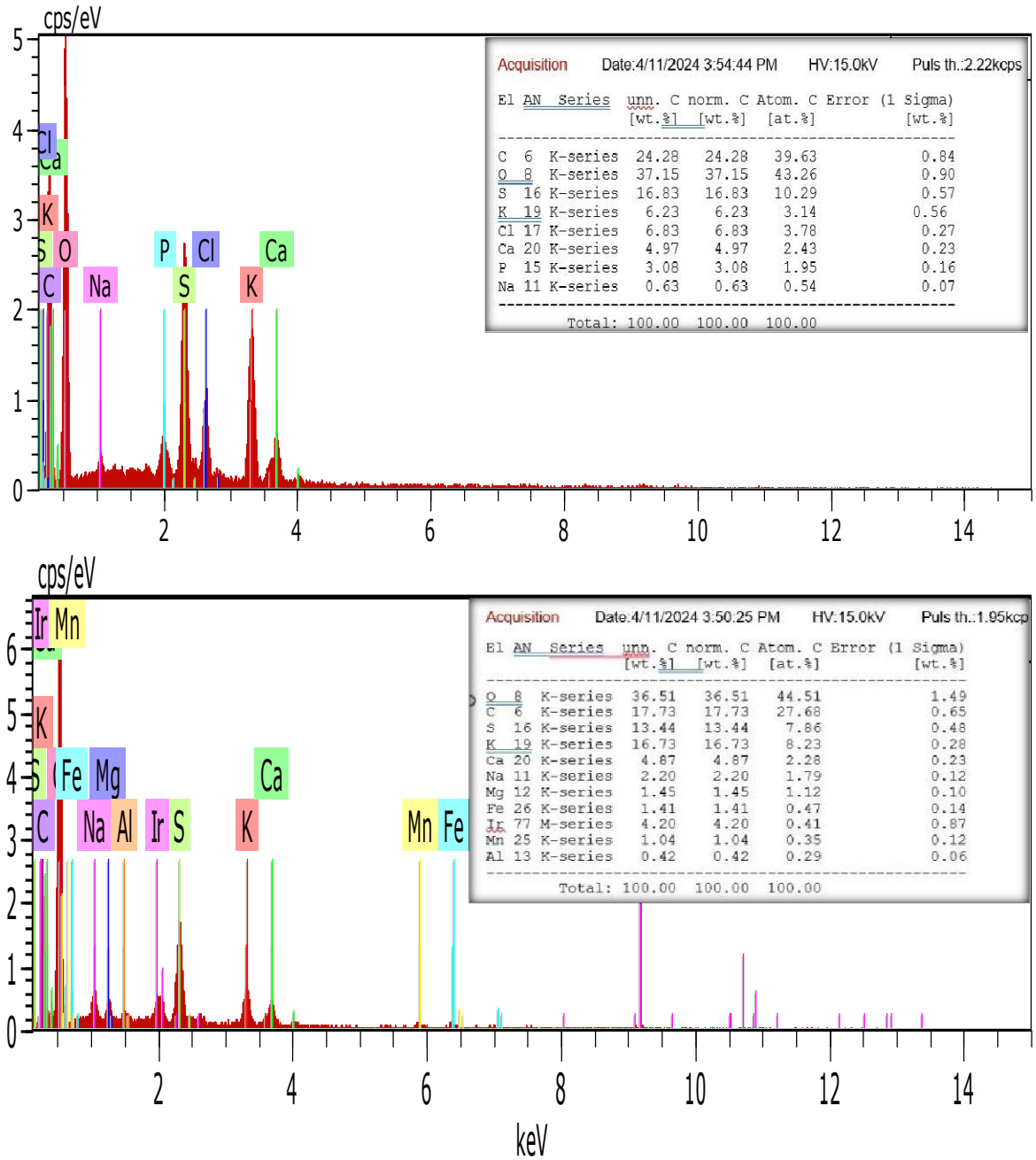


Figure S3. 2. The EDS analysis results for the kC AC/PEI hydrogel before and after treatment.

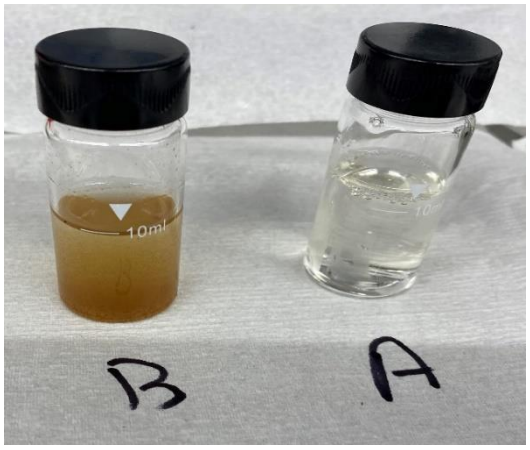


Figure S3. 3. Removal of color and reduction of turbidity.

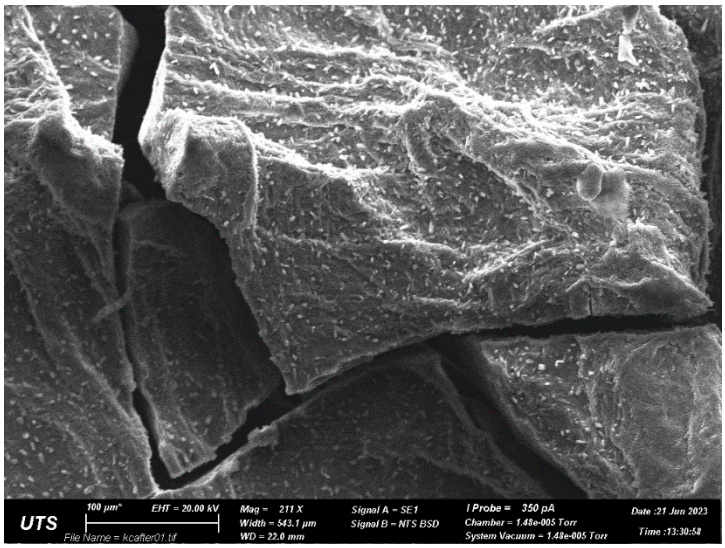


Figure S3. 4.SEM of the 3% kC hydrogel at 100 µm

Table S3. 1:Comparative of Ionic Radii, Hydration radii, and Electronegativity for Ions.

Ion	Ionic radii(nm)	Hydration radii (nm)	Electronegativity	Rejection %
Na^{+}	0.102	0.358	0.93	46.9
K^{+}	0.138	0.331	0.82	74.4
Mg^{2+}	0.072	0.428	1.31	82.9
Ca^{2+}	0.099	0.412	1.00	87.1
Cr^{3+}	0.073	0.400	1.66	84.3
Mn^{2+}	0.067	0.438	1.55	85.1
Co^{2+}	0.065	0.401	1.88	82.5
Ni^{2+}	0.069	0.404	1.91	83.9
Cu^{2+}	0.077	0.419	1.90	81
Zn^{2+}	0.074	0.430	1.65	81.6
Cd^{2+}	0.095	0.422	1.69	82.9
Pb^{2+}	0.202	0.401	2.33	85.8
Ba^{2+}	0.135	0.404	0.89	81.5

Chapter 6: Fabrication of kappa carrageenan-cellulose nanofiber/graphene oxide composite membrane for water purification

Alsaka, L., Altaee, A., Moghaddam, A., Khonakdar, H. A., AL-Ejji, M., Hawari, A. H., Hamdi, F., Aedan, Y., & Al Askar, A. (2025). Fabrication of kappa carrageenan-cellulose nanofiber/graphene oxide composite membrane for water purification. *Journal of Environmental Chemical Engineering*, 120445.

Author contributions statement:

Lilyan Alsaka: Writing – review & editing, Writing – original draft, Validation, Investigation, Formal analysis, Data curation, Conceptualization.Ali Altaee: Writing – review & editing, Writing – original draft, Validation, Supervision, Resources, Investigation, Funding acquisition, Formal analysis, Data curation. Armaghan Moghaddam: Writing – review & editing, Writing – original draft, Validation, Investigation, Formal analysis, Data curation. Alaa H. Hawari: Validation, Funding acquisition, Formal analysis, Data curation. Faris Hamdi: Writing – review & editing, Methodology, Investigation, Formal analysis. Hossein Ali Khonakdar: Writing – review & editing, Visualization, Validation, Formal analysis, Data curation. Ejji Maryam AL: Validation, Funding acquisition, Formal analysis, Data curation, Conceptualization. Yahia Aedan: Validation, Investigation. Abdulmajeed Al Askar: Methodology, Formal analysis, Data curation.

Abstract

This research investigates the synthesis, optimization, and assessment of kappa-carrageenan (kC)-cellulose nanofiber (CNF)/glutaraldehyde (GA)coated with graphene

oxide (GO) for seawater treatment. The kC hydrogel was crosslinked with GA to enhance mechanical strength and adsorption efficiency. The SEM, EDX, and FT-IR analyses revealed a well-defined porous structure, uniform coating, and significant functional groups. Based on swelling behavior, the average molecular weight between crosslinks (Mc) was calculated to evaluate network tightness. The addition of CNF increased the stiffness of the membranes and affected the internal network, resulting in reduced swelling, smaller Mc values, and decreased average pore radius. While this structural tightening reduced the water flux, it improved salt rejection. In the first stage, ion removal ranges from 85% to 92.7% but it decreased from 79.6% to 82.3% in the second stage, resulting in freshwater with a concentration of 692 mg/L. Reusability studies showed that the hydrogel maintained nearly consistent performance in multiple cycles, with a drop in rejection of 19% sodium chloride and 14% magnesium sulfate in 3rd cycle, while water flux declined by 25.8% and 17.6% for sodium chloride and magnesium sulfate. Antifouling experiments conducted in multiple cycles at a 90% recovery rate found 89.7% water flux recovered after DI water cleaning in 1st cycle and 82.5% in 3rd cycle. The kC-CNF/GO-GA hydrogel provides a solution for the treatment of seawater that is not only cost-effective but also sustainable and environmentally friendly.

6.1 Introduction

Water shortage and pollution are significant global challenges that threaten people's health and the environment's sustainability. The demand for water purification techniques has become more critical than ever because of the increasing population, industry water demands, and increased agricultural activities. Despite their effectiveness, conventional water purification methods consume high energy to be sustainable. These challenges

make hydrogel membranes, particularly those fabricated from natural and renewable resources, a potential technology for water purification.

Cellulose nanofibrils (CNFs) offer advantages such as their high length-to-diameter ratio, excellent tensile strength, large surface area, and ease of mixing with other substances. Because they are one-dimensional, they are perfect for making hybrid nanomaterials for water purification. When crosslinked, they make two-dimensional films, three-dimensional hydrogels, or aerogels. The carboxyl groups on CNF are essential for building a solid network, while electronegative oxygen and hydrogen atoms can make a weak bond, which is the essence of hydrogen bonding (T. Zhang et al., 2022). CNF-based products found applications in water treatment and purification. New research has focused on making, changing, and using CNF in water treatment that addresses environmental problems (Mahfoudhi & Boufi, 2017; Tshikovhi et al., 2020). For example, polyamidoxime-nanocellulose (PAO-CNF) hydrogels worked well to remove uranium from seawater, reaching 6.6 mg-U/g (Huang et al., 2024). When CNF was added to starch-g-poly (acrylic acid) hydrogels, the super-adsorbent products adsorbed Cu up to 0.957 g/g in a 0.6 g/L solution. As the Cu› concentration went up, so did the adsorption, particularly in an acidic environment of pH 1 to 2 (Baghbadorani et al., 2019).

Another natural polysaccharide material extracted from red seaweed and used for water purification is kappa carrageenan (kC). It has been studied extensively for its ability to gel and be compatible with living beings. Its special chemical structure, with sulfate groups and high molecular weight, makes it an excellent material for making hydrogels that can hold and absorb water (Rocha de Souza et al., 2007). Notably, the composite hydrogel from combining kC with CNFs exhibited exceptional mechanical strength, stability, and adsorption capacity.

In hydrogel formation, kC and CNF are particularly advantageous for desalination and water purification. The combination of kC with CNF has unique properties, including kC's ionic nature and swelling ability that facilitates the elimination of contaminants, while CNF provides structural reinforcement, enhancing the hydrogel's durability and reusability. Crosslinking CNF with acrylic acid (AA) produced cellulose nanofibers aerogel that was able to uptake about 40.01 mg/g Cu(II) and 130.36 mg/g Pb(II) (Tian et al., 2018). The kC/cellulose hydrogel demonstrated a maximum adsorption capacity of 486 ± 28.5 mg/g for Pb^{2+}. It maintained over 79% Pb^{2+} removal efficiency after eight adsorption-desorption cycles (Karbassiyazdi et al., 2023b). A study by Štefelová for dyes removal from wastewater by CNF adsorbent achieved 99.8% of methylene blue at 40 mg/L concentration as well as crystal violet and Congo red (Štefelová et al., 2017).

Wang et al. (2019), for example, fabricated a 3D network of cellulose/graphene oxide (CG) porous composites to make aerogels capable of adsorbing 421.9 mg/g of methylene blue and 163.4 mg/g of tetracycline (Wang et al., 2019). A new kC-g-PHEAA hydrogel with FeO_2 nanoparticles was able to absorb methylene blue (MB), rhodamine 6G (R6G), Cu(II), and Hg(II) (Kulal & Badalamoole, 2020a). kC-GO was used to coat the NF membrane to improve its fouling resistance and achieved 95.73% water flux recovery (Yadav, Ibrar, Altaee, et al., 2022b). Carrageenan and adjusted Carrageenan and nanocellulose-adjusted carrageenan beads were able to effectively remove Cu(II), Pb(II), Ca(II), Mg(II), and Fe(II) ions (Ali et al., 2019). A GO-kC/SA gel, synthesized by calcium hardening, exhibited improved mechanical strength. The gel exhibited maximum adsorption capacities of 272.18 mg/g for Ciprofloxacin (CIP) and 197.39 mg/g for Ofloxacin (OFL), with an adsorption capacity of 83.99 mg/g for simulated OFL wastewater (200 mg/L) in a fixed-bed column system (Yang et al., 2022).

In this study, a glutaraldehyde (GA) crosslinked kC-CNF/GO composite hydrogel membrane was fabricated for seawater desalination. Initially, kC and CNF were crosslinked with GA to produce a hydrogel base layer that was coated with a GO to enhance the rejection and antifouling characteristics of the kC-CNF/GO-GA composite membrane. The composite hydrogel membrane was investigated for i) the kC-CNF/GO-GA composite hydrogel efficiency to reject divalent and monovalent ions, ii) the effect of CNF on the water flux and ion rejection capabilities, and iii) the feasibility of seawater desalination by the kC-CNF/GO-GA composite hydrogel membrane. The performance and reusability of the kC-CNF/GO-GA composite hydrogel membrane were investigated in multiple cycles for seawater treatment as a sustainable desalination method.

6.2 Material and methods

6.2.1 Materials

The following materials were used in the research: the sulphated plant polysaccharide (kappa carrageenan kC), glutaraldehyde solution (GA), and graphene oxide (GO) were acquired from Sigma-Aldrich in Australia, while cellulose nanofiber (CNF) was acquired from Nanografi Company in Turkey. For the rejection and adsorption studies, analytical grade chemicals such as magnesium sulphate ($MgSO_4$) 2g/L, copper sulphate ($CuSO_4$) 2g/L, and sodium chloride (NaCl) 2g/L were procured from Sigma-Aldrich in Australia. Seawater was collected from a science lab at the University of Technology Sydney (Table 1). The real seawater samples were collected from the beach area in Sydney, Australia.

Table 6. 1:Properties of seawater used in the filtration experiments

Parameter	Seawater
pH	6.4
Conductivity	52 ± 2 ms/cm
Total dissolved Solids	34788 ± 100 mg/L
Turbidity	0.22 ± 1 NTU
Na^{+}	10933 ± 5 mg/L
K^{+}	383 ± 2 mg/L
Mg^{2+}	1303 ± 5 mg/L
Ca^{2+}	413 ± 2 mg/L
Cl^{-}	19592± 5 mg/L
Si^{4+}	0.151 ± 0. 1 mg/L
Cu^{2+}	0.021 ± 0. 1 mg/L
Li^{+}	0.188 ± 0.1 mg/L
B^{3-}	5 ± 0.1 mg/L
F^{-}	1.05 ± 0.01 mg/L
S^{2+}	914 ± 0.01 mg/L
Ba^{2+}	0.011 ± 0.01 mg/L
Br^{-}	64 ± 2 mg/L

6.2.2 Synthesis of kC-CNF/GO-GA hydrogel

The fabrication of the composite hydrogel consisted of the preparation of the base layer of kC-CNF/GA hydrogel coated with a thin layer of GO/GA to ensure the uniformity and structural stability of the membrane (Figure 6.1a). First, a 3%kC hydrogel was prepared by dissolving kC powder in deionized (DI) water, heating the mixture to 60 to 80°C, and stirring for 3 hours at 800 rpm. Concurrently, a CNF hydrogel is created by dissolving 1 to 2.5% CNF in DI water and using a hot water bath with sonication for 4 to 6 hours. The kC and CNF were mixed for 1 hour with 2%GA to form a uniform spreadable hydrogel blend. Then, a GO/GA solution was prepared by sonicating 12.5 mg of GO in 250 mL DI water at 45°C for 12 hours, mixed with a 2%GA at a 2:1 ratio, and the final solution was mixed at 600 rpm for 2 hours. To prepare the composite hydrogel membrane, the kC-CNF/GA hydrogel was packed in a filtration column and coated with a GO-GA layer using 0.5 bar for 2 hours.To prepare the composite hydrogel membrane, the kC-CNF/GA hydrogel was packed in a filtration column, then 2.7 mL of GO-GA solution was added on top of the hydrogel at 0.5 bar for 2 hours to produce a uniform 2 mm thick coating over the hydrogel membrane of 0.0013 m^2 active filtration area. It is noteworthy that excessive pressure could cause membrane defects and an uneven coating layer (Yadav et al., 2022).

Figure 6.1b illustrates the bonding techniques to create a stable structure in the kC-CNF/GA hydrogel with a thin GO/GA coating layer. The GA crosslinker promotes the formation of the following bonds: ether bonds (R–O–R'), acetal bonds ($R–CH(OR')_2$), and ester bonds (R–COO–R'). Ether bonds (R–O–R') are formed when GA interacts with hydroxyl groups (-OH) on kC and CNF via a ring-opening mechanism, resulting in a stable internal matrix. Acetal linkages ($R–CH(OR')_2$) enhance structural integrity and

stiffness since GA interlinks kC and CNF molecules via their hydroxyl groups. The GO coating is firmly bonded by ester linkages (R–COO–R') established between carboxyl groups (-COOH) on GO and hydroxyl groups in the hydrogel, ensuring robust adhesion and a cohesive multilayer architecture. The amalgamation of ether, acetal, and ester linkages produces a highly crosslinked network that improves the mechanical stability, surface area, and structural integrity of the hydrogel. The characterization of kC-CNF/GO-GA hydrogel is in Table S4.1 (Supplementary Materials). Table 6.2 shows the hydrogel membranes used in the experiments for seawater desalination.

Table 6. 2:Composition of hydrogel membranes used seawater desalination

Hydrogel membranes	kC (g/100mL)	CNF (g/100mL)	GO (mg/250mL)	GA (mL/100mL)	Hydrogel composition
M_1	3	1	12.5	2	3%KC-1%CNF/0.05%GO-2%GA
$M_{1.5}$	3	1.5	12.5	2	3%KC-1.5%CNF/0.05%GO-2%GA
M_2	3	2	12.5	2	3%KC-2%CNF/0.05%GO-2%GA
$M_{2.5}$	3	2.5	12.5	2	3%KC-2.5%CNF/0.05%GO-2%GA

a

Dissolve 3g kappa carrageenan(kC) in 100 mL of deionized water at 60 °C for 3 hours

Dissolve 1-2.5 g Cellulose nanofiber (CNF) in 100 mL of deionized water and sonicate for 4-6 hours.

0.05% Graphene oxide (GO) prepared by sonication,12.5mg of GO in 250 Ml deionized water at 45 °C for 12 hours.

Mix the kC hydrogel with CNF hydrogel in a 1:1 ratio with 2% GA for 1 hour until it becomes homogeneous and easy to spread on the support layer.

Mix 0.005%GO with 2%GA at a 2:1 ratio at 600rpm for 2 hours.

Spread kC-CNF hydrogel on the holder layer, add GO-GA to the hydrogel composite, and coat under 0.5 bar for 2 hours.

b

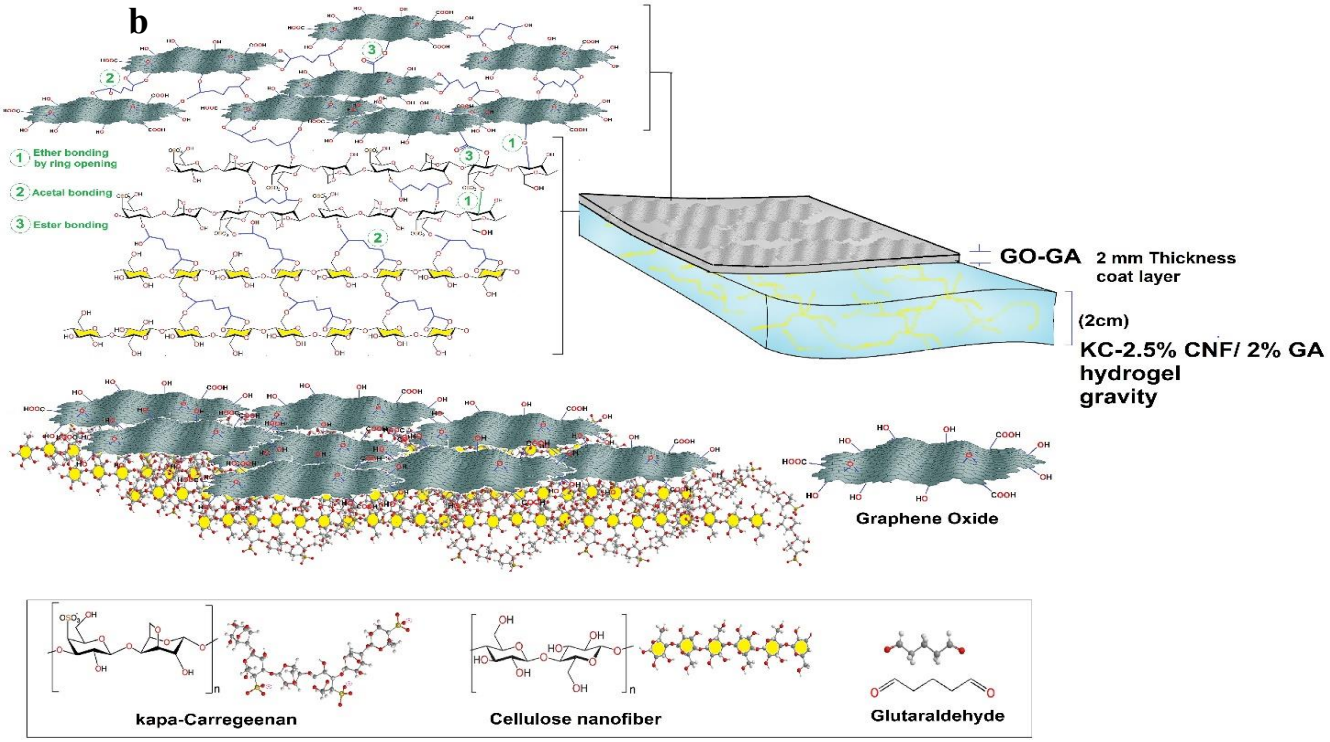


Figure 6.1. Hydrogel preparation a) Hydrogel formation process a) Hydrogel formation process, b) Synthesis and structural Composition of kC-CNF/GO-GA (M_1, $M_{1.5}$, M_2, and $M_{2.5}$) hydrogel and molecular interactions within hydrogel Network.

6.3 Hydrogel performance efficiency

6.3.1 Flux evaluation and rejection

The kC-(1-2.5)%CNF/GA hydrogel was cast on a lint support layer in a dead-end filtration column of 25 cm long and 0.0013 m² effective membrane area. After casting, the hydrogel was left to settle for 10-15 minutes; then, a 2 mm layer of the 0.05%GO-2%GA solution was added under 0.5 bar pressure for 2 hours. Pure water flux (*J*) was evaluated using DI water feed according to Equation 6.1:

$$J = \frac{V}{A*t} \qquad (6.1)$$

where *V* is the permeate volume in m³ over time t (hour), and *A* represents the effective surface area of the hydrogel (m²). The salt rejection studies utilized solutions of 2 g/L $MgSO_4$ and NaCl in separate experiments. The ion rejection rate (*%R*) was calculated from Equation 6.2:

$$R(\%) = (1 - \frac{Cp}{Cf}) * 100 \qquad (6.2)$$

In salt rejection studies, permeate concentration (*Cp*) and feed concentration (*Cf*) were quantified using ICP-MS (inductively coupled plasma-mass spectrometry). All experiments were conducted in triplicate, and results were presented with error bars.

6.3.2 Antifouling Study for Hydrogel

Antifouling experiments demonstrate the composite hydrogel's propensity to fouling. The experiments quantify the water flow before and after exposure to fouling materials to assess the hydrogel's capability to restore its filtering performance after cleaning. The

baseline experiment first measured pure water flow ($J1$) for DI water. Afterward, the water flux (Jf) of hydrogel filtering seawater was recorded. The hydrogel was rinsed with DI water at the end of this experiment, and the pure water flux ($J2$) was measured again. Water flux decline (DR%) and irreversible fouling (IFR%) were quantified in Equations 6.4 and 6.5 as follows:

$$FRR(\%) = (\frac{J2}{J1}) \times 100 \quad (6.3)$$

$$DR(\%) = (1 - \frac{Jf}{J1}) \times 100 \quad (6.4)$$

$$IFR(\%) = (1 - \frac{J2}{J1}) \times 100 \quad (6.5)$$

The water flux recovery (%FRR) reflects the antifouling effectiveness of the hydrogel in restoring the water flux after cleaning with DI water Equation 6.3. The IFR represents irreversible fouling that was not removed after cleaning.

6.3.3 Methodology hydrogel properties

Small pieces (2.5L×2.5W×2D cm) of the membrane were cut and soaked in distilled water for 15 hours to measure the hydrogel membrane's porosity. The wet membrane was weighed after carefully blotting excess water, and *weight1* was recorded. The samples were then dried in an oven at 60°C for 6 hours and weighed again (*weight2*). Then, porosity (P%) was calculated (Equation 6.6):

$$P\% = (\frac{weight1 - weight2}{A * l * \rho}) \quad (6.6)$$

Equation 6.7 calculates the hydrogel membrane's average pore radius size (rm) using the membrane porosity and pure water flux through the membrane. ΔP is the operation pressure, p is the membrane porosity, l and A are the thickness and effective membrane area, and Q is the volume of pure water flux per time (m^3/s)

$$rm = \sqrt{\frac{(2.9-1.75p)\times(8\times lQ\eta)}{(p\times A\times \Delta P)}} \quad (6.7)$$

Water uptake (*Wu*) of the hydrogel was quantified by cutting a pre-dried hydrogel into small pieces of 2×2×1 cm. Following a drying period of 6 hours at 105°C, the dry weight (Wdry) was recorded. The segments were then immersed in distilled water for 24 hours, and the wet weight (Wwet) was documented after the removal of surplus water by blotting. *Wu* was determined from Equation 6.8.

$$Wu = \left(\frac{Wwet-Wdry}{Wdry}\right) x100 \quad (6.8)$$

Equation 6.9 calculates the swelling degree (*SD*) by recording the starting and final weights after immersing the hydrogel samples in DI water and (0.5 to 2.5 g/L) NaCl solutions for 2 hours.

$$SD = \frac{(Wfinal-Winitial)}{Winitial} * 100 \quad (6.9)$$

kC-CNF/GA hydrogels, with different CNF concentrations, were tested for deswelling. Hydrogels pre-swollen in water for 24 hours were dried at 60°C, with weights declining every 30 minutes. Deswelling (*DS*) was calculated using Equation 6.10, where *Wswollen* is the swollen hydrogel weight and *Wdry* is the weight after 30 minutes of oven drying (Equation 6.10).

$$DS = \left(\frac{Wdry}{Wswollen}\right) \times 100 \quad (6.10)$$

To calculate the average molecular weight between crosslinks, the Flory-Rehner equation (without Gaussian chain correction) for hydrogels in water was used (Borges et al., 2020) as follows:

$$\frac{1}{M_C} = -\frac{\rho_P}{V_1} \cdot \frac{\ln(1-v_2)+v_2+Xv_2^2}{v_2^{\frac{1}{3}}-\frac{v_2}{2}} \quad (6.11)$$

where M_C represents the average molecular weight between crosslinks (g/mol), ρ_P represents the density of dry polymer constituents, V_1 represents the molar volume of the solvent (for water: 18.01 cm³/mol), and X represents the Flory–Huggins polymer–solvent interaction parameter (dimensionless). In addition, ν_2 represents volume fraction of polymer in the swollen hydrogel and was calculated by Equation 6.12 (Flory & Rehner Jr, 1943):

$$\nu_2 = \frac{1}{1+SD.\frac{\rho_P}{\rho_S}} \quad (6.12)$$

In Equation 6.12, SD represents the swelling degree, ρ_P represents the density of dry polymer constituents, and ρ_S represents the density of solvent (water = 1.00 g/cm^3).

6.3.4 Adsorption-desorption performance analysis

Adsorption-desorption experiments were conducted on the best-performance $M_{2.5}$ hydrogel membrane used in the multiple filtration cycles for seawater desalination. The experiment on the adsorption capability of Na^+ and Mg^{2+} was carried out using a thermostatic shaker at a temperature of 25ºC, a pH of 6.5, and a rotational speed of 150 revolutions per minute (rpm) over five hours. During the experiment, a solid-to-liquid ratio of 2 g/L was used to combine NaCl and $MgSO_4$. To achieve the separation performance of the $M_{2.5}$, centrifugation at 10000 rpm for 10 minutes was performed after the adsorption tests. ICP analysis was used to measure the concentration of ions in the filtration samples, and Equation 6.13 was used to compute the adsorption capacity in mg/g.

$$Adsorption\ capacity\ \left(\frac{mg}{g}\right) = (Ci - Cf) \times \frac{V}{W} \quad (6.13)$$

In Equation 6.11, *Ci* is ion concentration in mg/L, *Cf* is residual ion concentration at equilibrium in mg/L, *V* is solution volume in L, and *W* is hydrogel sample weight in grams. After adsorption, desorption experiments were conducted by introducing 30 mL of 0.1M hydrochloric acid (HCl) of pH 1.5 into vials containing 20 g of $M_{2.5}$ hydrogel. The desorption experiments were performed in a shaker at 25 °C, stirring at 150 rpm for 3 hours. Subsequently, the $M_{2.5}$ materials were separated by centrifugation at 10000 rpm for 10 minutes. Desorption capacity ($mg \cdot g^{-1}$) was calculated according to Equation 6.12.

$$Desorption\left(\frac{mg}{g}\right) = \frac{(CR \times V)}{Wgel} \quad (6.14)$$

CR represents the residual concentration of ions (mg/L), *V* is the volume of the HCl solution in Liters (L), and Wgel is the weight of the hydrogel in g.

6.4 Results

6.4.1 Rheology and Zeta potential of hydrogel composites

Figure 6.2a the rheological behavior of 3%kC hydrogel, 2.5%CNF hydrogel, and the $M_{2.5}$ hydrogel membrane. At a shear rate of 0.1 s^{-1}, 3%kC demonstrates the highest viscosity of $2.68*10^6$ mPa·s and shear stress 268 Pa, while 2.5%CNF starts with a viscosity of $1.21*10^6$ mPa·s and a shear stress of 120.87 Pa. The $M_{2.5}$ started with a low viscosity of 989,970 mPa·s and a shear stress of 99.01 Pa. With an increase in shear rate, all materials exhibited shear-thinning behaviour. For 3%kC, the viscosity decreased to 9180 mPa·s at a shear rate of 100 s^{-1}, with a shear stress of 919.85 Pa. For 2.5%CNF, the viscosity decreased steadily, reaching 12987 mPa·s at 100 s^{-1}, while the shear stress increased to 1300 Pa. The $M_{2.5}$ composite followed a similar shear-thinning behavior, with its viscosity decreasing to 8564.9 mPa·s at 100 s^{-1} and its shear stress increasing to 856.8 Pa. The attribute that the composite behaves in an intermediate manner between the kC and CNF

materials indicates that it can maintain a balance between fluidity and mechanical strength. On account of this, it is appropriate for applications that need structural integrity and shear resistance. Rheological analysis figure S4(Supplementary material) showed that increasing CNF concentration from M_1 to $M_{2.5}$ significantly enhanced viscosity and shear stress, indicating stronger network formation due to hydrogen bonding and fibril entanglement. $M_{2.5}$ exhibited the highest viscosity (9.89×10^5 mPa·s) and shear resistance, reflecting optimal reinforcement within the kC–GA matrix. All samples demonstrated shear-thinning behavior, confirming pseudoplasticity. These findings highlight CNF's role in enhancing mechanical stability and viscoelastic strength by densifying the network and improving polymer chain interactions. The M2.5 hydrogel membrane exhibits outstanding rheological properties suitable for water purification. It can retain a dense filtering matrix due to its shear-thinning properties, facilitating adequate water circulation at higher speeds and reducing the likelihood of accumulation. Figure 6.2b illustrates the zeta potential of various kC, CNF, and M_1 to $M_{2.5}$ hydrogel membranes. The pure kC, with a zeta potential of -41.4 mv ± -2.1, displays moderate colloidal stability, vital for contaminant adsorption. In contrast, pure CNF shows the highest stability with a zeta potential of -58.2 mv ± -2.9, showing enhanced electrostatic repulsion that facilitates the adsorption of positively charged ions, including heavy metals (Kim et al., 2017). As CNF concentration increases in the kC matrix, the zeta potential becomes more negative, improving the material's ability to interact with charged ions and pollutants. For example, the $M_{2.5}$ hydrogel, with a zeta potential of -49.2 mV ± -2.5, shows significantly enhanced stability, attracting and entrapping charged pollutants (Li et al., 2021). The zeta potential plays a significant function in influencing electrostatic interactions with pollutants, especially due to the sulfate groups in kC and carboxyl

groups in CNF, which enhance the adsorption of positively charged impurities via electrostatic attraction (Ahmed & Soundararajan, 2018). GA crosslinking stabilizes the hydrogel's structure without substantially reducing the zeta potential, assuring long-term effectiveness in water purification (Distantina et al., 2013). Further, a highly negative zeta potential (e.g., -40 to -60 mV) prevents aggregation, maintaining the hydrogel structure and increasing surface area for adsorption. The superior increase in negative zeta potential at higher CNF concentrations suggests that such hydrogel formulations could be highly efficient in removing positively charged contaminants from water while keeping structural integrity over time (Mohammed et al., 2018), specifically at neutral to basic pH, where the carboxyl groups in CNF are fully deprotonated, and the zeta potential is negative (Shaghaleh et al., 2022). Notably, a greater hydrogel negative charge also promotes the repulsion of negatively charged pollutants.

The contact angle measurements provide crucial knowledge of hydrogels' wettability and surface features. Figure 6.2c shows a contact angle of 72º ± 3.6 for kC, which is the highest contact angle, indicating a relatively low wettability and a more hydrophobic surface. Depending on the concentration of CNF, the kC-CNF hydrogels display various characteristics when crosslinked with GA. The M_1 exhibited the lowest contact angle, 47.3º ± 2.4, indicating the highest possible wettability and the most effective water adhesion. The contact angles steadily rose to 51.9º ± 2.6, 54.1º ± 2.7, and 60.3º ± 3.0 when the concentration of CNF increased to 1.5%, 2%, and 2.5%, respectively, indicating that an increase in CNF leads to a more settled structure and reduces the interaction of water with the surface. These findings highlight that kC-CNF/GO-GA hydrogels are tuneable, making them potential candidates for applications that need surface wettability customized to specific applications.

6.4.2 Porosity and pores size

Enforced with CNF and coated with GO, the GA crosslinked kC membrane has significant potential for desalinating seawater due to its selective absorption capabilities, porosity, and mechanical stability. Figure 6.2d shows that incorporating different amounts (1–2.5%) of CNF within the 3%kC hydrogel matrix affects the porosity and average pore radius. With increasing CNF concentration, porosity lessened from 86.8% ± 2.6 at 1%CNF to 81.5% ± 2.4 at 2.5%CNF (Equations 6.6), while the average pore radius concurrently reduced from 4.17 nm ± 0.08 to 3.74 nm ± 0.075 (Equations 6.7). GA forms covalent connections between kC and CNF chains, strengthening the hydrogel structure, while GA-induced crosslinking lowered pore size and stabilized the hydrogel network, making it more durable and performable after multiple filtration cycles. Selectivity-intensive applications recommend a greater CNF concentration, circa 2.5%, to create a compact network for rejecting ions. Instead, a small amount of CNF, circa 2%, can balance selectivity and water flux, making it suitable for applications that require good flow and large molecule rejection (Chen et al., 2021; Distantina et al., 2013).

The top coating layer of 0.05GO mixed with 2% GA enhances the hydrogel's selectivity and makes the surface more stable and fouling-resistant. GO's high surface area and functional groups increase heavy metal separation from the solution, while its hydrophilicity supports water permeability. Thus, the GO/GA layer acts as a selective barrier, capturing ions and pollutants, though it slightly reduces water flux due to denser pore structures (Mohammed et al., 2022). It shows the effect of variation in CNF concentration on the pore structure, changing the ability to adsorb and desorb substances. As CNF concentration increased from 1% to 2.5%, the adsorption surface area decreased from 68.5 to 39.25 m^2/g, while pore volume decreased from 0.079 to 0.025 cc/g, and pore

radius decreased from 3.75 to 2.98 nm. This pattern shows that more CNF concentration makes the structure dense and less porous by its shorter crosslinks or more physical crosslinks, further improving the antifouling property due to the tighter structure of the hydrogel substrate.

The desorption study also shows a similar pattern, with the surface area decreasing from 62.77 to 36.76 m^2/g. With an increase in the CNF concentration, the diameter of the pore gets smaller, decreasing from 3.62 nm in M_1 to 2.82 nm in $M_{2.5}$. These changes reflect a compact and highly crosslinked network at higher CNF levels, restricting pores size but increasing overall matrix density. GA crosslinking and higher CNF amplify this effect by reinforcing bonds within the structure, further restricting pores' size (Kalaiselvi et al., 2023; Kokol & Vivod, 2023).

Table S4.2(Supplementary Materials) illustrates the BET test of 3%kC hydrogels with different 1-2.5% CNF amounts. The pore size difference between the calculated value (3.7 nm) and the BET result (2.8 nm, Table S4.2) arises from the different measurement principles of the two methods. Equation (6.7) provides an estimated hydraulic pore size, while BET measures the textural (gas-accessible) pores.

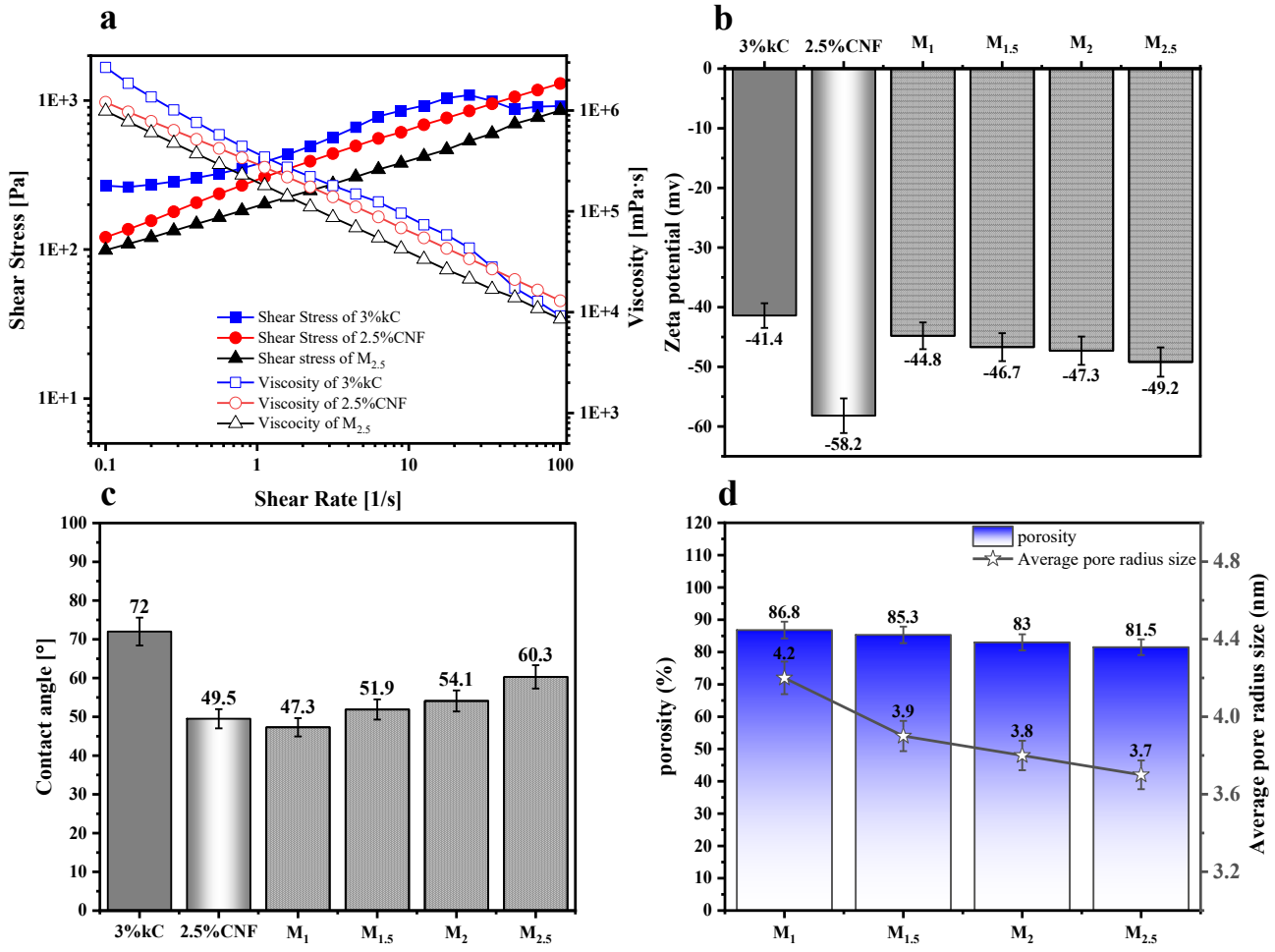


Figure 6. 2. a) viscosity and shear stress of kC, CNF, and $M_{2.5}$, b) Zeta potential of kC, CNF, M_1, $M_{1.5}$, M_2, and $M_{2.5}$, c) Contact angle measurements of kC, CNF, M_1, $M_{1.5}$, M_2 and $M_{2.5}$, d) porosity and pore size of the composite hydrogel of M_1, $M_{1.5}$, M_2, and $M_{2.5}$.

6.4.3 Hydrogel swelling, deswelling, and water uptake

The swelling properties of hydrogels in DI water are a critical indicator of their hydrophilic nature, network structure, and capacity to retain water. The microstructural characteristics, particularly crosslinking density, determine hydrogel swelling properties. When kC-CNF hydrogels crosslinked with GA were tested with DI water, their swelling degree decreased with increasing CNF concentration (Figure 6.3a). The CNF reinforces

the hydrogel network, hence reducing water uptake by restricting polymer chain mobility. The observed trend in swelling follows the calculated decrease in average crosslink length, as discussed in the following section. For example, M_1 exhibited the largest swelling (9.8 g/g ± 0.49), whereas $M_{2.5}$ had the lowest (8.0 g/g ± 0.40). Xu et al. (2019) found that network contraction decreased the swelling ratio (SR) with denser polymer crosslinking architectures (Xu et al., 2019). According to Bai et al. (2019), double-network hydrogels dissipate energy and have excellent anti-swelling properties (Bai et al., 2019). Chemically crosslinked hydrogels usually have properties that keep them stable and prevent them from swelling, but making them often requires complicated steps and chemicals (Xiang et al., 2020). Thus, membranes with elevated CNF concentration consistently displayed lower swelling degrees due to denser crosslinking and less hydrophilicity (Chang et al., 2011; Distantina et al., 2016; Hezaveh & Muhamad, 2012). Figure 6.3b shows the degree of swelling of M_1, $M_{1.5}$, M_2, and $M_{2.5}$ membranes in 0.5-2.5 g/L NaCl concentrations. There is a strong relationship between the concentration of NaCl and the swelling behavior of kC-CNF/GO-GA hydrogel membranes. The degree of swelling increased with the concentrations of sodium chloride because the ionic strength raises the osmotic pressure inside the hydrogel matrix, increasing the amount of water taken in. Also, neutralizing sulfate groups with Na^+ ions reduces electrostatic repulsion between the polymer chains, expanding the network for more water absorption. For $M_{2.5}$, which exhibits a rise in swelling from 5.4 g/g ± 0.2 at 0.5 g/L to 7.8 g/g ± 0.2 at 2.0 g/L. At 2.5 g/L NaCl concentration, the degree of swelling decreases due to the increased osmotic pressure in the opposite direction that draws water out of the hydrogel membrane. In addition, the stronger electrostatic shielding exerted by 2.5 g/L NaCl solution tightens the polymer chains, limiting the hydrogel's water absorption capacity.

The hydrogels' deswelling behavior was analyzed to understand their structural properties and capacity to retain water (Figure 6.3c). Standalone kC deswelling dropped from 64.8% to 0.2% after 270 min, while the standalone CNF deswelling dropped from 72% to 1.5% after 270 min. The deswelling rates for M_1, $M_{1.5}$, M_2, and $M_{2.5}$ at 30 minutes were 58.1%, 70.7%, 76.8%, and 86.5%, respectively, and reached circa 0.7% after 270 minutes. The membranes' compact polymer networks, strengthened by GA crosslinking, contributed to better water retention by the crosslinked kC-CNF/GO membranes and decreased water loss over time. Increasing the concentration of CNF improved water retention due to the denser and more stable polymer networks. Swelling and deswelling also induce structural changes in hydrogels and can produce various surface patterns. These surface patterns are stable in both dry and swollen states and enhance the potential of hydrogels for multiple applications (Kumar et al., 2023).

Figure 6.3d indicates that as the concentration of CNF increases, there is a corresponding decrease in the membrane water uptake percentage. Specifically, M_1 exhibits the highest water uptake at 2019.3% ± 101, while $M_{2.5}$ shows the lowest at 1197.5% ± 60. Based on this pattern, greater concentrations of CNF result in a denser polymer network, reducing the hydrogel's capacity to absorb water. This behavior is consistent with the findings that have been obtained, which state that an increase in the crosslinking density of hydrogels leads to a decrease in the swelling capacity. Therefore, it is feasible to adjust the swelling characteristics of kC-based hydrogels for specific applications by changing the concentrations of CNF.

The hydrogel membranes exhibited swelling and deswelling behaviors controlled by several circumstances. The enhanced crosslinking density results in a denser polymer network, reducing the swelling capacity and limiting the quantity of absorbed water.

Although the membrane's mechanical strength increases with the CNF concentration, the water absorption is further restricted owing to the denser network structure. The combined effects of increased crosslinking density and incorporation of CNF resulted in a reduction in porosity and pore size (Figure 6.2d), which in turn restricted the amount of space available for water molecules and reduced the swelling capacity.

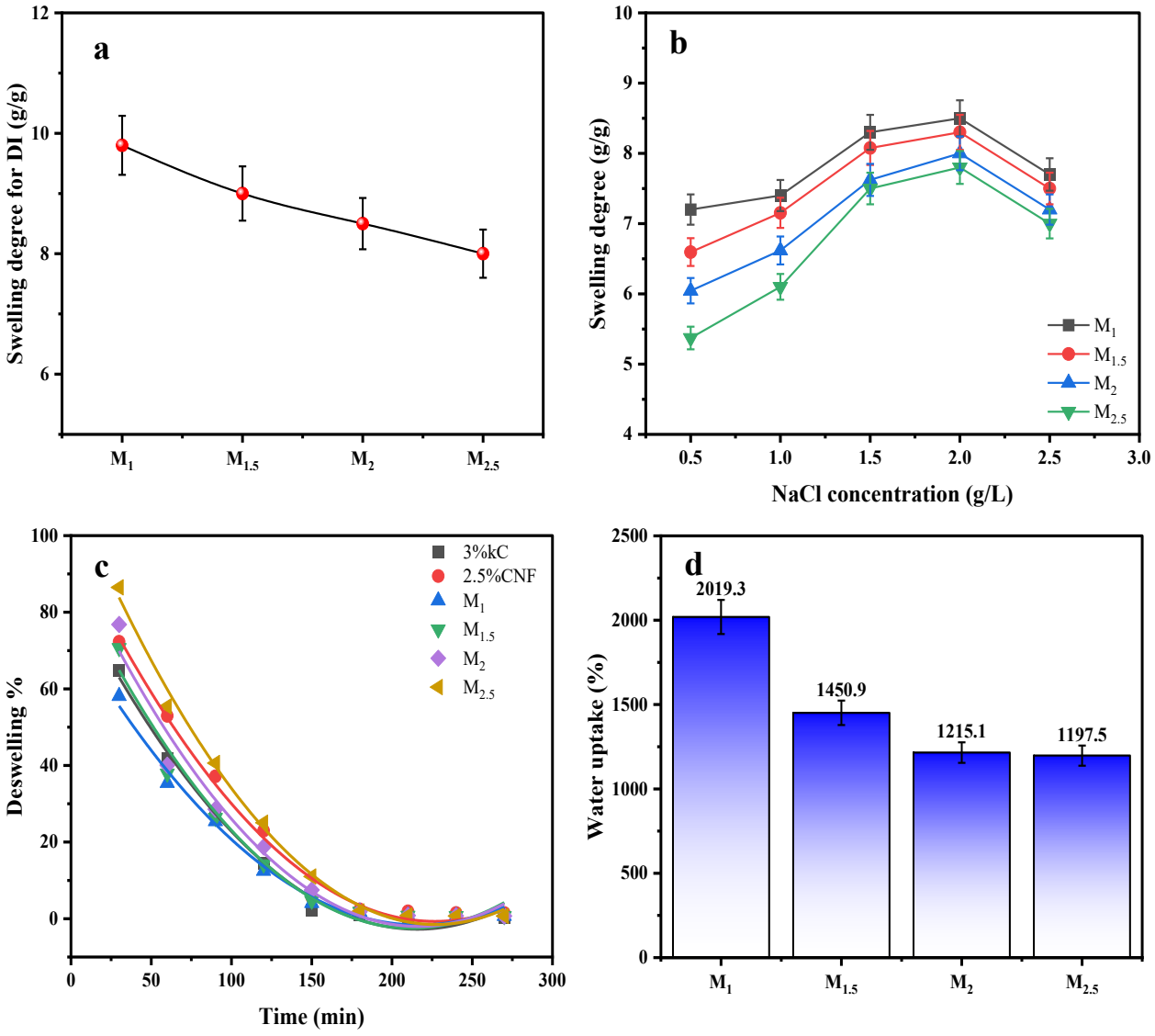


Figure 6. 3. a) Swelling degree in DI water of M_1, $M_{1.5}$, M_2, and $M_{2.5}$ for 2hr, b) Swelling degree of various hydrogels at various concentrations of NaCl, c) Deswelling of M_1, $M_{1.5}$, M_2, and $M_{2.5}$ hydrogel with time, d)Water uptake ability of M_1, $M_{1.5}$, M_2, and $M_{2.5}$ hydrogel.

6.4.4 Average molecular weight between crosslinks

In this study, the swelling data of the hydrogel samples were used to estimate the M_C values. Due to the complexity of the nanocomposite hydrogel system, particularly the presence of the top GO layer, the Mc calculations were performed based on simplified systems, where the GO layer was excluded. Accordingly, the obtained relative values were used to compare the properties. The calculated M_C was therefore regarded as an effective average molecular weight between all crosslinking points in the hydrogel bulk, integrating both covalent (GA-induced) and physical (CNF/kC) bonds. Full details of the methodology and assumptions used for these approximations, as well as the discussion on the effect of MC values on hydrogel properties, are provided in the Supplementary Materials.

GA plays a pivotal role as a crosslinker in the hydrogel membrane, forming covalent bonds, mostly with the hydroxyl groups in the CNF and the sulfate and hydroxyl groups in the kC. Such covalent crosslinks establish a stable 3D network, although physical interactions, including hydrogen bonding, ionic bonds, and chain entanglements, also support the stability and performance of the hydrogel. In contrast to covalent bonds, physical interactions are transient and reversible. Nonetheless, they contribute immensely to the hydrogel's mechanical integrity and dimensional stability under operational conditions(Grabska-Zielińska, 2024; Xu et al., 2022; Yang et al., 2023). Therefore, the M_C value represents the combined effect of both chemical and physical crosslinking. It reflects the average molecular weight of polymer segments between effective crosslinking points, whether those points are formed via covalent bonds or strong physical associations. As such, variations in Mc can be interpreted as changes in the overall

crosslinking density of the hydrogel network, encompassing the full range of interactions that govern its structural and functional behavior(Lu et al., 2018).

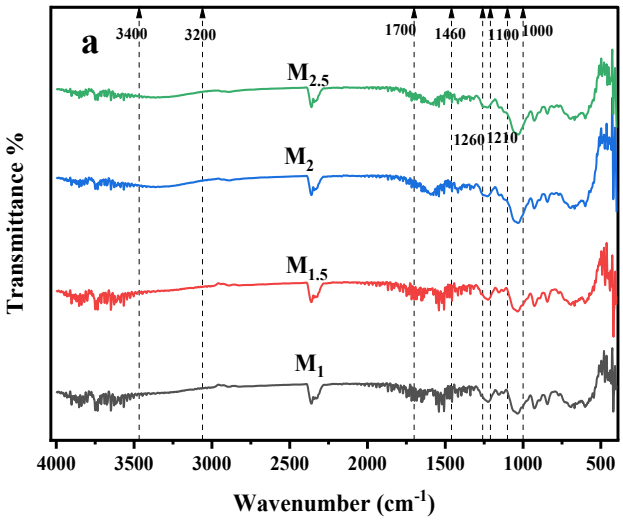
According to the swelling behavior, the estimated Mc values for the M1, M1.5, M2, and M2.5 samples were 10,535.5, 9,344.8, 8,639.9, and 7,914.6 g/mol, respectively. This decreasing trend suggests that increasing CNF content leads to a higher crosslink density within the hydrogel network. The probable mechanism involves improved interactions between the hydroxyl groups in the CNF and the aldehyde groups of GA, which promote the formation of a denser polymer network. As the network becomes more tightly crosslinked, the mesh size is reduced, thereby limiting the available free volume for water absorption. In addition, although CNF is hydrophilic, its network tightening effect dominates hydrophilicity; thus, MC values are reduced due to lower SD(Yue et al., 2016).

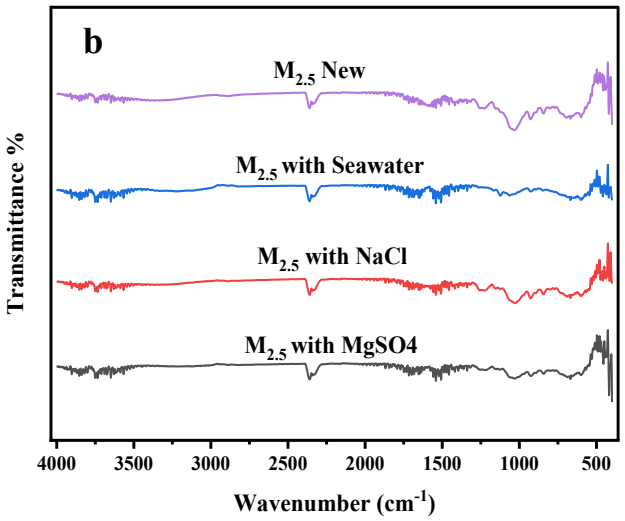
6.4.5 Hydrogel membrane characterization

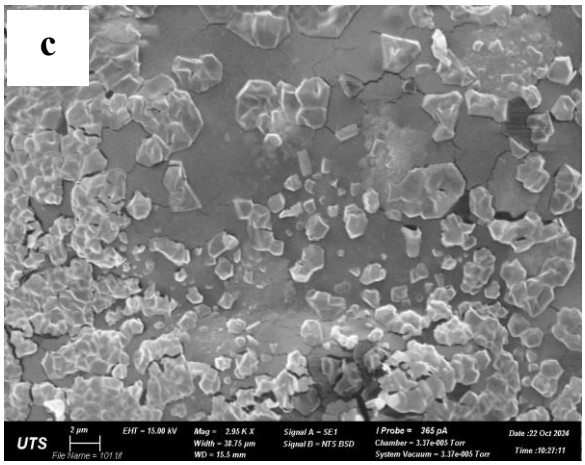
Figure 6.4a illustrates FT-IR analysis of M_1, $M_{1.5}$, M_2, and $M_{2.5}$. The analysis indicates that increasing CNF content enhances hydrogen bonding (3200–3400) $cm^{-1}$and C–O incorporation (1000–1100) cm^{-1} while reducing carbonyl C=O intensity 1700 cm^{-1}, indicating improved crosslinking and hydrogel stability. Figure 4b shows that the FT-IR of the new $M_{2.5}$ hydrogel membrane changes the intensity of its characteristic band when it is exposed to different types of water, such as seawater, NaCl, and $MgSO_4$ solutions. Interactions between the hydrogel's functional groups and the ions or molecules in its surroundings affect its swelling behavior, mechanical characteristics, and ion adsorption capacity. For instance, heavy metal ions produce coordination complexes that move the carbonyl stretching area. Saline solutions, such as seawater, NaCl and $MgSO_4$, change the hydrogen bonding network, which can be seen by the stretching of hydroxyl groups in Figure 6.4b.

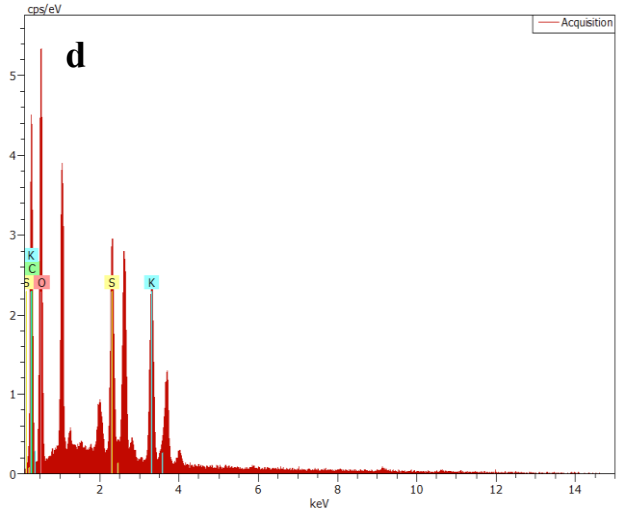
The scanning electron microscopy (SEM) of $M_{2.5}$ hydrogel showed structural alterations. Figure 6.4c shows new $M_{2.5}$ has a homogeneous, smooth surface with few fractures and imperfections. The production of crystalline structures, most likely by the deposition of salts and minerals from saline water, caused apparent morphological changes when filtering with seawater (Figure 6.4e). The surface of the new hydrogel, which was previously smooth and uniform, is changed by the deposits on its surface. These deposits provide evidence of metal ions captured by the membrane during seawater filtration.

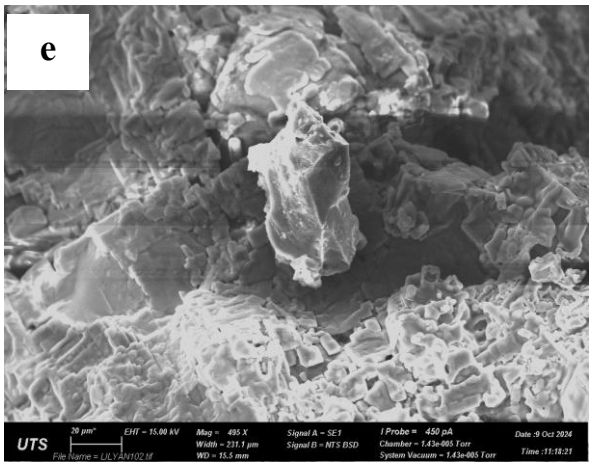
As shown in Table S4.3 and Figures 6.4d and 6.4f, the Energy Dispersive X-ray Spectroscopy (EDS) of the $M_{2.5}$ reveals that the composition of the hydrogen goes through changes after the filtration process. Oxygen (49.83 wt.%) and carbon (31.03 wt.%) are in the new hydrogel structure. Notable levels of sulfur (7.27 wt.%) and potassium (11.88 wt.%) are also present, indicative of the hydrogel's organic and polysaccharide-based composition. The hydrogel structure changes after seawater filtration. Carbon, oxygen, sulfur, and potassium concentrations decreased, suggesting salt replacement of these elements. On the other hand, there is a rise in the concentrations of sodium (31.90 wt.%) and chloride (44.23 wt.%), indicating a large amount of salt deposition (Figure 6.4e).


a
3400
3200
1700
1460
1100
1000
1260
1210
$M_{2.5}$
M_2
$M_{1.5}$
M_1
Transmittance %
4000 3500 3000 2500 2000 1500 1000 500
Wavenumber (cm^{-1})


b
$M_{2.5}$ New
$M_{2.5}$ with Seawater
$M_{2.5}$ with NaCl
$M_{2.5}$ with MgSO4
Transmittance %
4000 3500 3000 2500 2000 1500 1000 500
Wavenumber (cm^{-1})


c
UTS


d
cps/eV
Acquisition
K
C
O
S
K
keV


e
UTS

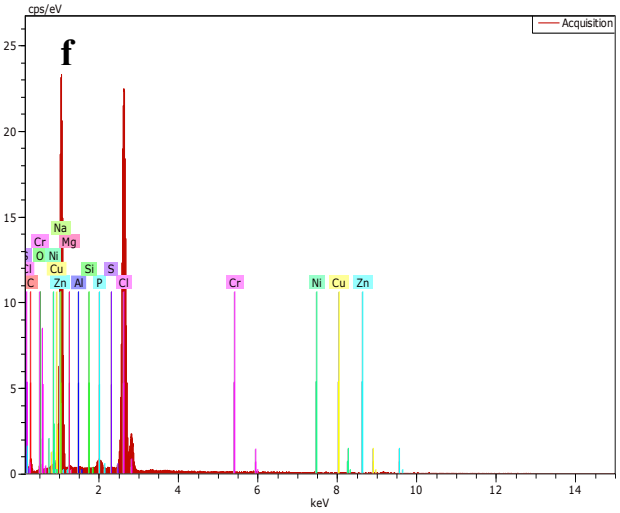

f
cps/eV
Acquisition
Na
Cr
Mg
O
Ni
Cu
Si
S
C
Zn
Al
P
Cl
Cr
Ni
Cu
Zn
keV

Figure 6. 4. a) FT-IR of the M_1, $M_{1.5}$, M_2, and $M_{2.5}$, b) FT-IR of the $M_{2.5}$ after filtration with $MgSO_4$, NaCl, and seawater, c and d) SEM and EDS for the new $M_{2.5}$, e, and f) SEM and EDS for the hydrogel after filtration with seawater.

6.4.6 Hydrogel DI water flux and salt rejection

DI water feed solution was utilized to evaluate the pure water flux of M_1, $M_{1.5}$, M_2, and $M_{2.5}$ membranes of 0.5, 1, 1.5, 2, and 2.5 cm thicknesses. Notably, hydrogel membrane M_3, with 3%CNF concentration, was not further considered in the comparison (Figure 6. 5) due to its low water flux and subtle rejection improvement compared to $M_{2.5}$ (Figures S4.2a and S4.2b, Supplementary Materials). Membrane M_3 membrane, with 3% CNF, is a good example that explains the relationship between CNF concentration and membrane performance with a slight increase in M_3 rejection, 0.4% to Mg and 0.5% to Na, due to CNF concentration increased from 2.5% to 3% (Figure S4.2b, Supplementary Materials). Figure 6.5a shows that the water flow declines as the hydrogel membrane's thickness and the CNF concentration increase. The 2 cm thickness membrane stands out with a balanced performance of excellent water flux and solute rejection. Membrane M_1 exhibited the maximum water flux of 78.7 LMH ± 3.9 at 0.5 cm, while the $M_{2.5}$ exhibited the lowest flux of 51.9 LMH ± 2.6 at 0.5 cm. As the thickness of the membrane increased to 2.0 cm, the water flux dropped to 44.6 LMH ± 2.2 for M_1 and 36.8 LMH for $M_{2.5}$, respectively. Increasing the thickness and CNF concentration in hydrogel membranes reduced water flux due to the tighter membrane structure, increased hydrophilicity, and increased hydraulic resistance. Thicker membranes provide increased hydraulic resistance, whereas higher CNF concentration densifies the hydrogel matrix, lowering porosity and permeability. Increasing the CNF content in the hydrogel improves the membrane's structural integrity by forming a more compact network (Acarer-Arat et al., 2024). This

densification enhances the membrane's structural stability at the expense of decreased pore size and porosity (Figure 6.2d), lowering water permeability.

While GA crosslinking is widely used in the field of hydrogels, its precise influence on hydrogel network structure and filtration properties is not always quantitatively assessed for water purification applications. In this work, M_C calculations offer a molecular-scale understanding of how crosslinking density impacts water permeability and solute rejection. Hence, the observed decrease in DI water flux with increasing CNF content can be further explained by examining the calculated M_C values. MC values decline with increasing CNF concentration, suggesting the formation of a denser and tightly crosslinked hydrogel network. A shorter MC corresponds to shorter polymer chains between crosslinks, which reduces the free volume and limits the number and size of interconnected water channels available for transport. This structural compactness directly prohibits water diffusion through the hydrogel, leading to a noticeable drop in pure water flux. Moreover, although CNF is hydrophilic and could, in theory, enhance water affinity and uptake, the dominating influence of crosslink density appears to override this effect. Water molecules encounter increased resistance due to the denser matrix, which suppresses bulk water transport despite any localized hydrophilicity from cellulose nanofibrils.

Figures 6.5b and 6.5c show an increase in the membranes' rejection with the thickness due to a more effective barrier against salt diffusion. For 2 g/L NaCl concentration and 0.5 cm thickness, the M_1 exhibited a 53.1% ± 1.6 rejection rate, increased to 63.8% ± 1.9 for $M_{1.5}$, reached 66.4% ± 2.0 for M_2 and 73.0% ± 2.2 for $M_{2.5}$ membrane. Membranes' rejection increased dramatically at 2 cm, achieving 76.3% ± 2.3, 85.2% ± 2.6, 94.1% ± 2.8, and 97.5% ± 2.9 for M_1, $M_{1.5}$, M_2, and $M_{2.5}$, respectively. The corresponding

membranes' rejection for 2 g/L $MgSO_4$ and 2 cm was 88.4% ± 1.8 for M_1, 90.1% ± 1.8 for $M_{1.5}$, 95.5% ± 1.9 for M_2, and 98.2% ± 1.9 for $M_{2.5}$ hydrogels. $MgSO_4$, a divalent salt, often exhibits higher rejection than monovalent NaCl due to the size and charge density differences. Figure 5d indicates that the water flux of NaCl decreased as the thickness and concentration of CNF increased. Specifically, water flux dropped from 50.3 LMH ± 5 to 27.9 LMH ± 2.8 for the M_1 and from 38.9 LMH ± 3.9 to 18.5 LMH ± 1.9 for the $M_{2.5}$ membranes. In addition to the physical restrictions imposed by lower M_C values, ionic screening effects from NaCl may reduce osmotic pressure-driven swelling, further reducing water uptake and flux in saline environments. These effects are more evident in samples with higher CNF content and shorter crosslink lengths.

At the same time, the rejection rate improved, increasing from 53.1% ± 1.6 to 76.3% ± 2.2 for the M_1 and 73.01% ± 2.2 to 97.5% ± 2.9 for the $M_{2.5}$. At a thickness of 2 cm, $MgSO_4$ was rejected by the membranes at a higher rate than NaCl. As the CNF concentration increased from 1% to 2.5%, the rejection rate for $MgSO_4$ increased from 88.4% to 98.5%, whereas NaCl's rejection rate increased from 76.3% to 97.5%. On the contrary, water flux for $MgSO_4$ dropped from 39.9 LMH in M_1 to 24.5 LMH in $M_{2.5}$, while for NaCl, it dropped from 28.2 LMH in M_1 to 19 LMH for NaCl $M_{2.5}$, indicating a reduction in the water flux at higher CNF concentrations (Figure 6.5e). For both $MgSO_4$ and NaCl feeds, the reduction in water flux at higher CNF concentrations was due to a decrease in the membrane's pore size that enhances its selectivity but reduces the water permeability. However, the greater rejection of $MgSO_4$ can be attributed to the larger hydrated radius of the Mg^{2+} ion (0.428 nm) compared to that of the Na^+ ion (0.356 nm), as well as the divalent valency of Mg^{2+} that encounters greater attraction by the negatively

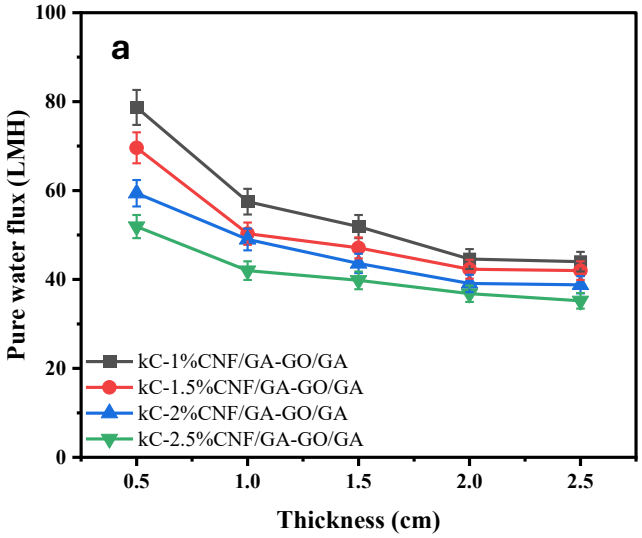
charged membrane surface. In contrast, the monovalent Na^+ ions are able to pass through more quickly.

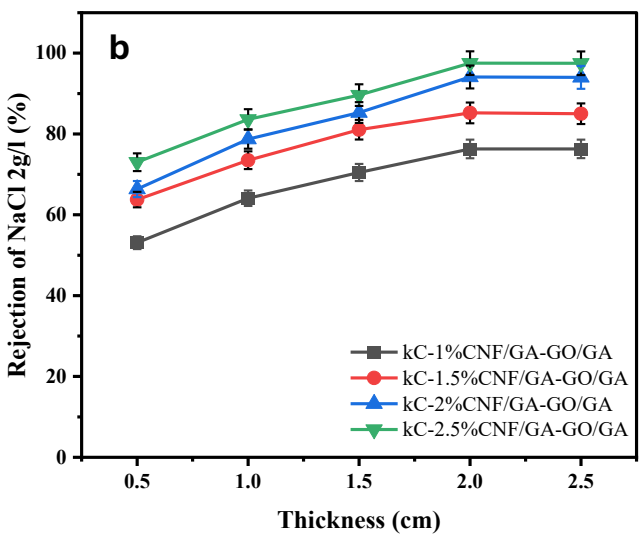
In all membranes, kC offers the fundamental structure with sulfate groups that engage with water and ions. At the same time, GA functions as a crosslinking agent to enhance the hydrogel's strength and reduce pore size, while the graphene oxide top layer increases the surface area and introduces functional groups that enhance the membrane's adsorption and mechanical stiffness. The concentration of CNF is critical to forming a denser hydrogel network of reduced pore sizes and augmented zeta potential for better ion rejection. A denser hydrogel matrix enhances the membrane's selectivity, improving the rejection of ions, and smaller pore sizes restrict ion passage, increasing ions' rejection (Ibrar et al., 2023).

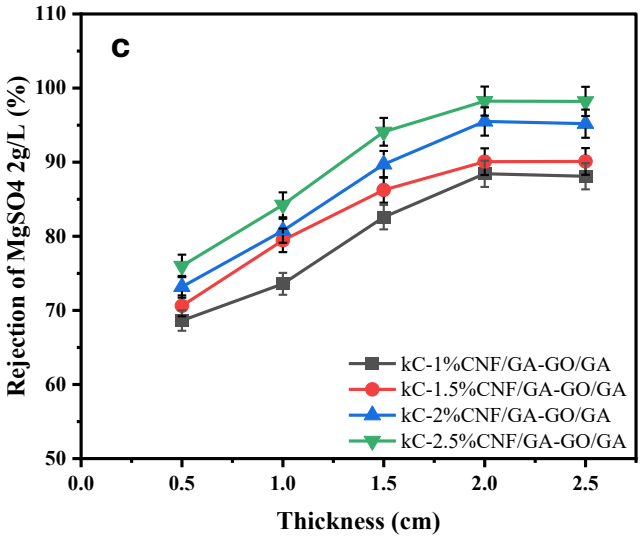
The hydrogel membranes' rejection of NaCl and $MgSO_4$ salts is influenced by the MC values. MC values decreased with increasing concentration of CNF, reflecting shorter distances between crosslinking points and a denser three-dimensional network. This tighter structure played a critical role in modulating ion transport and improving salt rejection efficiency. For both salts, lower Mc values enhanced the membrane's ability to act as a size-exclusion barrier. A smaller free volume within the matrix restricts the diffusion of solvated ions, especially those with large hydration shells, such as Mg^{2+} and SO_4^{2-}. This effect contributed to the consistently higher rejection rates observed for $MgSO_4$ compared to NaCl, as the hydrated Mg^{2+} ion (~8.6 Å) is substantially larger than Na^+ (~7.2 Å). The denser networks effectively limited the passage of these larger species while partially allowing smaller or monovalent ions to permeate.

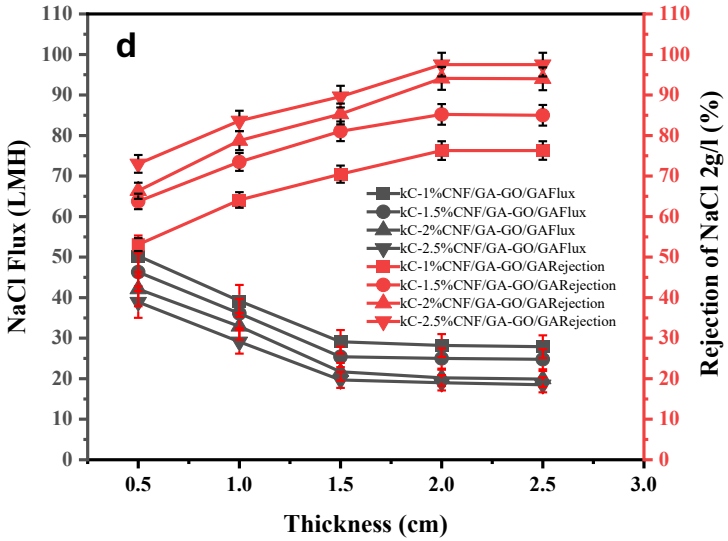
In addition, the reduced Mc enhances the Donnan exclusion mechanism by maintaining a more compact hydrogel structure. This can concentrate fixed charges in the network (e.g., carboxyl or hydroxyl groups from CNF or gelatin), which repel co-ions and reinforce the selectivity against multivalent ions. Although CNF is not strongly charged, the overall architecture and spatial constraint provided by a tighter network amplify these electrostatic exclusion effects. Therefore, it can be concluded that while lower Mc values decrease water flux, they improve salt rejection—especially for multivalent salts—by narrowing transport pathways and enhancing charge-based selectivity. The results highlight a fundamental trade-off in membrane design, where tighter networks (lower Mc) enhance selectivity, they reduce permeability, and an optimal balance must be tailored to application needs.

Thus, permselectivity of the hydrogel membranes is a trade-off between their rejection and water flux, with the membranes' water flux decreasing as their rejection increases. Since membrane $M_{2.5}$ at 2 cm thickness exhibited the best permselectivity, it was used for seawater desalination in multiple filtration cycles to evaluate its performance over time.


a
Pure water flux (LMH)
Thickness (cm)
kC-1%CNF/GA-GO/GA
kC-1.5%CNF/GA-GO/GA
kC-2%CNF/GA-GO/GA
kC-2.5%CNF/GA-GO/GA


b
Rejection of NaCl 2g/l (%)
Thickness (cm)
kC-1%CNF/GA-GO/GA
kC-1.5%CNF/GA-GO/GA
kC-2%CNF/GA-GO/GA
kC-2.5%CNF/GA-GO/GA


c
Rejection of MgSO4 2g/L (%)
Thickness (cm)
kC-1%CNF/GA-GO/GA
kC-1.5%CNF/GA-GO/GA
kC-2%CNF/GA-GO/GA
kC-2.5%CNF/GA-GO/GA


d
NaCl Flux (LMH)
Rejection of NaCl 2g/l (%)
Thickness (cm)
kC-1%CNF/GA-GO/GAFlux
kC-1.5%CNF/GA-GO/GAFlux
kC-2%CNF/GA-GO/GAFlux
kC-2.5%CNF/GA-GO/GAFlux
kC-1%CNF/GA-GO/GARejection
kC-1.5%CNF/GA-GO/GARejection
kC-2%CNF/GA-GO/GARejection
kC-2.5%CNF/GA-GO/GARejection

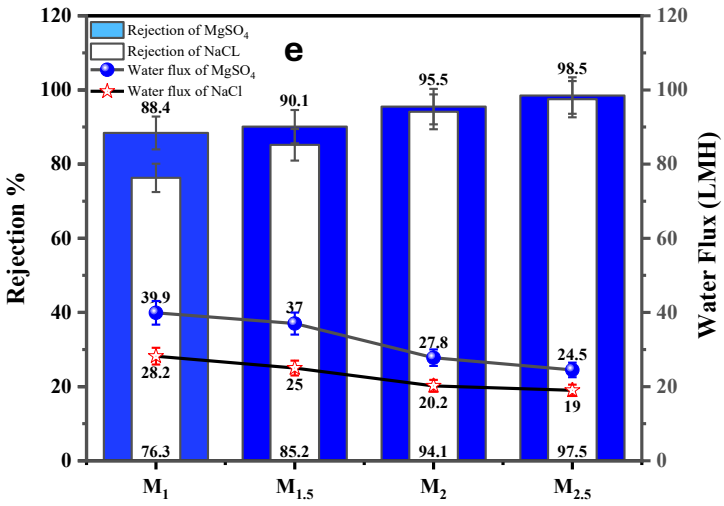

e
Rejection of MgSO4
Rejection of NaCL
Water flux of MgSO4
Water flux of NaCl
Rejection %
Water Flux (LMH)
88.4
90.1
95.5
98.5
39.9
37
27.8
24.5
28.2
25
20.2
19
76.3
85.2
94.1
97.5
M1
M1.5
M2
M2.5

Figure 6.5. a) Influence of hydrogel thickness on pure water flux, b) Influence of hydrogel thickness on 2 g/L NaCl rejection, c) Influence of hydrogel thickness on 2 g/L $MgSO_4$ rejection, d) Influence of hydrogel thickness on 2 g/L NaCl rejection and flux, e) Rejection and flux at 2 cm thickness for M_1, $M_{1.5}$, M_2, and $M_{2.5}$ with NaCl, and $MgSO_4$.

6.4.7 Seawater desalination

$M_{2.5}$ membrane was tested for seawater desalination experiments in a dead-end filtration column to achieve a recovery rate of 90%. In the two-stage filtration process, the permeate from the first stage was the feed for the second filtration stage, using a new hydrogel in each stage. In the first stage, the seawater TDS reduced from 34788 mg/L to 3500 mg/L, while it further reduced to 692 mg/L in the second stage. About a 98% reduction in ion concentration was achieved after the second filtration stage, as shown in Figure 6.6a, with the concentrations of Na^+ and SO_4^{2-} in the second stage permeate being 199 mg/L and 21 mg/L. The water flux in the first and second stages is shown in Figure 6.6b. In the first filtration stage, a stable water flux of 19.4 LMH was recorded after 20 minutes and dropped to 14.9 LMH after 90 minutes, whereas water flux in the second stage was 24.6 LMH after 35 minutes and decreased to 21.2 LMH after 90 minutes.

The drop in the water flux in stages one and two can be attributed to scale fouling from divalent ions deposition on the membrane surface, causing pore blockage. The EDX analysis shows divalent ion peaks on the $M_{2.5}$ membrane surface, including Mg^{2+} 0.12 wt.%, Si^{4+} 0.02 wt.%, and Cu^{2+} 0.24 wt.% (Table S4.3, supplementary material). Compared to divalent ions, Na^+ and K^+ exhibit low fouling characteristics due to weaker interaction with the membrane and their high solubility in solution, while Mg^{2+} and Ca^{2+} form complexes with negatively charged molecules, such as sulfate and carbonate, leading to the precipitation of insoluble salts. A gradual decline in water flux, therefore,

was inevitable over time, particularly when the membrane operates at 90%. The dead-end filtration of seawater also promotes fouling due to the accumulation of fouling materials on the membrane surface. The seawater was analyzed through a Malvern Particle analyzer for particle size distribution to study colloidal fouling (Figure 6.6c). Results show three peaks of particle size, 250-650 nm, 120-250 nm, and 60-120 nm, which are responsible for membrane fouling by blocking the 2.82 nm pore radius of the $M_{2.5}$ membrane (Table S4.2, Supplementary Materials).

The first filtration stage exhibited higher overall rejection percentages than the second stage, i.e., 89.9% vs. 80.2% (Figure 6d). For divalent ions, the membrane rejection of Mg^{2+} and Ca^{2+} was 91.7% ± 4.6 and 92.7% ± 4.6 in the first stage and 82.3% ± 4.1 and 80.4% ± 4.0 in the second stage. The greater Mg^{2+} and Ca^{2+} rejection in stage one was due to the high charge densities of ions that strengthened electrostatic repulsion with the negatively charged functional groups, such as carboxylate ($-COO^-$) and sulfate ($-SO_3^-$), of the membrane. Compared to Mg^{2+} and Ca^{2+}, SO_4^{2-} was rejected at a lower rate, 88.7% ± 4.4 in stage one and 79.7 ± 3.9 in stage two, due to its large size and lower charge density, which is responsible for its faster diffusion rate. Also, SO_4^{2-} can shed its large hydration shell more easily than Mg^{2+} and Ca^{2+}. Negatively charged membranes repel anions and attract cations through electrostatic interactions. Despite the more negative zeta potential at 2.5% CNF loading, the rejection of SO_4^{2-} was lower than that of Mg, which results from ion interactions with the membrane structure.The hydrated radius of SO_4^{2-} is significantly larger than that of Mg^{2+}, resulting in weaker electrostatic exclusion due to steric hindrance within the membrane pores. Moreover, SO_4^{2-} possesses a lower charge density and a more flexible hydration shell, allowing partial dehydration and diffusion through nanochannels. In contrast, Mg^{2+}, with a higher charge density, forms

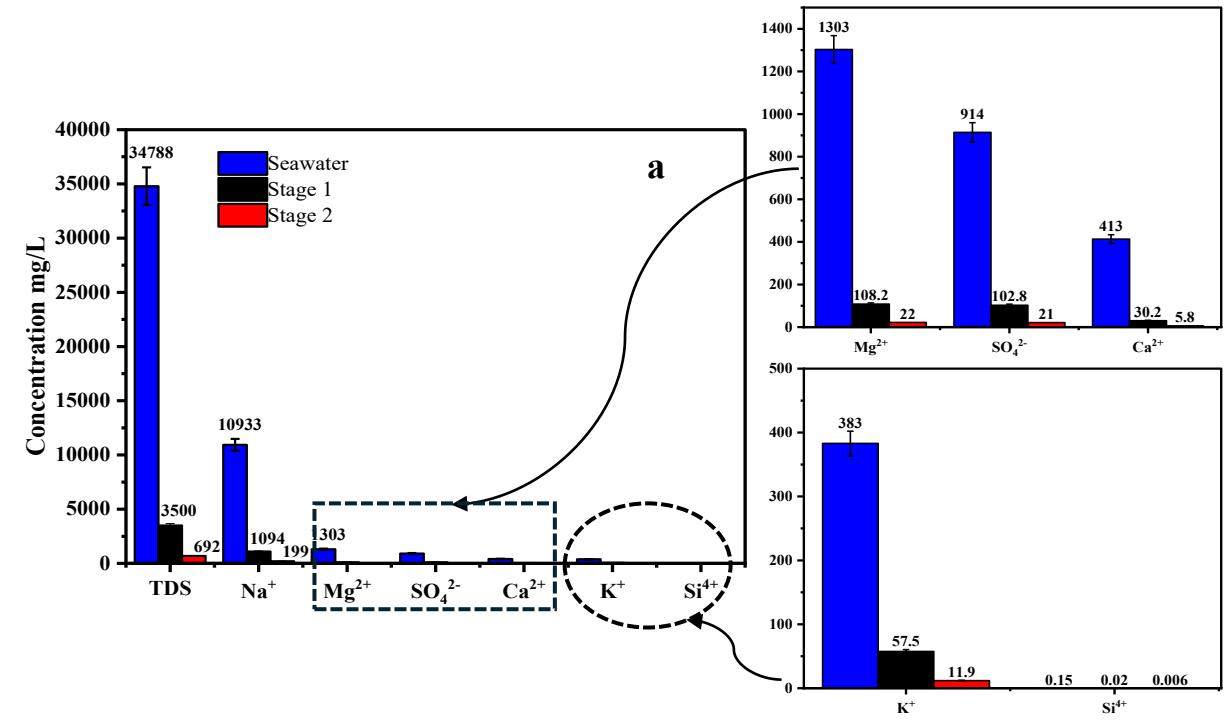
stronger electrostatic interactions with negatively charged groups such as $–COO^-$ and $–SO_3^-$, enhancing its rejection. The heterogeneous surface charge distribution of the kC–CNF/GA-GO-GA hydrogel may also create localized pathways of lower repulsion potential, further contributing to the relatively lower SO_4^{2-} rejection (Liu et al., 2025; Pintossi et al., 2020). For Na^+, the rejection was 90% ± 4.5 in stage one and 81.8% ± 4.0 in stage two, while K^+ rejection was 84.9% ± 4.2 in stage one and 79.6% ± 3.9 in stage two. The lower rejection rate of K^+ is owing to its greater ionic radius (0.132 nm) and lower charge density, which attenuates the influences of steric and electrostatic exclusion mechanisms. Compared to NaCl binary feed solution experiments, the lower Na^+ rejection in the seawater experiment is attributed to the complex ionic composition, competitive transport effects in natural seawater, which influence electrostatic exclusion and diffusion mechanisms. Also, the concentration of the feed solution in the NaCl experiment is 2 g/L, while in the seawater experiment is 34788 mg/L, which increases salt leakage across the hydrogel membrane.

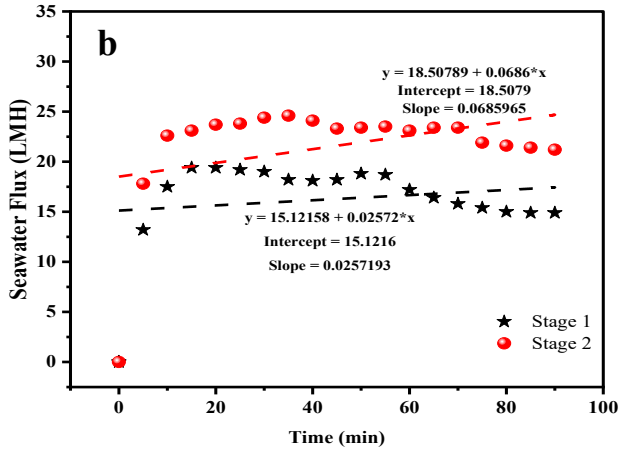
Figure 6.6e shows the $M_{2.5}$ membrane's performance in three seawater filtration cycles. The same membrane was used in the filtration cycles, with 1-hour DI water cleaning between cycles. The $M_{2.5}$ membrane has an FRR% of 89.7% ± 4.5 in cycle 1, 86.6% ± 4.3 in cycle 2, and 82.3% ± 4.1 in cycle 3, maintaining above 80% water flux recovery and strong capability for reuse in multiple filtration cycles. The IFR% was 10.3% ± 0.8 in the first cycle and increased to 17.5% ± 1.4 by the third cycle, indicating a gradual buildup of irreversible fouling due to the inadequate removal of pollutants by the DI water cleaning. However, the IFR increase was moderate, implying the durability and ability of the membrane to maintain functionality despite repeated use at a 90% recovery rate. The DR% increased from 43.1% ± 0.21 in cycle 1 to 48.3% ± 0.24 in cycle 3 as a result of

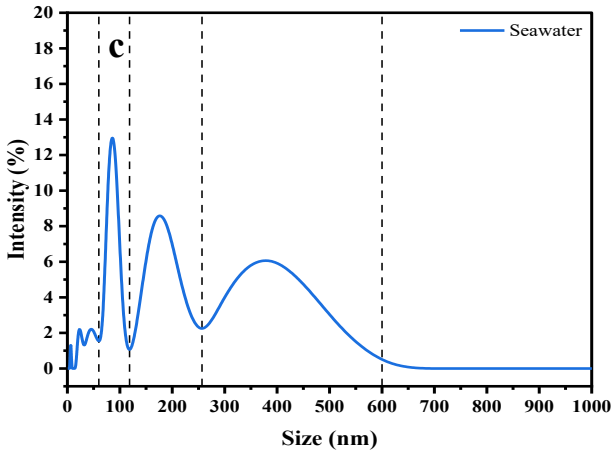
membrane fouling. Seawater changes the hydrogen bonding network in the $M_{2.5}$ membrane, which can be seen by the stretching of hydroxyl groups in **Figure 6.4b** and a rise in the concentrations of sodium (31.66 wt.%), chloride (44.23 wt.%), and silica (0.02 wt.%) indicating a large amount of salt deposition (Table S4.3, supplementary material). Membrane fouling was inevitable due to the elevated recovery rate in the filtration cycles and inadequate cleaning. The SEM images of the new and used hydrogel show an accumulation of fouling materials on the membrane surface after the seawater filtration (Figures 6.4c and 6.4e). The EDS images (Figures 6.4d and 6.4f) confirm high peaks of sulfate, silica, and divalent ions on the surface of the fouled membrane after seawater filtration (Figure 6.4f), indicating silica and metal sulfate fouling, such as magnesium sulfate. Figure 4b shows FT-IR spectra of the M2.5 hydrogel before and after exposure to NaCl, $MgSO_4$, and seawater, revealing spectral shifts in the O–H (3140–3380 cm^{-1}), C=O (1650–1700 cm^{-1}), S=O (1215–1240 cm^{-1}), and C–O–C (1030–1060 cm^{-1}) regions. These changes indicate ion–polymer interactions and hydrogen-bond rearrangement. The fouling propensity of the hydrogel membrane was severely exacerbated by the elevated recovery rate of the filtration process and membrane cleaning with DI water only, which is ineffective in the removal of silica and metal sulfate precipitates.

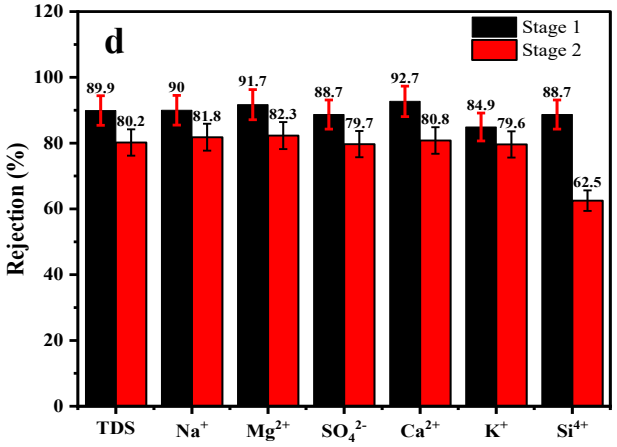
Table S4.6 (supplementary material) summarizes a comparison of research on CNF, GO, and kC hybrid membranes for water purification. The table shows water flux, rejection, and water flux recovery ratio (FRR) for several studies. In general, the water flux, FRR, and rejection rate of the kC-CNF/GO-GA are similar or competitive to those reported in the literature. Notably, the hydrogel membrane in this study is gravity-driven and hence does not require high energy for seawater desalination. Additionally, the hydrogel membrane operates at a 90% recovery rate, which is challenging for most pressure-driven

membrane processes. Previous studies (Ao et al., 2017; Lyu et al., 2018) fabricated a GO-based membrane for dye removal from wastewater. Although the studies reported 90 to 95% rejection of dyes, the rejection of divalent and monovalent ions was between 75% and 80%. Subsequent studies optimized the crosslinking and the composite design to enhance mechanical stability, ion selectivity, and antifouling performance of the GO NF membrane(Kong et al., 2024). Nevertheless, the membrane exhibited 95% removal of dyes and water flux recovery of 85% while water flux recovery in this study was 89.7% at a 90% recovery rate. In later studies, Kardani et al. fabricated a GO/PEI and hole-enriched GO/CNF membrane (Kardani et al., 2025), with superior ion transport and mechanical reinforcement for heavy metal recovery from wastewater. The membrane, with 93% rejection on NaCl and 94% to 99% rejection of divalent ions, exhibited a low water flux of 7.72 LMH and 90.93% FRR. The current kC–CNF/GO–GA hydrogel integrates a sustainable biopolymer with excellent ion rejection (≈98%) and water flux, providing a cost-effective solution for seawater desalination. The gravity-driven membrane achieved a 90% recovery rate and 89.7% FRR after three cycles of seawater filtration and DI water cleaning.


a
Seawater
Stage 1
Stage 2
Concentration mg/L
34788
3500
692
10933
1094
199
1303
TDS
Na+
Mg2+
SO4 2-
Ca2+
K+
Si4+
1303
108.2
22
914
102.8
21
413
30.2
5.8
Mg2+
SO4 2-
Ca2+
383
57.5
11.9
0.15
0.02
0.006
K+
Si4+


b
y = 18.50789 + 0.0686*x
Intercept = 18.5079
Slope = 0.0685965
y = 15.12158 + 0.02572*x
Intercept = 15.1216
Slope = 0.0257193
Stage 1
Stage 2
Seawater Flux (LMH)
Time (min)


c
Seawater
Intensity (%)
Size (nm)


d
Stage 1
Stage 2
Rejection (%)
89.9
80.2
90
81.8
91.7
82.3
88.7
79.7
92.7
80.8
84.9
79.6
88.7
62.5
TDS
Na+
Mg2+
SO4 2-
Ca2+
K+
Si4+

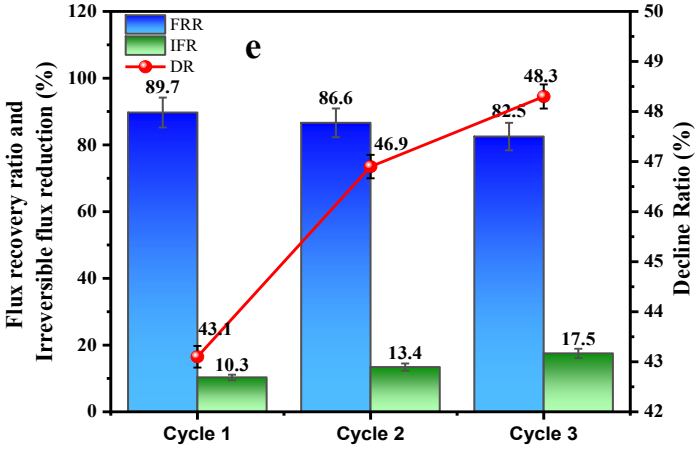

e
FRR
IFR
DR
Flux recovery ratio and
Irreversible flux reduction (%)
Decline Ratio (%)
89.7
43.1
10.3
86.6
46.9
13.4
82.5
48.3
17.5
Cycle 1
Cycle 2
Cycle 3

Figure 6. 6. a) Ion rejection and TDS reduction performance of $M_{2.5}$ hydrogel by seawater, stage 1, and stage 2, b) Water flux of the seawater with time for stage 1, and 2, c) Particle size distribution of the seawater conducted through the Malvern Particle Analyser, d) Removal of contaminants from seawater using $M_{2.5}$ for stage 1, and 2, e) Fouling (FRR, DR, and IFR) % for $M_{2.5}$ with seawater for three cycles.

6.4.8 Reusability

Desorption and reuse of the $M_{2.5}$ membrane are very important in practical applications from an economic point of view. Figure 6.7a illustrates the highest relative desorption capacity of $MgSO_4$ and NaCl in 2 g/L solution. Consecutive adsorption/desorption cycles were performed to assess the membrane reusability. The results show the robust adsorption/desorption characteristics of the $M_{2.5}$ membrane, even after three filtration cycles, with an adsorption efficiency of 79.4% ± 3.2 for Na^+ and 85% ± 3.4 for Mg^{2+} and desorption efficiency of 75.2% ± 3 for Na^+ and 83.3% ± 3.3 Mg^{2+}.

The efficiency of the $M_{2.5}$ membrane was also evaluated in multiple filtration cycles to investigate the rejection and water flux. After three filtration cycles, a reasonable reduction was noted in the rejection of $MgSO_4$ from 98.5% ± 4.9 to 85% ± 4.3 and for NaCl from 97.5% ± 4.9 to 79% ± 3.9. Water flux also dropped from 24.5 LMH ± 1.2 in cycle one to 20.2 LMH ± 1.0 in cycle three in the $MgSO_4$ tests and from 19 LMH ± 0.95 in cycle one to 14.1 LMH ± 0.71 in cycle three in the NaCl tests. The decline in the water flux was a consequence of Mg^{2+} and Na^+ ions blockage of the hydrogel's porous network. The $M_{2.5}$ membrane was rinsed with DI water between filtration cycles to remove the easily attached fouling materials. However, deeper impurities remain within the membrane structure, reducing water flux (Figures 6.7b and 6.7c). Consequently, the $M_{2.5}$ hydrogel membrane can be an efficient adsorbent to remove divalent and monovalent ions

in multiple filtration cycles since they can rapidly and effectively regenerate. The GO–GA layer exhibited strong adhesion to the hydrogel surface under dead-end filtration conditions, maintaining stability over three filtration cycles under 0.5 bar pressure. Minor delamination was observed after extending the filtration cycling due to normal interfacial fatigue during repeated swelling–deswelling, rather than poor adhesion of the GO-GA layer. Given that the membranes were designed for batch ion-removal and recovery applications rather than long-term continuous operation, the observed stability was satisfactory for their intended use. Nevertheless, future studies can focus on the improvement of interfacial bonding strategies to enhance long-term durability.

Based on retail prices, the cost of the filtration system, including the hydrogel filter for multiple uses, is very reasonable. The hydrogel costs about AU$ 6 per m^3 (of 2 cm thickness), producing more than 15 LMH of desalinated from seawater. The KC-CNF/GA-GO/GA hydrogel filter has a long shelf life, as long as it is kept in a closed container, and it would remain effective at least for more than a year from the date of preparation.

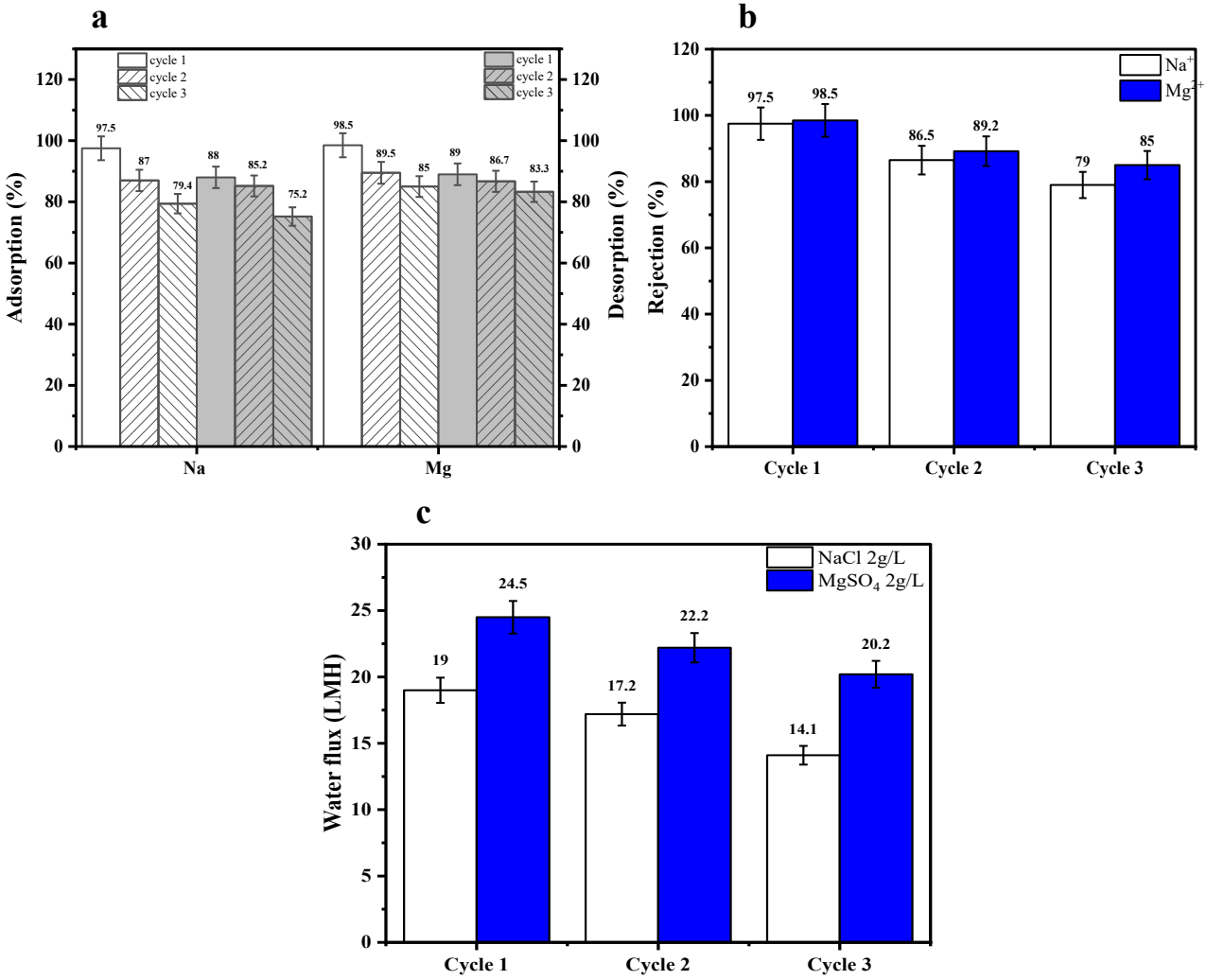


Figure 6. 7. a) Adsorption/desorption cycles for 2g/L NaCl and $MgSO_4$ on the $M_{2.5}$, b) Rejection of 2g/L NaCl and $MgSO_4$ during three cycles by $M_{2.5}$, and c) Water flux of NaCl 2g/L and $MgSO_4$ 2g/L during c cycles by $M_{2.5}$.

6.5 Conclusion

A gravity-driven kC-CNF composite hydrogel coated with GO and crosslinked with GA was fabricated for seawater desalination in stages from 34788 mg/L to 692 mg/L. The permeate water TDS falls within the fair water quality, TDS between 600 to 900 mg/L, which is applicable for irrigation and general use. Further treatment to reduce the TDS to ≤ 500 mg/L is required for drinking use. The water flux reduces when the concentration

of CNF increases in the hydrogel from 1% to 2.5%; in contrast, the rejection increases. CNF addition increased membrane stiffness and altered its structure, as evidenced by different analyses. The membranes were tested with DI water, NaCl and $MgSO_4$ solutions, and real seawater. Increasing CNF content lowered water and salt solution fluxes while enhancing NaCl and $MgSO_4$ rejection. This behavior was linked to the calculated M_C values, which decreased with CNF content, indicating a denser and more tightly crosslinked network. Such networks limited water mobility but improved selectivity and salt rejection.

The best hydrogel was the $M_{2.5}$ hydrogel, which achieved a rejection rate of 98.5% ±5 for divalent ions and 97.5% ±5 for monovalent ions. Furthermore, the hydrogel demonstrated a significant water flow, ranging from 24.5 LMH to 19 LMH for synthetic feed solutions and 18 LMH for seawater. The hydrogel exhibits efficient and selective ion extraction from saline solutions, with high rejection rates of 90% for Na^+, 91.7% for Mg^{2+}, and K^+ has a lower rejection rate of 84.9%. The hydrogel showed robustness to fouling conditions with a flux recovery ratio of 89.7% ± 4.5 for seawater 35 g/L with a decline ratio (DR) of 43.1 ± 0.2%. The hydrogel membrane exhibited 82.5% FRR after three filtration cycles with seawater. These results show the potential of molecular-level tailoring of hydrogels in allowing precise control over hydrogel behavior and performance. The next steps should be scaled manufacturing, real-world antifouling testing, and hydrogel regenerating capabilities. While this study focused on the optimization of the CNF crosslinking, the GA crosslinking degree and GO coating thickness should be further investigated in further studies to optimize the rejection-flux trade-off. The kC-2.5%CNF/GO-GA hydrogel is a major step towards sustainable and creative environmental solutions.

Supplementary material S4

Fabrication of kappa carrageenan-cellulose nanofiber/graphene oxide composite membrane for water purification

Lilyan Alsaka[1], Ali Altaee[1,*], Armaghan Moghaddam[2], Hossein Ali Khonakdar[3,4], John, Zhou[1], Maryam AL-Ejji[5], Alaa H. Hawari[6]



Figure S4. 1. An illustration of gravity-based filtration

Table S4. 1: Shows Analytic instruments were used to characterize M_1, $M_{1.5}$, M_2, and $M_{2.5}$

Analytical Instrument	Characteristics Studied
Fourier Transform Infrared (FTIR) (Thermo Scientific Nicolet Spectrometer)	To analyze the chemical structure and functional groups of M_1, $M_{1.5}$, M_2, and $M_{2.5}$ layers within 400–4000 cm^{-1}.
Field Emission Scanning Electron Microscopy (FESEM) (Zeiss EVO LS15 SEM, Zeiss, Sydney, Australia)	To test the surface morphology of M_1, $M_{1.5}$, M_2, and $M_{2.5}$

Energy Dispersive X-Ray Analysis (EDAX)(Bruker SDD XFlash 5030 detector, Zeiss, Australia)	To determine the elemental composition of $M_{1,}$ $M_{1.5}$, $M_{2,}$ and $M_{2.5}$
Surface Zeta Potential (Malvern Analytical)	To measure the surface charge of $M_{1,}$ $M_{1.5}$, $M_{2,}$ and $M_{2.5}$ and particle distribution in seawater.
Contact Angle Measurement (Kyowa Interface Science, Chennai, India)	To measure the contact angle to assess the hydrophilicity or hydrophobicity of $M_{1,}$ $M_{1.5}$, $M_{2,}$ and $M_{2.5.}$
Brunauer–Emmett–Teller (BET) Analysis	Analyzes the specific surface area, pore volume, and pore size distribution of $M_{1,}$ $M_{1.5}$, $M_{2,}$ and $M_{2.5.}$

Table S4. 2: Summaries of BET analysis

BET analysis		M_1	$M_{1.5}$	M_2	$M_{2.5}$
Adsorption BJH	Surface area m^2/g	68.5	45.24	40.18	39.25
	Pore Volume cc/g	0.079	0.061	0.045	0.025
	Pore Diameter nm	3.75	3.35	3.15	2.98
Desorption BJH	Surface area m^2/g	62.77	39.69	37.80	36.76
	Pore Volume cc/g	0.065	0.050	0.041	0.022
	Pore Diameter nm	3.62	3.13	2.95	2.82

Table S4.3: The EDS analysis results for the $M_{2.5}$ hydrogel.

Element	**Quantitative Results (wt.%)**	
	Pure hydrogel	Filtration with seawater
C	31.03	19.52
O	49.83	2.91
S	7.27	0.14
k	11.88	-
Cl	-	44.23
Na	-	31.66
Mg	-	0.12
Cu	-	0.24
Si	-	0.02

Al	-	0.1
Cr	-	0.11
Zn	-	0.36
P	-	0.59
Total	100	100

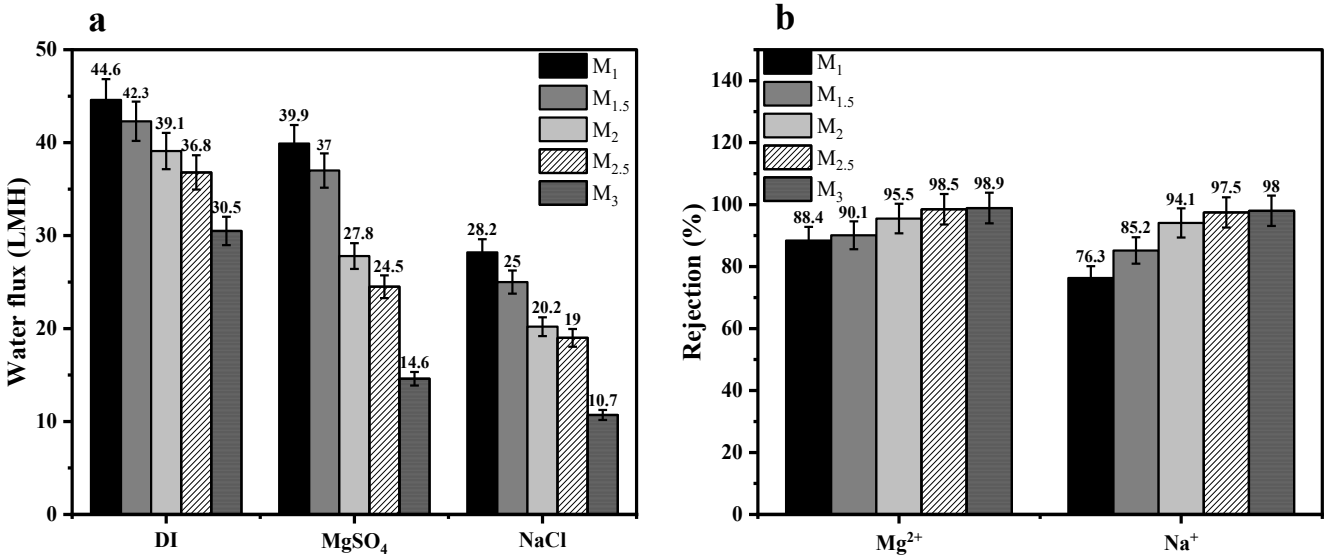


Figure S4. 2. a) Water flux at 2 cm thickness for M_1, $M_{1.5}$, M_2, $M_{2.5}$, and M_3 with, DI, NaCl, and $MgSO_4$, b) rejection at 2 cm thickness for M_1, $M_{1.5}$, M_2, $M_{2.5}$, and M_3 with, NaCl, and $MgSO_4$.

S4.1M_c calculations

In order to calculate M_c values for hydrogel samples, Equation 6.11 and Equation 6.12 were used. Following equation was used to calculate dry polymer density:

$$\rho_P = (\mathrm{wkC} \cdot \rho\mathrm{kC}) + (\mathrm{wCNF} \cdot \rho\mathrm{CNF}) \qquad \text{S4.1}$$

According Table 5.2, weight content of polymer constituents for the hydrogel samples was calculated, as shown in Table S4.4.

Table S4. 4:Weight content of polymer constituents in hydrogel samples

Sample	kC (g)	CNF (g)	Total Polymer (g)	wkC	wCNF
M_1	3	1	4	75%	25%

$M_{1.5}$	3	1.5	4.5	66.70%	33.30%
M_2	3	2	5	60%	40%
$M_{2.5}$	3	2.5	5.5	54.50%	45.50%

Considering ρkC=1.37 g/cm^3 and ρCNF=1.5 g/cm^3, ρ_p values were obtained. In addition, for the hydrogel systems, X was estimated using the rule of mixtures, and thus M_c values were approximated as shown in Table S4.5.

Table S4. 5: Density of polymer constituents in hydrogel samples

Sample	ρ_p (g/cm^3)	X	ν_2	M_C (g/mol)
M_1	1.4025	0.405	0.067822	10535.5365
$M_{1.5}$	1.4231	0.413	0.072422	9344.78619
M_2	1.4380	0.42	0.075626	8639.90133
$M_{2.5}$	1.4516	0.426	0.079285	7914.56583

S4.2 Effect of M_c values on properties of hydrogel samples

The M_C value is a critical parameter that provides insight into the internal network structure of hydrogels. In this study, M_C values were calculated using the Flory–Rehner equation based on swelling equilibrium data. The observed variations in M_C among different hydrogel samples directly reflect the density and compactness of the polymeric network formed during crosslinking. Here, the derived M_C values correspond to the effective crosslink density of the bulk hydrogel phase. While CNF contributes additional physical crosslinking, these effects are implicitly included in the measured swelling behaviour and polymer density parameters, yielding comparable trends to those expected from a dual-network model.

As expected, hydrogel samples with higher swelling degrees exhibited larger Mc values, indicating a looser network structure with longer polymer chains between crosslinking points. On the other hand, samples with lower swelling showed smaller M_C values, which meant a denser, more tightly crosslinked network. Increased crosslink density restricts the mobility of polymer chains and limits water uptake.

Porosity and pore size analyses also support the interpretation of M_C differences. Hydrogels with lower M_C values demonstrated more compact and less porous structures, while those with higher M_C values showed more open and interconnected porous networks. This morphological evidence aligns with the idea that tightly crosslinked networks (shorter M_C) form smaller, more constrained pore structures due to limited chain flexibility during gelation.

In addition, while CNF is intrinsically hydrophilic due to its abundance of hydroxyl groups, increasing its content in the hydrogel matrix did not result in a decrease in water contact angle (Nie et al., 2021). On the contrary, samples with higher CNF loading exhibited a slight increase in contact angle. This unexpected trend can be attributed to the overall densification of the hydrogel network, as confirmed by the reduced Mc values and lower swelling ratios. The denser crosslinked structure, which was characterized by shorter polymer chain lengths between crosslinks, likely restricted the diffusion and penetration of water molecules into the 3D network. As a result, although the surface may contain hydrophilic functional groups, the physical barrier posed by the tightly packed network reduces the apparent wettability, leading to an increase in the measured contact angle.

S4.3 Adsorption performance

Figure S4.3 illustrates different uptake behaviors for each ion; the adsorption qe mg/g of Na^+ and Mg^{2+} ions onto the $M_{2.5}$ hydrogel was observed for 300 minutes. At 30 minutes, both ions showed the ability of fast adsorption on the hydrogel composite, with Mg^{2+} reaching 1.54 mg/g ± 0.08 and Na^+ reaching 1.3 mg/g ± 0.06. One of the reasons the hydrogel's negatively charged functional groups, such as carboxylate ($-COO^-$) and sulfonate ($-SO_3^-$), which promote cations' electrostatic attraction and another reason provide many clean sites, are responsible for this rapid absorption. At 90 minutes, the adsorption was almost at equilibrium, with Mg^{2+} reaching an adsorption capacity of 1.73 mg/g ±0.08 and Na^+ reaching 1.8 mg/g ±0.09, leading to stronger electrostatic interactions with the hydrogel matrix. However, similar equilibrium adsorption capacities suggest that ion size and hydration energy also play significant roles in adsorption. After that, the amount of change became very slight. At the end of the adsorption period test at 300 min, the adsorption value of Na was 1.88mg/g ±0.09, and Mg was 1.81mg/g ±0.09. The results of this study are consistent with those of earlier research on polysaccharide-based hydrogels, which indicated the successful adsorption of metal ions by processes that included both electrostatic interactions and ion diffusion into the hydrogel network (Alsaka, Ibrar, Altaee, Zhou, Chowdhury, Maryam, et al., 2024; Ibrar et al., 2023). The adsorption capacity of the $M_{2.5}$ hydrogel is examined by analyzing its composite components, which include CNFs, kC, GO, and GA. CNFs' large surface area and mechanical strength strengthen the hydrogel and provide many ion adsorption sites(Zhang et al., 2021; Y. Zhang et al., 2020). kC increases adsorption capacity by introducing negatively charged sulphate groups ($-SO_3^-$), which facilitate electrostatic interactions with cationic species like Na^+ and Mg^{2+}. GO adds functional groups like

carboxyl (-COOH) and hydroxyl (-OH), boosting active site density and generating a porous network for ion transport(Deshwal et al., 2023). GA crosslinks polymer chains with covalent bonds to strengthen them. Overcrosslinking reduces the hydrogel's swelling ratio and functional groups needed for ion adsorption (Mohammed, Hegab, & Ou, 2022). These components work together to create a hydrogel with a strong, porous structure and a high functional group density that can adsorb cationic species from aqueous solutions.

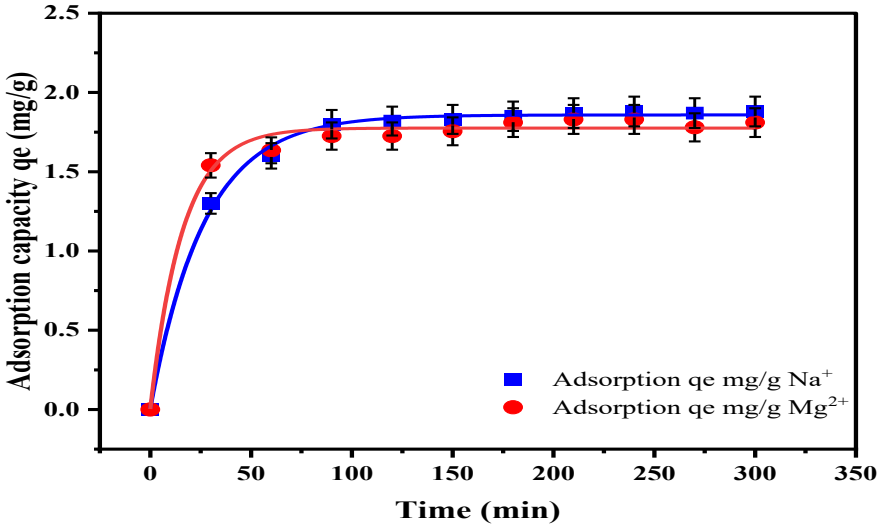


Figure S4. 3. The adsorption capacity of Na^{+} and Mg^{2+} on the hydrogel.

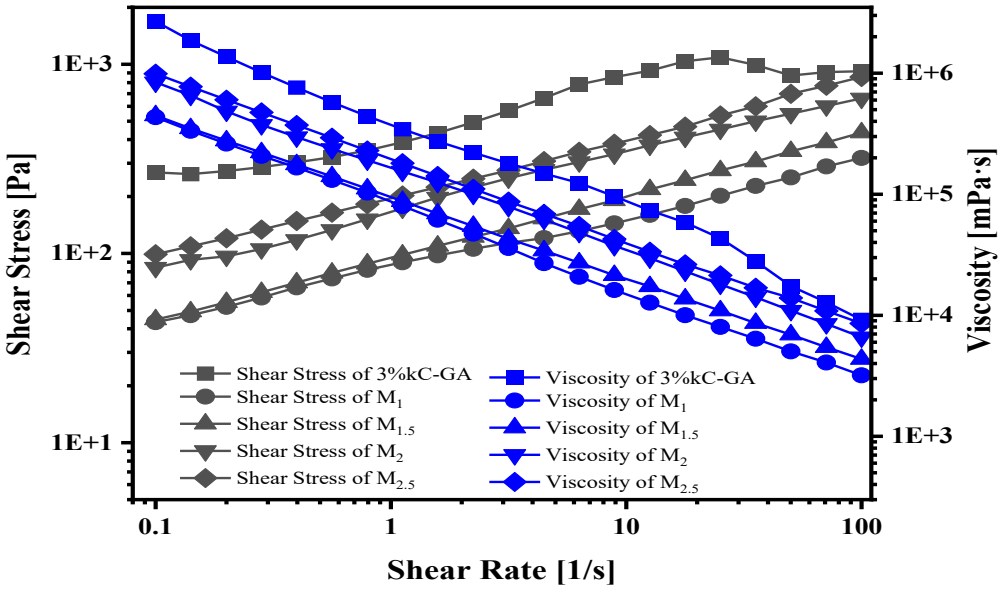


Figure S4. 4 .Viscosity and shear stress of the composite hydrogel membranes.

Table S4. 6: Comparative Summary of CNF, GO, and κc-Based Composite Membranes and Hydrogels for Advanced Water Treatment and Desalination.

Type of Hydrogel / Membrane	Type of Filtration	Water Flux /permeability	Rejection (Ion / Salt / TDS)	FRR (%) and Mechanical Strength (MPa)	Summary of Performance	Reference
GO/CNF network cross-linked with GA	Nanofiltration (aqueous & organic)	13.9 ± 1.9 (water); 4.1 ± 0.35 (ethanol) 13.9 $L \cdot m^{-2} \cdot h^{-1} \cdot bar^{-1}$	> 90% for Rose Bengal & Brilliant Blue dyes		An efficient combination of GO's molecular sieving and CNF's permeability. GA crosslinking improved selectivity and reduced swelling. Demonstrated stable nanofiltration performance across solvents.	(Mohammed et al., 2022)
GO–CCNC (carboxyl-modified nano-crystalline cellulose) membrane	Nanofiltration	12.74 L m^{-2} h^{-1} bar^{-1}	≥95% for dyes (SY, MB, RhB); 80.6% (Na_2SO_4); 75.5% ($MgSO_4$)	>90	CCNC intercalation increased GO interlayer spacing, improving flux. Membrane showed high dye rejection and moderate salt rejection.	(Lyu, Zhang, Wang, & Pu, 2018)

					Demonstrated strong antifouling and 90% flux recovery post-cleaning.	
Ultrathin GO layer on CNF membrane (crosslinker-free	Microfiltration / Nanofiltration	18123 ± 574 Lm^{-2} h^{-1} bar^{-1}	>90% for charged dyes (cationic & anionic)	High (dry & wet stability)	GO–CNF (1:100) layered membrane achieved ultrafast flux due to standing-inserted GO nanosheets forming nanochannels. Strong negative zeta potential improved electrostatic rejection. Excellent mechanical and chemical robustness.	(Liu, Zhu, & Mathew, 2019)
GO Composite Loose Nanofiltration (LNF) Membrane	Loose Nanofiltration (Dye–Salt Separation)	15–30 Lm^{-2} h^{-1} bar^{-1}	>95% (dyes); high salt permeability	>85	GO-based LNF membranes exhibit high dye retention and salt permeability via spatial and electrostatic repulsion mechanisms. Demonstrate	(Kong et al., 2024)

					excellent fouling resistance, antibacterial activity, and long-term stability for textile wastewater treatment.	
Superhydrophilic GO@Electrospun CNF Hybrid Membrane	Oil/Water Separation (Gravity-Driven)	0.96 $m^3 \cdot h^{-1} \cdot m^{-2}$ (~960 $L \cdot m^{-2} \cdot h^{-1}$)	99–99.8% (hexane, toluene, petroleum ether)	≈100 (10 cycles) High; corrosion-resistant	Fabricated via electrospinning and GO coating; superhydrophilic and underwater superoleophobic. High flux, antifouling, and stability in acidic, alkaline, and saline media. Environmentally friendly, no toxic reagents used.	(Ao et al., 2017)
kC–GO/PEI Nanocomposite Hydrogel Membrane	Nanofiltration / Heavy Metal Recovery & Wastewater Valorization	7.72 (optimized, 20% > baseline 6.44) LMH	NaCl: 93%; $MgSO_4$: 97.13%; Pb, Co: 99.7%; Cu: 94.11%; Li: 94.48%	90.93 (after 3 cycles)	GO enhanced hydrophilicity and permeability; PEI improved structural stability and metal selectivity. The membrane achieved near-complete removal of multiple	(Kardani et al., 2025)

					metals (Cd, Zn, Fe, Mn, Cr, Ni, Pb, Co, Cu, Li) with high flux recovery, demonstrating strong permselectivity and antifouling capability for sustainable wastewater treatment.	
kC/GO-Coated UA-60 Membrane	Nanofiltration / Leachate Wastewater Treatment	54–60 LMH	$MgSO_4$ 95%, NaCl 23%	95.7%	Cross-linked kC-GO layer increased hydrophilicity (WCA 29.9°), negative charge (−21.4 mV), and antifouling; excellent FRR and low fouling (18.9%).	(Yadav, Ibrar, Altaee, Samal, & Zhou, 2022)
kC / PSF/ (Ag–GO) Hybrid (GS3)	Nanofiltration / Heavy Metal Removal	213.12 LMH	Fe^{2+}: 98.1; Mn^{2+}: 99.8		Fabricated via wet phase inversion using **green solvent DMSO**. Incorporation of κ-Car and Ag–GO NPs increased hydrophilicity	(Baharudin et al., 2025)

					(WCA from 68.5° - 57.3°) and porosity (from 63% - 88%). Exhibited excellent Fe^{2+}/Mn^{2+} rejection (>98%) and sustainable membrane structure.	
kC-CNF/GA-GO-GA Hydrogel	Seawater Desalination / Ion Separation/gravity filtration	24.6 LMH	Stage 1: 92.7–85; Stage 2: 82.3–79.6; Final TDS = 692 $mg \cdot L^{-1}$ (≈98% ion removal)	89.7%	The κC–CNF/GO–GA hydrogel exhibited a well-defined porous morphology and a uniform GO coating. CNF addition enhanced stiffness and decreased pore size, resulting in lower flux but improved salt rejection. Reusability tests showed stable ion removal efficiency and high flux recovery across multiple cycles. The membrane provides an eco-friendly,	This Study

					low-cost approach for seawater treatment with consistent desalination performance.	

.

Chapter 7 Conclusions and recommendations for future work

Kappa-carrageenan-based hydrogels are characterized as surprisingly versatile materials, with a range of applications that is so broad. Biodegradable, highly adaptable, depending on what nanoparticles combine with and the method used to prepare. This kind of flexibility makes a strong option for treating various types of wastewater.

This study examined the development and application of hydrogels made from kappa-carrageenan (kC) for wastewater purification in various forms and modifications. The findings demonstrated the adaptability, sustainability, and excellent performance of kC-based hydrogels in treating different types of wastewater, including landfill leachate, soil remediation effluent, wastewater rich in metals, and seawater. Hydrogels are promising materials for purifying water. They purify water efficiently and cost-effectively due to their unique three-dimensional structures, large surface area, and quick regeneration capabilities. These hydrogels can absorb organic pollutants and heavy metals, making them suitable for emergency and environmentally friendly water treatment.

Chapter three investigated a kappa carrageenan-vanillin composite hydrogel filter for the treatment of ions and wastewater. The composite filter demonstrates excellent potential for contaminant removal from both synthetic and natural landfill leachate feed solutions. As a natural crosslinking and functionalizing agent, vanillin enhanced the chemical stability of the hydrogel matrix and increased adsorption efficiency. The results confirm the concept that such biopolymer-based materials can be effectively engineered for the removal of heavy metals and organic contaminants while maintaining biodegradability and cost-effectiveness. Among all the hydrogels, the 3% kC-V hydrogel achieved an 80% ±5 rejection rate for divalent ions and a 42% ±5 rejection rate for monovalent ions.

Furthermore, the hydrogel exhibited high water flux, ranging from 30.8 L/m²h to 44 L/m²h for synthetic feed solutions and 26 L/m²h for leachate wastewater, along with an excellent rejection rate for turbidity, organic matter, and metal ions. These features are significant for treating biomedical and hospital wastewater, where the waste contains potentially infectious materials, and their management is highly regulated, critical, and costly.

Chapter four of the thesis study developed an environmentally sustainable and cost-effective gravity-driven kappa-carrageenan (kC)-based hydrogel for the removal of perfluorooctanoic acid (PFOA) from both artificial and actual wastewater. Two kC hydrogel filters were prepared by mixing activated carbon (AC) or vanillin (V) with the kC hydrogel to optimize selectivity and water permeability. Experimental work revealed that both the PFOA rejection and water permeability increased with higher concentrations of AC and V in the kC hydrogel. The experiments also evaluated the impact of feed pH, PFOA concentration, hydrogel composition, and hydrogel thickness on performance. Incorporating vanillin and AC into the kC hydrogel significantly enhanced the porosity of the kC-3%V membrane from 62.8% ± 5 to 79.1% ± 5 and up to 89.7% in the kC-0.3%AC. When evaluating the hydrogel's performance against PFOA, notable pH-dependent variations in rejection were observed. The hydrogel rejection of PFOA is pH-dependent, with the kC-0.3%AC hydrogel achieving an 86.9% rejection at pH 4, while the kC-3%V showed an 85.7% rejection. The experiments also exhibited a decline in water flux at higher PFOA concentrations and pH levels for both kC-0.3%AC and kC-3%V hydrogels. The study revealed that PFOA rejection increased with concentration, indicating that elevated PFOA levels restrict water passage by occupying pore spaces. When tested for soil remediation wastewater treatment, the kC-0.3%AC hydrogel

removed 81.1% PFOA at a water flux of 25.6 LMH, while the kC-3%V hydrogel removed 79.3% PFOA at a water flux of 21.5 LMH. However, due to pore blocking, consecutive filtration cycles revealed a slight decline in the hydrogel's performance.

Chapter five investigated the feasibility of applying crosslinked kC-AC for wastewater treatment and resource recovery. The kC-AC hydrogel was crosslinked with PEI for wastewater treatment. The kC-AC/PEI hydrogel composite is characterized by a high rejection of divalent ions in wastewater, achieving selectivity of 87.1% for Ca^{2+} and 82.9% for Mg^{2+}. Monovalent ions such as Na^{+} and K^{+} were rejected at rates of 46.9% and 74.4%, respectively. The optimal rejection for divalent ions occurred at pH 4 and 35 °C. As for feed pressure, the water flux increased with the feed pressure while the rejection rate decreased slightly. The hydrogel removed 94%–97 % of turbidity and TOC, as well as 47% of sodium ions and 81%–87 % of divalent ions from leachate wastewater. The hydrogel, noted for its ability to maintain structural integrity and performance, remained stable over multiple cycles, showing only slight reductions in heavy metal rejection and water flux, from 32.3 LMH to 28.2 LMH. Furthermore, the study highlighted the feasibility of reusing the hydrogel after metal desorption without significantly reducing its rejection rate for divalent ions, which remained below 5%. Approximately 70% of heavy metals were reclaimed through a reverse osmosis (RO) system.

Chapter six exhibited the Kappa-carrageenan-cellulose nanofiber composite hydrogel, covered with graphene oxide and crosslinked with glutaraldehyde, exhibited efficient and selective ion extraction from seawater, with high rejection rates of 90% for Na^{+}, 91.7% for Mg^{2+}, and K^{+} had a lower rejection rate of 84.9%. With graphene oxide incorporation, the kC hydrogel acquired improved antifouling and rejection properties, eliminating etra and divalent ions (Si^{4+} and S^{2+}) at 88.7% to 89.4% and demonstrated robustness to fouling

with a flux recovery ratio of 89.7% ± 4.5 for seawater treatment, exhibiting a water flux decline ratio (DR) of 43.1 ± 0.2%. The antifouling properties are shown by only a 10.3% ± 0.8 irreversible water flux decline after three filtration cycles while maintaining above 80% for FRR%.

Another critical point is how effectively hydrogel can trap and remove heavy metals and nutrients, whether used as a bulk gel or as part of a membrane. kC hydrogel also appears to perform well under various environmental conditions, which is a significant advantage when dealing with fluctuating water quality. However, the optimal combinations and concentrations for specific situations need to be determined. Not every formulation functions the same way, and adjusting the mix is essential.

Notably, these hydrogels derived from natural sources make them significantly more appealing in the long run. They provide a unique balance between performance and sustainability. Future work should focus more on practical testing, experimenting with them on methanol, as well as short- and long-chain PFAS compounds to assess their reusability and obtain a clearer understanding of their environmental impact through thorough lifecycle studies. A pilot plant test is recommended to demonstrate the feasibility of scaling up the technology of kC hydrogels, which would play a crucial role in future water treatment strategies.

Further studies should move beyond controlled lab conditions and begin testing kC hydrogels in more realistic settings, such as pilot-scale systems or actual field sites. Real-world testing is essential to understand how these materials perform over time and under various environmental pressures. Regeneration and long-term performance are crucial for keeping costs low and enabling reuse. To enhance treatment accuracy, future studies

should concentrate on developing hydrogels that target specific pollutants like PFAS, heavy metals, and nitrogen and phosphorus nutrients in wastewater.

A comprehensive life cycle assessment, encompassing everything from hydrogel production to disposal, will clarify the true environmental impact. Without this crucial step, sustainability initiatives remain unfinished. Investigating these areas with a practical approach facilitates the transition of this technology from bench-scale potential to real-world effectiveness.

References

Abdeen, Z., Mohammad, S., & Mahmoud, M. (2015). Adsorption of Mn (II) ion on polyvinyl alcohol/chitosan dry blending from aqueous solution. *Environmental Nanotechnology, Monitoring & Management, 3*, 1-9.

Abdullah, N., Yusof, N., Lau, W., Jaafar, J., & Ismail, A. (2019). Recent trends of heavy metal removal from water/wastewater by membrane technologies. *Journal of Industrial and Engineering Chemistry, 76*, 17-38.

Abdullah, N., Yusof, N., Lau, W. J., Jaafar, J., & Ismail, A. F. (2019). Recent trends of heavy metal removal from water/wastewater by membrane technologies. *Journal of Industrial and Engineering Chemistry, 76*, 17-38. https://doi.org/https://doi.org/10.1016/j.jiec.2019.03.029

Acarer-Arat, S., Pir, İ., Tufekci, M., Güneş-Durak, S., Akman, A., & Tüfekci, N. e. (2024). Heavy Metal Rejection Performance and Mechanical Performance of Cellulose-Nanofibril-Reinforced Cellulose Acetate Membranes. *ACS omega, 9*(41), 42159-42171.

Acikgoz, C., Gül, Ü. D., Özan, K., & Borazan, A. A. (2016). Degradation of Reactive Blue by the mixed culture of Aspergillus versicolor and Rhizopus arrhizus in membrane bioreactor (MBR) system. *Desalination and Water Treatment, 57*(8), 3750-3756.

Aguilan, J. T., Broom, J., Hemmingson, J., Dayrit, F. M., Montano, M., Dancel, M., Ninonuevo, M., & Furneaux, R. (2003). Structural analysis of carrageenan from farmed varieties of Philippine seaweed.

Ahmed, E. M. (2015). Hydrogel: Preparation, characterization, and applications: A review. *Journal of advanced research, 6*(2), 105-121.

Ahmed, M. J. K., & Ahmaruzzaman, M. (2016). Investigation on the effective remediation of quinoline at solid/solution interface using modified agricultural waste: an inclusive study. *International journal of environmental science and technology (Tehran), 13*(4), 1177-1188. https://doi.org/10.1007/s13762-016-0952-0

Ahmed, N., Ehsan, A., Danish, S., Ali, M. A., Fahad, S., Dawar, K., Taban, S., Akça, H., Shah, A. A., Ansari, M. J., Babur, E., Süha Uslu, Ö., Datta, R., & Glick, B. R. (2022). Mitigation of lead (Pb) toxicity in rice cultivated with either ground water or wastewater by application of acidified carbon. *Journal of Environmental Management, 307*, 114521. https://doi.org/https://doi.org/10.1016/j.jenvman.2022.114521

Ahmed, S., & Soundararajan, A. (2018). *Marine polysaccharides: Advances and multifaceted applications*. CRC Press.

Akpor, O., & Muchie, M. (2010). Remediation of heavy metals in drinking water and wastewater treatment systems: processes and applications. *International Journal of Physical Sciences, 5*(12), 1807-1817.

Alam, J., Alhoshan, M., Shukla, A. K., Aldalbahi, A., & Ali, F. A. A. (2019). k-Carrageenan – A versatile biopolymer for the preparation of a hydrophilic PVDF composite membrane.

European polymer journal, 120, 109219. https://doi.org/10.1016/j.eurpolymj.2019.109219

Alam, J., Alhoshan, M., Shukla, A. K., Aldalbahi, A., Ali, F. A. A., Dass, L. A., & Muthumareeswaran, M. R. (2017). κ-Carrageenan as a promising pore-former for the preparation of a highly porous polyphenylsulfone membrane. *Materials letters, 204*, 108-111. https://doi.org/10.1016/j.matlet.2017.06.017

Alam, M. N., & Christopher, L. P. (2018). Natural cellulose-chitosan cross-linked superabsorbent hydrogels with superior swelling properties. *ACS Sustainable Chemistry & Engineering, 6*(7), 8736-8742.

Alam, M. N., Islam, M. S., & Christopher, L. P. (2019). Sustainable production of cellulose-based hydrogels with superb absorbing potential in physiological saline. *ACS omega, 4*(5), 9419-9426.

Ali, A. E.-H., Shawky, H., Abd El Rehim, H., & Hegazy, E. (2003). Synthesis and characterization of PVP/AAc copolymer hydrogel and its applications in the removal of heavy metals from aqueous solution. *European polymer journal, 39*(12), 2337-2344.

Ali, K., Wahba, M., Abou-Zeid, R., & Kamel, S. (2019). Development of carrageenan modified with nanocellulose-based materials in removing of Cu 2+, Pb 2+, Ca 2+, Mg 2+, and Fe 2+. *International Journal of Environmental Science and Technology, 16*, 5569-5576.

Aljeboree, A. M., Alkaim, A. F., Alsultany, F. H., & Issa, S. K. (2024). Highly reusable nano adsorbent based on clay-incorporated hydrogel nanocomposite for cationic dye adsorption. *Journal of Inorganic and Organometallic Polymers and Materials*, 1-22.

Alsaka, L., Ibrar, I., Altaee, A., Zhou, J., Chowdhury, M. H., Al-Ejji, M., & Hawari, A. H. (2024). Performance and analysis of kappa-carrageenan hydrogel for PFOA-contaminated soil remediation wastewater treatment. *Chemosphere, 365*, 143371.

Alsaka, L., Ibrar, I., Altaee, A., Zhou, J., Chowdhury, M. H., Maryam, A.-E., & Hawari, A. H. (2024). Performance and analysis of kappa-carrageenan hydrogel for PFOA-contaminated soil remediation wastewater treatment. *Chemosphere, 365*, 143371.

Alsalhy, Q. F., Rashid, K. T., Ibrahim, S. S., Ghanim, A. H., Van der Bruggen, B., Luis, P., & Zablouk, M. (2013). Poly(vinylidene fluoride-co-hexafluoropropylene) (PVDF-co-HFP) hollow fiber membranes prepared from PVDF-co-HFP/PEG-600Mw/DMAC solution for membrane distillation. *Journal of applied polymer science, 129*(6), 3304-3313. https://doi.org/10.1002/app.39065

AlSawaftah, N., Abuwatfa, W., Darwish, N., & Husseini, G. (2021). A Comprehensive Review on Membrane Fouling: Mathematical Modelling, Prediction, Diagnosis, and Mitigation. *Water (Basel), 13*(9), 1327. https://doi.org/10.3390/w13091327

Ambashta, R. D., & Sillanpää, M. (2010). Water purification using magnetic assistance: A review. *Journal of hazardous materials, 180*(1), 38-49. https://doi.org/10.1016/j.jhazmat.2010.04.105

Andreja Žgajnar, G., & Aleksander, P. (2015). Perspectives on Biological Treatment of Sanitary Landfill Leachate. In S. Mohamed (Ed.), *Wastewater Treatment Engineering* (pp. Ch. 5). IntechOpen. https://doi.org/10.5772/60924

Anis, S. F., Hashaikeh, R., & Hilal, N. (2019). Reverse osmosis pretreatment technologies and future trends: A comprehensive review. *Desalination, 452*, 159-195. https://doi.org/10.1016/j.desal.2018.11.006

Ansar, R., Saqib, S., Mukhtar, A., Niazi, M. B. K., Shahid, M., Jahan, Z., Kakar, S. J., Uzair, B., Mubashir, M., & Ullah, S. (2022). Challenges and recent trends with the development of hydrogel fiber for biomedical applications. *Chemosphere, 287*, 131956.

Appleman, T. D., Higgins, C. P., Quiñones, O., Vanderford, B. J., Kolstad, C., Zeigler-Holady, J. C., & Dickenson, E. R. V. (2014). Treatment of poly- and perfluoroalkyl substances in U.S. full-scale water treatment systems. *Water research (Oxford), 51*, 246-255. https://doi.org/10.1016/j.watres.2013.10.067

Arnal, J. M., García-Fayos, B., Sancho, M., Verdú, G., & Lora, J. (2010). Design and installation of a decentralized drinking water system based on ultrafiltration in Mozambique. *Desalination, 250*(2), 613-617. https://doi.org/10.1016/j.desal.2009.09.035

Arshad, F., Selvaraj, M., Zain, J., Banat, F., & Haija, M. A. (2019). Polyethylenimine modified graphene oxide hydrogel composite as an efficient adsorbent for heavy metal ions. *Separation and purification technology, 209*, 870-880.

Arthanareeswaran, G., Thanikaivelan, P., & Raajenthiren, M. (2009). Preparation and characterization of poly (methyl methacrylate) and sulfonated poly (ether ether ketone) blend ultrafiltration membranes for protein separation applications. *Materials Science & Engineering C, 29*(1), 246-252. https://doi.org/10.1016/j.msec.2008.06.015

Ashfaq, M. Y., Al-Ghouti, M. A., & Zouari, N. (2020). Functionalization of reverse osmosis membrane with graphene oxide to reduce both membrane scaling and biofouling. *Carbon, 166*, 374-387. https://doi.org/https://doi.org/10.1016/j.carbon.2020.05.017

Ateia, M., Alsbaiee, A., Karanfil, T., & Dichtel, W. (2019). Efficient PFAS Removal by Amine-Functionalized Sorbents: Critical Review of the Current Literature. *Environmental Science & Technology Letters, 6*(12), 688-695. https://doi.org/10.1021/acs.estlett.9b00659

Baghbadorani, N. B., Behzad, T., Etesami, N., & Heidarian, P. (2019). Removal of Cu2+ ions by cellulose nanofibers-assisted starch-g-poly (acrylic acid) superadsorbent hydrogels. *Composites Part B: Engineering, 176*, 107084.

Bai, C., Huang, Q., Zhang, X., & Xiong, X. (2019). Mechanical Strengths of Hydrogels of Poly (N, N-Dimethylacrylamide)/Alginate with IPN and of Poly (N, N-Dimethylacrylamide)/Chitosan with Semi-IPN Microstructures. *Macromolecular Materials and Engineering, 304*(11), 1900309.

Balasubramanian, R., Kim, S. S., & Lee, J. (2018). Novel synergistic transparent k-Carrageenan/Xanthan gum/Gellan gum hydrogel film: Mechanical, thermal and water

barrier properties. *International journal of biological macromolecules, 118*(Pt A), 561-568. https://doi.org/10.1016/j.ijbiomac.2018.06.110

Barakat, M., & Sahiner, N. (2008). Cationic hydrogels for toxic arsenate removal from aqueous environment. *Journal of environmental management, 88*(4), 955-961.

Barakat, M. A. (2011). New trends in removing heavy metals from industrial wastewater. *Arabian Journal of Chemistry, 4*(4), 361-377. https://doi.org/https://doi.org/10.1016/j.arabjc.2010.07.019

Bashir, S., Hina, M., Iqbal, J., Rajpar, A., Mujtaba, M., Alghamdi, N., Wageh, S., Ramesh, K., & Ramesh, S. (2020). Fundamental concepts of hydrogels: Synthesis, properties, and their applications. *Polymers, 12*(11), 2702.

Benguella, B., & Benaissa, H. (2002). Cadmium removal from aqueous solutions by chitin: kinetic and equilibrium studies. *Water Research, 36*(10), 2463-2474.

Bhat, M. P., Lee, J.-H., Kurkuri, M., Chen, T., Kim, C. S., & Lee, K.-H. (2025). Diatom contained alginate-chitosan hydrogel beads with enhanced hydrogen bonds and ionic interactions for extended release of gibberellic acid. *International journal of biological macromolecules, 291*, 138906.

Bhushan, B., & Yong Chae, J. (2011). Natural and biomimetic artificial surfaces for superhydrophobicity, self-cleaning, low adhesion, and drag reduction. *Progress in materials science, 56*(1), 1-108. https://doi.org/10.1016/j.pmatsci.2010.04.003

Bolisetty, S., Peydayesh, M., & Mezzenga, R. (2019). Sustainable technologies for water purification from heavy metals: review and analysis. *Chemical Society reviews, 48*(2), 463-487. https://doi.org/10.1039/c8cs00493e

Borges, F. T. P., Papavasiliou, G., & Teymour, F. (2020). Characterizing the molecular architecture of hydrogels and crosslinked polymer networks beyond Flory–Rehner—I. Theory. *Biomacromolecules, 21*(12), 5104-5118.

Bowen, W. R., & Welfoot, J. S. (2002). Modelling the performance of membrane nanofiltration—critical assessment and model development. *Chemical engineering science, 57*(7), 1121-1137. https://doi.org/10.1016/S0009-2509(01)00413-4

Buck, R. C., Franklin, J., Berger, U., Conder, J. M., Cousins, I. T., De Voogt, P., Jensen, A. A., Kannan, K., Mabury, S. A., & van Leeuwen, S. P. (2011). Perfluoroalkyl and polyfluoroalkyl substances in the environment: terminology, classification, and origins. *Integrated environmental assessment and management, 7*(4), 513-541.

Bustamante-Torres, M., Romero-Fierro, D., Arcentales-Vera, B., Palomino, K., Magaña, H., & Bucio, E. (2021). Hydrogels classification according to the physical or chemical interactions and as stimuli-sensitive materials. *Gels, 7*(4), 182.

Cai, J., Guo, J., Wang, S., Rodon-Fores, J., Swift, T., Haseeb, I., Cai, J., Guo, J., & Wang, S. (2023). Application of Polymer Hydrogels in the Prevention of Postoperative Adhesion: A Review. Gels 2023, 9, 98.

Caló, E., & Khutoryanskiy, V. V. (2015). Biomedical applications of hydrogels: A review of patents and commercial products. *European polymer journal, 65*, 252-267.

Cañizares, R. O., Rivas, L., Montes, C., Domínguez, A. R., Travieso, L., & Benitez, F. (1994). Aerated swine-wastewater treatment with K-carrageenan-immobilized Spirulina maxima. *Bioresource technology, 47*(1), 89-91. https://doi.org/10.1016/0960-8524(94)90035-3

Chang, C., He, M., Zhou, J., & Zhang, L. (2011). Swelling behaviors of pH-and salt-responsive cellulose-based hydrogels. *Macromolecules, 44*(6), 1642-1648.

Chang, E. E., Liang, C.-H., Huang, C.-P., & Chiang, P.-C. (2012). A simplified method for elucidating the effect of size exclusion on nanofiltration membranes. *Separation and purification technology, 85*, 1-7. https://doi.org/10.1016/j.seppur.2011.05.002

Chelu, M., Musuc, A. M., Popa, M., & Calderon Moreno, J. M. (2023). Chitosan hydrogels for water purification applications. *Gels, 9*(8), 664.

Chen, J., Jiang, X., Yin, D., & Zhang, W. (2020). Preparation of a hydrogel-based adsorbent for metal ions through high internal phase emulsion polymerization. *ACS omega, 5*(32), 19920-19927.

Chen, J. P., & Wu, S. (2004). Acid/base-treated activated carbons: characterization of functional groups and metal adsorptive properties. *Langmuir, 20*(6), 2233-2242.

Chen, W., Zhang, X., Mamadiev, M., & Wang, Z. (2017). Sorption of perfluorooctane sulfonate and perfluorooctanoate on polyacrylonitrile fiber-derived activated carbon fibers: in comparison with activated carbon. *RSC advances, 7*(2), 927-938. https://doi.org/10.1039/C6RA25230C

Chen, Y., Chen, L., Bai, H., & Li, L. (2013). Graphene oxide–chitosan composite hydrogels as broad-spectrum adsorbents for water purification. *Journal of Materials Chemistry A, 1*(6), 1992-2001.

Chen, Y., Zhang, L., Yang, Y., Pang, B., Xu, W., Duan, G., Jiang, S., & Zhang, K. (2021). Recent progress on nanocellulose aerogels: preparation, modification, composite fabrication, applications. *Advanced materials, 33*(11), 2005569.

Cheng, S., Zhang, L., Xia, H., Peng, J., Shu, J., & Li, C. (2016). Ultrasound and microwave-assisted preparation of Fe-activated carbon as an effective low-cost adsorbent for dyes wastewater treatment. *RSC advances, 6*(82), 78936-78946.

Cova, T. F., Murtinho, D., Pais, A. A., & Valente, A. J. (2018). Cyclodextrin-based materials for removing micropollutants from wastewater. *Current Organic Chemistry, 22*(22), 2150-2181.

Dalalibera, A., Vilela, P. B., Vieira, T., Becegato, V. A., & Paulino, A. T. (2020). Removal and selective separation of synthetic dyes from water using a polyacrylic acid-based hydrogel: characterization, isotherm, kinetic, and thermodynamic data. *Journal of environmental chemical engineering, 8*(5), 104465.

Das, S., & Ronen, A. (2022). A Review on Removal and Destruction of Per- and Polyfluoroalkyl Substances (PFAS) by Novel Membranes. *Membranes (Basel), 12*(7), 662. https://doi.org/10.3390/membranes12070662

de Andrade, J. l. R., Oliveira, M. F., da Silva, M. G. C., & Vieira, M. G. A. (2018). Adsorption of Pharmaceuticals from Water and Wastewater Using Nonconventional Low-Cost Materials: A Review. *Industrial & engineering chemistry research, 57*(9), 3103-3127. https://doi.org/10.1021/acs.iecr.7b05137

Deshwal, N., Singh, M. B., Bahadur, I., Kaushik, N., Kaushik, N. K., Singh, P., & Kumari, K. (2023). A review on recent advancements on removal of harmful metal/metal ions using graphene oxide: Experimental and theoretical approaches. *Science of the total environment, 858*, 159672.

Dil, E. A., Ghaedi, M., & Asfaram, A. (2017). The performance of nanorods material as adsorbent for removal of azo dyes and heavy metal ions: Application of ultrasound wave, optimization and modeling. *Ultrasonics Sonochemistry, 34*, 792-802. https://doi.org/https://doi.org/10.1016/j.ultsonch.2016.07.015

Distantina, S., Fadilah, F., & Kaavessina, M. (2016). Swelling behaviour of kappa carrageenan hydrogel in neutral salt solution. *International Journal of Chemical and Molecular Engineering, 10*(8), 998-1001.

Distantina, S., Rochmadi, R., Fahrurrozi, M., & Wiratni, W. (2013). Preparation and characterization of glutaraldehyde-crosslinked kappa carrageenan hydrogel. *Engineering Journal, 17*(3), 57-66.

Duman, O., Özcan, C., Polat, T. G., & Tunç, S. (2019). Carbon nanotube-based magnetic and non-magnetic adsorbents for the high-efficiency removal of diquat dibromide herbicide from water: OMWCNT, OMWCNT-Fe3O4 and OMWCNT-κ-carrageenan-Fe3O4 nanocomposites. *Environmental pollution, 244*, 723-732.

Eke, J., Banks, L., Mottaleb, M. A., Morris, A. J., Tsyusko, O. V., & Escobar, I. C. (2020). Dual-Functional Phosphorene Nanocomposite Membranes for the Treatment of Perfluorinated Water: An Investigation of Perfluorooctanoic Acid Removal via Filtration Combined with Ultraviolet Irradiation or Oxygenation. *Membranes (Basel), 11*(1), 18. https://doi.org/10.3390/membranes11010018

Erathodiyil, N., Chan, H.-M., Wu, H., & Ying, J. Y. (2020). Zwitterionic polymers and hydrogels for antibiofouling applications in implantable devices. *Materials Today, 38*, 84-98.

Esmaeili, M., Lahti, J., Virtanen, T., Mänttäri, M., & Kallioinen, M. (2020). The interplay role of vanillin, water, and coagulation bath temperature on formation of antifouling polyethersulfone (PES) membranes: Application in wood extract treatment. *Separation and purification technology, 235*, 116225.

Fan, L., Peng, K., Li, M., Wang, L., & Wang, T. (2013). Preparation and properties of carboxymethyl κ-carrageenan/alginate blend fibers. *Journal of biomaterials science. Polymer ed., 24*(9), 1099-1111. https://doi.org/10.1080/09205063.2012.739538

Fang, X., Zong, B., & Mao, S. (2018). Metal–Organic Framework-Based Sensors for Environmental Contaminant Sensing. *Nano-Micro Letters, 10*(4), 64. https://doi.org/10.1007/s40820-018-0218-0

Ferfera-Harrar, H., Benhalima, T., & Sadi, A. (2022). Development of functional chitosan-based superabsorbent hydrogel nanocomposites for adsorptive removal of Basic Red 46 textile dye. *Polymer Bulletin, 79*(8), 6141-6172.

Flores, C., Ventura, F., Martin-Alonso, J., & Caixach, J. (2013). Occurrence of perfluorooctane sulfonate (PFOS) and perfluorooctanoate (PFOA) in N.E. Spanish surface waters and their removal in a drinking water treatment plant that combines conventional and advanced treatments in parallel lines. *The Science of the total environment, 461-462*, 618-626. https://doi.org/10.1016/j.scitotenv.2013.05.026

Flory, P. J., & Rehner Jr, J. (1943). Statistical mechanics of cross-linked polymer networks II. Swelling. *The journal of chemical physics, 11*(11), 521-526.

Franke, V., McCleaf, P., Lindegren, K., & Ahrens, L. (2019). Efficient removal of per-and polyfluoroalkyl substances (PFASs) in drinking water treatment: nanofiltration combined with active carbon or anion exchange. *Environmental Science: Water Research & Technology, 5*(11), 1836-1843.

Gao, H., Sun, Y., Zhou, J., Xu, R., & Duan, H. (2013). Mussel-inspired synthesis of polydopamine-functionalized graphene hydrogel as reusable adsorbents for water purification. *ACS Applied Materials & Interfaces, 5*(2), 425-432.

Gao, X., & Chorover, J. (2012). Adsorption of perfluorooctanoic acid and perfluorooctanesulfonic acid to iron oxide surfaces as studied by flow-through ATR-FTIR spectroscopy. *Environmental chemistry, 9*(2), 148. https://doi.org/10.1071/EN11119

Geng, X., Wang, J., Ding, Y., Zhang, W., Wang, Y., & Liu, F. (2021). Poly(vinyl alcohol)/polydopamine hybrid nanofiltration membrane fabricated through aqueous electrospraying with excellent antifouling and chlorine resistance. *Journal of membrane science, 632*, 119385. https://doi.org/10.1016/j.memsci.2021.119385

Ghaemi, A., Torab-Mostaedi, M., & Ghannadi-Maragheh, M. (2011). Characterizations of strontium(II) and barium(II) adsorption from aqueous solutions using dolomite powder. *Journal of hazardous materials, 190*(1), 916-921. https://doi.org/https://doi.org/10.1016/j.jhazmat.2011.04.006

Gibas, I., & Janik, H. (2010). Synthetic polymer hydrogels for biomedical applications.

Godiya, C. B., Cheng, X., Li, D., Chen, Z., & Lu, X. (2019). Carboxymethyl cellulose/polyacrylamide composite hydrogel for cascaded treatment/reuse of heavy metal ions in wastewater. *Journal of hazardous materials, 364*, 28-38.

Gomri, C., Benkhaled, B. T., Chaix, A., Dorandeu, C., Chopineau, J., Petit, E., Aissou, K., Cot, D., Cretin, M., & Semsarilar, M. (2023). A facile approach to modify cellulose nanocrystal for the adsorption of perfluorooctanoic acid. *Carbohydrate Polymers, 319*, 121189.

Grabska-Zielińska, S. (2024). Cross-linking agents in three-component materials dedicated to biomedical applications: a review. *Polymers, 16*(18), 2679.

Grassi, M., Kaykioglu, G., Belgiorno, V., & Lofrano, G. (2012). Emerging compounds removal from wastewater. *Green Chem. Sustain, 2*, 15-38.

Gu, M., Hao, L., Wang, Y., Li, X., Chen, Y., Li, W., & Jiang, L. (2020). The selective heavy metal ions adsorption of zinc oxide nanoparticles from dental wastewater. *Chemical Physics, 534*, 110750.

Guo, H., Jiao, T., Zhang, Q., Guo, W., Peng, Q., & Yan, X. (2015). Preparation of graphene oxide-based hydrogels as efficient dye adsorbents for wastewater treatment. *Nanoscale research letters, 10*, 1-10.

Hamid, A. A., Alam, J., Shukla, A. K., Ali, F. A. A., & Alhoshan, M. (2023). Sustainable removal of phenol from wastewater using a biopolymer hydrogel adsorbent comprising crosslinked chitosan and κ-carrageenan. *International journal of biological macromolecules, 251*, 126340.

Hamid, M. F., Abdullah, N., Yusof, N., Lau, W. J., Ismail, A. F., Salleh, W. N. W., Jaafar, J., & Aziz, F. (2021). Innovative polymer-complex draw solution for copper (II) removal using forward osmosis. *Journal of environmental chemical engineering, 9*(1), 104854.

Hamid, M. F., Abdullah, N., Yusof, N., Lau, W. J., Ismail, A. F., Wan Salleh, W. N., Jaafar, J., & Aziz, F. (2021). Innovative polymer-complex draw solution for copper(II) removal using forward osmosis. *Journal of environmental chemical engineering, 9*(1), 104854. https://doi.org/10.1016/j.jece.2020.104854

Hamidi, M., Azadi, A., & Rafiei, P. (2008). Hydrogel nanoparticles in drug delivery. *Advanced drug delivery reviews, 60*(15), 1638-1649.

He, C., Yang, Y., Hou, Y.-J., Luan, T., & Deng, J. (2022). Chitosan-coated fluoro-functionalized covalent organic framework as adsorbent for efficient removal of per-and polyfluoroalkyl substances from water. *Separation and purification technology, 294*, 121195.

Hezaveh, H., & Muhamad, I. I. (2012). Effect of natural cross-linker on swelling and structural stability of kappa-carrageenan/hydroxyethyl cellulose pH-sensitive hydrogels. *Korean Journal of Chemical Engineering, 29*, 1647-1655.

Hezaveh, H., & Muhamad, I. I. (2013). Modification and swelling kinetic study of kappa-carrageenan-based hydrogel for controlled release study. *Journal of the Taiwan Institute of Chemical Engineers, 44*(2), 182-191.

Hilal, N., Al-Zoubi, H., Darwish, N., Mohamma, A., & Arabi, M. A. (2004). A comprehensive review of nanofiltration membranes: Treatment, pretreatment, modelling, and atomic force microscopy. *Desalination, 170*(3), 281-308.

Ho, T.-C., Chang, C.-C., Chan, H.-P., Chung, T.-W., Shu, C.-W., Chuang, K.-P., Duh, T.-H., Yang, M.-H., & Tyan, Y.-C. (2022). Hydrogels: properties and applications in biomedicine. *Molecules, 27*(9), 2902.

Hoare, T. R., & Kohane, D. S. (2008). Hydrogels in drug delivery: Progress and challenges. *Polymer, 49*(8), 1993-2007.

Hoekstra, A. Y. (2014). Water scarcity challenges to business. *Nature climate change, 4*(5), 318-320.

Hoffman, A. S. (2012). Hydrogels for biomedical applications. *Advanced drug delivery reviews, 64*, 18-23.

Hou, C., Zhang, Q., Li, Y., & Wang, H. (2012). P25–graphene hydrogels: Room-temperature synthesis and application for removal of methylene blue from aqueous solution. *Journal of hazardous materials, 205*, 229-235.

Huang, Y., Zou, S., Li, Z., Na, B., Lin, S., & Zhang, S. (2024). Tough polyamidoxime-nanocellulose supramolecular composite hydrogels for effective uranium extraction from seawater. *Polymer, 298*, 126895.

Huber, F., Berwanger, J., Polesya, S., Mankovsky, S., Ebert, H., & Giessibl, F. J. (2019). Chemical bond formation showing a transition from physisorption to chemisorption. *Science (American Association for the Advancement of Science), 366*(6462), 235-238. https://doi.org/10.1126/science.aay3444

Hydari, S., Sharififard, H., Nabavinia, M., & reza Parvizi, M. (2012). A comparative investigation on removal performances of commercial activated carbon, chitosan biosorbent and chitosan/activated carbon composite for cadmium. *Chemical engineering journal, 193*, 276-282.

Ibrar, I., Alsaka, L., Yadav, S., Altaee, A., Zhou, J. L., & Shon, H. K. (2023). Kappa carrageenan-vanillin composite hydrogel for landfill leachate wastewater treatment. *Desalination, 565*, 116826. https://doi.org/10.1016/j.desal.2023.116826

Jiang, S., Li, Y., & Ladewig, B. P. (2017). A review of reverse osmosis membrane fouling and control strategies. *Science of the total environment, 595*, 567-583.

Jin, T., Peydayesh, M., Joerss, H., Zhou, J., Bolisetty, S., & Mezzenga, R. (2021). Amyloid fibril-based membranes for PFAS removal from water. *Environmental science water research & technology, 7*(1), 1873-1884. https://doi.org/10.1039/d1ew00373a

Jin, W., Liu, H., Li, Z., Nie, P., Zhao, G., Cheng, X., Zheng, G., & Yang, X. (2022). Effect of Hydrogel Contact Angle on Wall Thickness of Artificial Blood Vessel. *International journal of molecular sciences, 23*(19), 11114. https://doi.org/10.3390/ijms231911114

Jin, X., Xiang, Z., Liu, Q., Chen, Y., & Lu, F. (2017). Polyethyleneimine-bacterial cellulose bioadsorbent for effective removal of copper and lead ions from aqueous solution. *Bioresource technology, 244*, 844-849.

Kalaiselvi, K., Mohandoss, S., Ahmad, N., Khan, M. R., & Manoharan, R. K. (2023). Adsorption of Pb2+ Ions from Aqueous Solution onto Porous Kappa-Carrageenan/Cellulose Hydrogels: Isotherm and Kinetics Study. *Sustainability, 15*(12), 9534.

Kalcioglu, Z. I., Mahmoodian, R., Hu, Y., Suo, Z., & Van Vliet, K. J. (2012). From macro-to microscale poroelastic characterization of polymeric hydrogels via indentation. *Soft Matter, 8*(12), 3393-3398.

Kalendova, P., Svoboda, L., Hroch, J., Honcova, P., Drobna, H., & Slang, S. (2021). Hydrogels based on starch from various natural sources: Synthesis and characterization. *Starch-Stärke, 73*(9-10), 2100051.

Karakoyun, N., Kubilay, S., Aktas, N., Turhan, O., Kasimoglu, M., Yilmaz, S., & Sahiner, N. (2011). Hydrogel–Biochar composites for effective organic contaminant removal from aqueous media. *Desalination, 280*(1-3), 319-325.

Karbassiyazdi, E., Altaee, A., Ibrar, I., Razmjou, A., Alsaka, L., Ganbat, N., Malekizadeh, A., Ghobadi, R., & Khabbaz, H. (2023a). Fabrication of carbon-based hydrogel membrane for landfill leachate wastewater treatment. *Desalination, 564*, 116783.

Karbassiyazdi, E., Altaee, A., Ibrar, I., Razmjou, A., Alsaka, L., Ganbat, N., Malekizadeh, A., Ghobadi, R., & Khabbaz, H. (2023b). Fabrication of carbon-based hydrogel membrane for landfill leachate wastewater treatment. *Desalination*, 116783.

Keller, A. A., Broje, V., & Setty, K. (2007). Effect of advancing velocity and fluid viscosity on the dynamic contact angle of petroleum hydrocarbons. *Journal of Petroleum Science and Engineering, 58*(1), 201-206. https://doi.org/https://doi.org/10.1016/j.petrol.2006.12.002

Keränen, A., Leiviskä, T., Salakka, A., & Tanskanen, J. (2015). Removal of nickel and vanadium from ammoniacal industrial wastewater by ion exchange and adsorption on activated carbon. *Desalination and Water Treatment, 53*(10), 2645-2654.

Khansari, M. M., Sorokina, L. V., Mukherjee, P., Mukhtar, F., Shirdar, M. R., Shahidi, M., & Shokuhfar, T. (2017). Classification of hydrogels based on their source: A review and application in stem cell regulation. *Jom, 69*, 1340-1347.

Khotimchenko, Y. S., Khozhaenko, E. V., Khotimchenko, M. Y., Kolenchenko, E. A., & Kovalev, V. V. (2010). Carrageenans as a new source of drugs with metal binding properties. *Mar Drugs, 8*(4), 1106-1121. https://doi.org/10.3390/md8041106

Kim, C. H., Youn, H. J., & Lee, H. L. (2017). Preparation of surface-charged CNF aerogels and investigation of their ion adsorption properties. *Cellulose, 24*, 2895-2902.

Klaus, M. V. X., Gutierrez, A. M., & Hilt, J. Z. (2023). Development of Poly (acrylamide)-Based Hydrogel Composites with Powdered Activated Carbon for Controlled Sorption of PFOA and PFOS in Aqueous Systems. *Polymers, 15*(22), 4384.

Kokol, V., & Vivod, V. (2023). Cation-exchange performance of a citric-acid esterified cellulose nanofibrous membrane for highly-selective proteins' permeability and adsorption capacity. *Carbohydrate Polymers, 318*, 121134.

Kostov, K. G., Nishime, T. M. C., Castro, A. H. R., Toth, A., & Hein, L. R. O. (2014). Surface modification of polymeric materials by cold atmospheric plasma jet. *Applied surface science, 314*, 367-375. https://doi.org/10.1016/j.apsusc.2014.07.009

Kuddushi, M., Rajput, S., Shah, A., Mata, J., Aswal, V. K., El Seoud, O., Kumar, A., & Malek, N. I. (2019). Stimuli responsive, self-sustainable, and self-healable functionalized hydrogel with dual gelation, load-bearing, and dye-absorbing properties. *ACS Applied Materials & Interfaces, 11*(21), 19572-19583.

Kulal, P., & Badalamoole, V. (2020a). Hybrid nanocomposite of kappa-carrageenan and magnetite as adsorbent material for water purification. *International journal of biological macromolecules, 165*(Pt A), 542-553. https://doi.org/10.1016/j.ijbiomac.2020.09.202

Kulal, P., & Badalamoole, V. (2020b). Hybrid nanocomposite of kappa-carrageenan and magnetite as adsorbent material for water purification. *International journal of biological macromolecules, 165*, 542-553.

Kumar, N., Gusain, R., Pandey, S., & Ray, S. S. (2023). Hydrogel nanocomposite adsorbents and photocatalysts for sustainable water purification. *Advanced Materials Interfaces, 10*(2), 2201375.

Kumarasamy, E., Manning, I. M., Collins, L. B., Coronell, O., & Leibfarth, F. A. (2020). Ionic Fluorogels for Remediation of Per- and Polyfluorinated Alkyl Substances from Water. *ACS central science, 6*(4), 487-492. https://doi.org/10.1021/acscentsci.9b01224

Kwak, H. W., Shin, M., Yun, H., & Lee, K. H. (2016). Preparation of silk sericin/lignin blend beads for the removal of hexavalent chromium ions. *International journal of molecular sciences, 17*(9), 1466.

Kwon, H. W., Gonzales, R. R., Zhang, P., Li, B., Im, K. S., Park, J. H., Lee, T. K., Matsuyama, H., & Nam, S. Y. (2025). Effective oil-in-water emulsion separation by self-cleaning superoleophobic hydrogel membrane composite with hierarchical structure. *npj Clean Water, 8*(1), 1-9.

Lee, A., Elam, J. W., & Darling, S. B. (2016). Membrane materials for water purification: design, development, and application. *Environmental science water research & technology, 2*(1), 17-42. https://doi.org/10.1039/c5ew00159e

Lei, X. (2023). *Perfluorooctanoic Acid (PFOA) Adsorption by Ordered Mesoporous Carbon (OMC) and Polyethyleneimine Modified Graphene Oxide (GO-PEI): Effects of Water Matrices and Understanding Mechanisms*. University of Louisiana at Lafayette.

Li, D., Lee, C.-S., Zhang, Y., Das, R., Akter, F., Venkatesan, A. K., & Hsiao, B. S. (2023). Efficient removal of short-chain and long-chain PFAS by cationic nanocellulose. *Journal of Materials Chemistry A, 11*(18), 9868-9883.

Li, D., Londhe, K., Chi, K., Lee, C. S., Venkatesan, A. K., & Hsiao, B. S. (2021). Functionalized bio-adsorbents for removal of perfluoroalkyl substances: A perspective. *AWWA Water Science, 3*(6), e1258.

Li, Z., Ma, Z., van der Kuijp, T. J., Yuan, Z., & Huang, L. (2014). A review of soil heavy metal pollution from mines in China: Pollution and health risk assessment. *Science of The Total Environment, 468-469*, 843-853. https://doi.org/https://doi.org/10.1016/j.scitotenv.2013.08.090

Li, Z., Qiu, J., Xu, X., Wan, R., Yao, M., Wang, H., Zhou, Z., & Xu, J. (2025). Solar driven kaolin-based hydrogels for efficient interfacial evaporation and heavy metal ion adsorption from wastewater. *Separation and purification technology, 354*, 129243.

Liang, H. W., Cao, X., Zhang, W. J., Lin, H. T., Zhou, F., Chen, L. F., & Yu, S. H. (2011). Robust and highly efficient free-standing carbonaceous nanofiber membranes for water purification. *Advanced Functional Materials, 21*(20), 3851-3858.

Liu, C., Omer, A., & Ouyang, X.-k. (2018). Adsorptive removal of cationic methylene blue dye using carboxymethyl cellulose/k-carrageenan/activated montmorillonite composite beads: Isotherm and kinetic studies. *International journal of biological macromolecules, 106*, 823-833.

Liu, S.-L., Wang, Y.-N., & Lu, K.-T. (2014). Preparation and pore characterization of activated carbon from Ma bamboo (Dendrocalamus latiflorus) by H 3 PO 4 chemical activation. *Journal of Porous Materials, 21*, 459-466.

Liu, S., & Li, L. (2016). Recoverable and Self-Healing Double Network Hydrogel Based on κ-Carrageenan. *ACS Applied Materials & Interfaces, 8*(43), 29749-29758. https://doi.org/10.1021/acsami.6b11363

Liu, Y., Lin, B., Liu, W., Li, J., Gao, C., & Pan, Q. (2018). Preparation and characterization of a novel nanofiltration membrane with chlorine-tolerant property and good separation performance. *RSC advances, 8*(64), 3643-3644. https://doi.org/10.1039/c8ra06755d

Liu, Y., Wang, J., Chen, H., & Cheng, D. (2022). Environmentally friendly hydrogel: A review of classification, preparation and application in agriculture. *Science of the total environment, 846*, 157303.

Liu, Z., Wang, H., Liu, C., Jiang, Y., Yu, G., Mu, X., & Wang, X. (2012). Magnetic cellulose–chitosan hydrogels prepared from ionic liquids as reusable adsorbent for removal of heavy metal ions. *Chemical Communications, 48*(59), 7350-7352.

Long, L., Hu, X., Yan, J., Zeng, Y., Zhang, J., & Xue, Y. (2019). Novel chitosan–ethylene glycol hydrogel for the removal of aqueous perfluorooctanoic acid. *Journal of Environmental Sciences, 84*, 21-28.

Lu, L., Yuan, S., Wang, J., Shen, Y., Deng, S., Xie, L., & Yang, Q. (2018). The formation mechanism of hydrogels. *Current stem cell research & therapy, 13*(7), 490-496.

Lu, Y., Wang, Z., Ouyang, X.-k., Ji, C., Liu, Y., Huang, F., & Yang, L.-Y. (2020). Fabrication of cross-linked chitosan beads grafted by polyethylenimine for efficient adsorption of diclofenac sodium from water. *International journal of biological macromolecules, 145*, 1180-1188.

Macedonio, F., Drioli, E., Gusev, A. A., Bardow, A., Semiat, R., & Kurihara, M. (2012). Efficient technologies for worldwide clean water supply. *Chemical engineering and processing, 51*, 2-17. https://doi.org/10.1016/j.cep.2011.09.011

Mahajan, P., & Kaushal, J. (2018). Role of Phytoremediation in Reducing Cadmium Toxicity in Soil and Water. *Journal of Toxicology, 2018*, 4864365. https://doi.org/10.1155/2018/4864365

Mahdavinia, G. R., Bazmizeynabad, F., & Seyyedi, B. (2015). kappa-Carrageenan beads as new adsorbent to remove crystal violet dye from water: adsorption kinetics and isotherm. *Desalination and Water Treatment, 53*(9), 2529-2539.

Mahdavinia, G. R., Massoudi, A., Baghban, A., & Shokri, E. (2014). Study of adsorption of cationic dye on magnetic kappa-carrageenan/PVA nanocomposite hydrogels. *Journal of environmental chemical engineering, 2*(3), 1578-1587. https://doi.org/10.1016/j.jece.2014.05.020

Mahfoudhi, N., & Boufi, S. (2017). Nanocellulose as a novel nanostructured adsorbent for environmental remediation: a review. *Cellulose, 24*, 1171-1197.

Maitra, J., & Shukla, V. K. (2014). Cross-linking in hydrogels-a review. *Am. J. Polym. Sci, 4*(2), 25-31.

Makhado, E., Pandey, S., Modibane, K. D., Kang, M., & Hato, M. J. (2020). Sequestration of methylene blue dye using sodium alginate poly (acrylic acid)@ ZnO hydrogel nanocomposite: kinetic, isotherm, and thermodynamic investigations. *International journal of biological macromolecules, 162*, 60-73.

Mehta, P., Sharma, M., & Devi, M. (2023). Hydrogels: An overview of its classifications, properties, and applications. *Journal of the Mechanical Behavior of Biomedical Materials*, 106145.

Miao, C., Huang, W., Li, K., & Yang, Y. (2024). Highly efficient removal of adsorbed cationic dyes by dual-network chitosan-based hydrogel. *Environmental Research, 263*, 120195.

Milley, S. A., Koch, I., Fortin, P., Archer, J., Reynolds, D., & Weber, K. P. (2018). Estimating the number of airports potentially contaminated with perfluoroalkyl and polyfluoroalkyl substances from aqueous film forming foam: A Canadian example. *Journal of environmental management, 222*, 122-131.

Miron, S. M., Dutournié, P., & Ponche, A. (2019). Filtration of Uncharged Solutes: An Assessment of Steric Effect by Transport and Adsorption Modelling. *Water (Basel), 11*(10), 2173. https://doi.org/10.3390/w11102173

Mishra, N., Reddy, R., Kuila, A., Rani, A., Nawaz, A., & Pichiah, S. (2017). A Review on Advanced Oxidation Processes for Effective Water Treatment. *Current world environment, 12*(3), 469-489. https://doi.org/10.12944/CWE.12.3.02

Mohammadzadeh Pakdel, P., & Peighambardoust, S. J. (2018). Review on recent progress in chitosan-based hydrogels for wastewater treatment application. *Carbohydrate Polymers, 201*, 264-279. https://doi.org/https://doi.org/10.1016/j.carbpol.2018.08.070

Mohammed, N., Grishkewich, N., & Tam, K. C. (2018). Cellulose nanomaterials: promising sustainable nanomaterials for application in water/wastewater treatment processes. *Environmental Science: Nano, 5*(3), 623-658.

Mohammed, S., Hegab, H. M., & Ou, R. (2022). Nanofiltration performance of glutaraldehyde crosslinked graphene oxide-cellulose nanofiber membrane. *Chemical Engineering Research and Design, 183*, 1-12.

Mokhtari, H., Kharaziha, M., Karimzadeh, F., & Tavakoli, S. (2019). An injectable mechanically robust hydrogel of Kappa-carrageenan-dopamine functionalized graphene oxide for promoting cell growth. *Carbohydrate Polymers, 214*, 234-249.

Mulder, M. (2012). *Basic principles of membrane technology*. Springer science & business media.

Mulyanti, R., & Susanto, H. (2018). Wastewater treatment by nanofiltration membranes. *IOP conference series. Earth and environmental science, 142*(1). https://doi.org/10.1088/1755-1315/142/1/012017

Naim Shaikh, M. A., & Nawaz, T. (2024). Highly Efficient Cationic Surfactant Functionalized Alginate Hydrogel for Perfluorooctanoic Acid Adsorption: Optimization through Response Surface Methodology and Performance Evaluation for Aqueous Media. *ACS ES&T Water*.

Nam, S. Y., Nho, Y. C., Hong, S. H., Chae, G. T., Jang, H. S., Suh, T. S., Ahn, W. S., Ryu, K. E., & Chun, H. J. (2004). Evaluations of poly (vinyl alcohol)/alginate hydrogels cross-linked by γ-ray irradiation technique. *Macromolecular Research, 12*, 219-224.

Nesic, A. R., Velickovic, S. J., & Antonovic, D. G. (2012). Characterization of chitosan/montmorillonite membranes as adsorbents for Bezactiv Orange V-3R dye. *Journal of hazardous materials, 209-210*, 256-263. https://doi.org/https://doi.org/10.1016/j.jhazmat.2012.01.020

Nie, S., Fu, Q., Lin, X., Zhang, C., Lu, Y., & Wang, S. (2021). Enhanced performance of a cellulose nanofibrils-based triboelectric nanogenerator by tuning the surface polarizability and hydrophobicity. *Chemical Engineering Journal, 404*, 126512.

Ouyang, Z., Huang, Z., Tang, X., Xiong, C., Tang, M., & Lu, Y. (2019). A dually charged nanofiltration membrane by pH-responsive polydopamine for pharmaceuticals and personal care products removal. *Separation and purification technology, 211*, 90-97. https://doi.org/10.1016/j.seppur.2018.09.059

Oves, M., Khan, M. S., Zaidi, A., & Ahmad, E. (2012). Soil contamination, nutritive value, and human health risk assessment of heavy metals: an overview. *Toxicity of heavy metals to legumes and bioremediation*, 1-27.

Ozay, O., Ekici, S., Baran, Y., Kubilay, S., Aktas, N., & Sahiner, N. (2010). Utilization of magnetic hydrogels in the separation of toxic metal ions from aqueous environments. *Desalination, 260*(1-3), 57-64.

Pacheco, D., Cotas, J., Rocha, C. P., Araújo, G. S., Figueirinha, A., Gonçalves, A. M. M., Bahcevandziev, K., & Pereira, L. (2021). Seaweeds' carbohydrate polymers as plant growth promoters. *Carbohydrate Polymer Technologies and Applications, 2*, 100097. https://doi.org/https://doi.org/10.1016/j.carpta.2021.100097

Parsons, S. (2004). *Advanced oxidation processes for water and wastewater treatment*. IWA publishing.

Pasqui, D., De Cagna, M., & Barbucci, R. (2012). Polysaccharide-based hydrogels: the key role of water in affecting mechanical properties. *Polymers, 4*(3), 1517-1534.

Patel, P., Gangwar, P., & Thareja, P. (2023). Preparation and rheology of titanium dioxide nanoparticles loaded κ-carrageenan hydrogel beads strengthened by mixed salts for multipollutant water remediation. *Journal of Vinyl and Additive Technology, 29*(4), 773-794.

Patra, S. K., Poddar, R., Brestic, M., Acharjee, P. U., Bhattacharya, P., Sengupta, S., Pal, P., Bam, N., Biswas, B., & Barek, V. (2022). Prospects of hydrogels in agriculture for enhancing crop and water productivity under water deficit condition. *International Journal of Polymer Science, 2022*(1), 4914836.

Pattarith, K., Nugroho, D., Nanan, S., & Benchawattananon, R. (2023). Cellulose Modified with Polyethylenimine (PEI) Using Microwave Methodology for Adsorption of Chromium from Aqueous Solutions. *Molecules, 28*(11), 4514.

Paulino, A. T., Belfiore, L. A., Kubota, L. T., Muniz, E. C., & Tambourgi, E. B. (2011). Efficiency of hydrogels based on natural polysaccharides in the removal of Cd2+ ions from aqueous solutions. *Chemical engineering journal, 168*(1), 68-76.

Pendergast, M. M., & Hoek, E. M. (2011). A review of water treatment membrane nanotechnologies. *Energy & environmental science, 4*(6), 1946-1971.

Pensini, E., Dinardo, A., Lamont, K., Longstaffe, J., Elsayed, A., & Singh, A. (2019). Effect of salts and pH on the removal of perfluorooctanoic acid (PFOA) from aqueous solutions through precipitation and electroflocculation. *Canadian journal of civil engineering, 46*(10), 881-886. https://doi.org/10.1139/cjce-2018-0705

Perumal, S., Atchudan, R., Edison, T. N. J. I., Babu, R. S., Karpagavinayagam, P., & Vedhi, C. (2021). A short review on recent advances of hydrogel-based adsorbents for heavy metal ions. *Metals, 11*(6), 864.

Pooresmaeil, M., & Namazi, H. (2020). Application of polysaccharide-based hydrogels for water treatments. In *Hydrogels based on natural polymers* (pp. 411-455). Elsevier.

Pradhan, D., Sukla, L. B., Sawyer, M., & Rahman, P. K. S. M. (2017). Recent bioreduction of hexavalent chromium in wastewater treatment: A review. *Journal of Industrial and Engineering Chemistry, 55*, 1-20. https://doi.org/https://doi.org/10.1016/j.jiec.2017.06.040

Prajapati, M., Shah, M., & Soni, B. (2021). A review of geothermal integrated desalination: A sustainable solution to overcome potential freshwater shortages. *Journal of cleaner production, 326*, 129412.

Qasim, M., Badrelzaman, M., Darwish, N. N., Darwish, N. A., & Hilal, N. (2019). Reverse osmosis desalination: A state-of-the-art review. *Desalination, 459*, 59-104. https://doi.org/10.1016/j.desal.2019.02.008

Qin, F., Yao, W., Liu, Y., Zhu, B., Yang, Q., & Zheng, Y. (2023). Polyethyleneimine functionalized cellulose-rich agroforestry residues for removing perfluorooctanoic acid: adsorption performance and mechanism. *Cellulose, 30*(6), 3653-3666.

Qin, Y., Long, M., Tan, B., & Zhou, B. (2014). RhB Adsorption Performance of Magnetic Adsorbent Fe3O4/RGO Composite and Its Regeneration through A Fenton-like Reaction. *Nano-Micro Letters, 6*(2), 125-135. https://doi.org/10.1007/BF03353776

Qiu, X., Kong, H., Li, Y., Wang, Q., & Wang, Y. (2022). Interface engineering of a Ti4O7 nanofibrous membrane for efficient solar-driven evaporation. *ACS Applied Materials & Interfaces, 14*(49), 54855-54866.

R, S. K., G, A., Y, L. T., & A.F, I. (2017). Enhancement of permeability and antibiofouling properties of polyethersulfone (PES) membrane through incorporation of quorum sensing inhibition (QSI) compound. *Journal of the Taiwan Institute of Chemical Engineers, 72*, 200-212. https://doi.org/10.1016/j.jtice.2017.01.012

Rabajczyk, A., Gniazdowska, J., Stojek, P., Czyżewska, K., Trusek, A., & Labus, K. (2024). Hydrogels and Their Functionalization—Analysis of the Possibility of Their Application in Post-Fire Water Treatment Processes. *Materials, 17*(23), 5820.

Rahmani, Z., Ghaemy, M., & Olad, A. (2022). Removal of heavy metals from polluted water using magnetic adsorbent based on κ-carrageenan and N-doped carbon dots. *Hydrometallurgy, 213*, 105915.

Ray, S. S., & Iroegbu, A. O. C. (2021). Nanocellulosics: Benign, Sustainable, and Ubiquitous Biomaterials for Water Remediation. *ACS omega, 6*(7), 4511-4526. https://doi.org/10.1021/acsomega.0c06070

Reshmy, R., Philip, E., Madhavan, A., Pugazhendhi, A., Sindhu, R., Sirohi, R., Awasthi, M. K., Pandey, A., & Binod, P. (2022). Nanocellulose as green material for remediation of hazardous heavy metal contaminants. *Journal of Hazardous Materials, 424*, 127516. https://doi.org/https://doi.org/10.1016/j.jhazmat.2021.127516

Ritt, C. L., Werber, J. R., Wang, M., Yang, Z., Zhao, Y., Kulik, H. J., & Elimelech, M. (2020). Ionization behavior of nanoporous polyamide membranes. *Proceedings of the National Academy of Sciences - PNAS, 117*(48), 30191-30200. https://doi.org/10.1073/pnas.2008421117

Rocha de Souza, M. C., Marques, C. T., Guerra Dore, C. M., Ferreira da Silva, F. R., Oliveira Rocha, H. A., & Leite, E. L. (2007). Antioxidant activities of sulfated polysaccharides from brown and red seaweeds. *Journal of applied phycology, 19*, 153-160.

Rocha, L. S., Nogueira, J., Daniel-da-Silva, A. L., Marques, P., Fateixa, S., Pereira, E., & Trindade, T. (2021). Water softening using graphene oxide/biopolymer hybrid nanomaterials. *Journal of environmental chemical engineering, 9*(1), 105045.

Rodrigues, F. H., Fajardo, A. R., Pereira, A. G., Ricardo, N. M., Feitosa, J. P., & Muniz, E. C. (2012). Chitosan-graft-poly (acrylic acid)/rice husk ash based superabsorbent hydrogel composite: preparation and characterization. *Journal of Polymer Research, 19*, 1-10.

Roy, Y., Warsinger, D. M., & Lienhard, J. H. (2017). Effect of temperature on ion transport in nanofiltration membranes: Diffusion, convection and electromigration. *Desalination, 420*, 241-257. https://doi.org/10.1016/j.desal.2017.07.020

Saito, T., Nishiyama, Y., Putaux, J.-L., Vignon, M., & Isogai, A. (2006). Homogeneous suspensions of individualized microfibrils from TEMPO-catalyzed oxidation of native cellulose. *Biomacromolecules, 7*(6), 1687-1691.

Salgueiro, A. M., Daniel-da-Silva, A. L., Girão, A. V., Pinheiro, P. C., & Trindade, T. (2013). Unusual dye adsorption behavior of κ-carrageenan coated superparamagnetic nanoparticles. *Chemical engineering journal, 229*, 276-284.

Sanyang, M., Ghani, W. A. W. A. K., Idris, A., & Ahmad, M. B. (2016). Hydrogel biochar composite for arsenic removal from wastewater. *Desalination and Water Treatment, 57*(8), 3674-3688.

Sargeant, T. D., Desai, A. P., Banerjee, S., Agawu, A., & Stopek, J. B. (2012). An in situ forming collagen–PEG hydrogel for tissue regeneration. *Acta biomaterialia, 8*(1), 124-132.

Şengil, İ. A., & Özacar, M. (2009). Competitive biosorption of Pb2+, Cu2+ and Zn2+ ions from aqueous solutions onto valonia tannin resin. *Journal of hazardous materials, 166*(2-3), 1488-1494.

Service, R. F. (2006). Desalination freshens up. American Association for the Advancement of Science.

Shaghaleh, H., Hamoud, Y. A., Xu, X., Wang, S., & Liu, H. (2022). A pH-responsive/sustained release nitrogen fertilizer hydrogel based on aminated cellulose nanofiber/cationic copolymer for application in irrigated neutral soils. *Journal of cleaner production, 368*, 133098.

Shon, H. K., Phuntsho, S., Chaudhary, D. S., Vigneswaran, S., & Cho, J. (2013). Nanofiltration for water and wastewater treatment – a mini review. *Drinking water engineering and science, 6*(1), 47-53. https://doi.org/10.5194/dwes-6-47-2013

Singh, N., Nagpal, G., & Agrawal, S. (2018). Water purification by using adsorbents: a review. *Environmental technology & innovation, 11*, 187-240.

Singhal, R., & Gupta, K. (2016). A review: tailor-made hydrogel structures (classifications and synthesis parameters). *Polymer-Plastics Technology and Engineering, 55*(1), 54-70.

Soares, S. F., Simoes, T. R., Trindade, T., & Daniel-da-Silva, A. L. (2017). Highly efficient removal of dye from water using magnetic carrageenan/silica hybrid nano-adsorbents. *Water, Air, & Soil Pollution, 228*, 1-11.

Štefelová, J., Slovák, V., Siqueira, G., Olsson, R. T., Tingaut, P., Zimmermann, T., & Sehaqui, H. (2017). Drying and pyrolysis of cellulose nanofibers from wood, bacteria, and algae for char application in oil absorption and dye adsorption. *ACS Sustainable Chemistry & Engineering, 5*(3), 2679-2692.

Sun, X., Peng, B., Ji, Y., Chen, J., & Li, D. (2009). Chitosan (chitin)/cellulose composite biosorbents prepared using ionic liquid for heavy metal ions adsorption. *AIChE Journal, 55*(8), 2062-2069.

Sun, Y., Yu, F., Li, C., Dai, X., & Ma, J. (2019). Nano-/Micro-confined Water in Graphene Hydrogel as Superadsorbents for Water Purification. *Nano-Micro Letters, 12*(1), 2. https://doi.org/10.1007/s40820-019-0336-3

Sun YaJie, S. Y., Ma YanLi, M. Y., Fang GuiZhen, F. G., Li ShuJun, L. S., & Fu YuJie, F. Y. (2016). Synthesis of acid hydrolysis lignin-g-poly-(acrylic acid) hydrogel superabsorbent composites and adsorption of lead ions.

Tang, C. Y., Fu, Q. S., Robertson, A. P., Criddle, C. S., & Leckie, J. O. (2006). Use of Reverse Osmosis Membranes to Remove Perfluorooctane Sulfonate (PFOS) from Semiconductor Wastewater. *Environmental science & technology, 40*(23), 7343-7349. https://doi.org/10.1021/es060831q

Tang, S. C., Yin, K., & Lo, I. M. (2011). Column study of Cr (VI) removal by cationic hydrogel for in-situ remediation of contaminated groundwater and soil. *Journal of contaminant hydrology, 125*(1-4), 39-46.

Tansel, B., Sager, J., Rector, T., Garland, J., Strayer, R. F., Levine, L., Roberts, M., Hummerick, M., & Bauer, J. (2006). Significance of hydrated radius and hydration shells on ionic permeability during nanofiltration in dead end and cross flow modes. *Separation and purification technology, 51*(1), 40-47.

Thakur, S., Govender, P. P., Mamo, M. A., Tamulevicius, S., Mishra, Y. K., & Thakur, V. K. (2017). Progress in lignin hydrogels and nanocomposites for water purification: Future perspectives. *Vacuum, 146*, 342-355.

Tian, C., She, J., Wu, Y., Luo, S., Wu, Q., & Qing, Y. (2018). Reusable and cross-linked cellulose nanofibrils aerogel for the removal of heavy metal ions. *Polymer Composites, 39*(12), 4442-4451.

Tranquilan-Aranilla, C., Nagasawa, N., Bayquen, A., & Dela Rosa, A. (2012). Synthesis and characterization of carboxymethyl derivatives of kappa-carrageenan. *Carbohydrate Polymers, 87*(2), 1810-1816. https://doi.org/https://doi.org/10.1016/j.carbpol.2011.10.009

Tshikovhi, A., Mishra, S. B., & Mishra, A. K. (2020). Nanocellulose-based composites for the removal of contaminants from wastewater. *International journal of biological macromolecules, 152*, 616-632.

Ullah, F., Othman, M. B. H., Javed, F., Ahmad, Z., & Akil, H. M. (2015). Classification, processing and application of hydrogels: A review. *Materials Science and Engineering: C, 57*, 414-433.

Umoren, S. A., & Eduok, U. M. (2016). Application of carbohydrate polymers as corrosion inhibitors for metal substrates in different media: A review. *Carbohydrate Polymers, 140*, 314-341. https://doi.org/https://doi.org/10.1016/j.carbpol.2015.12.038

Vaid, V., & Jindal, R. (2022). An efficient pH-responsive kappa-carrageenan/tamarind kernel powder hydrogel for the removal of brilliant green and rose bengal from aqueous solution. *Journal of applied polymer science, 139*(21), 52218.

Van der Bruggen, B., & Vandecasteele, C. (2002). Modelling of the retention of uncharged molecules with nanofiltration. *Water Research, 36*(5), 1360-1368.

Verliefde, A., Cornelissen, E., Amy, G., Van der Bruggen, B., & van Dijk, H. (2007). Priority organic micropollutants in water sources in Flanders and the Netherlands and assessment of removal possibilities with nanofiltration. *Environmental pollution (1987), 146*(1), 281-289. https://doi.org/10.1016/j.envpol.2006.01.051

Wakeel, M., Chen, B., Hayat, T., Alsaedi, A., & Ahmad, B. (2016). Energy consumption for water use cycles in different countries: A review. *Applied Energy, 178*, 868-885. https://doi.org/https://doi.org/10.1016/j.apenergy.2016.06.114

Wang, J., & Li, Z. (2015). Enhanced selective removal of Cu (II) from aqueous solution by novel polyethylenimine-functionalized ion imprinted hydrogel: Behaviors and mechanisms. *Journal of hazardous materials, 300*, 18-28.

Wang, S., Ma, X., & Zheng, P. (2019). Sulfo-functional 3D porous cellulose/graphene oxide composites for highly efficient removal of methylene blue and tetracycline from water. *International journal of biological macromolecules, 140*, 119-128.

Wang, Y.-N., Li, W., Wang, R., & Tang, C. Y. (2017). Enhancing boron rejection in FO using alkaline draw solutions. *Water Research, 118*, 20-25. https://doi.org/https://doi.org/10.1016/j.watres.2017.04.016

Wang, Z., Li, Y., Liu, F., Shao, H., Yang, Y. n., Wang, L., Jin, Z., Li, D., He, X., & Chen, N. (2025). Embedded solar-powered hydrogel evaporator for enhancing uranium extraction from seawater. *Chemical engineering journal, 505*, 159063.

Wang, Z., Zhang, G., & Li, Y. (2020). Preparation of chitosan/polyacrylamide/graphene oxide composite membranes and study of their methylene blue adsorption properties. *Materials, 13*(19), 4407.

Weerasundara, L., Gabriele, B., Figoli, A., Ok, Y.-S., & Bundschuh, J. (2021). Hydrogels: Novel materials for contaminant removal in water—A review. *Critical reviews in environmental science and technology, 51*(17), 1970-2014.

Xiang, X., Chen, G., Chen, K., Jiang, X., & Hou, L. (2020). Facile preparation and characterization of super tough chitosan/poly (vinyl alcohol) hydrogel with low temperature resistance and anti-swelling property. *International journal of biological macromolecules, 142*, 574-582.

Xu, J., Liu, J., Ling, P., Zhang, X., Xu, K., He, L., Wang, Y., Su, S., Hu, S., & Xiang, J. (2020). Raman spectroscopy of biochar from the pyrolysis of three typical Chinese biomasses: A novel method for rapidly evaluating the biochar property. *Energy, 202*, 117644.

Xu, J., Zhang, M., Du, W., Zhao, J., Ling, G., & Zhang, P. (2022). Chitosan-based high-strength supramolecular hydrogels for 3D bioprinting. *International journal of biological macromolecules, 219*, 545-557.

Xu, S., Li, H., Ding, H., Fan, Z., Pi, P., Cheng, J., & Wen, X. (2019). Allylated chitosan-poly (N-isopropylacrylamide) hydrogel based on a functionalized double network for controlled drug release. *Carbohydrate Polymers, 214*, 8-14.

Xu, X., Liu, Q., Qiu, J., Zhao, Q., Yuan, S., Li, H., Li, Z., Fu, A., Xu, J., & Lu, B. (2025). Photothermal-photocatalytic bifunctional highly porous hydrogel for efficient coherent sewage purification-clean water generation. *Desalination, 597*, 118364.

Xu, X., Zhao, Q., Liu, Q., Qiu, J., Li, J., Zheng, W., Cao, J., Wang, L., Wang, W., & Yuan, S. (2024). Full-spectrum-responsive Ti4O7-PVA nanocomposite hydrogel with ultrahigh evaporation rate for efficient solar steam generation. *Desalination, 577*, 117400.

Yadav, M., & Chiu, F.-C. (2019). Cellulose nanocrystals reinforced κ-carrageenan based UV resistant transparent bionanocomposite films for sustainable packaging applications. *Carbohydrate Polymers, 211*, 181-194. https://doi.org/https://doi.org/10.1016/j.carbpol.2019.01.114

Yadav, S., Ibrar, I., Altaee, A., Samal, A. K., & Zhou, J. (2022a). Surface modification of nanofiltration membrane with kappa-carrageenan/graphene oxide for leachate wastewater treatment. *Journal of Membrane Science*, 120776.

Yadav, S., Ibrar, I., Altaee, A., Samal, A. K., & Zhou, J. (2022b). Surface modification of nanofiltration membrane with kappa-carrageenan/graphene oxide for leachate wastewater treatment. *Journal of membrane science, 659*, 120776.

Yadav, S., Ibrar, I., Samal, A. K., Altaee, A., Déon, S., Zhou, J., & Ghaffour, N. (2022a). Preparation of fouling resistant and highly perm-selective novel PSf/GO-vanillin nanofiltration membrane for efficient water purification. *Journal of hazardous materials, 421*, 126744-126744. https://doi.org/10.1016/j.jhazmat.2021.126744

Yadav, S., Ibrar, I., Samal, A. K., Altaee, A., Déon, S., Zhou, J., & Ghaffour, N. (2022b). Preparation of fouling resistant and highly perm-selective novel PSf/GO-vanillin nanofiltration membrane for efficient water purification. *Journal of Hazardous Materials, 421*, 126744. https://doi.org/https://doi.org/10.1016/j.jhazmat.2021.126744

Yan, E., Cao, M., Ren, X., Jiang, J., An, Q., Zhang, Z., Gao, J., Yang, X., & Zhang, D. (2018). Synthesis of Fe3O4 nanoparticles functionalized polyvinyl alcohol/chitosan magnetic composite hydrogel as an efficient adsorbent for chromium (VI) removal. *Journal of Physics and Chemistry of Solids, 121*, 102-109.

Yang, B., Yang, X., Liu, B., Chen, Z., Chen, C., Liang, S., Chu, L.-Y., & Crittenden, J. (2017). PVDF blended PVDF-g-PMAA pH-responsive membrane: Effect of additives and solvents on membrane properties and performance. *Journal of membrane science, 541*, 558-566. https://doi.org/10.1016/j.memsci.2017.07.045

Yang, C. H., Wang, M. X., Haider, H., Yang, J. H., Sun, J.-Y., Chen, Y. M., Zhou, J., & Suo, Z. (2013). Strengthening alginate/polyacrylamide hydrogels using various multivalent cations. *ACS Applied Materials & Interfaces, 5*(21), 10418-10422.

Yang, D., Li, L., Chen, B., Shi, S., Nie, J., & Ma, G. (2019). Functionalized chitosan electrospun nanofiber membranes for heavy-metal removal. *Polymer, 163*, 74-85.

Yang, J., Chen, Y., Zhao, L., Zhang, J., & Luo, H. (2023). Constructions and properties of physically cross-linked hydrogels based on natural polymers. *Polymer Reviews, 63*(3), 574-612.

Yang, P., Yu, F., Yang, Z., Zhang, X., & Ma, J. (2022). Graphene oxide modified κ-carrageenan/sodium alginate double-network hydrogel for effective adsorption of antibiotics in a batch and fixed-bed column system. *Science of the total environment, 837*, 155662.

Yaroshchuk, A. E. (1998). Rejection mechanisms of NF membranes. *Membrane Technology, 1998*(100), 9-12.

Yoon, Y., & Lueptow, R. M. (2005). Removal of organic contaminants by RO and NF membranes. *Journal of membrane science, 261*(1-2), 76-86.

Yu, F., Cui, T., Yang, C., Dai, X., & Ma, J. (2019). κ-Carrageenan/Sodium alginate double-network hydrogel with enhanced mechanical properties, anti-swelling, and adsorption capacity. *Chemosphere, 237*, 124417.

Yu, Q., Deng, S., & Yu, G. (2008). Selective removal of perfluorooctane sulfonate from aqueous solution using chitosan-based molecularly imprinted polymer adsorbents. *Water research (Oxford), 42*(12), 3089-3097. https://doi.org/10.1016/j.watres.2008.02.024

Yue, N. L., Jennings, M. C., & Puddephatt, R. J. (2016). Dimerization of an organoplatinum complex triggered by oxidative addition: A model for dynamic ring-opening polymerization. *Journal of Organometallic Chemistry, 803*, 45-50.

Zeng, C., Tanaka, S., Suzuki, Y., & Fujii, S. (2017a). Impact of feed water pH and membrane material on nanofiltration of perfluorohexanoic acid in aqueous solution. *Chemosphere (Oxford), 183*, 599-604. https://doi.org/10.1016/j.chemosphere.2017.05.132

Zeng, C., Tanaka, S., Suzuki, Y., & Fujii, S. (2017b). Impact of feed water pH and membrane material on nanofiltration of perfluorohexanoic acid in aqueous solution. *Chemosphere, 183*, 599-604.

Zeng, C., Tanaka, S., Suzuki, Y., Yukioka, S., & Fujii, S. (2017). Rejection of Trace Level Perfluorohexanoic Acid (PFHxA) in Pure Water by Loose Nanofiltration Membrane. *Journal of Water and Environment Technology, 15*(3), 120-127. https://doi.org/10.2965/jwet.16-072

Zeng, Q., Qi, X., Zhang, M., Tong, X., Jiang, N., Pan, W., Xiong, W., Li, Y., Xu, J., Shen, J., & Xu, L. (2020). Efficient decontamination of heavy metals from aqueous solution using pullulan/polydopamine hydrogels. *International Journal of Biological Macromolecules, 145*, 1049-1058. https://doi.org/https://doi.org/10.1016/j.ijbiomac.2019.09.197

Zhang, L., Guo, L., & Wei, G. (2021). Recent advances in the fabrication and environmental science applications of cellulose nanofibril-based functional materials. *Materials, 14*(18), 5390.

Zhang, L., Lu, H., Yu, J., Fan, Y., Yang, Y., Ma, J., & Wang, Z. (2018). Synthesis of lignocellulose-based composite hydrogel as a novel biosorbent for Cu 2+ removal. *Cellulose, 25*, 7315-7328.

Zhang, Q., Deng, S., Yu, G., & Huang, J. (2011). Removal of perfluorooctane sulfonate from aqueous solution by crosslinked chitosan beads: Sorption kinetics and uptake mechanism. *Bioresource technology, 102*(3), 2265-2271. https://doi.org/10.1016/j.biortech.2010.10.040

Zhang, Q., Wang, Z., Zhang, C., Aluko, R. E., Yuan, J., Ju, X., & He, R. (2020). Structural and functional characterization of rice starch-based superabsorbent polymer materials. *International journal of biological macromolecules, 153*, 1291-1298.

Zhang, R., Tian, J., Gao, S., & Van der Bruggen, B. (2020). How to coordinate the trade-off between water permeability and salt rejection in nanofiltration? *Journal of materials chemistry. A, Materials for energy and sustainability, 8*(18), 8831-8847. https://doi.org/10.1039/d0ta02510k

Zhang, T., Xiao, S., Fan, K., He, H., & Qin, Z. (2022). Preparation and adsorption properties of green cellulose-based composite aerogel with selective adsorption of methylene blue. *Polymer, 258*, 125320.

Zhang, X., Fang, X., Li, J., Pan, S., Sun, X., Shen, J., Han, W., Wang, L., & Zhao, S. (2018). Developing new adsorptive membrane by modification of support layer with iron oxide microspheres for arsenic removal. *Journal of colloid and interface science, 514*, 760-768.

Zhang, X., He, A., Guo, R., Zhao, Y., Yang, L., Morita, S., Xu, Y., Noda, I., & Ozaki, Y. (2022a). A new approach to removing interference of moisture from FTIR spectrum. *Spectrochimica Acta Part A: Molecular and Biomolecular Spectroscopy, 265*, 120373. https://doi.org/https://doi.org/10.1016/j.saa.2021.120373

Zhang, X., He, A., Guo, R., Zhao, Y., Yang, L., Morita, S., Xu, Y., Noda, I., & Ozaki, Y. (2022b). A new approach to removing interference of moisture from FTIR spectrum. *Spectrochimica acta. Part A, Molecular and biomolecular spectroscopy, 265*, 120373. https://doi.org/10.1016/j.saa.2021.120373

Zhang, X., Wang, S., Zhu, X., Zhu, D., Wang, W., Wang, B., Deng, S., & Yu, G. (2024). Efficient removal of per/polyfluoroalkyl substances from water using recyclable chitosan-coated covalent organic frameworks: Experimental and theoretical methods. *Chemosphere, 356*, 141942.

Zhang, Y., Chi, H., Zhang, W., Sun, Y., Liang, Q., Gu, Y., & Jing, R. (2014). Highly Efficient Adsorption of Copper Ions by a PVP-Reduced Graphene Oxide Based On a New Adsorptions Mechanism. *Nano-Micro Letters, 6*(1), 80-87. https://doi.org/10.1007/BF03353772

Zhang, Y., & Li, Z. (2017). Heavy metals removal using hydrogel-supported nanosized hydrous ferric oxide: Synthesis, characterization, and mechanism. *Science of the total environment, 580*, 776-786.

Zhang, Y., Zhao, X., Yang, W., Jiang, W., Chen, F., & Fu, Q. (2020). Enhancement of mechanical property and absorption capability of hydrophobically associated polyacrylamide hydrogels by adding cellulose nanofiber. *Materials Research Express, 7*(1), 015319.

Zhang, Z., Xiao, F., Guo, Y., Wang, S., & Liu, Y. (2013). One-pot self-assembled three-dimensional TiO2-graphene hydrogel with improved adsorption capacities and photocatalytic and electrochemical activities. *ACS Applied Materials & Interfaces, 5*(6), 2227-2233.

Zhao, C., Nie, S., Tang, M., & Sun, S. (2011). Polymeric pH-sensitive membranes—A review. *Progress in polymer science, 36*(11), 1499-1520. https://doi.org/10.1016/j.progpolymsci.2011.05.004

Zhao, K., Chen, M., Zhang, Y., Miao, J., Jiang, J., Xie, W., Yang, Z., Lin, L., Zhang, W., Chu, R., Shi, W., & Hu, Y. (2022). Anti-fouling and anti-bacterial graphene oxide/calcium alginate hybrid hydrogel membrane for efficient dye/salt separation. *Desalination, 538*, 115908. https://doi.org/https://doi.org/10.1016/j.desal.2022.115908

Zhao, L., Zhou, Y., Zhang, J., Liang, H., Chen, X., & Tan, H. (2023). Natural polymer-based hydrogels: From polymer to biomedical applications. *Pharmaceutics, 15*(10), 2514.

Zhao, Q., Liu, J., Wu, Z., Xu, X., Ma, H., Hou, J., Xu, Q., Yang, R., Zhang, K., & Zhang, M. (2022). Robust PEDOT: PSS-based hydrogel for highly efficient interfacial solar water purification. *Chemical engineering journal, 442*, 136284.

Zhao, Q., Wu, Z., Xu, X., Yang, R., Ma, H., Xu, Q., Zhang, K., Zhang, M., Xu, J., & Lu, B. (2022). Design of poly (3, 4-ethylenedioxythiophene): polystyrene sulfonate-polyacrylamide dual network hydrogel for long-term stable, highly efficient solar steam generation. *Separation and purification technology, 300*, 121889.

Zheng, B., Liu, X., Guo, R., Fu, Q., Zhao, X., Wang, S., Chang, S., Wang, X., Geng, M., & Yang, G. (2017). Distribution characteristics of poly-and perfluoroalkyl substances in the Yangtze River Delta. *Journal of environmental sciences (China), 61*(11), 97-109. https://doi.org/10.1016/j.jes.2017.09.015

Zhou, D., Zhang, L., & Guo, S. (2005). Mechanisms of lead biosorption on cellulose/chitin beads. *Water Research, 39*(16), 3755-3762.

Zhou, J., Saeidi, N., Wick, L. Y., Kopinke, F.-D., & Georgi, A. (2021). Adsorption of polar and ionic organic compounds on activated carbon: Surface chemistry matters. *The Science of the total environment, 794*, 148508-148508. https://doi.org/10.1016/j.scitotenv.2021.148508

Zhou, M., Tan, Q., Wang, Q., Jiao, Y., Oturan, N., & Oturan, M. A. (2012). Degradation of organics in reverse osmosis concentrate by electro-Fenton process. *Journal of Hazardous Materials, 215-216*, 287-293. https://doi.org/https://doi.org/10.1016/j.jhazmat.2012.02.070

Zhou, Y., Tang, Y., Liao, C., Su, M., & Shih, K. (2023). Recent advances toward structural incorporation for stabilizing heavy metal contaminants: A critical review. *Journal of hazardous materials, 448*, 130977.

Zhu, Y., Tang, J., Li, M., Wang, H., & Yang, H. (2021). Contamination Status of Perfluorinated Compounds and Its Combined Effects with Organic PollZutants. *Asian J. Ecotoxicol, 16*, 86-99.